MODEL MEMBRANES AND THEIR INTERACTIONS WITH NATIVE AND ARTIFICIAL LIPOPROTEINS

Malmö University Health and Society Doctoral Dissertation
Model Membranes and Their Interactions with Native and Artificial Lipoproteins 2020:4

Front Illustration: Lipid Exchange Between Lipoprotein and Model Membrane
ISBN 978-91-7877-131-8 (print)
ISBN 978-91-7877-132-5 (pdf)
ISSN 1653-5383
DOI 10.24834/isbn.9789178771325
Printing: Holmbergs, Malmö 2020

SARAH WALDIE

MODEL MEMBRANES AND THEIR INTERACTIONS WITH NATIVE AND ARTIFICIAL LIPOPROTEINS

Malmö University, 2020
Faculty of Biomedical Science
Life Sciences Group, Institut Laue-Langevin

CONTENTS

LIST OF PUBLICATIONS

Paper 1

The production of matchout-deuterated cholesterol and the study of bilayer-cholesterol interactions

S. Waldie, M. Moulin, L. Porcar, H. Pichler, G. A. Strohmeier, M. Skoda, V. T. Forsyth, M. Haertlein, S. Maric, M. Cárdenas

Scientific Reports (2019), 9:5118

Paper 2

Localisation of cholesterol within supported lipid bilayers made of a natural extract of tailor-deuterated phosphatidylcholine

S. Waldie, T. K. Lind, K. Browning, M. Moulin, M. Haertlein, V. T. Forsyth, A. Luchini, G. A. Strohmeier, H. Pichler, S. Maric, M. Cárdenas

Langmuir (2018), 34(1), 472-479

Paper 3

Lipoprotein ability to exchange and remove lipids from model membranes as a function of fatty acid saturation and presence of cholesterol

S. Waldie, F. Sebastiani, K. Browning, S. Maric, T. K. Lind, N. Yepuri, T. A. Darwish, M. Moulin, G. Strohmeier, H. Pichler, M. W. A. Skoda, A. Maestro, M. Haertlein, V. T. Forsyth, E. Bengtsson, M. Malmsten, M. Cárdenas

Biochemica Biophysica Acta – Molecular and Cell Biology of Lipids (2020), 1865, 158769

Paper 4

The interaction of ApoE and ApoE nascent-like HDL particles with model cellular membranes: Effect of protein allele and membrane composition

S. Waldie, F. Sebastiani, M. Moulin, Y. Gerelli, S. Prevost, F. Roosen-Runge, J. C. Voss, T. A. Darwish, N. Yepuri, R. Del Giudice, G. Strohmeier, H. Pichler, S. Maric, V. T. Forsyth, M. Haertlein, M. Cárdenas

Manuscript

Paper Contributions

Paper 1

Planned for and produced matchout cholesterol, performed NR and SANS experiments, data analysis, wrote first draft of the manuscript and was responsible for submitting the manuscript.

Paper 2

Performed NR experiments, data analysis, and contributed to the discussions and the writing of the manuscript.

Paper 3

Planned and carried out NR experiments, majority of data analysis, wrote the first draft of the manuscript and was responsible for writing and submitting the manuscript.

Paper 4

Produced proteins and lipoproteins used in experiments. Planned and carried out NR and SANS experiments, data analysis and was responsible for writing of the manuscript.

ABBREVIATIONS

CVD	Cardiovascular Disease
LDL	Low-Density Lipoprotein
HDL	High-Density Lipoprotein
RCT	Reverse Cholesterol Transport
GGE	Gradient Gel Electrophoresis
ApoA1	Apolipoprotein A1
ApoB100	Apolipoprotein B100
VLDL	Very Low-Density Lipoprotein
IDL	Intermediate-Density Lipoprotein
ABCA1	ATP-Binding Cassette A1
ABCG1	ATP-Binding Cassette G1
LCAT	Lecithin:Cholesterol Acyltransferase
SR-B1	Scavenger Receptor Class B Type-1
CETP	Cholesteryl Ester Transfer Protein
LDLR	Low-Density Lipoprotein Receptor
PLTP	Phospholipid Transfer Protein
HL	Hepatic Lipase
EL	Endothelial Lipase
LPL	Lipoprotein Lipase
FC	Free Cholesterol
CE	Cholesterol Esters
TG	Triglycerides
rHDL	Reconstituted High-Density Lipoprotein
ApoE	Apolipoprotein E
AD	Alzheimer’s Disease
DSC	Differential Scanning Calorimetry
PC	Phosphatidylcholine
SM	Sphingomyelin
PE	Phosphatidylethanolamine
PS	Phosphatidylserine
PI	Phosphatidylinositol

SUV	Small Unilamellar Vesicle
LUV	Large Unilamellar Vesicle
GUV	Giant Unilamellar Vesicle
SLB	Supported Lipid Bilayer
POPC	1-palmitoyl-2-oleoyl-glycero-3-phosphocholine
DPPC	1,2-dipalmitoyl-sn-glycero-3-phosphocholine
AFM	Atomic Force Microscopy
DLS	Dynamic Light Scattering
QCMD	Quartz Crystal Microbalance with Dissipation
ATR-FTIR	Attenuated Total Reflection-Fourier Transform Infra-Red Spectroscopy
SANS	Small-Angle Neutron Scattering
NR	Neutron Reflectometry
SAXS	Small-Angle X-ray Scattering
SEC-SAXS	Size-Exclusion Chromatography Small-Angle Scattering
His-tag	Histidine-Tag
UC	Ultra Centrifugation
DMPC	1,2-dimyristoyl-sn-glycero-3-phosphocholine
SAS	Small-Angle Scattering
SLD	Scattering Length Density
TOF	Time-of-Flight
cmSi	Contrast Matched Silicon
DLPC	1,2-dilauroyl-sn-glycero-3-phosphocholine

ABSTRACT

Atherosclerosis arises from build-up of plaque in the blood, can result in cardiovascular disease and is the largest killer in the west. Low- and high-density lipoproteins are involved in the disease development by depositing and removing lipids to and from artery walls. These processes are complex and not fully understood however, therefore determining the specific roles of the components involved is of fundamental importance in the treatment of the disease.

The work presented in this thesis investigates the production of recombinant tailor-deuterated cholesterol, the structure of cholesterol-containing model membranes and interactions of both native and reconstituted lipoproteins with model membranes. Deuteration is commonly used in neutron scattering for biological samples to provide highly important contrast and the complexity of the native lipoproteins leads to the use of more simple model systems where the compositions can be altered and investigated systematically.

A protocol was developed to produce matchout-deuterated cholesterol for use in neutron scattering studies, as cholesterol is a hugely important component in membranes. The verification of the matchpoint of cholesterol was determined by small-angle neutron scattering and the localisation of cholesterol in model membranes was determined through the use of neutron reflectometry. The interactions of the native and reconstituted lipoproteins with model membranes were also followed by neutron reflectometry, while the structural characterisation of the reconstituted lipoproteins was carried out by small-angle scattering.

INTRODUCTION

Atherosclerosis

Atherosclerosis

Atherosclerosis is the largest killer in the west[1]. It comes from plaque build-up in artery walls and can lead to cardiovascular diseases (CVD), giving rise to heart attacks and strokes[2]. The plaque build-up originates from low-density lipoproteins (LDL) depositing into the artery walls[3] which are then oxidised and taken up by macrophages. These then become foam cells, essentially filled with fat, and they continue to build up and can form a plaque. When this plaque ruptures, thrombus material enters the blood stream and can lead to heart attacks or other CVD related phenomena. High-density lipoproteins (HDL), on the other hand, have been shown to play a preventative role in the development to atherosclerosis by a process known as reverse cholesterol transport (RCT)[4]. Here, cholesterol is removed from the lipid-filled foam cells and deposited in the liver where it is cleared from the body[5–7]. The cholesterol removal occurs via efflux by various means, including aqueous diffusion or receptor/transporter mediated transfer[8]. The presence of HDL has been shown to prevent the oxidation of the LDL and therefore helps prevent the development to atherosclerosis[9]. In turn, HDL and LDL are commonly known as ‘good’ and ‘bad’ cholesterol respectively. Whilst HDL has been shown to prevent the development to atherosclerosis via this RCT pathway, in which a reduction of atherosclerotic risk is seen with increasing RCT efficiency[7], increased levels of HDL have also been shown to have a neutral[10] or even negative correlation[11] to the prevention of atherosclerotic development. Although the molecular mechanisms involved in the advancement of CVD are highly complex, the absolute ratios of LDL to HDL have been found to be of great importance for the onset of atherosclerosis[12].

Lipoproteins

Lipoproteins consist of a core of cholesterol esters and triglycerides, with an outer monolayer of lipids and cholesterol all encased by apolipoproteins[13]. Lipoproteins come in various sizes and are categorised by their density and composition[13]. These

variations can be large between distinct groups of lipoproteins; for example, HDL and LDL vary drastically in protein composition, size and density, however within these categories further distinctions can be made. This is more prominent in HDL where there are generally five distinct subpopulations, with slight variations in composition but most notably differences in size and density. HDL was first described by differences in density according to ultra-centrifugation techniques categorising HDL into two distinct groups[14]: HDL2 which is lower in density due to a higher lipid content (1.063-1.125 g mL^{-1}); and HDL3 which is slightly higher in density owing to its higher protein content (1.125-1.21 g mL^{-1}). These groups can further be characterised by their size, using polyacrylamide gradient gel electrophoresis (GGE) resulting in five further subclasses ranging in size from 7.2-12.0 nm in diameter[15].

The main protein present in HDL is Apolipoprotein A1 (ApoA1) contributing roughly 70% of total protein content in all HDL[16]. The second most abundant is ApoA2[16] followed by a combination of various other proteins including Apolipoproteins C, E and J. While almost all HDL contain ApoA1[17], the remaining proteins are varied across different HDL types and subclasses[16]. The main protein present in LDL is Apolipoprotein B100 (ApoB100)[13]; this is a large protein also found on very low-density lipoproteins (VLDL) and intermediate-density lipoproteins (IDL), although never found in HDL. ApoC and ApoE are also commonly found in VLDL[16].

Another key difference between HDL and LDL is the way in which they are formed in the body (see Figure 1). HDL is metabolised from lipid-poor ApoA1 produced in the intestine and liver[18]. This ApoA1 is lipidated with both phospholipids and cholesterol via the ATP-binding cassette A1 (ABCA1), which in turn forms nascent discoidal HDL on the addition of further phospholipids and cholesterol via peripheral tissues. The nascent HDL obtains free cholesterol transferred via macrophage ABCA1 and ABCG1 transporters. This free cholesterol is then esterified by lecithin-cholesterol acyltransferase (LCAT) resulting in mature spherical HDL with a core full of cholesterol esters[18]. Both discoidal and mature HDL can interact with the scavenger receptor class B type-1 (SR-B1) in the liver and undergo transfer of cholesterol esters towards SR-B1 and exchange of unesterified cholesterol in both directions[19]. The transfer of cholesterol esters also occurs via the cholesteryl ester transfer protein (CETP) to VLDL and LDL for eventual uptake by the LDL receptor (LDLR) in the liver[20]. The transfer of phospholipids and triglycerides from VLDL to HDL is facilitated by phospholipid transfer protein (PLTP) resulting in HDL remodelling. The hydrolysis of HDL phospholipids and triglycerides via hepatic and endothelial lipases (HL and EL) also results in HDL remodelling[21].

On the other hand, LDL has a much simpler formation pathway. Chylomicrons, the largest and least dense lipoprotein type, are produced in the intestine and undergo hydrolysis of triglycerides resulting in chylomicron remnants which are cleared via the liver[22]. VLDL are produced in the liver and are the next least dense lipoproteins rich in triglycerides. These particles are hydrolysed by lipoprotein lipases (LPL) resulting in the removal of the triglycerides and the formation of IDL which are cholesterol rich[23]. Further hydrolysis via LPL occurs and results in LDL, which is even richer in cholesterol (see Figure 1).

In summary, the structural and compositional differences between HDL and LDL play a large role in their contributions to atherosclerosis[24]. While both lipoprotein types are lipid binding, their abilities to exchange lipids and transport cholesterol differ drastically. LDL deposits more lipids and cholesterol to artery walls, whereas the main role of HDL in the blood is to carry out cholesterol efflux thereby removing excess cholesterol from artery walls[24].

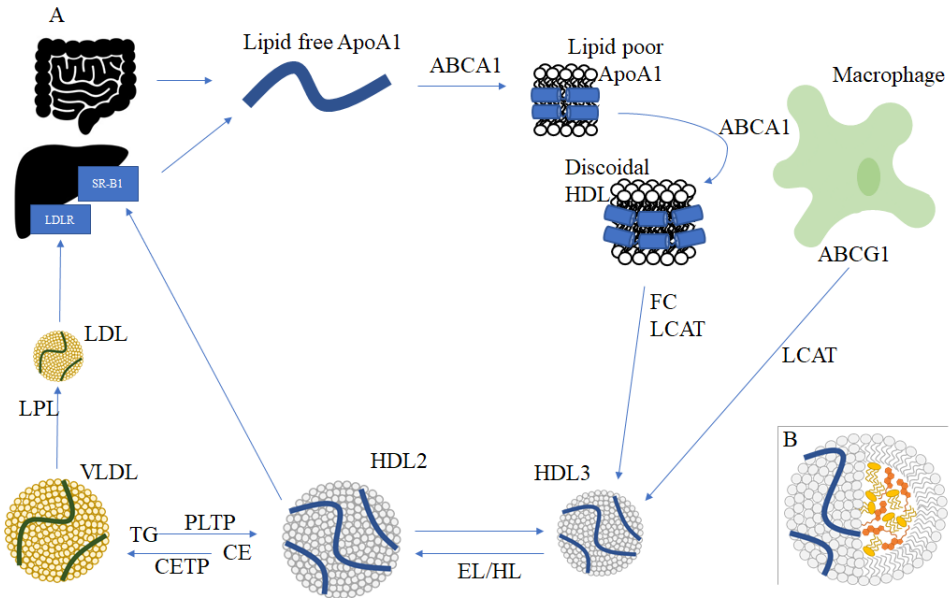

Figure 1A. Lipoprotein metabolism: Lipid-free ApoA1 is produced in both the intestine and the liver. It gains phospholipids and cholesterol via the ATP binding cassette A1 (ABCA1) to form lipid-poor ApoA1; it gains further lipids from peripheral tissues to form nascent discoidal HDL which obtains free cholesterol (FC) from macrophages via ABCA1 and ABCG1. The FC is esterified by lecithin-cholesterol acyltransferase (LCAT) to form mature spherical HDL. Mature HDL can interact with the scavenger receptor class B type-1 (SR-B1) in the liver resulting in the exchange of unesterified cholesterol in both directions. Cholesteryl esters (CE) are transferred to VLDL via the cholesteryl ester transfer protein (CETP) for eventual uptake by the LDLR in the liver. The progression from VLDL to LDL occurs via hydrolysis by lipoprotein lipases (LPL). Phospholipids and triglycerides (TG) are transferred to HDL from VLDL via the phospholipid transfer protein (PLTP) resulting in HDL remodelling. Hepatic and endothelial lipases (HL/EL) also promote HDL remodelling. Insert: B. Lipoprotein structure with a core of cholesterol esters and triglycerides.

Plaque Remodelling

As increased HDL levels had previously been shown to reduce the risk of atherosclerosis by slowing down plaque formation via lipid and cholesterol removal[5], potential treatments were introduced to mimic this process. One such method, the so-called plaque remodelling method, injected reconstituted HDL-like particles (rHDL) into the blood stream to increase the efficiency of cholesterol efflux and therefore reduce the progression to atherosclerosis[25,26]. Another plaque remodelling technique works on a similar basis but uses ApoA1-like peptides instead of rHDL to carry out the same function[27,28]. Pre-clinical trials for plaque remodelling therapies seemed to give positive indications of success in diminishing atherosclerotic plaque[29], however clinical trials failed to deliver statistically significant regression of atherosclerotic plaque[30]. In coronary heart disease, derived from the plaque build-up in atherosclerosis, HDL levels have been shown to have both protective[31] and non-protective[32] capabilities in patients after coronary interventions or bypass operations respectively. The latter also supported discussions that neither the concentration nor the quantity of HDL alone in the blood is important, but that it is functionally beneficial HDL (*i.e.* those that increase RCT for example) which have a positive impact in providing atheroprotective behaviour[33,34]. It is though, to date, not known which HDL have beneficial function in order to prepare relevant rHDL for therapy.

Apolipoprotein E (ApoE)

Structure and Roles

ApoE is a 299 amino acid protein encoded by the ApoE gene found on human chromosome 19[35]. There are three alleles of ApoE: E2, E3 and E4, each differ by only two amino acids in positions 112 and 158. Either arginine or cysteine are found in these positions depending on the isoform[36]: E2: Cys-112, Cys-158; E3: Cys-112, Arg-158; E4: Arg-112, Arg-158. Even though these differences are only small they have dramatic effects on the structure and function of the proteins[37].

ApoE present in the periphery (the rest of the body apart from the brain) is mostly produced in the liver[38,39], whereas all ApoE found in the brain is produced therein as it cannot cross the blood-brain barrier[40]. The roles ApoE plays within these distinct regions (the brain versus the periphery) are also varied[41]. In the periphery ApoE circulates in blood serum and is found on most HDL particles, but more commonly on large HDL2 particles which are rich in lipids and triglycerides[42]. ApoE takes part in cholesterol efflux and also binds to lipoproteins and ApoE receptors[43,44]. Receptor

binding is of great importance to the role that ApoE plays in the clearance of cholesterol from the body[45,46]. However, within the brain ApoE-enriched HDL-like particles do not behave as HDL in the periphery: ApoE plays a role in maintaining cholesterol homeostasis by transporting cholesterol around the brain but distinctly not clearing it from plasma as elsewhere in the body[38,47].

Different parts of the protein's structure are responsible for the ability to bind various components in the blood, for example ApoE's N-terminal binds to LDL receptors[48], whereas its C-terminal domain is most commonly associated with lipid binding capabilities[49]. There has been some discussion as to whether ApoE4 can bind a fewer or greater number of lipids compared to ApoE3[49,50]. The difference in abilities to bind lipids has been discussed at length and has mostly been attributed to the structural differences arising from the changes in composition across the protein isoforms[51]. The presence of the arginine at residue 112 in allele E4 forms a salt bridge with Glu-109, leading to Arg-61 facing away from the four-helical bundle comprising the N-terminal. This in turn leads to another salt bridge to occur between Arg-61 and Glu-255 in the C-terminal domain. Even though it is probable that salt bridges occur to some extent in ApoE3 and ApoE2, it is to a much lesser extent than for ApoE4[39]. This interaction between Arg-61 and Glu-255 is known as the 'domain interaction' leading to ApoE4's more compact structure[52] and is likely the cause of many functional differences between the isoforms. Indeed, when small molecules are introduced to inhibit this interaction, or mutations are introduced to prohibit the domain interaction, the ApoE4-like isoform behaves in a much more similar way to ApoE3[37,53,54]. On one hand, it is argued that ApoE4 can bind fewer lipids due to this domain interaction causing restrictions on the structure and therefore not allowing it to bind as many lipids as the other isoforms[50]. On the other hand, this salt bridge is said to have some causal effects in the increased lipid affinity of ApoE4[49,55], including ApoE4's reduced ability to form tetramers[56] and therefore increased ability to bind lipids, as monomers are more able to bind lipids than tetramers[57]. This structural difference is reflected in different binding abilities for some LDL receptors[58]; despite this, overall ApoE3 and ApoE4 have been shown to have equal binding capacity for the ApoE receptors in the liver[59]. .

Relevance in Disease

ApoE is a biomarker for certain diseases such as atherosclerosis and Alzheimer's disease (AD), however the positive or negative correlation to these diseases is allele dependent. ApoE3 is a neutral indicator for these diseases, *i.e.* it does not have a positive or negative connotation with either. ApoE2 is thought to be protective against AD[60,61];

however, in certain cases indicative of atherosclerotic development due to its impaired binding of the LDLR in Type III hyperlipoproteinemia cases. This impaired binding leads to lesser capabilities to clear triglyceride rich VLDL remnants from plasma and in turn increase atherosclerotic risk[39,62]. ApoE4 has been linked to the progression of both atherosclerosis and AD[37]. As previously discussed, the use of ApoA1-rHDL has previously been employed to aid in the treatment of atherosclerosis, and more recently the use of ApoE-based rHDL has also been introduced and has encouraging potential, though clinical trials are required to determine if it would be a suitable treatment route for atherosclerosis[63].

The main links to these diseases, while not fully understood, have been put down to their different binding abilities to both lipids and receptors. In the blood ApoE4 has a greater tendency to bind to VLDL than HDL; however for both ApoE2 and ApoE3 the opposite phenomenon occurs[49]. This preference for VLDL of ApoE4 has been suggested to be due to structural restrictions arising from the domain interaction[64,65] leading to an extended helical segment in the C-terminal domain. An extended configuration results in ApoE4 having a preference for the lesser curved surfaces found on VLDL, due to the latter's increased size and higher lipid surface content: 60% lipids vs. 80% protein in HDL[49]. Another suggestion is that ApoE3 has a more stable N-terminal domain and therefore can bind proteins more easily hence the preference for HDL, whereas ApoE4 is less stable and therefore less likely to bind to proteins and so has a stronger affinity for VLDL[49]. This preference of ApoE4 for VLDL gives rise to greater VLDL receptor binding and downregulation, leading to higher levels of LDL found in serum resulting in higher risk for atherosclerosis[39,64]. Conversely, in the brain both ApoE3 and ApoE4 preferentially bind to HDL sized particles[38,66]. The different binding capabilities of the isoforms lead, for ApoE4, to a deficiency both in lipid and cholesterol transport in the brain, and in cholesterol deposition to neuronal sites[67]. This deficiency is seen across many processes in the brain and leads to ApoE4 displaying a greater production of amyloid beta peptides which is an indicator of the beginning stages of AD[68]. It is though not clear if the development of AD comes from the amyloid beta peptide production directly or from a lack of clearance of the amyloid plaques[69].

Lipids and Biomembranes

Cell Membranes

Biological membranes comprise the outer layer of a cell providing protection from its surrounding environment and regulating material in and out of the cell. Human cell membranes are comprised of mainly phospholipids, cholesterol and proteins, but specific composition can vary per cell type[70]. Each component in cell membranes has a specific role[71], such as communication within and between cells[72] or transport of material[73].

The "fluid mosaic model" was reported in the early 1970s as a way to describe cell membranes which comprised membrane proteins set in a fluid lipid bilayer[74] (Figure 2). The viscous fluidity allows for translational diffusion to occur, resulting in a dynamic membrane[75]. The composition of the membrane strongly influences the bilayer's features such as fluidity, curvature and potential domain formation. A more recent model known as the "flexible surface model" was introduced in the 1990s which provided further information about how proteins and lipids interact in the membrane, giving rise to distinct curvatures and insight into membrane protein stability[76,77].

As phospholipids make up a large proportion of the cell membrane, they have an important role in deciding what can or cannot enter the cell. They form a bilayer at the rim of the cell due to their amphipathic nature, preventing unwanted molecules from passing through the membrane. Another main role of the phospholipids is to maintain fluidity, dependent on the temperature and composition[78]. Membranes can be characterised via various techniques such as differential scanning calorimetry (DSC), which can be used to measure the melting temperature of lipids to determine what phase the lipids are in[79].

Proteins within cell membranes also play an important role: they can communicate signals from intracellular to extracellular environments[80]; enable the movement of molecules across the membrane[81]; and some proteins allow recognition of other cells[82].

The way in which lipids come together can be determined by their composition and environment. The "packing parameter" of a certain lipid type is related to the ratio between its hydrophilic headgroup and hydrophobic tail region[83]. Distinct packing parameters determine the overall shape that the spontaneous assemblies form. For planar bilayers, as in the case for membranes, this packing parameter is equal to 1, since the relative areas of the headgroups and tail regions should be equal and result in flat bilayers. For packing parameters smaller than 1, various shapes can occur with

positive curvature, whereas for packing parameters larger than 1 the same shapes occur but in an inverted manner[84], for example, reverse micelles where the headgroups form the micelle core and the tails are part of the continuous solution phase.

In general, cell membranes are in a fluid state. However, their highly complex composition can cause some phase separation to occur due to limited miscibility or certain interactions between lipid types; these nanodomains are called lipid rafts. These rafts are often comprised of cholesterol and sphingolipids which show strong interactions in the membrane[85,86] and play important physiological roles in protein signalling[87,88] and function[89]. Studies of lipid rafts *in vivo* have been successfully carried out using fluorescence techniques with various cell types[90–92]. Neutron scattering techniques have been used to investigate domains in membrane models, including determining the co-existence of fluid and gel domains within a membrane[93], and investigating the domain size and morphology within a model environment[94].

Another aspect of cellular membranes, is the asymmetric nature of the composition[95]. Generally, in eukaryotic cells, there is a prevalent asymmetry in the distribution of the lipids in the membranes. A large proportion of the phosphatidylcholine (PC) and sphingomyelin (SM) is found in the outer membrane, whereas the inner membrane leaflet is more commonly comprised of phosphatidylethanolamine (PE), phosphatidylserine (PS) and phosphatidylinositol (PI)[96]. This distinct distribution can in part be down to the packing parameters of the lipids: PC and SM prefer neutral or positive curvature, whereas PE and PS prefer negative curvature. This arrangement of lipids is also thought to provide certain functions to the membrane, including stability, surface charge and permeability.

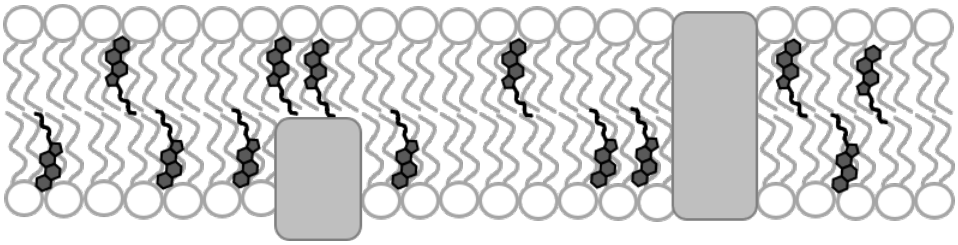

Figure 2. Pictorial representation of a cell membrane. The phospholipids are the main component, the cholesterol is represented by the hexagonally comprised molecules and the large solid colour blocks are proteins.

Lipid Types

Lipids come in many shapes and sizes. They are amphipathic molecules generally comprised of a hydrophilic headgroup and a hydrophobic tail region. Phospholipids make up roughly 70% of all lipids in human cell membranes[96], containing a phosphate-based head group and an acyl chain tail region. PC is the most common type of phospholipid in humans[97], with two acyl chains comprising the tail. While all PC headgroups are the same, the tail regions can vary in both chain length and saturation.

Another common type of lipid found in cell membranes are sphingolipids. This group is not derived from glycerol, unlike many others, and consists of a headgroup, a fatty acyl chain and sphingosine (an 18-carbon length amino alcohol hydrocarbon). SM is the most common sphingolipid in cell membranes[96] with either a PC or PE headgroup, a sphingosine and a fatty acyl chain of varying length and saturation.

Cholesterol

Cholesterol is another key component of cellular membranes. As a lipid it contains a polar hydroxyl headgroup and a non-polar tail region. The tail region consists of four bulky hydrocarbon rings with a short acyl chain, together forming the sterol structure. The steroid ring group interacts strongly with phospholipid tails which helps to maintain the membrane's structure[98]. Key roles of cholesterol include balancing both membrane fluidity and rigidity, depending on temperature[99–101], and also altering the thickness of membranes, by condensation[102] or by fluctuations in the gel and fluid phases[103].

The presence of cholesterol in membranes induces a liquid ordered phase as a function of cholesterol concentration – this highly ordered phase has characteristics of both gel and liquid crystalline phases[104]. Neutron scattering techniques have been used to show the presence of micro-domains of highly ordered lipids (with high concentrations of cholesterol in particular), amongst an otherwise liquid disordered phase[105], known as rafts.

Model Membranes

As cell membranes are very complex, model membranes are often used as a bio-mimetic to simplify the environment but allow for specific questions about the composition, structure, morphology and size to be answered. When exploring phenomena occurring in human membranes, PC lipids are often used as the main component as

they constitute a large proportion of human cell membranes. Different phospholipids can be used depending on the specific question being asked: information to be obtained and what the model symbolises.

There are various ways in which to represent cell membranes, from monolayers[106], to vesicles and various forms of supported bilayers[107], each type providing a different property to be probed. One way to represent lipid bilayers is via the use of vesicles: thermodynamically unstable aggregates which are created via sonication or extrusion. Vesicles can be categorised by size from small unilamellar vesicles (SUVs) through to large and giant unilamellar vesicles (LUVs and GUVs respectively), ranging from 20 nm in radius to a few microns in diameter, dependent on their use and what they represent. SUVs may be used as a pre-cursor to forming supported lipids bilayers (SLBs)[108] whereas GUVs are in the size range to be comparable to eukaryotic cells[109] and have also been used to study phase behaviour in membranes[110,111].

While vesicles are free standing in solution, SLBs provide a flat membrane to be studied. The most common ways in which SLBs are formed are the vesicle fusion or Langmuir-Blodgett methods. Vesicle fusion is a simple method for bilayer deposition: small vesicles are introduced onto a hydrophilic surface and spontaneously rupture after initially adsorbing onto the surface. Small vesicles formed by tip sonication have an increased chance of rupturing and forming a uniform bilayer[108,112,113]. Langmuir-Blodgett/Schaefer deposition is another way in which bilayers can be formed in a controlled manner, and it is commonly used to create asymmetrical bilayers[114,115]. However, this method can be a very time-consuming process and requires highly controlled conditions for good coverage. SLBs can be used to study membrane composition[108] as well as the morphology of the bilayer *i.e.* the detection of microdomains or inhomogeneity present[116].

Vesicle fusion, on the other hand, can give rise to spontaneous asymmetry in SLBs such as for mixtures of low and high melting lipids[117]. It was shown that asymmetry occurs in vesicle compositions close to the two phase boundaries between fluid and gel phases for 1-palmitoyl-2-oleoyl-glycero-3-phosphocholine (POPC) – 1,2-dipalmitoyl-sn-glycero-3-phosphocholine (DPPC) mixtures. This is due to vesicles having a range of sizes and lipid distributions at the single vesicle level, dependent on vesicle size[108].

While SLBs provide a lot of information about a membrane, the contact it has with the surface could potentially cause artefacts or different properties to be seen[118]. The development of floating lipid bilayers removes the bilayer from being in direct contact with the substrate and could therefore help circumvent this problem[119].

These methods for representing model membranes can be studied via various techniques such as atomic force microscopy (AFM)[116], dynamic light scattering (DLS)[120], quartz crystal microbalance with dissipation (QCMD)[121], attenuated total reflection-Fourier transform infra-red spectroscopy (ATR-FTIR)[122], small-angle neutron scattering (SANS)[123] and neutron reflectometry (NR)[124], some of which will be discussed later on in more detail.

The chosen membrane composition is determined by the purpose of the model and what it represents. Most commonly symmetrical membranes are used if standard cell membranes are the subject of choice for simplicity purposes. Cell membranes are often asymmetrical; however, in model membranes this is often not considered unless the outer layer is drastically different or plays a significant role. For example, the outer layer of certain native cell membranes may consist of particular lipids or proteins that are key to function and are the component in question.

Use of Membranes to Study Interactions

Model membranes can be of interest to study the membrane itself, however, they often serve as a tool to study interactions with the membrane[125] or as carriers for membrane proteins. In either case, the simplest model which suitably represents the membrane in question should be used.

One recent example of a study of lipoprotein interactions occurring at model membranes is the work carried out by Browning *et al*.[126,127] to follow interactions of human lipoproteins with model membranes as SLBs. The initial work investigated the difference in interaction between HDL and LDL with model PC membranes[126] and found NR was a suitable tool to follow this exchange. The study showed HDL removed more lipids from the SLBs whereas LDL deposited more. Following this work, an investigation into the effect that the charge of the bilayer has on exchange capabilities was carried out[127] through the introduction of PS lipids into PC bilayers to give varying levels of charge across the membranes. Whilst the quantity of lipids deposited was unaffected by the charge on the bilayer, the amount of material removed by HDL increased for membranes with higher charge. A further example is from Maric *et al*.[128] who investigated interaction of human lipoproteins with model PC membranes in the form of vesicles, free standing in solution. As with the work by Browning *et al*. deuteration was used to aid the quantification of lipid exchange. The mode of interaction was determined in more detail whereby the interaction was seen to be influenced not only by diffusion-limited monomer exchange but collision and tethering-determined exchange also, along with the lipoprotein type present.

Gerelli *et al*. used NR to follow lipid exchange between SLBs and vesicles[129]. The use of the deuterated SLBs and non-deuterated vesicles, and vice versa, allowed the exchange to be followed by changes in the reflectivity signal. This method also gave rise to information on the flip-flop rates of lipids within the SLBs, another phenomenon of cellular membranes that has also been measured in bulk[123].

Another interaction type that has been studied at membrane surfaces is that between nanodiscs (formed by lipids and membrane scaffold proteins reminiscent of apolipoproteins[130] or polymers[131]) and SLBs. Hall *et al*. incubated polymer-based nanodiscs with SLBs and followed both lipid and polymer exchange using ATR-FTIR and NR respectively[122]. The combined use of these techniques allowed distinction to be made between the lipid and polymer exchange as the polymer exchange was less detectable via ATR-FTIR.

Use of Scattering

To be able to study the structure and dynamics of soft matter systems, such as lipids and proteins, scattering is a powerful technique often employed. The scattering comes from an interaction of an incoming source of either X-rays or neutrons with a sample. X-rays interact with the electron cloud of the sample whereas neutrons interact with the nucleus of the atoms (see Materials and Methods section for theory).

In X-ray scattering, the scattering power is directly proportional to the number of electrons in the sample (Figure 3). In this way smaller components, such as hydrogen, have weak scattering power. This also means that isotopes of the same element have an equal scattering power as they have the same number of electrons. The scattering lengths of the main components in these soft matter systems can be found in Table 1. From these values it is clear to see that hydrogen gives little contrast compared to other components, however hydrogen often makes up a large proportion of these samples, so a lot of information is lost.

Neutrons, on the other hand, behave very differently. The scattering ability of different elements is not linked to the number of electrons but is seemingly more random and interacts with the nucleus of the atom. Again, the scattering lengths of the main components of soft matter systems can be found in Table 1. From these values the contrast is again notable, however the largest difference is of that between hydrogen and deuterium. This difference in scattering power enables different features to be distinguished in samples through isotope substitution. Both buffer solutions and the samples themselves can be modified via this method.

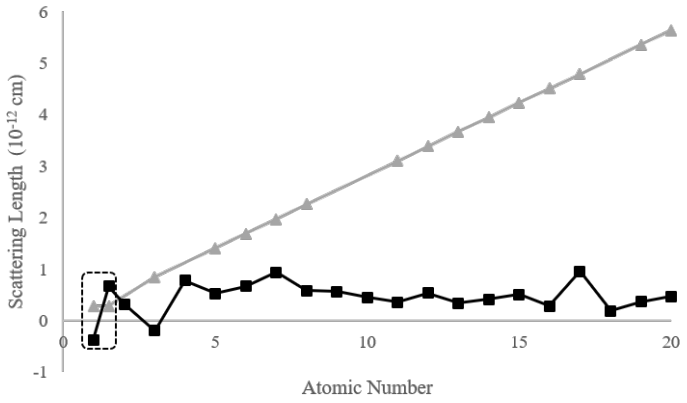

Figure 3. X-ray (triangles) and neutron (squares) scattering lengths of the first twenty atoms of the periodic table (including most common atoms found in biological samples). Deuterium is given as atomic number 1.5 to separate from hydrogen at 1. Hydrogen and deuterium are highlighted in dotted square box.

Table 1. X-ray and Neutron scattering lengths (*b*) for atoms commonly found in soft matter systems[132].

Atom (Isotope)	$b_{\text{X-ray}}$ **(10^{-12} cm)**	b_{neutron} **(10^{-12} cm)**
Hydrogen (^{1}H)	0.28	-0.37
Deuterium (^{2}H)	0.28	0.67
Carbon (^{12}C)	1.69	0.67
Oxygen (^{16}O)	1.97	0.58
Nitrogen (^{14}N)	2.25	0.94
Phosphorous (^{31}P)	4.23	0.52
Sulphur (^{32}S)	4.50	0.28

A key factor in obtaining the most information from using low-resolution scattering techniques is creating good contrast. Often this scattering contrast comes from the difference in scattering ability of the sample compared to the solvent it is in. When working with X-rays, this contrast often comes from the introduction of heavy metal salts into the sample environment[133,134]. For neutrons, on the other hand, this contrast comes from the use of isotope labelling, most commonly via the use of deuteration for biological samples[123,129,135].

Another key benefit that can be gained from the use of isotopes is that of rendering certain components 'invisible', also known as contrast matching[136]. As hydrogen has a negative scattering length where deuterium has a positive one, a specific isotope ratio can be utilised to obtain a sample with no net scattering. This can be highly beneficial when measuring samples with more than one component. Using a heavy water or D_2O based buffer, certain components can be rendered invisible or 'matched-out' at certain percentages of D_2O. Different components have standard D_2O levels at which they no longer give net coherent scattering, for example lipids, protein and DNA have matchout values of roughly 12%, 42% and 65% D_2O buffer, respectively[137] (Figure 4). This means that no scattering from those components will be seen in those specific percentages of D_2O as there is no contrast between the sample and the buffer it is in. Using deuteration in the sample as well as in the buffer gives another level of possibility when determining the best contrast for a sample. Measuring a non-deuterated sample in 100% D_2O buffer will likely give the best contrast, enabling the most amount of information to be obtained from the data. However, the technique of matching out can also be used to add complexity to a sample whilst reducing its scattering. This can be beneficial in procuring further information about a sample without adding layers of complexity in the scattering data. To determine the matchpoint of a sample as a whole or specific components within, a matchout series can be carried out in a range of D_2O buffer contrasts to extract the relevant information.

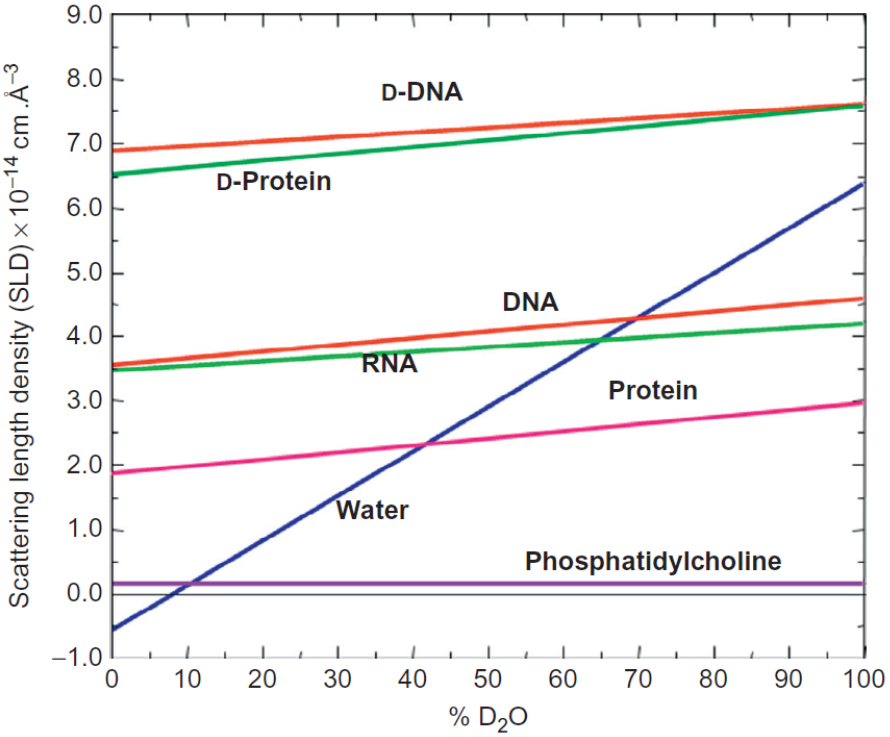

Figure 4. Level of deuteration in buffer required to provide matchout conditions for various biological macromolecules. (Reviewed in Haertlein et. al 2016)[135]

Deuteration can be carried out chemically[138] or biologically[139]. Chemical deuteration is performed by exposing whole molecules or building blocks to D_2O in the presence of a catalyst. The final products are then synthesised from these deuterated starting materials using organic chemistry techniques. Biological deuteration is accomplished by using microorganisms such as bacteria or yeast grown in deuterated media, followed by extraction and purification. The specific level of deuteration can be obtained using a deuterated or non-deuterated carbon source[139,140] or solvent. The benefits of using biological deuteration is that the specific level of deuteration can be fine-tuned according to experimental needs, and chiral specific molecules can be obtained. Different sections within the same molecule can be modified to have differing final levels of deuteration, this can be done by knowing the synthesis pathway and how each component in the medium will affect the final product. For example, the production of

natural PC lipids using *Escherichia coli* and differing levels of deuteration across different sections of the lipids renders the whole molecule matched-out in 100% deuterated solutions even though the level of deuteration differs across the molecule[140].

Scattering can be used in various ways to determine valuable structural or dynamic information about a sample, depending on the sample type and environment it is in. One example is the use of neutron spin echo to follow the dynamics of a molecule by analysing the speed of scattered neutrons to determine dynamic properties of the molecule in question[141]. Another example is the use of crystallography to determine the structure of molecules and to aid in determining their potential importance or use for further studies[142]. Other techniques include small-angle X-ray and neutron scattering (SAXS and SANS respectively) and neutron reflectometry (NR) which will be the main focus explored here. The principles of these techniques will be discussed in the materials and methods section.

Small-Angle Scattering and Neutron Reflectometry

SAXS is an effective tool used to determine the structure of a sample in solution[143–145]. It can also be used to follow kinetics or interactions in solution[146]. Size-exclusion chromatography coupled with SAXS (SEC-SAXS)[147] can be used alongside normal SAXS measurements for various reasons, including to improve sample quality and to study samples which might be unstable or aggregate quickly. The use of the SEC to directly measure samples into the beamline ensures the sample is as fresh as it can be and has not had the chance to degrade or aggregate before analysis is carried out. A low flow rate is used during this process to maximise the amount of time the sample is exposed to the beam, to obtain as much information as possible. SAXS measurements (like any X-ray measurements) cannot be carried out over extended periods as the samples often suffer radiation damage after exposure to the X-ray beam, in turn rendering them no longer in a biologically relevant state[148]. However, the potential larger intensity from SAXS measurements gives rise to shorter measurement times (if using a synchrotron source) and greater detail to be obtained from the sample.

SANS is also an extremely useful tool to determine structural information about a sample in solution or follow interactions and kinetics in solution[128,137], and can also be used in combination with SAXS to maximise information obtained[149]. While using SANS is often a slower technique compared to SAXS (due to lower flux resulting in longer exposures), the main benefit of using neutrons comes from the ability to gain more contrasts with the use of deuteration (as discussed previously)[150]. Using several isotopic contrasts for the same sample gives more detailed information, which aids in

the data fitting procedure and provides more accurate and representative models. To determine which contrasts to use a matchout series can be performed which allows for the determination of the level of deuteration required to render a sample invisible[151]. Kinetics and interactions can also be followed by neutron scattering, provided the timescales are suitable[123,128]. If the timescale is too short, the neutrons will not be able to provide suitable information as long measurement times are required for good statistical data.

NR is a technique which allows investigation into samples on surfaces[152–154] or interactions with said samples[155,156]. The structural information obtained will only see what is adsorbed to the surface and not any presence of molecules in the bulk solution. Again, due to the use of neutrons as probe, deuteration can be beneficial in gaining various contrasts of the same sample aiding the restraining when fitting data. It is also possible to follow kinetics of interactions with NR as the changes at the surface can be followed with time[126,127,129]. If the timescale is suitably long NR can be a very good way to follow a process occurring in real time.

AIMS

The overall aim of this thesis is to understand the specific role that the apolipoprotein ApoE plays on lipid exchange events at the onset of atherosclerosis. To be able to understand such phenomena, several methodological requirements were necessary, resulting in several specific aims, including: the advancement of model membrane systems to increase their similarity to real membranes and their complexity; deuteration of membrane components; and advancement in the reconstitution of artificial lipoproteins with controlled composition. Previously, most exchange work was done for lipoproteins extracted from human blood which are very complex in terms of both protein and lipid content. Here, artificial rHDL was prepared from ApoE (alleles 3 and 4) in order to better understand their role in phospholipid and cholesterol exchange. Additionally, previous work investigated the effect of charge within the membrane on lipoprotein interactions. In this thesis, SLBs that include the second most important component in membranes, cholesterol, were used as model membranes to follow lipid exchange with lipoproteins.

The specific aims are:

1. To produce matchout cholesterol for advanced biomolecular complex studies using NR and SANS (Paper 1).

2. To form model membranes comprising cholesterol and determine its co-localisation within the membranes by NR. Here deuterated and non-deuterated cholesterol as well as natural and synthetic lipids are used to determine localisation of cholesterol in model membranes (Paper 1 and Paper 2).

3. To determine lipid exchange for human lipoproteins and model membranes in the presence and absence of cholesterol and using lipids with differing saturation levels using NR (Paper 3).

4. To determine ApoE interactions with model membranes of differing saturation levels using NR (Paper 4).

5. To form artificial lipoproteins made of ApoE, and to structurally characterise them by SANS (Paper 4).

6. To determine lipid exchange for artificial ApoE based lipoproteins and model membranes in the presence and absence of cholesterol using NR (Paper 4)

MATERIALS AND METHODS

Bio-deuteration

Deuteration plays an important role throughout this project. The use of bio-deuteration is a key tool and used here to fine tune the level of deuteration required in the final samples. While protein deuteration is possible, only non-deuterated protein was used throughout. Instead, various lipids including cholesterol were produced in a deuterated environment. Lipo-engineered *E. coli* and *Pichia pastoris* (a yeast strain) were used to produce PC lipids[140] and cholesterol[157] respectively. Deuteration is toxic to cells[158]; however, when introduced gradually to a strain it can adapt and produce the required samples much in the same way as if in a non-deuterated environment. The benefit of using this method allows the level of deuteration to be chosen precisely for the needs of the experiments.

Sample Preparation

Protein Production

There are various methods that can be used to purify proteins; these largely depend on whether the protein construct used includes a tag to aid purification. Whilst it is possible to purify proteins with no tag, the presence of a tag can reduce the number of steps required in the purification process. One of the most common tags used for protein purification is the inclusion of a histidine tag (His-tag: 6 or occasionally 10 successive histidine amino acids included at one end of the protein sequence), enabling a short one or two step purification process. The main goal behind using this tag is to separate proteins with a tag from those without, using affinity chromatography. A Nickel-NTA column is used for this process, whereby the protein with the His-tag will attach to the column, whereas the unwanted proteins go straight through and are removed from the sample. The protein can then be released from the column and is often quite pure, a further size-exclusion chromatography step can be carried out to increase the purity of the sample.

Whilst His-tags were included in the constructs used throughout this project, and indeed were used as a purification method to begin with, other tags can be used in the purification process such as a thioredoxin tag as used here. Thioredoxin is a small protein which can be added to the sequence for the protein of interest, resulting in what is known as a fusion protein, aiding the solubility and purification of said protein.

The His-tag present in the construct is situated between the ApoE protein and the thioredoxin tag making it difficult to purify via this method. Due to the lipid-binding nature of ApoE, a purification method using ultra-centrifugation (UC) is possible. The protein is incubated with lipids to protect the hinge-region during the cleaving process required to remove the thioredoxin tag. After the cleaving step, ApoE remains lipid bound whereas the thioredoxin is not. Using a density gradient obtained via UC, a separation of lipid-bound protein from other unwanted cellular proteins, including the thioredoxin, is possible.

rHDL Preparation

rHDL preparation can be carried out via different methods. The most common is with the use of cholate which helps solubilise the protein and lipids and is then later removed via Bio-Beads™ or dialysis. Another method is forming the discs via self-assembly, where protein and lipids are incubated together and left to form discs over time. There are benefits to both methods: the first allows for different lipid types to be used and obtain the same final result; the second does not require the use of detergents therefore reducing the risk of unfolding the protein and deactivating it. Different ratios of protein to lipid can also be used, sometimes resulting in different sized nanodiscs.

Here, different methods were tested including the use of cholate and removal via Bio-Beads™ or dialysis, and self-assembly. However, as only 1,2-dimyristoyl-sn-glycero-3-phosphocholine (DMPC) lipids were used in the rHDL, self-assembly was found to be the most suitable method. To obtain the final rHDL samples, protein-lipid mixtures were incubated at 24 °C for at least 12 hours, and purified via size-exclusion chromatography to separate them from any potentially remaining lipid-free protein or excess lipids.

Small-Angle Scattering

The principles of small-angle scattering (SAS) with both X-rays and neutrons are very similar, apart from the main key difference of what the incoming source of X-rays (SAXS) or neutrons (SANS) interacts with; however, for the purposes of elastic neutron scattering studies, the same principles apply to both.

The incoming beam of X-rays or neutrons interacts with the sample and is scattered. The scattered intensity is measured as a function of momentum transfer, q, and defined as thus:

$$|q| = |k_f - k_i| = \frac{4\pi sin\theta}{\lambda}$$

Equation 1

where θ is shown in Figure 5 and λ is the wavelength of the incoming source of X-rays or neutrons.

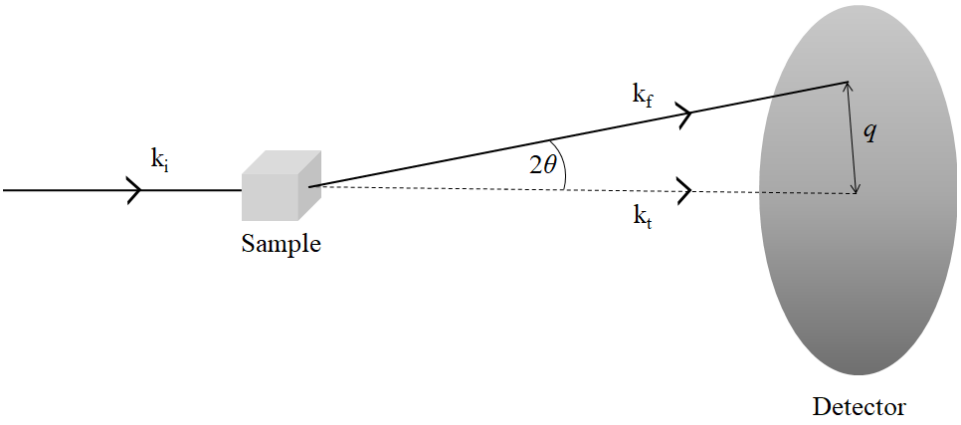

Figure 5. Schematic of small-angle scattering principle. Where k_i, k_f and k_t are the incident, scattered and transmitted scattering vectors and q is the momentum transfer.

Scattered intensity is measured as a function of q and gives an average of scattering from the sample as is defined as follows:

$$I(q) = \frac{N}{V} {V_p}^2 (\rho - \rho_{solv})^2 |F(q)|^2$$

Equation 2

where N refers to the number of molecules in solution, V is the total sample volume, V_p is the molecular volume, (ρ-ρ_{solv}) is the scattering contrast defined as the scattering length density of the sample minus that of the solvent, and $|F(q)|$ is the sample form factor giving information about the sample shape in solution. The detector image gives the structure of the sample in reciprocal space and after Fourier transform treatment is converted to real space for size and structure determination.

Data Analysis

For both SAXS and SANS similar models can be used and co-refined together; however, it is important not to over-fit the data or try to obtain information that is not available, with the use of co-refinement. As X-ray data is generally recorded to higher resolution, further information can be obtained from these data sets. Therefore it is important not to force the fitting to be simultaneous for both if the SANS data do not give that level of information.

Three contrasts for the SANS data are measured for this very reason: to help alleviate the uncertainty in the measurements. Data are fitted based on models which translate raw data into structures. Measurements for the empty cell and buffer backgrounds are subtracted from sample data; and different detector distances (from the sample) are also used to ensure the whole q-range of interest is covered when measuring. As the scattering from the sample is related to the size of the molecule being studied, shorter detector distances are required for longer length scales and vice versa.

Multiple contrasts are often measured with SANS providing further information about a sample, adding a constraint to the fitting process thereby obtaining more accurate fitting parameters. The use of 0%, 42% and 100% D_2O based buffer solutions provides further constraints and multiple contrasts for the components, particularly important for protein-lipid complexes. The 100% D_2O buffer provides the greatest contrast between the non-deuterated sample overall and the buffer environment providing the most information. The 42% D_2O buffer is the level at which proteins give no net coherent scattering, which is useful when studying protein-lipid complexes: even though the contrast is not the largest between the lipids and the buffer, as there is no signal coming from the protein, all the information that can be obtained from this data set is related to the lipid signal. The 0% D_2O buffer contrast gives an overall view of the complex but with less contrast, the lipids will also have very low

scattering signal in H_2O as they matchout at around 10% D_2O. Therefore, more information can be obtained about the protein itself at this contrast: 10% D_2O buffer could be used in its place here if it is preferable to have zero scattering from the lipids.

To determine the level of deuteration required in the buffer solution to result in no net scattering from a sample, a contrast-match series can be carried out. This series involves a succession of samples to be measured in varying ratios of H_2O:D_2O buffer to determine the point at which no scattering is seen. The graph obtained gives the level of deuteration required to matchout the sample when the intensity is zero. This can be done with a singular component or a combination of two components where one value is already known leaving only one unknown[159]. It is important to note however, that the distribution of components across the sample must be uniform to obtain a reliable and informative value. If a sample is not uniform this can lead to difficulties in obtaining a suitable series, as an average will be taken across the sample. Different detector distances (from the sample) are also used to ensure the whole *q*-range of interest is covered when measuring. As the scattering from the sample is related to the size, shorter detector distances are required for longer length scales and vice versa.

Neutron Reflectometry

Scattering with neutron reflectometry is, in principle, similar to small-angle scattering in that it is the intensity as a function of momentum transfer that is measured. Instead of the beam of neutrons travelling directly to the sample, they are introduced at an angle to the surface and reflected according to the scattering length density of each layer. In specular reflection, the angle of incidence is the same as the angle of reflection giving rise to a scattering length density (SLD) profile of the sample, perpendicular to the surface.

Theory

Specular reflection describes the reflectivity signal of a flat smooth surface (interfacial roughness of the sample gives rise to off-specular reflection detailing composition in the lateral direction). The scattering principle is similar to small-angle scattering; the incident angle θ, of wave vector k_i is equal to the reflected angle of wave vector k_r (Figure 6). The incident and reflected wave vectors are equal and defined by:

$$k_i = k_r = \frac{2\pi}{\lambda}$$

Equation 3

The ratio of incident to reflected intensities gives information about the change in k when reflected at the surface and is defined as the momentum transfer denoted by *Q*:

$$Q = k_r - k_i = 2k_i = \frac{4\pi sin\theta}{\lambda}$$

Equation 4

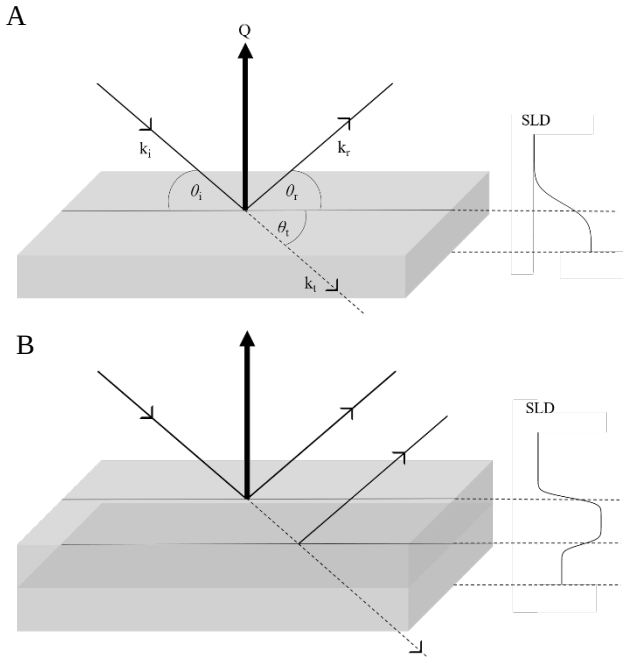

Figure 6. Reflectometry scattering principle and accompanying SLD profiles. Reflection and refraction occur depending on the structure of the interface, hereby described by SLD profiles. A. Neutron beam reflecting from surface with incoming, reflected and transmitted wave vectors k_i, k_r and k_t with corresponding angles θ_i, θ_r and θ_t and scattering vector *Q*. B. Neutron scattering from thin layer. The SLD profiles vary according to the changes in SLD across the layers.

Time-of-flight (TOF) reflectometry is used to capture a whole *q*-range in one snapshot, providing better resolution. If it is necessary to use only one wavelength of neutrons, a large proportion of neutrons are not used giving lower flux. As neutrons are produced using either a nuclear reactor (as at the Institut Laue-Langevin, ILL) or a spallation source (as at ISIS neutron source), the incoming beam needs to be regulated to produce a pulse to tune the *q*-range. At ISIS the pulsed nature of the source already provides conditions for the TOF technique; however at the ILL the TOF approach is possible via the use of choppers which allow only a small range of neutrons through to form the beam. The settings of the choppers can be modified to obtain the wavelength of neutrons desired. On FIGARO at the ILL (Figure 7), where most data in this thesis was collected, the wavelength range of neutrons was from 2-20 Å in turn giving a measurable *q*-range of 0.004-4 $Å^{-1}$. To capture the full *q*-range desired two incident angles were used: 0.8° and 2.3°.

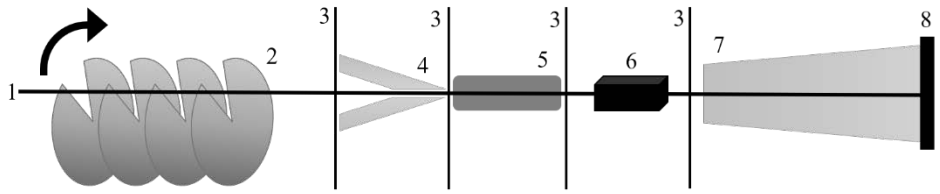

Figure 7. FIGARO instrument setup. (1) The neutron beam entering (2) four choppers which rotate to refine the wavelength of neutrons allowed through; (3) hitting various slits which further refine the beam. (4) Guiding mirrors and a (5) collimator direct the beam before hitting the (6) sample and a (8) detector under (7) vacuum.

Data Analysis

The data obtained are presented as reflectivity as a function of *q* where the reflectivity is defined as relative intensity I/I_0: I corresponding to reflected intensity and I_0 to the incident signal. As an SLD profile is not directly obtained from scattering data, models are used to fit the data to the profile. These models represent each layer within a sample. For each SLD change it is possible to distinguish the thickness, solvent percentage (in relation to coverage of sample) and roughness of each layer. Multiple contrasts are often used for reflectivity measurements; this gives more information on the same sample and allows constraints to be put in place to derive more accurate models. Three contrasts are used in this work: 0%, 38% and 100% D_2O-based buffers. The 0% and

100% D_2O buffers give maximum contrasts for deuterated and non-deuterated samples respectively, whereas the 38% D_2O contrast gives an SLD value which matches the small oxide layer present on the silicon blocks, often denoted cmSi (contrast-matched Silicon). For the 100% D_2O buffer, a critical edge is seen in this *q*-range. This is due to the refractive index of the D_2O being higher than the Si block and therefore gives total external reflection resulting in a reflectivity signal of 1. When the contrast is of lower refractive index, the neutrons are refracted giving a reflectivity signal of less than 1.

For each sample measured an initial characterisation of the silicon block is carried out before any sample deposition occurs, enabling the fitting of this layer which then can be fixed for the remaining steps during an experiment. For the samples themselves, each model is derived by the addition of layers corresponding to each SLD change which are simultaneously fitted with all three buffer contrasts. Various models are tried for each sample, the final chosen model is the one that best fits the data and makes most physical sense.

To ensure the model makes physical sense for the lipid samples seen here, the area of the headgroup should roughly equal the area of the lipid tail region, for each lipid. This can be calculated using the solvent penetration value with respect to each layer as there should be equal numbers of heads to tails and as the bilayer is flat, each component must take up equal space and can be defined as such:

$$A = \frac{V}{d\phi}$$

Equation 5.1

$$\frac{V_{head}}{d_{head}\phi_{head}} = \frac{2V_{tail}}{d_{tail}\phi_{tail}}$$

Equation 5.2

where V is the volume of the head or tail regions, d is the thickness and ϕ is the volume fraction. Two tails are present per headgroup, hence the requirement for doubling the tail volume.

To add further complexity to the bilayer model, asymmetry can be applied in a multi component system if enough contrast is seen between components. To determine the respective volume fractions of the components, the known SLD values are necessary to be able to determine the positioning of one component in favour of another (causing said asymmetry). If the layer is comprised of solvent and two further

components, e.g. varying lipids with differing enough SLD values, the following equation can be used with the overall SLD value obtained from the model:

$$SLD_{layer} = SLD_{l1}\phi_{l1} + SLD_{l2}\phi_{l2} + SLD_{solv}\phi_{solv}$$

Equation 6

where $\phi_{l1} + \phi_{l2} + \phi_{solv} = 1$.

Bilayer characterisation

As mentioned briefly, all silicon surfaces are characterised prior to introducing samples onto them, both in D_2O and H_2O buffers, to be able to fit the SiO_2 layer. Once the surfaces are verified to be clean and ready for use, the lipid vesicles are injected onto them. Supported lipid bilayers (SLBs) are characterised in three contrasts to gain optimum information when fitting (0%, 38% and 100% D_2O based buffers). To start with a basic three-layer model was chosen to fit the SLBs to represent the inner headgroup, tail and outer headgroup regions, assuming a symmetrical bilayer. During the fitting process various other models were tested including four- or five-layer symmetrical or asymmetrical options. Between the SiO_2 layer and the SLB sometimes a small solvent layer is also required. The final model is selected on the basis of the best fit (the χ^2 value), in combination with what makes sense from a physical point of view. When a suitable model is found, this is then generally used as a guide for other SLB fittings.

Exchange experiments

Three different types of exchange experiments were carried out with various SLB conformations: native lipoproteins (HDL and LDL); ApoE protein alone; and ApoE-based rHDL. During the exchange process the first hour of kinetics was measured then every other hour subsequent, *i.e.* the first, third, fifth and sometimes seventh hours were measured depending on the overall incubation times. Samples were incubated with the SLBs for either 6 or 8 hours in total before rinsing with buffer. During the incubation process, measurements were carried out in H_2O buffer to give the most contrast, as the SLBs used were deuterated to some extent (either tail-only deuterated or fully deuterated). A full characterisation in the three contrasts was then carried out again at the end and the same fitting process was performed. An additional rinse with H_2O was performed to confirm that no further changes in reflectivity occurred after rinsing with excess buffer. To simplify the fitting as much as possible, the starting points of the fitting parameters were the initial bilayer values, allowing only the least

number of parameters to change, for example, the SLD and the solvent penetration of the tail region. For some experiments, this was sufficient to get a good enough fit after the exchange, however some bilayers changed more drastically than others and so further structural changes were required to reach a suitable fit. After the incubation, in each case at least one further layer was required on top of the bilayer to represent the lipoprotein/protein/rHDL attached to the surface that stayed after washing. The quantities of lipids exchanged and removed in each of these experiments could be determined from the changes in SLD and solvent coverage respectively, following Equation 6.

RESULTS AND DISCUSSION

Bio-deuteration for Advancing Model Membranes

Cholesterol

As discussed previously, cholesterol is a highly important component in cellular membranes and plays an important role in the development of atherosclerosis. In order to use neutron scattering to probe membrane structures and lipid exchange, deuterated cholesterol, and in particular, matchout-deuterated cholesterol, was ideal.

At the beginning of this project, perdeuterated cholesterol was produced using already established protocols[139]. The production of matchout cholesterol required further advances in methods and modification of these protocols. As cholesterol plays a such a large role in membranes and throughout the body, the need for matchout-deuterated cholesterol for use in neutron scattering experiments for biological applications (SANS in particular) is very high. It was in the original plan to measure liposomes with the matchout-cholesterol incorporated against matchout-lipoproteins, however difficulties arose owing to the stability of these liposomes in solution leading to sedimentation during the course of the SANS experiment. This in turn led to a change in scattering signal arising from a combination of lipid exchange (the phenomenon of interest) and loss of sample (through sedimentation) and an impossible task to determine which effect gave which result. Therefore, the studies with lipoproteins presented here focus on interactions with membranes using NR.

To determine the appropriate modifications required, the synthesis pathway of cholesterol was looked into and the quantity of hydrogen required to give an overall SLD value that would fit the matchout requirements was determined (roughly 6H in a total of 46H). The deuteration of cholesterol was carried out via the use of a lipo-engineered *P. pastoris* strain[157] with non-deuterated glycerol as a carbon source. As such a small proportion of hydrogen atoms were required to remain as protium and not be replaced by deuterium the simplest way to carry this out was via the change in carbon source. Another carbon source that is often used is glucose, though more expensive than glycerol. If glucose had been used instead, it is most likely the same end product would have been obtained due to the similar synthesis of glucose in the biosynthetic pathway. The initial steps would be different; however, they reach the same precursor molecule

relatively early on in the synthesis. Thus, there is little room for differences to occur. Another option would be to change the level of deuteration in the medium. In this instance, 100% deuterated medium was used to grow the yeast in. A lower percentage of D_2O based medium could have been used; however, in this case at every step there would be an increased chance of a protium being up taken by the molecule rather than a deuterium. Possibly more so than just the 1 in 10 chance if a 90% D_2O medium was used, as hydrogen bonding with a bridging H is more energetically favourable than having a bridging D[160]. Therefore, H could potentially be preferentially taken from the medium. Another benefit of using a non-deuterated carbon source over a lesser deuterated medium is the cost: it is cheaper to use non-deuterated glycerol instead of 10% less D_2O medium. The benefit of using bio-systems to deuterate a molecule is usually the increased control that can be obtained during the synthesis process, for example with the production of matchout-deuterated PC[140]. However, due to the nature of this synthetic pathway (as compared with that of PC), the numerous steps lead to many uncertainties and apart from the hydrogen atoms the carbon source starts with, all remaining hydrogen atoms come from the medium so each step is a game of statistics and probability.

An alternative route to deuterate cholesterol is through chemical deuteration[161]. However, this is a complicated process and not an easy route to go down to obtain fully deuterated systems. Partial deuteration is possible this way, but to get to the level of deuteration required for matchout conditions, this is an unsuitable method to follow. That being so, if it were possible to deuterate chemically, there may be more specific reactions targeting certain areas of the cholesterol molecule that could be tuned towards deuteration. For the time being, however, chemical synthesis is not a viable option for the matchout-deuteration of cholesterol and would lead to a racemic mixture of products, rather than a naturally obtained singularly chiral end product.

In Paper 1, SANS was used to determine the match-point of cholesterol. To determine this (the level of D_2O required in the buffer to result in a matched-out sample), the cholesterol was required to be incorporated into vesicles of another lipid to obtain good scattering data. Cholesterol has a very low solubility limit in water and forms micelles at roughly 25- 40 nM at 25 °C[162]. The micelles are very small and only scatter weakly, hence multi-component vesicles were used. The lipids chosen were POPC, as cholesterol had already been shown to be soluble at quite high concentrations in these vesicles, and the same protocol was followed as for the tail-deuterated POPC vesicles alone[151]. Measuring series for both POPC alone and POPC with cholesterol at different H_2O/D_2O ratios enabled the matchpoint to be determined as 101%. This value

obtained by SANS also corroborated the NMR and MS data for the level of deuteration of the cholesterol at 89% (see Figures 1-3 in Paper 1).

Membrane Structure with Cholesterol

The outcome of using a non-deuterated carbon source with a cholesterol-producing lipo-engineered yeast strain for matchout-deuterated cholesterol production was successful and enabled it to be used in NR and SANS studies (Paper 1). As with the perdeuterated cholesterol[139], NR was also used to characterise SLBs with cholesterol incorporated and determine the position of the cholesterol within the bilayer.

The localisation of cholesterol in model membranes is highly important, especially for the later studies, which will follow lipid exchange processes. Therefore, both deuterated and non-deuterated cholesterol were used to locate the molecule and to cross-check that the deuteration does not itself affect the positioning and is therefore a suitable tool to use in future studies. The membranes were prepared using vesicle fusion to form SLBs for use in NR studies. The membranes were chosen for variation of tail length and level of saturation and included both naturally and synthetically derived lipids. To obtain good scattering contrast, we used matchout-deuterated cholesterol within non-deuterated membranes (Paper 1) and both non-deuterated and deuterated cholesterol within deuterated membranes (Paper 2) to ensure the variations in cholesterol deuteration did not affect its localisation in the membrane.

We prepared model membranes of synthetic (Paper 1) and naturally derived (Paper 2) PC lipids to determine the localisation of the cholesterol. The use of different lipid species ensured the localisation of cholesterol was determined over a range of membranes with different tail lengths and at varying cholesterol concentration. Initially single layer models for the tail region were tested, however they failed to give suitable fits for the data, implying the cholesterol was not symmetrically situated throughout the bilayer. Other models of increasing complexity were also tested; however these still did not give suitable and acceptable fits for the data. In the end, a five-layer model for the bilayer was determined, including an inner headgroup, a tail region and an outer headgroup where the tail region itself was split into a further three layers (Figure 8). All models also included a SiO_2 layer and most included a small solvent layer between the SiO_2 and in the inner headgroup, commonly seen in SLBs for NR[163].

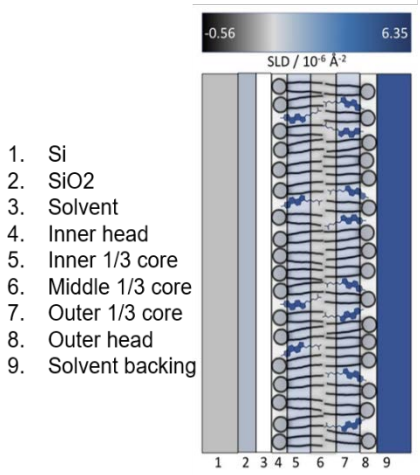

Figure 8. Model determined for cholesterol localisation. (Figure 4A in Paper 1).

The use of both synthetic and naturally derived lipids was important to ensure the same model could be used across all model membranes, and that the cholesterol behaved the same way when non-deuterated and deuterated. In all cases cholesterol was found to thicken the bilayer, which was expected due to the induction of the liquid ordered phase, or combination of liquid ordered and liquid disordered[164]. For the naturally derived lipids, with increasing levels of cholesterol came an increasingly thickened core. For the synthetic lipids an increase in core thickness was also seen when compared to the same bilayers without cholesterol. It is important to note however, that while values in Paper 2 imply a linear increase is seen with increasing cholesterol quantities, it can be seen from the values in Paper 1 that a plateau is reached and the bilayer does not thicken much further (see Table 2 below). The cholesterol was situated in the outer two sections of the overall tail region closer to the headgroups. This was determined via the differences in SLD seen throughout these three layers.

Table 2. Comparison of cholesterol inducing increase in core thicknesses from cholesterol-containing SLBs in Papers 1 and 2. *Values taken from literature for comparison. (DLPC: 1,2-dilauroyl-sn-glycero-3-phosphocholine)

Paper	SLB	0% chol	10% chol	20% chol	40% chol
Paper 1	DLPC mo	21.8*[165]	28.2*[166]	-	30.3
	POPC mo	30*[121]	-	-	31.5
	DMPC mo	25.8*[165]	34.1*[166]	-	29.7
Paper 2	dPC hchol	29.5	30.9	32.8	-
	dPC dchol	29.5	30.8	33.5	-

Cholesterol positioning in the naturally derived membranes was not found to be symmetrical with increasing concentration, *i.e.* greater levels of cholesterol were seen in the outer-most section of the core compared to that closest to the inner headgroups. On the other hand, symmetric distribution was found for the SLB with a lower percentage of cholesterol (Table 2 and Figure 4 in Paper 2). This is likely due to an asymmetry within the vesicles prior to vesicle fusion due to cholesterol's affinity for higher curvature found within the inner-leaflet of the vesicles[167,168]. It is also important to note that where deuterated and non-deuterated cholesterol was used, very little difference was seen in the structure and thickness of the layers implying no effects were seen on the phospholipid-cholesterol interactions, verifying the suitability of using deuterated cholesterol and the absence of significant isotope effects.

The synthetic lipids were of varying length and level of saturation and showed the same positioning of cholesterol throughout the SLBs regardless of lipid species. The cholesterol was also found to be located towards the headgroups in all bilayers and not localised towards the centre of the core as previously suggested[165]. Marquardt *et al.* (2016)[165] had proposed a model whereby cholesterol remained horizontal within the bilayer and not towards the head-tail interface, if the core thickness was below 30 Å. This was not found to be the case for any of the bilayers in Paper 1 as all of them showed the location of the cholesterol in the upright position towards the head-tail interface; however within errors all the SLBs were 30 Å or more after the addition of cholesterol. The importance of the model fitting all bilayer types verifies the relevance of the use of model membranes and synthetic lipids, in particular, as the cholesterol behaves in the same way across the board.

The concentration of cholesterol in cells in the periphery is roughly 20 mol% in endothelial cells[169] compared to 40 mol% in neural cells in the brain[170,171]. Whilst the concentration of cholesterol varies throughout the body in differing cell types, the results here show that regardless of that, the cholesterol localises in a similar way. The asymmetry of the cholesterol from inner to outer leaflets seen here may not mirror live cells since it likely arises as a consequence of the method of SLB formation. However, structurally it can be said the cholesterol thickens a membrane and is located towards the head-tail interface, irrespective of the lipid species it is surrounded by, in said membrane.

The quantities of cholesterol in the bilayers in Paper 2 were nominally given as 10 and 20 mol%. From the analysis of the data these values were 9% and 15% respectively, for the non-deuterated cholesterol in the deuterated PC bilayer. This shows that while in later experiments there is little contrast between cholesterol and phospholipid

in the SLBs, and therefore as the concentration of cholesterol may be difficult to determine, it can be assumed to be the nominal composition within error.

Native/Artificial Lipoproteins and Model Membranes

Native Lipoproteins with Membranes

The use of native lipoproteins for interaction studies with model membranes via NR has been shown to be a suitable method as reported previously[126,127]. During these studies HDL was shown to remove more lipids than LDL and the presence of charged lipids within the membrane also increased the ability of HDL to remove lipids.

During the studies presented here the effect of the level of saturation and the presence of cholesterol in the membrane was investigated (Paper 3). Two types of lipoproteins were used: HDL and LDL, purified from plasma from 3 healthy males and pooled together. No clinical background information exists for these samples.

The level of saturation in the bilayer made a huge difference in the level of interaction of the lipoproteins with the SLBs (Figure 9). The presence of unsaturation dramatically decreased the quantities of lipids exchanged and removed by the lipoproteins, regardless of lipoprotein type. In this way, HDL and LDL have a greater affinity for saturated rather than unsaturated lipids, though LDL to a lesser extent. The absolute values of the quantities of saturated lipids both exchanged and removed was greater for HDL than LDL, as seen before[126]. The difference in ease of lipid removal between the lipoprotein types could be explained by variance in the specific protein-lipid interactions. Different conformations of ApoA1 (the main protein in HDL) were shown to have varying binding affinities to POPC vesicles[172]. The increased ease for saturated lipid removal is likely due to the increased mobility of said lipids. Saturated phospholipids were shown to have greater mobility than their unsaturated counterparts in both gel and fluid phases[173].

The presence of cholesterol in the SLBs also had a large impact on the quantities of lipids exchanged and removed (Figure 9). In the bilayers comprising saturated lipids, the presence of cholesterol decreased the amount of lipids exchanged and removed with HDL, whereas for the unsaturated lipids, the presence of cholesterol made little difference when interacting with HDL. LDL, on the other hand, did not follow the same pattern. Including 10 mol% cholesterol in the saturated bilayer increased the amount of lipids exchanged. Upon further increasing to 20 mol% a similar value was found to that of the saturated bilayer alone. For the unsaturated SLBs, the presence of 20 mol% cholesterol also gave similar values to that of the bilayer alone. However, in

terms of removal, for both the saturated and unsaturated bilayers, the presence of cholesterol increasingly reduced the quantity of lipids removed. It is possible that the presence of cholesterol may inhibit the mobility of phospholipids[174], and cause it to localise preferentially towards saturated lipids[175]. However, there were no clear systematic changes when cholesterol was incorporated into the bilayer so it is difficult to pinpoint the exact cause of the changes seen. LDL has also been shown to preferentially bind to rafts of saturated lipid with cholesterol[176]. Since no reduction or increase in exchange was seen due to cholesterol, it is likely the specific lipoprotein-lipid interactions determine the final quantities of lipids exchanged and removed.

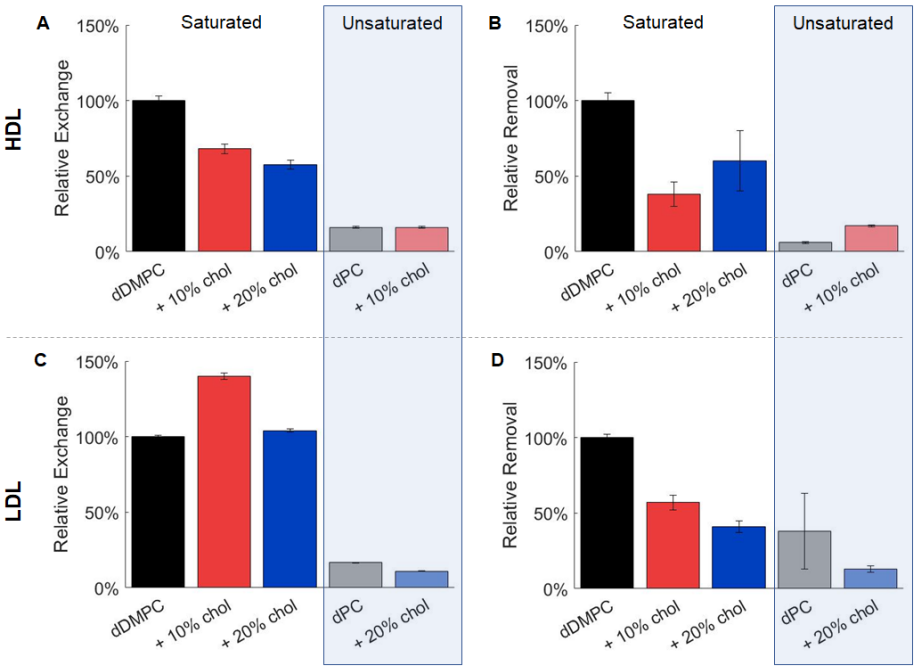

Figure 9. Relative lipid exchange and removal for HDL or LDL particles interacting with membranes formed with saturated (dDMPC) and unsaturated (dPC) phospholipids with and without cholesterol. Results are shown for HDL (A, B) and LDL (C, D) regarding exchange (A, C) and removal (B, D). (Figure 2 from Paper 3)

As already discussed, some of the differences seen are likely due to specific interactions between the lipoprotein particles and the SLBs. To further look into this, differences were compared between levels of interactions of LDL with differing compositions. It was found that with increasing density of LDL, *i.e.* increasing percentage of protein, greater levels of exchange were observed (Figure 3 in Paper 3). These findings can be explained by the difference in ApoB100 (the main protein in LDL) found on smaller more dense LDL particles. Denser LDL particles contain regions with altered epitopes[177] that may house part of the lipid-binding region of LDL[178] and thus affect their binding and interactive activities.

The effect of the presence of deuteration in the lipid headgroups was also investigated. Little difference was seen in terms of the quantity of lipids removed. However, with increasing levels of deuteration in the headgroups, increased amounts of lipids exchanged were observed (Figure 4 in Paper 3). This difference is again likely due to specific protein-lipid interactions, influenced by the presence of deuterium[160,179], which therefore could impact the outcome of these types of exchange studies; however this was most notable only when the headgroups were *per*deuterated. Tail deuteration should not affect this to such an extent, as the lipoproteins do not interact with the tail groups specifically upon initial interaction.

Structure of rHDL

Reconstituted HDL-like particles are commonly used to represent native discoidal HDL as they are structurally similar and behave in comparable ways – namely in their lipid exchange capacity. To structurally characterise rHDL, SAXS and SANS are commonly used tools[180]. Various models have been proposed for these protein-lipid complexes including the picket-fence model[181] and the double superhelix[182], but the most common and widely used model is that of the double belt model[183].

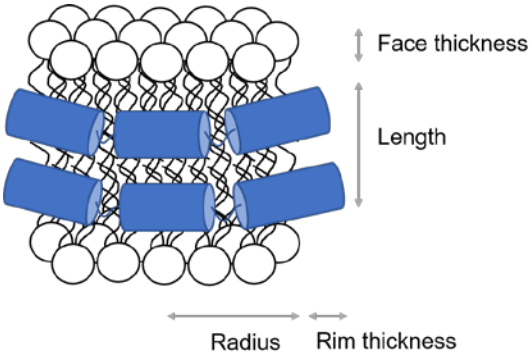

Figure 10. Model used to fit SAXS and SANS data for ApoE-rHDL. (Figure 3A in Paper 4).

This last model is the one used to fit the data presented here resulting in a protein rim encircling a bilayer of lipids as seen in Figure 10 (Figure 3A inset, Paper 4). The number of proteins present in ApoE-DMPC complexes has been discussed and has shown some variation but always resulting in 2 or more protein molecules per disc[46,184,185]. The conformation of the ApoE protein has also been proposed to vary according to the allele present[38]. It has been suggested that ApoE3 is capable of adopting an elongated belt conformation which extends around the perimeter of the disc and two separate molecules are stacked to form the double belt[184]. On the other hand, ApoE4 is proposed to form a looped-back arrangement due to decreased flexibility arising from the salt bridge, giving a more compact structure in which one molecule covers both leaflets of the bilayer[185,186]. The complete list of parameters determined from fitting the data are presented in Table 3.

Table 3. Parameters for ApoE3 and ApoE4 rHDL. *Fitted values. **Calculated values. ***Fixed value.

Parameters	**ApoE3 rHDL**	**ApoE4 rHDL**
Radius* Å	39.6	43.3
Ellipticity ratio*	1.8	1.5
Rim thickness* Å	9	9.8
Face thickness* Å	7.9	7.6
Length*** Å	28	28
Diameter** Å	97.2-160.6	106.2-149.5
Circumference** Å	417	407
No. amino acids**	278	272
Area per lipids** $Å^2$	55.9	55.9
No. lipids per leaflet**	159	158
No. proteins per disc**	2	2

The values for the differing proteins are very similar, giving the same number of proteins and lipids per disc and the same rim and face thicknesses. They differ slightly in radius and ellipticity ratio, though still only within a few Ångstroms. These values are in line with previously reported data for discs of similar composition[187]. The number of amino acids which are in contact with the bilayer is roughly 20 short of the full length protein which has 299, however this has also been seen before with similar proteins[180,188] and allows for some flexibility in the protein and potential expansion. The size is slightly larger than what has been seen for ApoA1 rHDL[183]. However, as the ApoE protein is significantly larger than ApoA1, it is a reasonable increase and is similar to previously reported data for proteins of similar length[187].

Protein and Artificial HDL with Membranes

As native lipoproteins are highly complex structures, to determine specific roles of components reconstituted lipoproteins can be used in their place. As with the native lipoproteins, both lipid-free protein and the reconstituted HDL particles were incubated with model membranes and the interaction and lipid exchange followed, again as a function of saturation and presence of cholesterol respectively. The main focus of the rHDL study was comparing ApoE3 with ApoE4; however it also included rHDL made with ApoA1 (the main protein in HDL).

The interaction of protein alone against both saturated and unsaturated model membranes resulted in differences seen across protein alleles and lipid species. However, an overall similar model was seen for all SLBs and both protein types (Paper 4): some lipids were removed, some protein incorporated into the tail region of the bilayers and some protein formed an extra layer on top of the SLBs. When comparing the saturation of the membranes, regardless of allele, ApoE had a preference to remove saturated lipids over unsaturated ones. This is similar to what was seen with the HDL and is again likely to be due to the increased mobility of saturated lipids compared to unsaturated ones[173]. However, again regardless of allele, more ApoE was found within the tail region of the unsaturated membranes than saturated ones (Figure 11). As for the alleles, more ApoE4 was found within the tail region of the SLBs than ApoE3, regardless of saturation level, whereas on the other hand, more ApoE3 was found on top of the SLBs than ApoE4, again regardless of lipid saturation (see Figures 2D and E, Paper 4). These differences are likely explained by differences in the modes of interaction of ApoE with the specific lipid species. ApoE4 is said to have a greater ability to bind lipids than ApoE3 due to slight structural differences[56,57]. ApoE4 is thought to have a more rigid structure and prefer less curved lipid surfaces such as

VLDL than ApoE3, whereas ApoE3 is more flexible and can interact with other proteins more easily as with on the surface of HDL[49]. Thus, ApoE3 probably prefers to interact with lipid headgroups and is found on top of the SLBs whereas ApoE4 is found within. Though it is important to bear in mind that the NR data cannot distinguish whether the ApoE3 proteins are separate molecules on top from those within. The increased flexibility of ApoE3 means it is likely that the same molecules can adapt different conformations, part of which resides within the tails and part on the heads, to a larger extent than the ApoE4 protein.

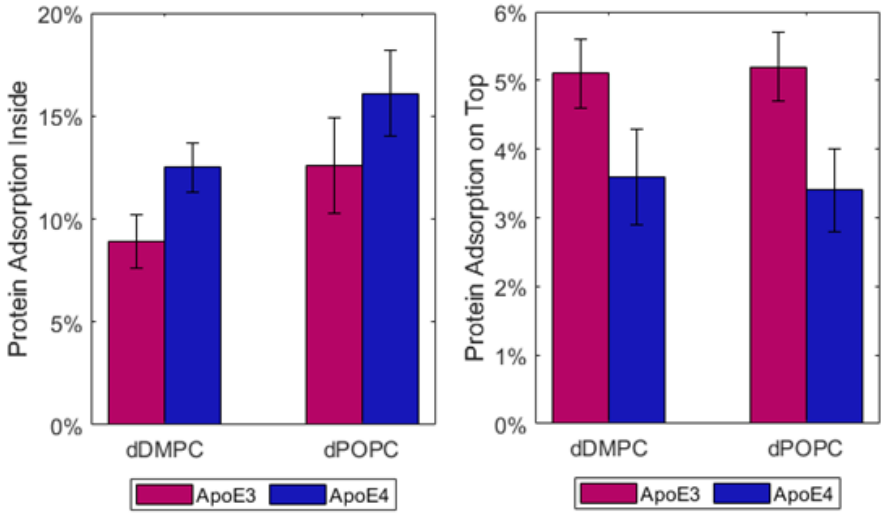

Figure 11. Percentages of protein adsorbed within the bilayer cores (left) and on top of the bilayers (right). (Figures 2D and E in Paper 4).

The lipid exchange studies showed mixed results comparing the two ApoE-rHDL with the native and ApoA1-based rHDL (Figure 12 and Paper 4). In terms of lipid removal, no distinct pattern was seen for the interaction of ApoE-rHDL with the SLBs in the presence and absence of cholesterol. ApoA1-rHDL, on the other hand, behaved in a much more similar way to native mature HDL by removing a noticeable quantity of lipids from the bilayer, though not quite to the same extent. Conversely ApoE-rHDL displayed a distinct ability to exchange lipids with the SLBs, in a manner similar to both the native and ApoA1-rHDL. The presence of cholesterol hindered the ability of the ApoE-rHDL to exchange lipids, as had been seen previously with the native HDL (Paper 3). While ApoE3-rHDL exchanged similar quantities of lipids to the native and

ApoA1-based counterparts, ApoE4-rHDL exchanged the highest values of all of them. The differences seen here are likely to be due to the different apolipoprotein-specific, including allele-specific[189,190], interactions with lipids. The differences seen between ApoE3 and ApoE4 could also be due to potential differences in protein arrangement in the rHDL leading to differing abilities to exchange lipids. ApoA1-rHDL show similar behaviour to the native plasma HDL, which is to be expected. ApoE, on the other hand, performs different roles to ApoA1 in the brain, where both alleles are found on ApoE-enriched HDL-like particles and help to maintain cholesterol homeostasis by moving lipids around the brain to maintain membrane plasticity rather than clearing cholesterol straight from the body as elsewhere in the periphery[191].

Following the journey of cholesterol was also possible during these experiments through the use of optimised deuteration and contrast. Both deuterated and non-deuterated cholesterol were used in SLBs to determine if cholesterol was selectively exchanged by the rHDL or not. As the lipids replacing those in the SLB would be non-deuterated, any uptake of cholesterol would cause a change in the SLD of the tail core. However, this was not the case showing cholesterol was not selectively taken, but only phospholipids exchanged. This work highlights the differences between ApoE and ApoA1 as mirrored in their differing roles in the body[192], and confirms the relevance of our model systems to understand functional processes in the body and then further find ways to regulate interactions for finding cures to diseases such as atherosclerosis or Alzheimer's disease.

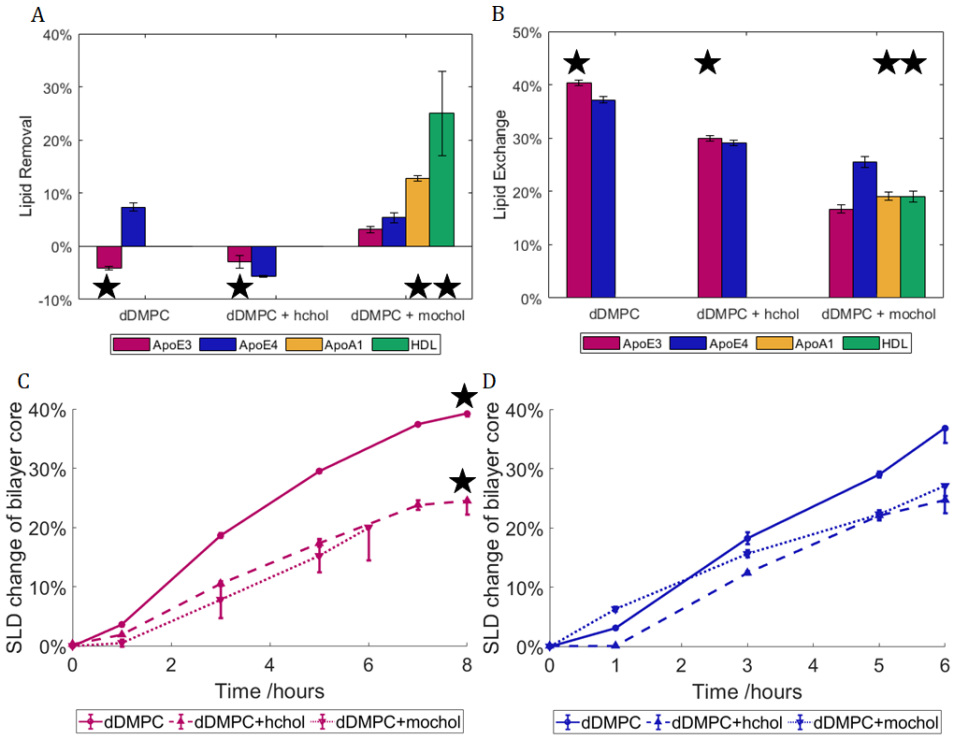

Figure 12. Lipid A. removal and B. exchange by ApoE-rHDL. SLD change in bilayer core for DMPC and DMPC-cholesterol SLBs against C. ApoE3-rHDL and D. ApoE4-rHDL. The stars represent incubation periods of 8 hours compared to 6 hours of those without.

CONCLUSIONS

This thesis describes the characterisation of model membranes and their interactions with lipoproteins. It also includes the production of tailor-deuterated cholesterol and reconstituted lipoproteins used throughout the experiments. The initial characterisation of the model membranes was important to ensure a greater understanding of the systems that would be used throughout the rest of the work. Results from Papers 1 and 2 shed light on the structure of cholesterol-containing membranes highlighting not only the importance of the use of deuterated cholesterol in these studies but also verifying their suitability, as few differences between deuterated and non-deuterated were seen. The NR technique used for the study of the cholesterol-containing membranes showed its applicability to the study of model membranes. While it is not a new technique to be used to structurally characterise membranes, it proved to be a powerful tool in combination with the use of deuterated lipids to obtain satisfactory detail about the model systems in question.

Model membranes have often been used to follow interactions as biomimetics. Papers 3 and 4 exploit this powerful technique with the use of NR and SANS. Paper 3 explores the interactions of native lipoproteins with model membranes investigating the important roles that the composition of the membrane can play; more specifically the presence of saturation vs. unsaturation and presence and absence of cholesterol. The class of lipoprotein as well as the more specific composition can impact the interaction seen with model membranes, as displayed by the HDL and LDL. This was further discovered in Paper 4 where only small changes were made in the composition – the change of a protein allele differing in only one amino acid – and still differences were seen, as reflected in the diseases associated with these proteins.

The findings here show the importance of understanding how the smallest change in lipoprotein composition can make a large difference and can aid the understanding behind fundamental processes that occur in the onset of certain diseases such as atherosclerosis. Development in treatment for these diseases will be aided in the understanding of the initial processes which occur.

FUTURE PERSPECTIVES

During this work there was a focus on the composition of the model membranes and the effect this would have on the systems investigated. However, following on from these experiments, various other questions could be asked to gain further understanding on these processes, including further systematic studies of lipoprotein composition.

In terms of the native lipoproteins, using sub-fractionated LDL to separate the large buoyant particles from the small dense ones would already give some information on the effect of composition. As we found within our studies the smaller denser particles exchanged more lipids, it would be interesting to carry out a more systematic approach to this method to ensure continuity and well-defined sub-classes.

This could also be linked to the use of native lipoproteins from people with underlying health conditions, specifically CVD related. Only samples from healthy males were used during these studies, however it would be interesting to see how or if the lipoprotein profile differed between these groups of people and how this might affect their lipid exchange capabilities. In turn this could be used to aid treatment development if the interactions of these lipoproteins differ dramatically and therefore a more suitable alternative could be determined.

Since our protein-lipid interactions showed that the alleles have different ways of interacting with lipids, it would be interesting to see if discs of different lipid compositions also have differing interactions with model membranes. Indeed, we have already acquired preliminary data on ApoA1 discs made with POPC and DMPC which behave differently in the same environment (Figure 13).

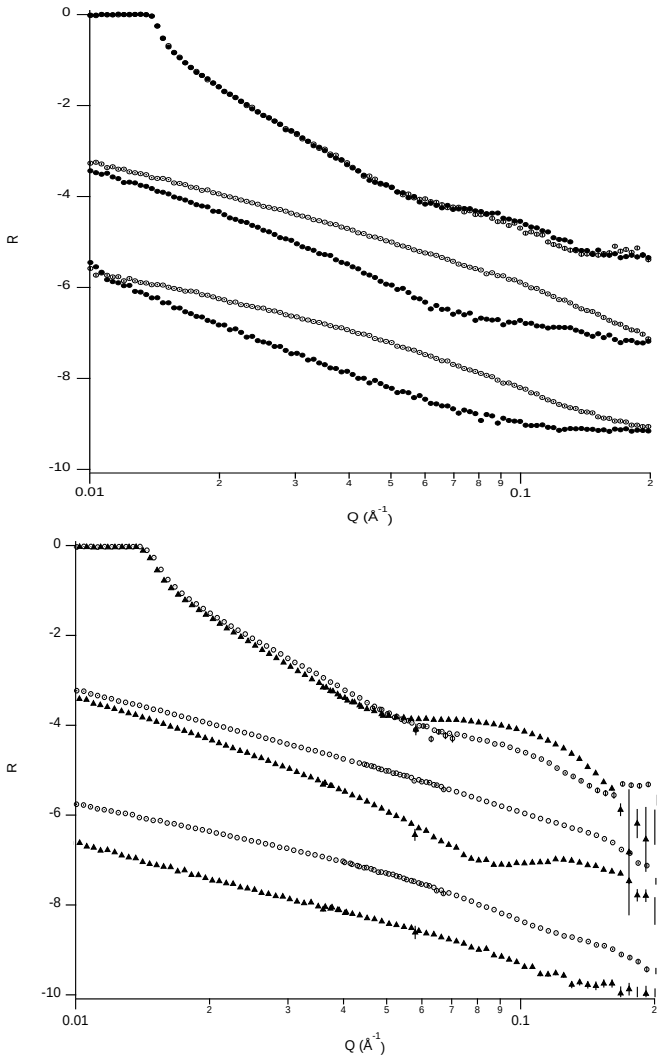

Figure 13. Preliminary NR data for ApoA1-rHDL made with POPC (top) or DMPC (bottom) against DMPC SLBs. Pristine bilayer before shown in hollow circles in both, whereas POPC rHDL are shown in full circles (top) and DMPC rHDL are shown in full triangles (bottom).

Another route that could be explored is that of the complexity itself of the rHDL composition. Different components can affect the properties of the model systems drastically, however if a combination of proteins was used it would be interesting to see if one protein would overshadow the properties of the other or if it would sit somewhere in the middle.

During experimentation, we also observed allele-dependent self-assembly of lipid-free proteins. ApoE3 was found to form large random aggregates, whereas ApoE4 formed more rigid structures (Figure 14). This work still needs to be completed and will then be published. Other work that was started and needs a little more to complete it, is the study of the way in which specific interactions between the apolipoproteins and lipids occur: of key interest is whether the protein binds before integration and removal or if it all happens at the same time. SANS studies have been carried out following the formation of the rHDL and demonstrated the gradual increase in scattering from the formation of the discs.

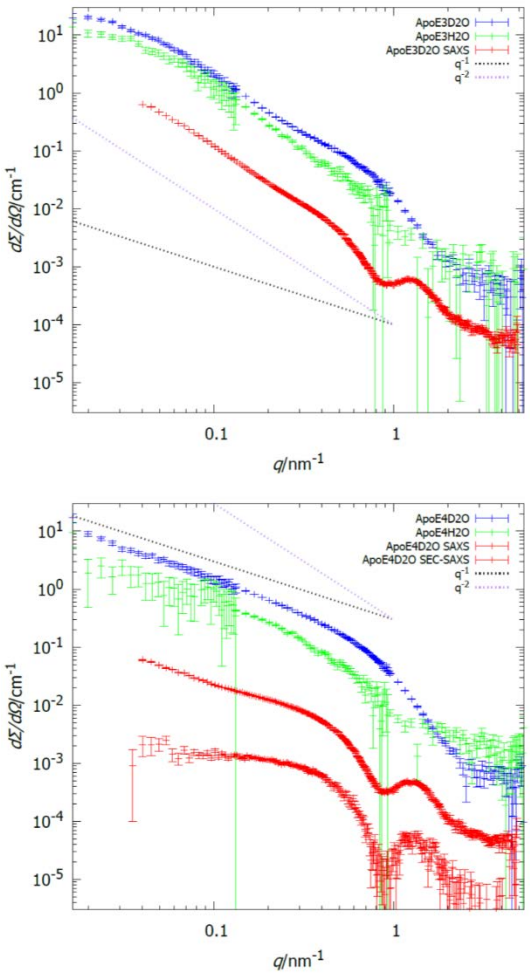

Figure 14. SANS and SAXS data for ApoE3 (top) and ApoE4 (bottom) protein.

POPULÄRVETENSKAPLIG SAMMANFATTNING

Åderförkalkning är den främsta orsaken till tidig död bland människor i västvärlden. Det uppstår genom uppbyggnad av plack (fett) i artärväggarna, något som i sin tur kan leda till hjärtinfarkt och stroke. Fett och kolesterol transporteras runt kroppen med hjälp av nanopartiklar som kallas lipoproteiner. Lipoproteiner bär fettet till och från cellerna. Det finns olika typer av lipoproteiner såsom 1) lågdensitetslipoproteiner (LDL, också kallad för det onda kolesterolet) som levererar fett till cellerna, och 2) högdensitetslipoproteiner (HDL, också kallad för det goda kolesterolet) som avlägsnar fett från cellerna. När det finns en obalans i lipidmetabolismen, börjar LDL ackumulera fett som eventuellt bildar ett plack vid artärväggarna, medan HDL kan hjälpa till att förhindra ansamling av plack och minska risken för hjärt-kärlsjukdom. Dessa processer är mycket komplexa och inte helt utredda, varför det krävs enklare modeller som delar upp processerna i separata komponenter så att man kan förstå var och en för sig. De kunskaper man får genom enklare modeller kan leda till ytterligare förståelse för sjukdomsutveckling och i sin tur hjälpa utvecklingen av behandlingar för sjukdomen. Kolesterol är en viktig komponent i cellmembran som denna avhandling fokuserar på: modellmembran skapas för att representera de som finns i kroppen, där kolesterol spelar en viktig roll. Dessa modeller kan modifieras för att i sin tur fokusera på en viss aspekt av membranet och studera den systematiskt: här studeras rollen av mättat och omättat fett som kan innehålla kolesterol. Eftersom lipoproteiner består av många olika komponenter används båda nativa och förenklade modeller för dessa också. Neutronreflektans har använts för att följa växelverkan mellan lipoproteiner och modellmembran. På detta sätt kunde membrankomponenternas roller bestämmas och variationen bland de nativa proven och deras enklare modeller belysas. Slutligen bestämdes strukturen hos modellipoproteinerna genom lågvinkel neutronspridning. Resultaten bekräftade lämpligheten av modellerna för att kartlägga lipoproteinernas roll i fettutbyte.

ACKNOWLEDGEMENTS

My first and biggest thanks goes to my supervisor Marité; your enthusiasm and positive attitude is truly inspiring. Thank you for your encouraging words and for always motivating and supporting me.

A huge thank you also goes to my other supervisors who have provided support and invaluable knowledge throughout this time. Martine: for teaching me everything in the lab, answering my incessant questions and always making time for me; Michael: for always taking the time to go through things thoroughly with me; Selma: for your advice and always excellent feedback and Trevor: for your support and encouragement.

A thank you to all the members of the Life Sciences Group during the last few years, so many good times were had and always the perfect distraction from the hectic world of lab work. To Val, thanks for letting me share your corner of the office and to Juliette thank you for always being happy to help with lab queries and for being such a great friend in the last few years. To other friends in Grenoble who made my time there so enjoyable: Charlotte thanks always for such great advice and encouragement with work, and to Ashley thanks for always being so positive and encouraging! Another special thanks to Lauren, whilst not in Grenoble, you have always encouraged and supported me! Thank you also to my new colleagues in Malmö, for welcoming me in for what has been quite the unexpected year.

A special thanks goes to everyone who helped during many (many) beamtimes, Federica, Nico, Dainius, Yubexi, Kate and Tania, thanks for all your advice, extra pairs of hands and unwavering enthusiasm even when working through the night!

My final thanks go to my family who have always supported me, to George and Harry who always have wise words or at least distraction to offer, to Mum and Dad who always manage to put a smile back on my face – your endless love and support is everything to me. And to Ash, thanks for keeping me sane and putting things into perspective when I couldn’t.

REFERENCES

1. World Health Organization. Cardiovascular Disease. https://www.who.int/news-room/fact-sheets/detail/cardiovascular-diseases-(cvds) (2017).
2. Rader, D. J. & Daugherty, A. Translating molecular discoveries into new therapies for atherosclerosis. *Nature* **451**, 904–913 (2008).
3. Ference, B. A. *et al.* Low-density lipoproteins cause atherosclerotic cardiovascular disease. 1. Evidence from genetic, epidemiologic, and clinical studies. A consensus statement fromthe European Atherosclerosis Society Consensus Panel. *Eur. Heart J.* **38**, 2459–2472 (2017).
4. Ouimet, M., Barrett, T. J. & Fisher, E. A. HDL and Reverse Cholesterol Transport. *Circ. Res.* **124**, 1505–1518 (2019).
5. Feig, J. E., Hewing, B., Smith, J. D., Hazen, S. L. & Fisher, E. A. HDL and Atherosclerosis Regression: Evidence from Pre-clinical and Clinical Studies. *Circ Res* **114**, 205–213 (2014).
6. Marques, L. R. *et al.* Reverse cholesterol transport: Molecular mechanisms and the non-medical approach to enhance HDL cholesterol. *Front. Physiol.* **9**, 1–11 (2018).
7. Rosenson, R. S. *et al.* Cholesterol efflux and atheroprotection: Advancing the concept of reverse cholesterol transport. *Circulation* **125**, 1905–1919 (2012).
8. Yancey, P. G. *et al.* Importance of different pathways of cellular cholesterol efflux. *Arterioscler. Thromb. Vasc. Biol.* **23**, 712–719 (2003).
9. Brites, F., Martin, M., Guillas, I. & Kontush, A. Antioxidative activity of high-density lipoprotein (HDL): Mechanistic insights into potential clinical benefit. *BBA Clin.* **8**, 66–77 (2017).
10. Voight, B. F. *et al.* Plasma HDL cholesterol and risk of myocardial infarction: A mendelian randomisation study. *Lancet* **380**, 572–580 (2012).
11. Madsen, C. M., Varbo, A. & Nordestgaard, B. G. Extreme high high-density lipoprotein cholesterol is paradoxically associated with high mortality inmen and women: Two prospective cohort studies. *Eur. Heart J.* **38**, 2478–2486 (2017).
12. Fernandez, M. L. & Webb, D. The LDL to HDL Cholesterol Ratio as a Valuable Tool to Evaluate Coronary Heart Disease Risk. *J. Am. Coll. Nutr.* **27**, 1–5 (2008).
13. Jonas, A. *Lipoprotein structure*. *Biochemistry of Lipids, Lipoproteins and Membranes* (2002). doi:10.1042/bst0100143a.
14. de Lalla, O. F. & Gofman, J. W. Ultracentrifugal Analysis of Serum Lipoproteins. *Methods Biochem. Anal.* **1**, (1954).
15. Nichols, A. V, Krauss, R. M. & Musliner, T. A. Nondenaturing Polyacrylamide Gradient Gel Electrophoresis. *Methods Enzymol.* **128**, 417–31 (1986).

16. von Eckardstein, A. & Kardassis, D. *High Density Lipoproteins*. *Handbook of Experimental Pharmacology* vol. 224 (2015).
17. Sacks, F. M. & Jensen, M. K. From high-density lipoprotein cholesterol to measurements of function: Prospects for the development of tests for high-density lipoprotein functionality in cardiovascular disease. *Arterioscler. Thromb. Vasc. Biol.* **38**, 487–499 (2018).
18. Zannis, V. I. *et al.* Probing the pathways of chylomicron and HDL metabolism using adenovirus-mediated gene transfer. *Curr. Opin. Lipidol.* **15**, 151–166 (2004).
19. Zannis, V. I., Chroni, A. & Krieger, M. Role of apoA-I, ABCA1, LCAT, and SR-BI in the biogenesis of HDL. *J. Mol. Med.* **84**, 276–294 (2006).
20. Hafiane, A. & Genest, J. HDL, atherosclerosis, and emerging therapies. *Cholesterol* **2013**, (2013).
21. Kardassis, D., Mosialou, I., Kanaki, M., Tiniakou, I. & Thymiakou, E. Metabolism of HDL and its Regulation. *Curr. Med. Chem.* **21**, 2864–2880 (2014).
22. Almer, G., Mangge, H., Zimmer, A. & Prassl, R. Lipoprotein-Related and Apolipoprotein-Mediated Delivery Systems for Drug Targeting and Imaging. *Curr. Med. Chem.* **22**, 3631–3651 (2015).
23. Feingold, K. R. & Grunfeld, C. Introduction to Lipids and Lipoproteins. *Endotext* 1–19 (2000).
24. Badimon, L. & Vilahur, G. LDL-cholesterol versus HDL-cholesterol in the atherosclerotic plaque: Inflammatory resolution versus thrombotic chaos. *Ann. N. Y. Acad. Sci.* **1254**, 18–32 (2012).
25. Gille, A., Easton, R., D'Andrea, D., Wright, S. D. & Shear, C. L. CSL112 enhances biomarkers of reverse cholesterol transport after single and multiple infusions in healthy subjects. *Arterioscler. Thromb. Vasc. Biol.* **34**, 2106–2114 (2014).
26. Van Capelleveen, J. C., Brewer, H. B., Kastelein, J. J. P. & Hovingh, G. K. Novel therapies focused on the high-density lipoprotein particle. *Circ. Res.* **114**, 193–204 (2014).
27. Garber, D. W. *et al.* A new synthetic class A amphipathic peptide analogue protects mice from diet-induced atherosclerosis. *J. Lipid Res.* **42**, 545–552 (2001).
28. White, C. R., Garber, D. W. & Anantharamaiah, G. M. Anti-inflammatory and cholesterol-reducing properties of apolipoprotein mimetics: A review. *J. Lipid Res.* **55**, 2007–2021 (2014).
29. Ibanez, B. *et al.* Recombinant HDL Milano exerts greater anti-inflammatory and plaque stabilizing properties than HDL wild-type. *Atherosclerosis* **220**, 72–77 (2012).
30. Chenevard, R. *et al.* Reconstituted HDL in Acute Coronary Syndromes. *Cardiovasc. Ther.* **30**, 51–57 (2012).
31. Sattler, K. J. E. *et al.* High high-density lipoprotein-cholesterol reduces risk and extent of percutaneous coronary intervention-related myocardial infarction and improves long-term outcome in patients undergoing elective percutaneous

coronary intervention. *Eur. Heart J.* **30**, 1894–1902 (2009).
32. Angeloni, E. *et al.* Lack of protective role of HDL-C in patients with coronary artery disease undergoing elective coronary artery bypass grafting. 3557–3562 (2013) doi:10.1093/eurheartj/eht163.
33. Kypreos, K. E., Gkizas, S., Rallidis, L. S. & Karagiannides, I. HDL particle functionality as a primary pharmacological target for HDL-based therapies. *Biochem. Pharmacol.* **85**, 1575–1578 (2013).
34. Tsompanidi, E. M., Brinkmeier, M. S., Fotiadou, E. H., Giakoumi, S. M. & Kypreos, K. E. HDL biogenesis and functions: Role of HDL quality and quantity in atherosclerosis. *Atherosclerosis* **208**, 3–9 (2010).
35. Moreno-grau, S. *et al.* Genome-wide significant risk factors on chromosome 19 and the APOE locus. **9**, 24590–24600 (2018).
36. Weisgraber, K. H., Rall, S. C. & Mahley, R. W. Human E Apoprotein Heterogeneity. *Journey Biol. Chem.* **256**, 9077–9083 (1981).
37. Mahley, R. W., Weisgraber, K. H. & Huang, Y. Apolipoprotein E : structure determines function , from atherosclerosis to Alzheimer ' s disease to AIDS. 183–188 (2009) doi:10.1194/jlr.R800069-JLR200.
38. de Chaves, E. P. & Narayanaswami, V. Apolipoprotein E and cholesterol in aging and disease in the brain. *Futur. Lipidol.* **3**, 505–530 (2008).
39. Mahley, R. W. Apolipoprotein E : from cardiovascular disease to neurodegenerative disorders. *J. Mol. Med.* 739–746 (2016) doi:10.1007/s00109-016-1427-y.
40. Linton, M. F. *et al.* Phenotypes of apolipoprotein B and apolipoprotein E after liver transplantation. *J. Clin. Invest.* **88**, 270–281 (1991).
41. Chernick, D., Ortiz-valle, S., Jeong, A., Qu, W. & Li, L. Neuroscience Letters Peripheral versus central nervous system APOE in Alzheimer ' s disease : Interplay across the blood-brain barrier. *Neurosci. Lett.* **708**, 134306 (2019).
42. Davidson, W. S. *et al.* Proteomic analysis of defined HDL subpopulations reveals particle-specific protein clusters: Relevance to antioxidative function. *Arterioscler. Thromb. Vasc. Biol.* **29**, 870–876 (2009).
43. Koo, C., Innerarity, T. L. & Mahley, R. W. Obligatory Role of Cholesterol and Apolipoprotein E in the Formation of Large Cholesterol-enriched and Receptor-active High Density Lipoproteins. **260**, 11934–11943 (1985).
44. Mahley, R. W., Huang, Y. & Weisgraber, K. H. Putting cholesterol in its place : apoE and reverse cholesterol transport. **116**, 3–6 (2006).
45. Brown, M. S. & Goldstein, J. L. A receptor-mediated pathway for cholesterol homeostasis. *Science (80-.).* **232**, 34–47 (1986).
46. Yamamoto, T., Choi, H. W. & Ryan, R. O. Apolipoprotein E isoform-specific binding to the low-density lipoprotein receptor. *Anal. Biochem.* **372**, 222–226 (2008).
47. Mauch, D. H. *et al.* CNS Synaptogenesis Promoted by Glia-Derived Cholesterol. *Science (80-.).* **294**, 1354–1357 (2001).
48. Innerarity, T. L., Friedlander, E. J., Rall, S. C., Weisgraber, K. H. & Mahley, R.

W. The receptor-binding domain of human apolipoprotein E. Binding of apolipoprotein E fragments. *J. Biol. Chem.* **258**, 12341–12347 (1983).
49. Nguyen, D. *et al.* Molecular Basis for the Differences in Lipid and Lipoprotein Binding Properties of Human Apolipoproteins E3 and E4. **49**, 10881–10889 (2010).
50. Xu, Q., Brecht, W. J., Weisgraber, K. H., Mahley, R. W. & Huang, Y. Apolipoprotein E4 Domain Interaction Occurs in Living Neuronal Cells as Determined by Fluorescence Resonance Energy Transfer *. **279**, 25511–25516 (2004).
51. Mahley, R. W. & Rall, S. C. Apolipoprotein E : Far More Than a Lipid Transport Protein. *Annu. Rev. Genomics Hum. Genet.* 507–37 (2000).
52. Hatters, D. M., Budamagunta, M. S., Voss, J. C. & Weisgraber, K. H. Modulation of apolipoprotein E structure by domain interaction: Differences in lipid-bound and lipid-free forms. *J. Biol. Chem.* **280**, 34288–34295 (2005).
53. Ye, S. *et al.* Apolipoprotein (apo) E4 enhances amyloid β peptide production in cultured neuronal cells: ApoE structure as a potential therapeutic target. *Proc. Natl. Acad. Sci. U. S. A.* **102**, 18700–18705 (2005).
54. Mahley, R. W. & Huang, Y. Small-molecule Structure Correctors Target Abnormal Protein Structure and Function: The Structure Corrector Rescue of Apolipoprotein E4-associated Neuropathology. *J Med Chem* **55**, 8997–9008 (2012).
55. Saito, H. *et al.* Effects of Polymorphism on the Lipid Interaction of Human Apolipoprotein E. *J. Biol. Chem.* **278**, 40723–40729 (2003).
56. Chetty, P. S., Mayne, L., Lund-katz, S., Englander, S. W. & Phillips, M. C. Helical structure, stability, and dynamics in human apolipoprotein E3 and E4 by hydrogen exchange and mass spectrometry. *PNAS* **114**, 968–973 (2017).
57. Garai, K., Baban, B. & Frieden, C. Dissociation of apoE oligomers to monomers is required for high affinity binding to phospholipid vesicles. **50**, 2550–2558 (2011).
58. Ruiz, J. *et al.* The apoE isoform binding properties of the VLDL receptor reveal marked differences from LRP and the LDL receptor. *J. Lipid Res.* **46**, 1721–1731 (2005).
59. Weisgraber, K. H., Innerarity, T. L. & Mahley, R. W. Abnormal lipoprotein receptor-binding activity of the human E apoprotein due to cysteine-arginine interchange at a single site. *J. Biol. Chem.* **257**, 2518–2521 (1982).
60. Reiman, E. M. Exceptionally low likelihood of Alzheimer ' s dementia in APOE2 homozygotes from a 5,000-person neuropathological study. **11**, (2020).
61. Wu, L., Zhao, L. & Ph, D. ApoE2 and Alzheimer ' s disease : time to take a closer look. **11**, 412–413 (2020).
62. Elmadbouh, I. *et al.* Relationship of apolipoprotein E polymorphism with lipid profiles in atherosclerotic coronary artery disease. *Egypt. Hear. J.* **65**, 71–78 (2013).
63. Valanti, E. K., Dalakoura-Karagkouni, K. & Sanoudou, D. Current and emerging

reconstituted hdl-apoa-i and hdl-apoe approaches to treat atherosclerosis. *J. Pers. Med.* **8**, 1–12 (2018).
64. Dong, L. & Weisgraber, K. H. Human Apolipoprotein E4 Domain Interaction. **271**, 19053–19057 (1996).
65. Dong, L. M. *et al*. Human apolipoprotein E. Role of arginine 61 in mediating the lipoprotein preferences of the E3 and E4 isoforms. *J. Biol. Chem.* **269**, 22358–22365 (1994).
66. Fagan, A. M. & Holtzman, D. M. Astrocyte lipoproteins, effects of apoE on neuronal function, and role of apoE in amyloid-β deposition in vivo. *Microsc. Res. Tech.* **50**, 297–304 (2000).
67. Arendt, T. *et al.* Plastic neuronal remodeling is impaired in patients with Alzheimer's disease carrying apolipoprotein ε4 allele. *J. Neurosci.* **17**, 516–529 (1997).
68. Sanan, D. A. *et al.* Apolipoprotein E associates with β amyloid peptide of Alzheimer's disease to form novel monofibrils. Isoform ApoE4 associates more efficiently than ApoE3. *J. Clin. Invest.* **94**, 860–869 (1994).
69. Castellano, J. M. *et al.* Human apoE isoforms differentially regulate brain amyloid-B peptide clearance. *Sci Transl Med* **3**, (2011).
70. Harayama, T. & Riezman, H. Understanding the diversity of membrane lipid composition. *Nat. Rev. Mol. Cell Biol.* **19**, 281–296 (2018).
71. Gatenby, R. A. The role of cell membrane information reception, processing, and communication in the structure and function of multicellular tissue. *Int. J. Mol. Sci.* **20**, 3609 (2019).
72. Frieden, B. R. & Gatenby, R. A. Signal transmission through elements of the cytoskeleton form an optimized information network in eukaryotic cells. *Sci. Rep.* **9**, 1–10 (2019).
73. Quick, M. & Javitch, J. A. Monitoring the function of membrane transport proteins in detergent-solubilized form. *Proc. Natl. Acad. Sci. U. S. A.* **104**, 3603–3608 (2007).
74. Singer, S. . & Nicolson, G. L. The Fluid Mosaic Model of the Structure of Cell Membranes. *Science* vol. 175 720–731 (1972).
75. Singer, S. J. A Fluid Lipid-Globular Protein Mosaic Model of Membrane Structure. *Ann. N. Y. Acad. Sci.* **195**, 16–23 (1972).
76. Brown, M. F. Modulation of rhodopsin function by properties of the membrane bilayer. *Chem. Phys. Lipids* **73**, 159–180 (1994).
77. Botelho, A. V., Huber, T., Sakmar, T. P. & Brown, M. F. Curvature and Hydrophobic forces drive oligomerization and modulate activity of rhodopsin in membranes. *Biophys. J.* **91**, 4464–4477 (2006).
78. Seu, K. J., Cambrea, L. R., Everly, R. M. & Hovis, J. S. Influence of lipid chemistry on membrane fluidity: Tail and headgroup interactions. *Biophys. J.* **91**, 3727–3735 (2006).
79. Fidorra, M., Heimburg, T. & Seeger, H. M. Melting of individual lipid components in binary lipid mixtures studied by FTIR spectroscopy, DSC and

Monte Carlo simulations. *Biochim. Biophys. Acta - Biomembr.* **1788**, 600–607 (2009).
80. Luttrell, L. M. *et al.* B-Arrestin-Dependent Formation of B2 Adrenergic Receptor-Src Protein Kinase Complexes. *Science (80-.).* **283**, 655–661 (1999).
81. Mademidis, A. & Köster, W. Transport activity of FhuA, FhuC, FhuD, and FhuB derivatives in a system free of polar effects, and stoichiometry of components involved in ferrichrome uptake. *Mol. Gen. Genet.* **258**, 156–165 (1998).
82. Briard, J. G., Jiang, H., Moremen, K. W., MacAuley, M. S. & Wu, P. Cell-based glycan arrays for probing glycan-glycan binding protein interactions. *Nat. Commun.* **9**, 1–11 (2018).
83. Frolov, V. A., Shnyrova, A. V. & Zimmerberg, J. Lipid polymorphisms and membrane shape. *Cold Spring Harb. Perspect. Biol.* **3**, 1–14 (2011).
84. Gruner, S. O. L. M. Intrinsic curvature hypothesis for biomembrane lipid composition : A role for nonbilayer lipids. **82**, 3665–3669 (1985).
85. Simons, K. & Ikonen, E. Functional rafts in cell membranes. *Nature* **387**, 569–572 (1997).
86. Ramstedt, B. & Slotte, J. P. Interaction of cholesterol with sphingomyelins and acyl-chain-matched phosphatidylcholines: A comparative study of the effect of the chain length. *Biophys. J.* **76**, 908–915 (1999).
87. McGraw, C., Yang, L., Levental, I., Lyman, E. & Robinson, A. S. Membrane cholesterol depletion reduces downstream signaling activity of the adenosine A 2A receptor. *Biochim. Biophys. Acta - Biomembr.* **1861**, 760–767 (2019).
88. Armstrong, C. L. *et al.* Effect of cholesterol on the lateral nanoscale dynamics of fluid membranes. *Eur. Biophys. J.* **41**, 901–913 (2012).
89. Klein, U., Gimpl, G. & Fahrenholz, F. Alteration of the Myometrial Plasma Membrane Cholesterol Content with β-Cyclodextrin Modulates the Binding Affinity of the Oxytocin Receptor. *Biochemistry* **34**, 13784–13793 (1995).
90. Stöckl, M., Plazzo, A. P., Korte, T. & Herrmann, A. Detection of lipid domains in model and cell membranes by fluorescence lifetime imaging microscopy of fluorescent lipid analogues. *J. Biol. Chem.* **283**, 30828–30837 (2008).
91. Nickels, J. D. *et al.* The in vivo structure of biological membranes and evidence for lipid domains. *PLoS Biol.* **15**, 1–22 (2017).
92. Renner, L. D. & Weibel, D. B. Cardiolipin microdomains localize to negatively curved regions of Escherichia coli membranes. *Proc. Natl. Acad. Sci. U. S. A.* **108**, 6264–6269 (2011).
93. Armstrong, C. L. *et al.* Co-existence of gel and fluid lipid domains in single-component phospholipid membranes. *Soft Matter* **8**, 4687–4694 (2012).
94. Heberle, F. A. *et al.* Bilayer thickness mismatch controls raft size in model membranes. *J. Am. Chem. Soc.* **135**, 6853–6859 (2013).
95. Marquardt, D., Geier, B. & Pabst, G. Asymmetric lipid membranes: Towards more realistic model systems. *Membranes (Basel).* **5**, 180–196 (2015).
96. Verkleij, A. J. *et al.* The Asymmetric Distribution of Phospholipids in the Human Red Cell Membrane A combined Study Using Phospholipases and Freeze-Etch

Electron Microscopy. *BBA - Biomembr.* **323**, 178–193 (1973).
97. Van Meer, G., Voelker, D. R. & Feigenson, G. W. Membrane lipids: Where they are and how they behave. *Nat. Rev. Mol. Cell Biol.* **9**, 112–124 (2008).
98. Smaby, J. M., Brockman, H. L. & Brown, R. E. Cholesterol's Interfacial Interactions with Sphingomyelins and Phosphatidylcholines: Hydrocarbon Chain Structure Determines the Magnitude of Condensation. *Biochemistry* **33**, 9135–9142 (1994).
99. Bag, N., Yap, D. H. X. & Wohland, T. Temperature dependence of diffusion in model and live cell membranes characterized by imaging fluorescence correlation spectroscopy. *Biochim. Biophys. Acta - Biomembr.* **1838**, 802–813 (2014).
100. Fernández-Pérez, E. J. *et al.* Effect of cholesterol on membrane fluidity and association of Aβ oligomers and subsequent neuronal damage: A Double-Edged Sword. *Front. Aging Neurosci.* **10**, 1–14 (2018).
101. Crocke, E. L. Cholesterol function in plasma membranes from ectotherms: Membrane-specific roles in adaptation to temperature. *Am. Zool.* **38**, 291–304 (1998).
102. Demel, R. A., Van Deenen, L. L. M. & Pethica, B. A. Monolayer interactions of phospholipids and cholesterol. *Biochim. Biophys. Acta* **135**, 11–19 (1967).
103. Léonard, A. *et al.* Location of Cholesterol in DMPC Membranes . A Comparative Study by Neutron Diffraction and Molecular Mechanics Simulation †. *Langmuir* **17**, 2019–2030 (2001).
104. Marquardt, D., Kučerka, N., Wassall, S. R., Harroun, T. A. & Katsaras, J. Cholesterol's location in lipid bilayers. *Chem. Phys. Lipids* **199**, 17–25 (2016).
105. Armstrong, C. L. *et al.* The Observation of Highly Ordered Domains in Membranes with Cholesterol. *PLoS One* **8**, 1–10 (2013).
106. Nobre, T. M. *et al.* Interactions of bioactive molecules & nanomaterials with Langmuir monolayers as cell membrane models. *Thin Solid Films* **593**, 158–188 (2015).
107. Chan, Y.-H. M. & Boxer, S. G. Model Membrane Systems and Their Applications. *Curr. Opin. Chem. Biol.* **11**, 581–587 (2007).
108. Åkesson, A. *et al.* Composition and structure of mixed phospholipid supported bilayers formed by POPC and DPPC. *Soft Matter* **8**, 5658–5665 (2012).
109. Jenkins, E. *et al.* Reconstitution of immune cell interactions in free-standing membranes. *J. Cell Sci.* **132**, 1–21 (2019).
110. Konyakhina, T. M. & Feigenson, G. W. Phase diagram of a polyunsaturated lipid mixture: Brain sphingomyelin/1-stearoyl-2-docosahexaenoyl-sn-glycero-3-phosphocholine/cholesterol. *Biochim. Biophys. Acta - Biomembr.* **1858**, 153–161 (2016).
111. Goñi, F. M. *et al.* Phase diagrams of lipid mixtures relevant to the study of membrane rafts. *Biochim. Biophys. Acta - Mol. Cell Biol. Lipids* **1781**, 665–684 (2008).
112. Cho, N. J., Hwang, L. Y., Solandt, J. J. R. & Frank, C. W. Comparison of extruded and sonicated vesicles for planar bilayer self-assembly. *Materials (Basel).* **6**,

3294–3308 (2013).
113. Lind, T. K. & Cárdenas, M. Understanding the formation of supported lipid bilayers via vesicle fusion—A case that exemplifies the need for the complementary method approach (Review). *Biointerphases* **11**, 020801-1–12 (2016).
114. Kurniawan, J., Ventrici De Souza, J. F., Dang, A. T., Liu, G. Y. & Kuhl, T. L. Preparation and Characterization of Solid-Supported Lipid Bilayers Formed by Langmuir-Blodgett Deposition: A Tutorial. *Langmuir* **34**, 15622–15639 (2018).
115. Paracini, N., Clifton, L. A., Skoda, M. W. A. & Lakey, J. H. Liquid crystalline bacterial outer membranes are critical for antibiotic susceptibility. *Proc. Natl. Acad. Sci. U. S. A.* **115**, E7587–E7594 (2018).
116. Lv, Z., Banerjee, S., Zagorski, K. & Lyubchenko, Y. L. Supported Lipid Bilayers for Atomic Force Microscopy Studies. *Methods Mol Biol* **1814**, 129–143 (2018).
117. Wacklin, H. P. & Thomas, R. K. Spontaneous formation of asymmetric lipid bilayers by adsorption of vesicles. *Langmuir* **23**, 7644–7651 (2007).
118. Przybylo, M. *et al.* Lipid diffusion in giant unilamellar vesicles is more than 2 times faster than in supported phospholipid bilayers under identical conditions. *Langmuir* **22**, 9096–9099 (2006).
119. Clifton, L. A. *et al.* Self-Assembled Fluid Phase Floating Membranes with Tunable Water Interlayers. *Langmuir* **35**, 13735–13744 (2019).
120. Arriaga, L. R. *et al.* Stiffening effect of cholesterol on disordered lipid phases: A combined neutron spin echo + dynamic light scattering analysis of the bending elasticity of large unilamellar vesicles. *Biophys. J.* **96**, 3629–3637 (2009).
121. Luchini, A. *et al.* Towards biomimics of cell membranes: structural effect of phosphatidylinositol triphosphate (PIP3) on a lipid bilayer. *Colloids Surfaces B Biointerfaces* **173**, 202–209 (2019).
122. Hall, S. C. L. *et al.* Adsorption of a styrene maleic acid (SMA) copolymer-stabilized phospholipid nanodisc on a solid-supported planar lipid bilayer. *J. Colloid Interface Sci.* **574**, 272–284 (2020).
123. Nakano, M., Fukuda, M., Kudo, T., Endo, H. & Handa, T. Determination of interbilayer and transbilayer lipid transfers by time-resolved small-angle neutron scattering. *Phys. Rev. Lett.* **98**, 30–33 (2007).
124. Åkesson, A., Lind, T. K., Barker, R., Hughes, A. & Cárdenas, M. Unraveling dendrimer translocation across cell membrane mimics. *Langmuir* **28**, 13025–13033 (2012).
125. Clifton, L. A. *et al.* Design and use of model membranes to study biomolecular interactions using complementary surface-sensitive techniques. *Adv. Colloid Interface Sci.* **277**, 102118 (2020).
126. Browning, K. L. *et al.* Human Lipoproteins at Model Cell Membranes: Effect of Lipoprotein Class on Lipid Exchange. *Sci. Rep.* **7**, 1–11 (2017).
127. Browning, K. L. *et al.* Effect of bilayer charge on lipoprotein lipid exchange. *Colloids Surfaces B Biointerfaces* **168**, 117–125 (2018).
128. Maric, S. *et al.* Time-resolved small-angle neutron scattering as a probe for the

dynamics of lipid exchange between human lipoproteins and naturally derived membranes. *Sci. Rep.* **9**, 7591 (2019).
129. Gerelli, Y., Porcar, L., Lombardi, L. & Fragneto, G. Lipid exchange and flip-flop in solid supported bilayers. *Langmuir* **29**, 12762–12769 (2013).
130. Bayburt, T. H., Grinkova, Y. V. & Sligar, S. G. Self-Assembly of Discoidal Phospholipid Bilayer Nanoparticles with Membrane Scaffold Proteins. *Nano Lett.* **2**, 853–856 (2002).
131. Hall, S. C. L. *et al.* Influence of Poly(styrene-co-maleic acid) Copolymer Structure on the Properties and Self-Assembly of SMALP Nanodiscs. *Biomacromolecules* **19**, 761–772 (2018).
132. Mahieu, E. & Gabel, F. Biological small-angle neutron scattering : recent results and development research papers. 715–726 (2018) doi:10.1107/S2059798318005016.
133. Grishaev, A., Anthis, N. J. & Clore, G. M. Contrast-Matched Small-Angle X - ray Scattering from a Heavy-Atom- Labeled Protein in Structure Determination: Application to a Lead- Substituted Calmodulin − Peptide Complex. **134**, 14686–14689 (2012).
134. Hura, G. L. *et al.* DNA conformations in mismatch repair probed in solution by X-ray scattering from gold nanocrystals. *PNAS* **110**, 17308–17313 (2013).
135. Haertlein, M. *et al. Biomolecular Deuteration for Neutron Structural Biology and Dynamics*. *Methods in Enzymology* vol. 566 (2016).
136. Dunne, O. *et al.* Matchout deuterium labelling of proteins for small-angle neutron scattering studies using prokaryotic and eukaryotic expression systems and high cell-density cultures. *Eur. Biophys. J.* **46**, 425–432 (2017).
137. Castellanos, M. M., McAuley, A. & Curtis, J. E. Investigating Structure and Dynamics of Proteins in Amorphous Phases Using Neutron Scattering. *Comput. Struct. Biotechnol. J.* **15**, 117–130 (2017).
138. Klenner, M. *et al.* Decagram scale production of deuterated mineral oil and polydecene as solvents for polymer studies in neutron scattering. *Polym. Chem.* **11**, 4986–4994 (2020).
139. Moulin, M. *et al.* Perdeuteration of cholesterol for neutron scattering applications using recombinant Pichia pastoris. *Chem. Phys. Lipids* **212**, 80–87 (2018).
140. Maric, S. *et al.* Biosynthetic preparation of selectively deuterated phosphatidylcholine in genetically modified Escherichia coli. *Appl. Microbiol. Biotechnol.* **99**, 241–254 (2015).
141. Ricci, C. *et al.* Amyloid β-Peptide Interaction with Membranes: Can Chaperones Change the Fate? *J. Phys. Chem. B* **123**, 631–638 (2019).
142. Manzoni, F. *et al.* Elucidation of Hydrogen Bonding Patterns in Ligand-Free, Lactose- and Glycerol-Bound Galectin-3C by Neutron Crystallography to Guide Drug Design. *J. Med. Chem.* **61**, 4412–4420 (2018).
143. Maric, S., Lind, T. K., Lyngsø, J., Cárdenas, M. & Pedersen, J. S. Modeling Small-Angle X-ray Scattering Data for Low-Density Lipoproteins: Insights into the Fatty Core Packing and Phase Transition. *ACS Nano* **11**, 1080–1090 (2017).

144. Korasick, D. A. & Tanner, J. J. Determination of protein oligomeric structure from small-angle X-ray scattering. *Protein Sci.* **27**, 814–824 (2018).
145. Mertens, H. D. T. & Svergun, D. I. Structural characterization of proteins and complexes using small-angle X-ray solution scattering. *J. Struct. Biol.* **172**, 128–141 (2010).
146. Fekry, M. *et al.* SAXS and stability studies of iron-induced oligomers of bacterial frataxin CyaY. *PLoS One* **12**, 1–22 (2017).
147. Bucciarelli, S. *et al.* Size-exclusion chromatography small-angle X-ray scattering of water soluble proteins on a laboratory instrument. *J. Appl. Crystallogr.* **51**, 1623–1632 (2018).
148. Hopkins, J. B. & Thorne, R. E. Quantifying radiation damage in biomolecular small-angle X-ray scattering. *J. Appl. Crystallogr.* **49**, 880–890 (2016).
149. Mirandela, D. *et al.* Merging In-Solution X - ray and Neutron Scattering Data Allows Fine Structural Analysis of Membrane − Protein Detergent Complexes¨. 8–12 (2018) doi:10.1021/acs.jpclett.8b01598.
150. Zhang, F. *et al.* Hydration and interactions in protein solutions containing concentrated electrolytes studied by small-angle scattering. *Phys. Chem. Chem. Phys.* **14**, 2483–2493 (2012).
151. Garg, S. *et al.* Cholesterol solubility limit in lipid membranes probed by small angle neutron scattering and MD simulations. *Soft Matter* **10**, 9313–9317 (2014).
152. Gerelli, Y. Phase Transitions in a Single Supported Phospholipid Bilayer: Real-Time Determination by Neutron Reflectometry. *Phys. Rev. Lett.* **122**, 248101 (2019).
153. Moulin, M. *et al.* Towards a molecular understanding of the water purification properties of Moringa seed proteins. *J. Colloid Interface Sci.* **554**, 296–304 (2019).
154. Rodriguez-Loureiro, I., Latza, V. M., Fragneto, G. & Schneck, E. Conformation of Single and Interacting Lipopolysaccharide Surfaces Bearing O-Side Chains. *Biophys. J.* **114**, 1624–1635 (2018).
155. Rodriguez-Loureiro, I. *et al.* Neutron reflectometry yields distance-dependent structures of nanometric polymer brushes interacting across water. *Soft Matter* **13**, 5767–5777 (2017).
156. Nylander, T. *et al.* Neutron reflectometry to investigate the delivery of lipids and DNA to interfaces (Review). *Biointerphases* **3**, FB64–FB82 (2008).
157. Hirz, M., Richter, G., Leitner, E., Wriessnegger, T. & Pichler, H. A novel cholesterol-producing Pichia pastoris strain is an ideal host for functional expression of human Na,K-ATPase α3β1 isoform. *Appl. Microbiol. Biotechnol.* **97**, 9465–9478 (2013).
158. Katz, J. J., Crespi, H. L., Czajka, D. M. & Finkel, A. J. Course of deuteriation and some physiological effects of deuterium in mice. *Am. J. Physiol.* **203**, 907–913 (1962).
159. Garg, S. *et al.* Cholesterol solubility limit in lipid membranes probed by small angle neutron scattering and MD simulations. *Soft Matter* **10**, 9313–9317 (2014).

160. Scheiner, S. & Martin, C. Relative Stability of Hydrogen and Deuterium Bonds. *J. Am. Chem. Soc.* 1511–1521 (1996) doi:10.1021/ja9530376.
161. Hanashima, S. *et al.* Biomolecular Chemistry. 8601–8610 (2019) doi:10.1039/c9ob01342c.
162. Haberland, M. E. & Reynolds, J. A. Self-association of Cholesterol in Aqueous Solution. *Proc. Natl. Acad. Sci.* **70**, 2313–2316 (1973).
163. Vitiello, G. *et al.* Cholesterol modulates the fusogenic activity of a membranotropic domain of the FIV glycoprotein gp36. *Soft Matter* **9**, 6442–6456 (2013).
164. de Almeida, R. F. M., Fedorov, A. & Prieto, M. Sphingomyelin / phosphatidylcholine / cholesterol phase diagram : boundaries and composition of lipids rafts. *Biophys. J.* **85**, 2406–2416 (2003).
165. Marquardt, D. *et al.* Lipid bilayer thickness determines cholesterols location in model membranes. *Soft Matter* **12**, 9417–9428 (2016).
166. Kučerka, N., Nieh, M. P. & Katsaras, J. Fluid phase lipid areas and bilayer thicknesses of commonly used phosphatidylcholines as a function of temperature. *Biochim. Biophys. Acta - Biomembr.* **1808**, 2761–2771 (2011).
167. Wang, W., Yang, L. & Huang, H. W. Evidence of Cholesterol Accumulated in High Curvature Regions : Implication to the Curvature Elastic Energy for Lipid Mixtures. **92**, 2819–2830 (2007).
168. Yesylevskyy, S. O., Demchenko, A. P., Kraszewski, S. & Ramseyer, C. Cholesterol Induces Uneven Curvature of Asymmetric Lipid Bilayers. **2013**, (2013).
169. Rastogi, B. K. & Nordby, A. Lipid composition of cultured human endothelial cells. *Thromb. Res.* **18**, 629–641 (1980).
170. Ingólfsson, H. I. *et al.* Computational lipidomics of the neuronal plasma membrane. *Biophys. J.* **113**, 2271–2280 (2017).
171. Ingólfsson, H. I. *et al.* Lipid organization of the plasma membrane. *J. Am. Chem. Soc.* **136**, 14554–14559 (2014).
172. Tricerri, M. A. *et al.* Interaction of apolipoprotein A-I in three different conformations with palmitoyl oleoyl phosphatidylcholine vesicles. *J. Lipid Res.* **43**, 187–197 (2002).
173. Nanda, H. *et al.* Relaxation dynamics of saturated and unsaturated oriented lipid bilayers. *Soft Matter* **14**, 6119–6127 (2018).
174. Orädd, G., Lindblom, G. & Westerman, P. W. Lateral diffusion of cholesterol and dimyristoylphosphatidylcholine in a lipid bilayer measured by pulsed field gradient NMR spectroscopy. *Biophys. J.* **83**, 2702–2704 (2002).
175. Pitman, M., Suits, F., MacKerell, A. & Feller, S. Molecular-Level Organization of Saturated and Polyunsaturated Fatty Acids in a Phosphatidylcholine Bilayer Containing Cholesterol. *Biochemistry* **43**, 15318–15328 (2004).
176. Pike, L. J. Rafts defined: A report on the Keystone symposium on lipid rafts and cell function. *J. Lipid Res.* **47**, 1597–1598 (2006).
177. Wang, X., Pease, R., Bertinato, J. & Milne, R. W. Well-defined regions of

apolipoprotein B-100 undergo conformational change during its intravascular metabolism. *Arterioscler. Thromb. Vasc. Biol.* **20**, 1301–1308 (2000).
178. Segrest, J. P., Jones, M. K., De Loof, H. & Dashti, N. Structure of apolipoprotein B-100 in low density lipoproteins. *J. Lipid Res.* **42**, 1346–1367 (2001).
179. Guengerich, F. P. Kinetic Deuterium Isotope Effects in Cytochrome P450 Reactions. *Methods Enzymol.* 217–238 (2017) doi:10.1016/bs.mie.2017.06.036.Kinetic.
180. Skar-Gislinge, N. *et al.* Elliptical structure of phospholipid bilayer nanodiscs encapsulated by scaffold proteins: Casting the roles of the lipids and the protein. *J. Am. Chem. Soc.* **132**, 13713–13722 (2010).
181. Jonas, A. & Wald, J. H. Defined Apolipoprotein A-I Conformations in Reconstituted High Density Lipoprotein Discs *. 4818–4824 (1989).
182. Wu, Z. *et al.* Double superhelix model of high density lipoprotein. *J. Biol. Chem.* **284**, 36605–36619 (2009).
183. Midtgaard, S. R., Pedersen, M. C. & Arleth, L. Small-Angle X-Ray Scattering of the Cholesterol Incorporation into Human ApoA1-POPC Discoidal Particles. *Biophys. J.* **109**, 308–318 (2015).
184. Narayanaswami, V. *et al.* Helix Orientation of the Functional Domains in Apolipoprotein E in Discoidal High Density Lipoprotein Particles *. **279**, 14273–14279 (2004).
185. Raussens, V. *et al.* The Low Density Lipoprotein Receptor Active Conformation of Apolipoprotein E. **273**, 25825–25830 (1998).
186. Drury, J. & Narayanaswami, V. Examination of lipid-bound conformation of apolipoprotein E4 by pyrene excimer fluorescence. *J. Biol. Chem.* **280**, 14605–14610 (2005).
187. Bayburt, T. H. & Sligar, S. G. Membrane protein assembly into Nanodiscs. *FEBS Lett.* **584**, 1721–1727 (2010).
188. Denisov, I. G., Grinkova, Y. V., Lazarides, A. A. & Sligar, S. G. Directed Self-Assembly of Monodisperse Phospholipid Bilayer Nanodiscs with Controlled Size. *J. Am. Chem. Soc.* **126**, 3477–3487 (2004).
189. Gong, J. *et al.* Apolipoprotein E (ApoE) Isoform-dependent Lipid Release from Astrocytes Prepared from Human ApoE3 and ApoE4 Knock-in Mice *. **277**, 29919–29926 (2002).
190. Michikawa, M., Fan, Q., Isobe, I. & Yanagisawa, K. Apolipoprotein E Exhibits Isoform-Specific Promotion of Lipid Efflux from Astrocytes and Neurons in Culture. *J. Neurochem* **74**, 1008–1016 (2000).
191. Mahley, R. W. Central Nervous System Lipoproteins ApoE and Regulation of Cholesterol Metabolism. 1305–1315 (2016) doi:10.1161/ATVBAHA.116.307023.
192. Filou, S. *et al.* Distinct Roles of Apolipoproteins A1 and E in the Modulation of High-Density Lipoprotein Composition and Function. *Biochemistry* **55**, 3752–3762 (2016).

Paper 1

SCIENTIFIC REPORTS

OPEN

The Production of Matchout-Deuterated Cholesterol and the Study of Bilayer-Cholesterol Interactions

Received: 10 January 2019
Accepted: 7 March 2019
Published online: 26 March 2019

Sarah Waldie[1,2], Martine Moulin[1], Lionel Porcar[1], Harald Pichler[3,4], Gernot A. Strohmeier[3,5], Maximilian Skoda[6], V. Trevor Forsyth[1,7], Michael Haertlein[1], Selma Maric[2,8] & Marité Cárdenas[2]

The deuteration of biomolecules provides advanced opportunities for neutron scattering studies. For low resolution studies using techniques such as small-angle neutron scattering and neutron reflection, the level of deuteration of a sample can be varied to match the scattering length density of a specific D_2O/H_2O solvent mixture. This can be of major value in structural studies where specific regions of a complex system can be highlighted, and others rendered invisible. This is especially useful in analyses of the structure and dynamics of membrane components. In mammalian membranes, the presence of cholesterol is crucial in modulating the properties of lipids and in their interaction with proteins. Here, a protocol is described for the production of partially deuterated cholesterol which has a neutron scattering length density that matches that of 100% D_2O solvent (hereby named matchout cholesterol). The level of deuteration was determined by mass spectrometry and nuclear magnetic resonance. The cholesterol match-point was verified experimentally using small angle neutron scattering. The matchout cholesterol was used to investigate the incorporation of cholesterol in various phosphatidylcholine supported lipid bilayers by neutron reflectometry. The study included both saturated and unsaturated lipids, as well as lipids with varying chain lengths. It was found that cholesterol is distributed asymmetrically within the bilayer, positioned closer to the headgroups of the lipids than to the middle of the tail core, regardless of the phosphatidylcholine species.

Cholesterol is a key component of cellular membranes that modulates the structure and organisation of the lipid bilayer including the formation of so-called lipid rafts[1]. Lipid rafts are naturally existing nano-sized domains which are thought to regulate transmembrane proteins, some of which are linked to signalling mechanisms throughout the membrane[2,3]. Cholesterol provides rigidity in membranes by inducing liquid-ordered phases, and also affects structure by bringing about changes in the thickness of lipid monolayers (by condensation)[4,5] and bilayers (by altering the fluid and gel phases)[6–8].

It has recently been suggested that cholesterol positions itself in a lipid bilayer in a manner that depends on its environment: in polyunsaturated or very thin saturated bilayers, cholesterol will preferentially locate towards the core of the bilayer[9–11], while for thicker bilayers made of saturated or monounsaturated lipids, the cholesterol molecules will sit closer to the hydrophilic head groups of the lipid core[11]. It was suggested that the displacement of cholesterol towards the core is due to a solubility limit related to the order parameter of the lipids in which it is

[1]Institut Laue-Langevin, 71 Avenue des Martyrs, 38042, Grenoble, Cedex 9, France. [2]Biofilm-Research Centre for Biointerfaces and Biomedical Science Department, Faculty of Health and Society, Malmo University, Malmo, 20506, Sweden. [3]Austrian Centre of Industrial Biotechnology, Petersgasse 14, 8010, Graz, Austria. [4]Graz University of Technology, Institute of Molecular Biotechnology, NAWI Graz, BioTechMed Graz, Petersgasse 14, 8010, Graz, Austria. [5]Graz University of Technology, Institute of Organic Chemistry, NAWI Graz, Stremayrgasse 9, 8010, Graz, Austria. [6]Rutherford Appleton Laboratory, Harwell, Didcot, OX11 0QX, UK. [7]Life Sciences Department, Faculty of Natural Sciences, Keele University, Staffordshire, ST5 5BG, UK. [8]MAX IV Laboratory, Fotongatan 2, 225 92, Lund, Sweden. Correspondence and requests for materials should be addressed to M.H. (email: haertlein@ill.fr) or S.M. (email: selma.maric@mau.se) or M.C. (email: marite.cardenas@mau.se)

found[9,10,12]. This is quite a surprising result that requires further investigation. An excellent technique to study the structure and composition of thin membranes is neutron reflectometry (NR), as it is a highly sensitive structural tool with a resolution of a few angstroms perpendicular to the plane of the solid-liquid interface[13,14].

The availability of deuterated lipids is crucial for neutron scattering studies that exploit the very large difference in the scattering length densities (ρ) of protium and deuterium. This approach provides a way to study the positioning of a lipid molecule with respect to different environments and has successfully been used for the study of several systems including mixtures of deuterated phospholipids[15–17] and unlabelled sterols[18]. The deployment of D_2O matched-deuteration, referred to herein as simply matchout-deuteration, (in contrast to *per*deuteration) in neutron structural studies has been discussed recently by Dunne *et al.*[19] and Haertlein *et al.*[20]. This approach is based on the concept of deuterating specific molecules (in this case cholesterol) to a level that endows them with a ρ that is equal to that of pure D_2O, and as such is invisible to small angle neutron scattering (SANS) or NR at this solvent condition. The matchout-deuteration regime allows more sophisticated neutron-based experiments to be designed whereby within a single sample preparation, different components of a complex can be rendered "invisible" to neutron scattering techniques such as SANS and NR. This matchout deuteration technique allows components to be invisible to a *per*deuterated environment, however different mixtures of H_2O and D_2O can give the same effect when the ρ of the solvent mixture matches the ρ of a component of a system (typically having a value in between that of H_2O and D_2O) which is in turn rendered invisible. The benefits of this contrast matching allows a simplification of a complex system by focussing on certain parts and not having any extra scattering from those parts that are not of interest. Using solely a mixture of H_2O and D_2O to contrast match components might not be sufficient, for example in the case that the ρ values for the phospholipids compared to non-deuterated cholesterol are very similar. *Per*deuteration gives a different advantage, in that it provides maximum contrast to a non-deuterated solvent background. This is beneficial if a greater signal is necessary or if a single component sample is under investigation.

Despite the benefits of molecular deuteration in scattering techniques, there are some considerations to bear in mind; namely if the deuteration of lipid components truly reflects the same system when non-deuterated. Deuteration is known to affect the phase transition temperature of phospholipids[21,22] and the high resolution structural composition of lipid systems[22,23]. For low resolution studies, however, hydrogenous and deuterated lipid systems are often considered to be interchangeable.

In this work, a new protocol based on *in vivo* biosynthetic methods for the production of deuterated cholesterol is presented. The cholesterol was characterised by mass spectrometry (MS), nuclear magnetic resonance (NMR), and SANS. Moreover, the matchout cholesterol is used to further investigate its location in different lipid bilayers by NR. Specifically, we use supported lipid bilayers (SLBs) of matchout deuterated cholesterol-containing phosphatidylcholine (PC) with various saturated lengths (C14:0 DMPC and C12:0 DLPC) and level of unsaturation (1-palmitoyl-2-oleoyl-glycero-3-phosphocholine, C16:0,18:1 or POPC).

Results

Growth and Fermentation Conditions for the Production of Matchout-Deuterated Cholesterol.

*Per*deuteration of cholesterol can be achieved in high cell density cultures using lipo engineered strains of *Pichia pastoris* grown in a medium containing the solvent (D_2O) and a carbon source (d8-glycerol) in their deuterated forms[24]. To reduce the deuteration level to a level required for matchout labelling, a medium containing D_2O and unlabelled glycerol was used. Cells were adapted to growth in the deuterated medium prior to high cell density cultures. At the end of the fermenter run, the final optical density measured at 600 nm (OD_{600}) was 42 and the cellular wet weight (CWW) was 37 g, giving a final yield of 66.5 mg of matchout-deuterated cholesterol for 1 litre of culture.

Structural Characterisation of Matchout-Deuterated Cholesterol. The analysis of the lipid fractions from the purified cell paste, as carried out by gas chromatography coupled with mass spectrometry (GC-MS) (in duplicate – green and orange curves), showed a peak eluting at 28.1 min (Fig. 1A). This peak corresponds to cholesterol. The retention times and composition as estimated by the area under the chromatographic peaks are given in Table 1. The presence of cholesterol is demonstrated by the MS spectrum that shows a main peak at 499 m/z (Fig. 1B). This main peak corresponds to cholesterol with a mass of 427 g/mol. The cholesterol shown has undergone silylation during the derivatisation process, where a trimethylsilyl moiety with a mass of 72 g/mol leading to the total mass of the complex at 499 m/z was added. This step is required to ensure sufficient volatility of the sample, enabling accurate and efficient GC-MS analysis[25]. The remaining peaks were assigned by comparison to a non-deuterated sample, as was reported previously[24]. These sterols also had additional peaks in their MS chromatograms arising from various intermediates during their synthesis.

The cholesterol produced, labelled MO-chol in Fig. 2 and Table 2, was found to have an 89% level of deuteration by ^{1}H-NMR. This level of deuteration accounts for 41 deuterium atoms and 5 protiums, giving a mass of 427 g/mol; this is supported by the GC-MS data.

Contrast Match Point Determination. The scattering intensities of each series (either pure non-deuterated POPC or its mixtures with matchout cholesterol) are shown in Fig. 3A. The contrast match point (CMP) was determined for the composition of the solvent at $y = 0$ in Fig. 3B. The CMP for non-deuterated POPC including 40 mol% matchout cholesterol is an overall value and corresponds to the presence of both lipids and cholesterol.

Using the CMP for both series and Eqs 3–5 the CMP for cholesterol alone was found to be 101%, corresponding to a ρ value of 6.5×10^{-6} Å^{-2}, as summarised in Table 2. The value obtained for the ρ is in excellent agreement with both the MS and NMR data. The errors given were determined using standard deviation analysis.

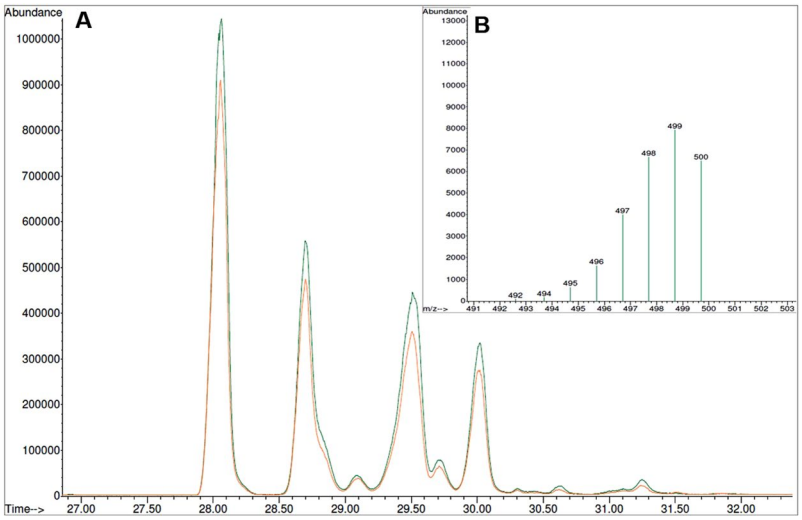

Figure 1. GC-MS analysis of the sterol components extracted from the partially deuterated cell paste. (**A**) GC-MS chromatogram showing the total sterol components, each sample was run in duplicate (green and orange curves). The first and main peak corresponds to cholesterol. Further details relating to the remaining peaks are given in Table 1. (**B**) MS spectrum for the isolated cholesterol component showing the main mass peak.

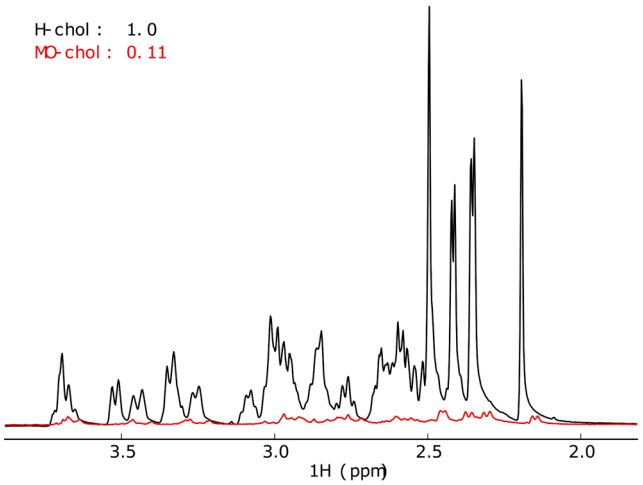

Figure 2. ^{1}H-NMR spectra for non-deuterated and matchout-deuterated cholesterol in black and red respectively. These spectra were measured in CD_3OD and at a concentration of 2 mM. The spectra were collected on a Bruker 1D NMR spectrometer at 600 MHz.

Peak	Compound	Retention Time (RT) (min)	Rel. RT	% of Total Sterols
1	Cholesterol	28.1	1.000	47.1 ± 1.3
2	7-DHC	28.7	1.023	23.2 ± 0.3
3	Zymosterol	29.1	1.037	1.3 ± 0.0
4	Cholesta-5,7,14,24(25)-tetraenol	29.5	1.052	26.1 ± 1.4
5	Cholesta-7,24(25)-dienol	29.7	1.059	2.2 ± 0.2
6	Ergosterol (IS)	30.0	1.070	
Total sterols	4.5 ± 0.2 ug/mg (CWW)			

Table 1. Table of sterol components in GC-MS sample.

Structure and Localisation of Matchout-Deuterated Cholesterol in Saturated and Monounsaturated Phospholipid Bilayers. Three different SLBs were studied using NR to determine the positioning of the cholesterol within the bilayer: non-deuterated DMPC, POPC and DLPC each containing 40 mol% matchout-deuterated cholesterol. The three Tris buffer contrasts in D_2O, H_2O and a mixture giving the same ρ to

POPC	% POPC	% CHOL	$\rho_{POPC} \times 10^{-6}$ Å^{-2}	$\rho_{MO\text{-}CHOL} \times 10^{-6}$ Å^{-2}	CMP_{TOT}	$CMP_{MO\text{-}CHOL}$
Without MO-CHOL	100	0	0.44 ± 0.02		15 ± 1	
With MO-CHOL	60	40	0.44 ± 0.02	6.5 ± 0.2	37 ± 2	101 ± 2

Table 2. Summary of the experimentally determined CMPs and ρ values obtained for the lipid vesicles.

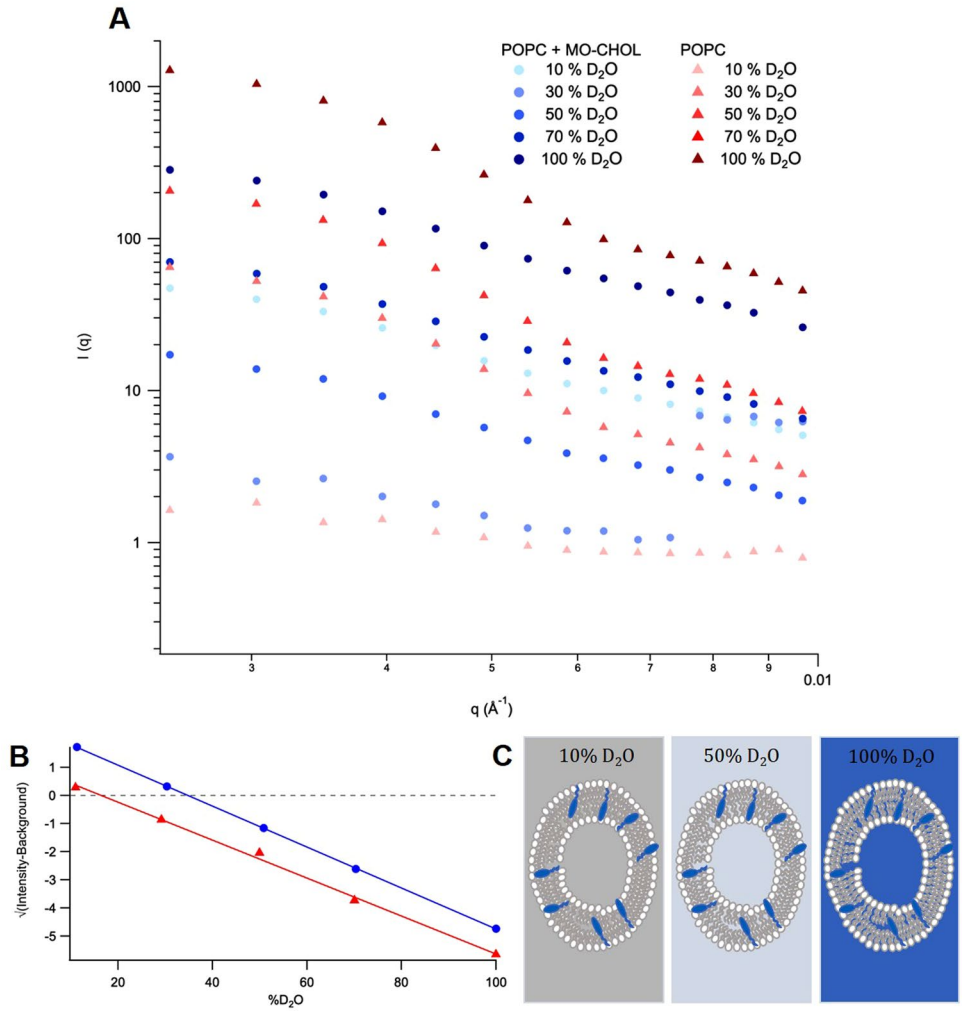

Figure 3. (**A**) The SANS spectra for the non-deuterated POPC series in the absence (red triangles) and presence (blue circles) of matchout cholesterol (MO-CHOL) in 10%, 30%, 50%, 70% and 100% D_2O (v/v) contrasts. (**B**) The contrast match point series measured for non-deuterated POPC in the absence (red triangles) and presence (blue circles) of matchout cholesterol, measured in 10%, 30%, 50%, 70% and 100% (v/v) D_2O contrasts. The lines are a linear fit to the data given by the symbols. (**C**) Pictorial representation of the model for the vesicles used in the SANS matchout series with POPC in the presence of 40 mol% cholesterol at contrasts of 10% D_2O matching out the lipids tails, 50% D_2O showing all components of the vesicles and 100% D_2O matching out the cholesterol.

contrast match the silicon block (cmSi) gave structural and compositional information on the bilayer and the data were fitted to a model as shown in Fig. 4A. The model includes the silicon block with a small silicon dioxide layer in contact with a small solvent layer followed by the bilayer. The bilayer is broken up into five-layers: an inner head group, three distinct tail regions and an outer head group exposed to the solvent contrast. The three sections of the tail core allow for an asymmetric distribution of cholesterol, as reported previously[26]. The thickness, coverage and roughness of the tail regions were all constrained during the fitting process to be symmetric (each of these parameters were kept equal throughout all three core layers) to limit the number of variables. However, the ρ for each section of the core was allowed to vary, granting the distribution of cholesterol throughout the bilayer.

Alternative models with only one or two layers in the lipid core were also tried. However, the fits were not satisfactory, suggesting an oversimplification of the composition of the SLB, assumed to be symmetrical and uniform throughout the core. A five-layer model was therefore necessary to understand where the cholesterol was located

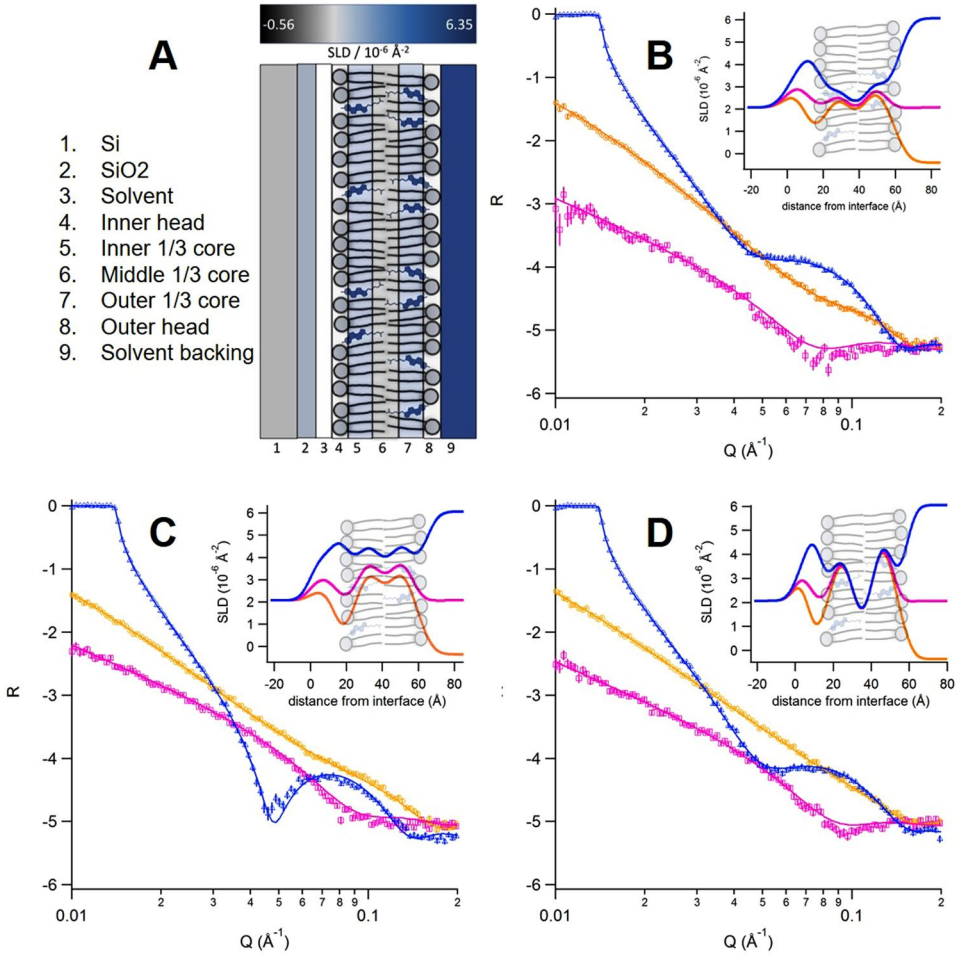

Figure 4. (**A**) Five layer model used to fit the SLBs at the SiO_2-aqueous interface, and reflectivity curves for cholesterol-containing (**B**) DMPC, (**C**) DLPC and (**D**) POPC SLBs. The SLBs were formed by vesicle fusion at 37 °C using a vesicle composition of 60 mol% PC and 40 mol% cholesterol. The blue triangle, orange circle and pink square curves coincide with different contrasts (100% deuterated Tris buffer, 100% non-deuterated Tris buffer and cmSi respectively). The insets in (**B**–**D**) show the ρ profile for the best fits to the five layer model.

in the core - whether it accumulates in the centre of the bilayer core or positions itself at the edges of the bilayer close to the headgroups as seen previously[11,26].

Figure 4B–D shows the NR curves for the three different SLBs studied, in each of the three isotopic contrasts (D_2O, H_2O and cmSi, in blue, pink and orange respectively). The best fitting parameters are given in Table 3. The total (and core) thickness for the bilayers are 45 (29.7) Å, 46 (31.5) Å and 44 (30.3) Å for the cholesterol-containing DMPC, POPC and DLPC SLBs respectively. In all three SLBs, the outer regions of the lipid core are enriched with cholesterol; this can be seen with the increase in ρ in the outer regions of the core, corresponding to the increased ρ value of the cholesterol compared to the lipid tails alone. In the DMPC bilayer, the inner (that closer to the Si block surface) and outer sections of the lipid core present an enrichment in cholesterol with 52 mol% and 61 mol% while only 20 mol% cholesterol is present in the central region of the lipid core. This gives an average of 45 mol% cholesterol content in the SLB, which is expected and very close to the nominal value of the parent vesicles used for the SLB formation. In the POPC bilayer, the inner and outer regions of the tail core contain 64 mol% and 75 mol% cholesterol while only 21 mol% is present in the middle section of the core, thus giving an overall 53 mol% cholesterol in the SLB. This is slightly higher than the nominal value to be expected from the parent vesicles. The DLPC SLB also contained enriched outer regions of the tail core with 72 mol% and 75 mol% for the inner and outer leaflets respectively, and only 47 mol% in the middle region. This in turn gives an average of 65 mol% cholesterol present in the DLPC SLB, which is again higher than the expected nominal value. Compositional deviations in SLBs from their parental vesicles for a two component system containing PC lipids close to its phase separation boundary and when using the vesicle fusion approach have been reported previously[15].

Sample		$\rho \times 10^{-6}$/Å^{-2}	MO-Chol %	Thickness/Å	Coverage %	MMA/Å^2
DMPC +40 mol% cholesterol	Inner Head	1.89*		8.2 ± 0.5**	92 ± 2**	43 ± 3
	Tail (3 sublayers)	3.2 ± 0.3	52 ± 5	29.7 ± 0.8**	93 ± 1**	50 ± 2
		1.0 ± 0.5	20 ± 9			54 ± 2
		3.8 ± 0.3**	61 ± 5			49 ± 2
	Outer Tail	1.89*		8.2 ± 0.5**	92 ± 2**	43 ± 3
			Average: 45 ± 11	**Total: 46 ± 1**		
POPC +40 mol% cholesterol	Inner Head	1.89*		7.2 ± 0.2**	87 ± 3**	52 ± 2
	Tail	4.06 ± 0.07	64 ± 1	31.5 ± 0.3**	99 ± 1**	47 ± 1
		1.11 ± 0.08	21 ± 1			56 ± 1
		4.83 ± 0.07**	75 ± 1			45 ± 1
	Outer Tail	1.89*		7.2 ± 0.2**	87 ± 3**	52 ± 2
			Average: 53 ± 2	**Total: 45.9 ± 0.4**		
DLPC +40 mol% cholesterol	Inner Head	1.89*		7.0 ± 0.3**	74 ± 3**	63 ± 4
	Tail	4.6 ± 0.2	72 ± 3	30.3 ± 0.5**	83 ± 1**	50 ± 2
		2.9 ± 0.2	47 ± 3			51 ± 2
		4.8 ± 0.1**	75 ± 2			50 ± 2
	Outer Tail	1.89*		7.0 ± 0.3**	74 ± 3**	63 ± 4
			Average: 65 ± 5	**Total: 44.4 ± 0.7**		

Table 3. Structural parameters obtained from fitting of derived model to the reflectivity curves for the bilayers. *Values kept constant during the fitting process. **The errors are given in Table 3 and are calculated using a Monte-Carlo analysis as embedded in the motofit software[43].

Discussion

In this paper, a new protocol is presented for the production of matchout-deuterated cholesterol in a yeast host. The method is based on growing a genetically modified yeast strain[27] in deuterated media using a non-deuterated carbon source (glycerol) to obtain the required level of deuteration. Both MS (Fig. 1) and ^{1}H NMR (Fig. 2) suggest a level of deuteration of the cholesterol of 89%, corresponding to 41 deuterium and 5 protium atoms. The asymmetric distribution of ions for the main peak in the MS spectrum (Fig. 1B) implies no compounds have a higher deuteration level than 89% (there is otherwise a Gaussian distribution of deuteration around the main ion)[24,28]. This demonstrates the efficacy of the production method and its practical application for the matchout deuterium labelling that is often extremely helpful in neutron scattering work[29,30]. From the biosynthetic pathway, an outline of which can be seen in the Supplementary Information Scheme SI1, it is obvious that the presence of *per*deuterated solvent largely determines the level of deuteration in cholesterol. Since the non-deuterated glycerol is the only carbon source in the growth media, it provides the carbon backbone of cholesterol and all the original protiums. Certain protium atoms in this carbon backbone have a lower likelihood to undergo deuterium exchange during the biosynthesis process. The tautomerisation of Acetyl CoA (see Scheme 2 in Supplementary Information) results in an equilibrium of products which largely determines the level of deuteration in the final product, as it is during this step there is most uncertainty in the resulting hydrogen atoms. These equilibrium products react together to continue along the biosynthetic pathway. Therefore, from the biosynthesis of cholesterol we can expect that the use of non-deuterated glycerol as the sole carbon source will result in at least five protiums not being exchanged by deuterium - four present in methyl groups and one labile protium on the oxygen. The number of protium atoms incorporated into matchout cholesterol as determined by MS and NMR allowed the calculation of a theoretical ρ of 6.5×10^{-6} Å^{-2}. The experimental SANS data (Fig. 3) confirmed the ρ of the matchout deuterated cholesterol preparation to be 6.5×10^{-6} Å^{-2}. This corresponds to the (notional) CMP of 101% D_2O solvent.

This D_2O matchout cholesterol preparation was used to investigate the positioning of the cholesterol molecules within the leaflets of SLBs made of various PC lipids. NR was chosen due to it being a highly suitable technique for studying density profiles of lipid films in a direction perpendicular to an interface and having down to a few Angstroms resolution[13,14]. In a previous study, a five-layer model for SLBs made of natural, D_2O matchout deuterated PC extracts has been used to show the asymmetrical distribution of both non-deuterated and *per*deuterated cholesterol throughout the lipid core and that the molecule is located close to the PC headgroups[26]. In that work, *per*deuterated cholesterol and non-deuterated cholesterol was mixed with D_2O matched natural PC bilayers specifically to give contrast and highlight the cholesterol, whereas here we use non-deuterated bilayers and D_2O matched cholesterol to ensure minimal signal from the cholesterol while being able to specifically compare the scattering from the lipid bilayers. An advantage of the previous work was the use of a lipid extract to determine the structure and positioning of cholesterol within a bilayer made of natural lipids. However, a drawback to the use of a natural lipid extract, and in turn an advantage of using singular lipid species in this instance, is the well-defined lipid volumes attainable and necessary for the detailed structural information extracted. A systematic study of single lipid structures is possible, in turn verifying the model previously determined. The 5 layer (head layer- 3 equally thick lipid core sublayers - head layer) model was used here to determine the location

of cholesterol within the bilayer as a function of the length of saturated lipids (C12 vs C14) and the presence of unsaturation (POPC). This is relevant to recent NMR, MD and SANS analyses that suggest that the PC species determines the positioning of cholesterol within the lipid bilayer[11]. In particular, it has been suggested that the thickness of the bilayer core may determine the position and orientation of cholesterol - with thin bilayers forcing the cholesterol out of the bilayer structure and into the middle section of the lipid core: for cholesterol-containing lipid films where the half core thickness is shorter than the extended length of a cholesterol molecule (15 Å) the steroid moiety tilts and descends into the bilayer centre.

In the absence of (and presence of 10 mol%) cholesterol, the lipid bilayer core thickness was reported to be 30 Å[31], 25.8 (34.1) Å[11,32] and 21.8 (28.2) Å[11,32] for POPC, DMPC and DLPC respectively at similar experimental conditions. Therefore, these SLBs should probe whether the bilayer core thickness affects the positioning of cholesterol within the lipid bilayer structure: the thicker DMPC and POPC bilayers should lead to cholesterol being closer to the headgroups, while DLPC should lead to cholesterol being gathered in the middle of the core.

The results obtained here show that the cholesterol was located nearer the headgroups in all of the SLBs studied, as can be seen from the difference in ρ values for the different regions in the hydrophobic core arising from the cholesterol-rich regions (insets in Fig. 4). The core thicknesses were found to be (within the experimental error) 30 Å for DMPC and DLPC, and slightly thicker (by 1.5 Å) for POPC. As already discussed, Marquardt *et al.*[11] hypothesised a limit of 30 Å for the displacement of cholesterol from the upright positioning towards the centre of the bilayer core. Kučerka *et al.*[33] found when polyunsaturated lipids alone in the presence of cholesterol induced the cholesterol positioning to be in the centre of the bilayer, whereas the co-addition of as few as 5 mol% DMPC induced the upright positioning of cholesterol near the lipid headgroups due to the increased level of order it provided. Both phenomena are in agreement with the data provided here whereby the high cholesterol content (>45 mol%) provides a high level of order in the bilayers thus inducing the cholesterol to remain in an upright position, regardless of saturation level or chain length.

The concentration of cholesterol present (65 mol%) in the DLPC SLB means the bilayer is likely to be in a liquid-ordered phase or even on the boundary of a crystalline and lamellar phase, which is cholesterol-rich, at 37 °C[34]. This increase in cholesterol concentration could lead to the formation of crystalline cholesterol regions, especially near the headgroups. Similarly, the DMPC SLB contained 45 mol% cholesterol which would imply that the bilayer would be in a quite rigid liquid-ordered phase[35].

For the cholesterol containing POPC bilayers, the sole unsaturated lipid studied, cholesterol was located at the head-tail interface. This is expected as it has been previously reported that for unsaturated bilayers the cholesterol tends to be located nearer the headgroups[26]. Interestingly, the phase of the cholesterol containing POPC bilayer was also likely to be liquid-ordered due to the slightly increased level of cholesterol. At 40 mol% cholesterol, the POPC-cholesterol phase diagram[36] predicts the coexistence of the liquid-ordered and liquid-disordered phases at 37 °C. However, the NR data showed slightly higher levels of cholesterol present (53 mol%) thus pushing the phase slightly over into the liquid-ordered region of the phase diagram. Earlier it has been found that the composition of SLB can differ from that of the nominal vesicles, and this has to do with differences in composition at the single vesicle level that are size dependent and is more marked for mixtures that are close to a phase transition boundary[15].

The experiments performed by Marquardt *et al.*[11] contained phospholipids with only 10 mol% cholesterol. Under these conditions, the bilayers are likely to be in the liquid-disordered phase. Hence, it would seem possible that the liquid crystalline phase of the cholesterol containing lipids may also play a key role in determining the positioning of the molecules in addition to the total thickness of the core or level of saturation of the core.

It is well known that *per*deuteration of lipids can impact their phase transition behaviour[22]. Recently, it was reported that the *per*deuteration of lipids reduced their bilayer thickness besides reducing their melting temperature. Even though the phase transition reported is not of that between a co-existing mixture of liquid disordered and liquid ordered to solely liquid ordered (as shown here), a similar effect is likely to be seen. However, it is important to note that it was also reported that the bilayer structure was not much altered away from the melting temperature. Their suggestion to overcome the differences induced by the deuteration is to use only partial deuteration to benefit from the difference in ρ without perturbing the bilayer itself significantly. The work here uses non-deuterated lipids and partially deuterated cholesterol which meets these requirements, thus implying there should be little interference and the use of the partially deuterated cholesterol is suitable to verify the previously established protocol and model.

Understanding the data presented here can help to determine the effect that cholesterol exerts on a bilayer, which can in turn give further insight into the function of cholesterol itself and how bilayers, and therefore cellular membranes, behave. This is particularly important for the structure and function of endothelial membranes (that contain about 20 mol% cholesterol[37]) and neural cells (that contain up to 40 mol% cholesterol[38,39]). Additional experiments using a wider range of cholesterol contents are needed to clarify the role of bilayer thickness for the distribution of cholesterol, however it should be emphasised that the accuracy of NR decreases sharply with reduced contrast (which would be the case of a SLB containing only 10 mol% cholesterol).

The availability of matchout-deuterated cholesterol opens up a range of additional possibilities of for membrane, cholesterol and protein structural studies. For example studies of matchout deuterated cholesterol may be used in combination with matchout deuterated PC[28] to enable studies of the role that cholesterol plays in membrane protein structure and function in matchout deuterated nanodiscs[40] and lipid-exchange studies in lipoproteins (unpublished results).

Conclusions

A method has been developed for the production of matchout deuterated cholesterol for use in neutron scattering studies by the simple incorporation of non-deuterated glycerol in the otherwise deuterated growth medium, further demonstrating how the carbon source used in cultures can be used to control the level of deuteration in biomass.

The development of matchout-deuterated cholesterol allows for studies of its positioning within the lipid membrane, as demonstrated in the NR studies described here. It also opens up other options including the study of its regulation of membrane proteins[17], its metabolism and uptake by cellular complexes such as lipoproteins, and other aspects that impact in terms of both structure and function in relation to other components in the cell membrane. In general, the inclusion of cholesterol in lipid bilayers gives a more realistic model membrane than phospholipids alone.

Materials and Methods

Theoretical D_2O Match Point of Cholesterol. During the biosynthetic synthesis of cholesterol many protons are exchanged during enzymatic processes, therefore if a *per*deuterated growth medium is used the majority of protium atoms will be exchanged for deuterium atoms present in the medium. A ρ calculator was used to determine a theoretical ρ value for matchout cholesterol whereby only 5 hydrogen atoms would be required to remain as protium whereas the remaining 41 hydrogens could be exchanged to deuterium. Throughout the process most hydrogen atoms are exchanged meaning using a non-deuterated carbon source provides the correct level of non-deuteration in the overall solution mixture.

Production of Yeast Biomass. Matchout-deuterated cholesterol was produced in the Deuteration Laboratory of ILL's Life Sciences Group and purified using a protocol modified from that described by Moulin *et al.*[24] for the production of perdeuterated cholesterol. In order to achieve a matchout level of deuteration, the previously genetically modified *Pichia pastoris* yeast strain was grown in the presence of non-deuterated glycerol as the sole carbon source in D_2O minimal medium. One litre of deuterated basal salts medium (BSM) containing 10 g non-deuterated glycerol was inoculated ($OD_{600} = 2.7$) and grown in a three litre fermenter (Labfors, Infors) for a duration of three weeks. The pD level was monitored and adjusted by the addition of NaOD. After about a week when all of the glycerol had been consumed, the fed-batch phase was initiated by continuous feeding of a further 30 g of glycerol over 12 days.

Purification of Partially Deuterated Cholesterol. Cholesterol was extracted and purified from the cell paste and analysed as reported previously[24]. The cell paste (batches between 27.5 and 34.5 g) was transferred into a 500 mL round-bottomed flask into which 60 g potassium hydroxide, 200 mL water, 100 mL methanol and 400 mg pyrogallol was added. The mixture was heated under gentle reflux for 3 h under a nitrogen atmosphere with minimal stirring to avoid foaming. After cooling to room temperature, 100 mL cyclohexane was added and the mixture stirred for another hour. Insoluble materials were then removed by filtration, once the mixture had cooled to room temperature, and the cyclohexane layer formed was separated using a separatory funnel. The methanolic solution was extracted a further two times each with 100 mL cyclohexane. The combined three cyclohexane extracts were washed with 100 mL water, dried over sodium sulphate and concentrated under reduced pressure. From a total of 123.7 g cell paste, 788 mg crude solid extract was obtained. To pre-purify the matchout-deuterated cholesterol, a flash chromatography on silica gel (silica gel 60, 0.040–0.063 mm, No. 109385, Marck, Darmstadt, Germany) using cyclohexane/ethyl acetate mixtures from 20:1 to 3:1 (v/v) was conducted. After removing the solvents under reduced pressure, 317 mg pre-purified material was obtained and, thus, the final HPLC separation could be done in a single run with the available equipment. Propan-1-ol proved to be a highly suitable solvent for dissolving the crude material in 2 mL volume. The cholesterol was isolated in pure form using a ThermoFisher UltiMate 3000 binary semi-preparative HPLC system equipped with a NUCLEODUR® 100-10 C18ec column (125 mm × 21 mm, 5 µm, Macherey-Nagel, Düren, Germany) attached to a VP 20/16 NUCLEODUR® C18ec guard column. Using an isocratic mixture consisting of acetonitrile/methanol (95:5) at a flow rate of 20 mL/min at 30 °C, the desired product eluted baseline-separated between 27.9 and 34.3 min as monitored by UV-detection at 210 nm. After removing the solvent under reduced pressure, 66.5 mg pure matchout-deuterated cholesterol was obtained. Analytical HPLC analysis of the final product purity was conducted on an Agilent 1100 system, equipped with a DAD detector and a NUCLEODUR® C18 gravity column (150 mm × 3 mm, 3 µm, No. 760083.30, Macherey-Nagel, Düren, Germany) using an isocratic mixture of acetonitrile/methanol 1:1 at a flow rate of 0.70 mL/min at 30 °C. The eluting peak at 8.24 min represents the desired product with a purity of >99% as checked by UV at 210 nm detection wavelength.

Structural Characterisation of Partially Deuterated Cholesterol. *Gas Chromatography Mass Spectrometry of Cholesterol.* Gas chromatography coupled with mass spectrometry (GCMS) was carried out as reported previously[24]. 1 mL 0.2% pyrogallol in methanol and 400 µL 60% potassium hydroxide was used to resuspend 15 mg cell paste in Pyrex tubes. 10 µg ergosterol (1 mg/mL) were used as an internal standard and the sample was saponified at 90 °C for 2 h. The sample was extracted with *n*-heptane three times over and dried under a constant stream of nitrogen. 10 µL pyridine was used to dissolve the dried extracts, then derivatised with 10 µL *N*,*O*-bis(trimethylsilyl)trifluoracetamide. Samples were diluted in 50 µL ethyl acetate and analysed by GC-MS.

Nuclear Magnetic Resonance. The level of deuteration of the cholesterol was determined by ^{1}H-NMR, measured at the Institut de Biologie Structurale (IBS), Grenoble, France. The samples were measured at a 4 mM concentration in deuterated chloroform. No internal standard was used. However, the non-deuterated cholesterol sample was set as a reference for 0% deuteration. The instrument used was a 600 MHz Bruker NMR spectrometer with an avance III HD console. A spectral width of 25 ppm was obtained, 32 scans were carried out with a relaxation delay of 20 sec and an acquisition time of 0.5 sec per scan. Bruker TopSpin software was used to analyse the data.

Lipid Vesicle and Supported Lipid Bilayer Formation. The lipids; 1-Palmitoyl-2-oleoyl-glycero-3-phosphocholine (POPC), 1,2-dimyristoyl-sn-glycero-3-phosphocholine (DMPC or C14 PC), 1,2-dilauroyl-sn-glycero-3-phosphocholine (DLPC or C12 PC), non-deuterated cholesterol and the extruder setup were purchased from Avanti Polar Lipids (Alabaster, AL).

For SANS, non-deuterated POPC lipid films were prepared in the presence and absence of 40 mol% partially deuterated cholesterol. The lipids were mixed from chloroform stocks of both POPC and cholesterol. The chloroform was evaporated using a nitrogen stream and the resulting films were put under vacuum overnight. The films were hydrated in D_2O to a concentration of 50 mg/mL, extruded using a 100 nm filter and thereafter diluted 10-fold with varying H_2O/D_2O ratios. The lipids were used at a final concentration of 5 mg/mL in 10%, 30%, 50%, 70% and 100% D_2O/H_2O (v/v). By using a lipid stock prepared in 100% D_2O for each lipid type, the same vesicle preparation was ensured for each series.

The lipids films required for NR were further hydrated in Milli-Q water to a concentration of 0.2 mg/mL and bath sonicated for 1 h. The lipid solutions were then tip sonicated for 5 min, at 10% power 5 sec on, 5 sec off, just before use. For optimum vesicle fusion, a 0.1 mg/mL solution of lipids in the presence of 2 mM $CaCl_2$ was used[15], by mixing equal volumes of the tip sonicated lipids with a 4 mM $CaCl_2$ solution[26,41]. The sample was then introduced into the flow cell by a syringe injection and left to incubate at 37 °C for 20 min before rinsing the excess off in water followed by Tris buffer (50 mM Tris-HCl, 150 mM NaCl).

Neutron Scattering. SANS and NR data were collected where the scattered intensity as a function of the momentum transfer vector $q = 4\pi * sin(\theta)/\lambda$, were measured.

Determination of Contrast Match Point using SANS. SANS data were collected on the D22 instrument at the Institut Laue-Langevin (ILL) in Grenoble. The experiments were carried out at 25 °C using detector distances of 1.4, 5.6 and 17.6 m, providing a total q range of $0.002 < q < 0.56$ Å^{-1}. The CMP was obtained from the graph shown in Fig. 3B which plots $\sqrt{}$(intensity-background) against D_2O concentration (ϕ). Here, the intensity value corresponds to the average of the intensities between $0.003 < q < 0.012$ Å^{-1} and the background value corresponds to the average of the intensities between $0.45 < q < 0.55$ Å^{-1}. The data were corrected for the empty cell, background and used in absolute scale compared to the direct beam measurement. The cell thickness was 1 mm quartz glass Helma SANS cuvettes and the data reduction was carried out using GRASP.

The scattered intensity, $I(q)$, of a vesicle solution is related to the form factor, $P(q)_{lipid}$, volume, V_{lipid}, number density, n, of the vesicles, and the difference in ρ between the vesicles (ρ_{lipid}) and the solvent ($\rho_{solvent}$):

$$I(q) = n * V_{lipid}^2 * (\rho_{lipid} - \rho_{solvent})2 * P(q)_{lipid} + I_{incoherent} \quad (1)$$

where ρ is given by the total sum of scattering lengths (b_i) over the total volume (V):

$$(\rho) = \Sigma b_i / V \quad (2)$$

From the contrast match point (CMP), the ρ of sample can be acquired using the equation:

$$\rho_{sample} = CMP_{TOT} * \rho_{D2O} + (1 - CMP_{TOT}) * \rho_{H2O} \quad (3)$$

For the two component systems, the overall ρ can be broken down into the following equation that combines each components ρ and volume ratio (ϕ):

$$\rho_{sample} = \phi_{POPC} * \rho_{POPC} + \phi_{CHOL} * \rho_{CHOL} \quad (4)$$

For the two component systems, the CMP can be broken down into the following equation that combines component CMP and ϕ:

$$CMP_{TOT} = \phi_{POPC} * CMP_{POPC} + \phi_{CHOL} * CMP_{CHOL} \quad (5)$$

By rearranging this equation, the ρ of the cholesterol can be found from the overall CMP and the subsequent overall ρ.

Neutron Reflectometry Study. NR data were collected on the INTER instrument at the ISIS neutron facility, Didcot, UK[42], and fitted using the MOTOFIT package[43]. The experiments were carried out at 37 °C using bespoke solid-liquid flow cells. The resolution was set to $\Delta q/q = 3\%$ and the incident angles used were 0.7° and 2.3°. The area illuminated by the neutron beam was 30×60 mm^2. The polyether ether ketone (PEEK) components of the cell were cleaned thoroughly using bath sonication in 2% (v/v) Hellmanex twice and MilliQ water, with rinsing in MilliQ water between each sonication. The Silicon (111) blocks used for depositing the bilayer were cleaned using Piranha solution (H_2SO_4/H_2O_2, 7:3) for 10 min at 80 °C before thorough rinsing with MilliQ water.

The DMPC, POPC and DLPC all containing 40 mol% matchout deuterated cholesterol SLBs were deposited in 2 mM $CaCl_2$ and measured in three contrasts: D_2O, H_2O and a mixture which contrasts matches the silicon (cmSi) using Tris buffer, as previously mentioned.

References

1. Simons, K. & Ikonen, E. Functional rafts in cell membranes. *Nature* **387**, 569–572 (1997).
2. Armstrong, C. L. *et al.* Effect of cholesterol on the lateral nanoscale dynamics of fluid membranes. *Eur. Biophys. J.* **41**, 901–913 (2012).
3. de Almeida, R. F. M. & Joly, E. Crystallization around solid-like nanosized docks can explain the specificity, diversity, and stability of membrane microdomains. *Front. Plant Sci.* **5**, 1–14 (2014).

4. Smaby, J. M., Momsen, M., Kulkarni, V. S. & Brown, R. E. Cholesterol-induced interfacial area condensations of galactosylceramides and sphingomyelins with identical acyl chains. *Biochemistry* **35**, 5696–5704 (1996).
5. Demel, R. A., Van Deenen, L. L. M. & Pethica, B. A. Monolayer interactions of phospholipids and cholesterol. *Biochim. Biophys. Acta* **135**, 11–19 (1967).
6. Léonard, A. *et al*. Location of Cholesterol in DMPC Membranes. A Comparative Study by Neutron Diffraction and Molecular Mechanics Simulation†. *Langmuir* **17**, 2019–2030 (2001).
7. Karmakar, S. & Raghunathan, V. A. Structure of phospholipid-cholesterol membranes: An x-ray diffraction study. *Phys. Rev. E - Stat. Nonlinear, Soft Matter Phys.* **71**, 1–10 (2005).
8. Gallová, J. *et al*. The effects of cholesterol and β;-sitosterol on the structure of saturated diacylphosphatidylcholine bilayers. *Eur. Biophys. J.* **40**, 153–163 (2011).
9. Harroun, T. A., Katsaras, J. & Wassall, S. R. Cholesterol hydroxyl group is found to reside in the center of a polyunsaturated lipid membrane. *Biochemistry* **45**, 1227–1233 (2006).
10. Harroun, T. A., Katsaras, J. & Wassall, S. R. Cholesterol hydroxyl group is found to reside in the center of a polyunsaturated lipid membrane. *Biochemistry* **47**, 7090–7096 (2008).
11. Marquardt, D. *et al*. Lipid bilayer thickness determines cholesterols location in model membranes. *Soft Matter* **12**, 9417–9428 (2016).
12. Brzustowicz, M. R., Cherezov, V., Caffrey, M., Stillwell, W. & Wassall, S. R. Molecular organization of cholesterol in polyunsaturated membranes: Microdomain formation. *Biophys. J.* **82**, 285–298 (2002).
13. Lind, T. K. & Cárdenas, M. Understanding the formation of supported lipid bilayers via vesicle fusion—A case that exemplifies the need for the complementary method approach (Review). *Biointerphases* **11** (2016).
14. Fragneto, G. Neutrons and model membranes. *Eur. Phys. J. Spec. Top.* **213**, 327–342 (2012).
15. Åkesson, A. *et al*. Composition and structure of mixed phospholipid supported bilayers formed by POPC and DPPC. *Soft Matter* **8**, 5658–5665 (2012).
16. Vacklin, H. P., Tiberg, F., Fragneto, G. & Thomas, R. K. Composition of supported model membranes determined by neutron reflection. *Langmuir* **21**, 2827–2837 (2005).
17. Jagalski, V. *et al*. Grafted biomembranes containing membrane proteins - the case of the leucine transporter. *Soft Matter* **11**, 7707–7711 (2015).
18. De Ghellinck, A. *et al*. Lipid polyunsaturation determines the extent of membrane structural changes induced by Amphotericin B in Pichia pastoris yeast. *Biochim. Biophys. Acta* **1848**, 2317–2325 (2015).
19. Dunne, O. *et al*. Matchout deuterium labelling of proteins for small-angle neutron scattering studies using prokaryotic and eukaryotic expression systems and high cell-density cultures. *Eur. Biophys. J.* **46**, 425–432 (2017).
20. Haertlein, M. *et al*. Biomolecular Deuteration for Neutron Structural Biology and Dynamics. *Methods in Enzymology* **566** (2016).
21. Guard-Friar, D., Chen, C. & Engle, A. S. Deuterium Isotope Effect on the Stability of Molecules: Phospholipids. *J. Phys. Chem.* **89**, 1810–1813 (1985).
22. Bryant, G. *et al*. Effect of deuteration on the phase behaviour and structure of lamellar phases of phosphatidylcholines - Deuterated lipids as proxies for the physical properties of native bilayers. *Colloids Surfaces B Biointerfaces* **177**, 196–203 (2019).
23. Luchini, A. *et al*. The impact of deuteration on natural and synthetic lipids: A neutron diffraction study. *Colloids Surfaces B Biointerfaces* **168**, 126–133 (2018).
24. Moulin, M. *et al*. Perdeuteration of cholesterol for neutron scattering applications using recombinant Pichia pastoris. *Chem. Phys. Lipids* **212**, 80–87 (2018).
25. Dettmer-Wilde, K. & Engewald, W. Practical Gas Chromatography. (Springer - Verlag Berlin Heidelberg, 2014).
26. Waldie, S. *et al*. Localization of Cholesterol within Supported Lipid Bilayers Made of a Natural Extract of Tailor-Deuterated Phosphatidylcholine. *Langmuir* **34**, 472–479 (2018).
27. Hirz, M., Richter, G., Leitner, E., Wriessnegger, T. & Pichler, H. A novel cholesterol-producing Pichia pastoris strain is an ideal host for functional expression of human Na,K-ATPase α3β1 isoform. *Appl. Microbiol. Biotechnol.* **97**, 9465–9478 (2013).
28. Maric, S. *et al*. Biosynthetic preparation of selectively deuterated phosphatidylcholine in genetically modified Escherichia coli. *Appl. Microbiol. Biotechnol.* **99**, 241–254 (2015).
29. Banc, A. *et al*. Small angle neutron scattering contrast variation reveals heterogeneities of interactions in protein gels. *Soft Matter* **12**, 5340–5352 (2016).
30. Laux, V. *et al*. Selective deuteration of tryptophan and methionine residues in maltose binding protein: A model system for neutron scattering. *Eur. Biophys. J.* **37**, 815–822 (2008).
31. Luchini, A. *et al*. Towards biomimics of cell membranes: structural effect of phosphatidylinositol triphosphate (PIP3) on a lipid bilayer. *Colloids Surfaces B Biointerfaces* **173**, 202–209 (2019).
32. Kučerka, N., Nieh, M. P. & Katsaras, J. Fluid phase lipid areas and bilayer thicknesses of commonly used phosphatidylcholines as a function of temperature. *Biochim. Biophys. Acta - Biomembr.* **1808**, 2761–2771 (2011).
33. Kučerka, N. *et al*. Cholesterol in bilayers with PUFA chains: Doping with DMPC or POPC results in sterol reorientation and membrane-domain formation. *Biochemistry* **49**, 7485–7493 (2010).
34. Chiang, Y. W., Shimoyama, Y., Feigenson, G. W. & Freed, J. H. Dynamic molecular structure of DPPC-DLPC-cholesterol ternary lipid system by spin-label electron spin resonance. *Biophys. J.* **87**, 2483–2496 (2004).
35. Almeida, P. F. F., Vaz, W. L. C. & Thompson, T. E. Lateral diffusion in the liquid phases of dimyristoylphosphatidylcholine/cholesterol lipid bilayers: a free volume analysis. *Biochemistry* **31**, 6739–6747 (1992).
36. de Almeida, R. F. M., Fedorov, A. & Prieto, M. Sphingomyelin/phosphatidylcholine/cholesterol phase diagram: boundaries and composition of lipids rafts. *Biophys. J.* **85**, 2406–2416 (2003).
37. Rastogi, B. K. & Nordby, A. Lipid composition of cultured human endothelial cells. *Thromb. Res.* **18**, 629–641 (1980).
38. Ingólfsson, H. I. *et al*. Lipid organization of the plasma membrane. *J. Am. Chem. Soc.* **136**, 14554–14559 (2014).
39. Ingólfsson, H. I. *et al*. Computational lipidomics of the neuronal plasma membrane. *Biophys. J.* **113**, 2271–2280 (2017).
40. Josts, I. *et al*. Conformational states of ABC transporter MsbA in a lipid environment investigated by small-angle scattering using stealth carrier nanodiscs. *Structure* **26**, 1072–1079 (2018).
41. Browning, K. L. *et al*. Human lipoproteins at model cell membranes: effect of lipoprotein class on lipid exchange. *Sci. Rep.* **7**, 1–11 (2017).
42. Webster, J., Holt, S. & Dalgliesh, R. INTER the chemical interfaces reflectometer on target station 2 at. *ISIS. Phys. B Phys. Condens. Matter* **385–386**, 1164–1166 (2006).
43. Nelson, A. Co-refinement of multiple-contrast neutron/X-ray reflectivity data using MOTOFIT. *J. Appl. Crystallogr.* **39**, 273–276 (2006).

Acknowledgements

V.T.F. acknowledges support from the EPSRC under grant numbers GR/R99393/01 and EP/C015452/1 which funded the creation of the Deuteration Laboratory (D-Lab) in the Life Sciences group of the ILL. G.A.S. acknowledges the support of this work by the Federal Ministry of Science, Research and Economy (BMWFW), the Federal Ministry of Traffic, Innovation and Technology (bmvit), the Styrian Business Promotion Agency SFG, the Standortagentur Tirol, the Government of Lower Austria and Business Agency Vienna through the

COMET-Funding Program managed by the Austrian Research Promotion Agency FFG. M.C. and S.M. thank the Swedish Research Council for funding. The authors also thank the ILL and STFC for the provision of beam time with corresponding DOI numbers: 10.5291/ILL-DATA.INTER-371, 10.5286/ISIS.E.92924368 and 10.5286/ISIS.E.98002370. This work used the platforms of the Grenoble Instruct-ERIC Center (ISBG: UMS 3518 CNRS-CEA-UGA-EMBL) with support from FRISBI (ANR-10-INBS-05-02) and GRAL (ANR-10-LABX-49-01) within the Grenoble Partnership for Structural Biology (PSB).

Author Contributions

S.W. produced the matchout cholestesterol, H.P. and G.A.S. purified and performed the GC-MS analysis on the matchout cholesterol, S.W. and L.P. performed the SANS experiments and analysis, M.M. and M.H. supported the production of matchout cholesterol, S.W., M.S. and M.C. performed the NR experiments, S.W. analysed the NR data and performed the NMR experiments, S.W., T.F., M.H., S.M. and M.C planned for producing matchout cholesterol and for its characterisation, M.C. secured the research funding, conceived and designed the NR study. S.W. and M.C. wrote the manuscript. All authors contributed to data interpretation and discussion, read and approved the final version of the manuscript.

Additional Information

Supplementary information accompanies this paper at https://doi.org/10.1038/s41598-019-41439-z.

Competing Interests: The authors declare no competing interests.

Publisher's note: Springer Nature remains neutral with regard to jurisdictional claims in published maps and institutional affiliations.

The Production of Matchout-Deuterated Cholesterol and the Study of Bilayer-Cholesterol Interactions

Sarah Waldie[1,2], Martine Moulin[1], Lionel Porcar[1], Harald Pichler[3,4], Gernot A. Strohmeier[3,5], Maximilian Skoda[6], V. Trevor Forsyth[1,7], Michael Haertlein[1*], Selma Maric[2,8*], Marité Cárdenas[2*]

1. Institut Laue-Langevin, 71 Avenue des Martyrs, 38042 Grenoble, Cedex 9, France
2. Biofilm-Research Centre for Biointerfaces and Biomedical Science Department, Faculty of Health and Society, Malmo University, Malmo 20506, Sweden
3. Austrian Centre of Industrial Biotechnology, Petersgasse 14, 8010 Graz, Austria
4. Graz University of Technology, Institute of Molecular Biotechnology, NAWI Graz, BioTechMed Graz, Petersgasse 14, 8010 Graz, Austria
5. Graz University of Technology, Institute of Organic Chemistry, NAWI Graz, Stremayrgasse 9, 8010 Graz, Austria
6. Rutherford Appleton Laboratory, Harwell, Didcot OX11 0QX, UK
7. Life Sciences Department, Faculty of Natural Sciences, Keele University, Staffordshire ST5 5BG, UK
8. MAX IV Laboratory, Fotongatan 2, 225 92 Lund, Sweden.

*Corresponding Authors
Michael Haertlein: haertlein@ill.fr
Selma Maric: selma.maric@mau.se
Marité Cárdenas: marite.cardenas@mau.se

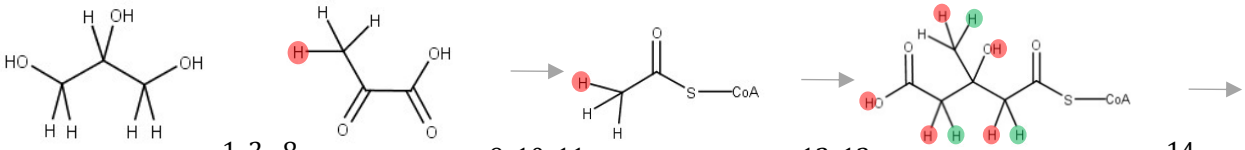

Glycerol — 1, 2…8 → Pyruvate — 9, 10, 11 → Acetyl CoA — 12, 13 → HMG-CoA — 14 →

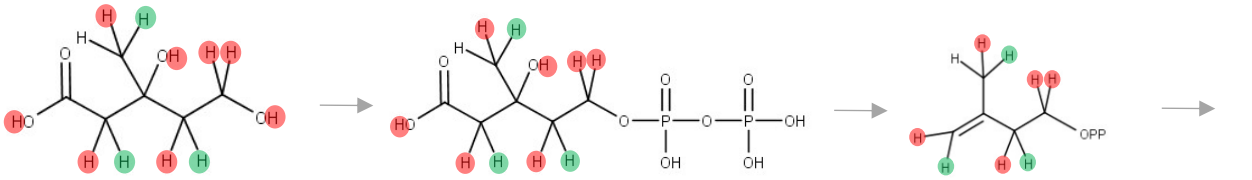

Melavonic Acid — 15, 16 → Melavonate Pyrophosphate — 17 → Isopentyl Pyrophosphate — 18, 19 →

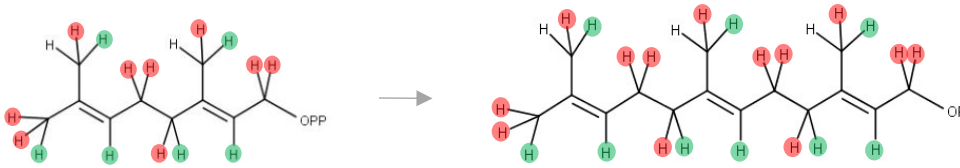

Geranyl Pyrophosphate — 20 → Farnesyl Pyrophosphate — 21 →

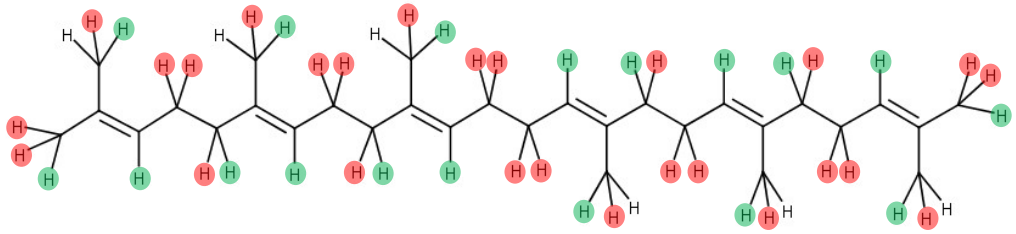

Squalene — 22, 23 →

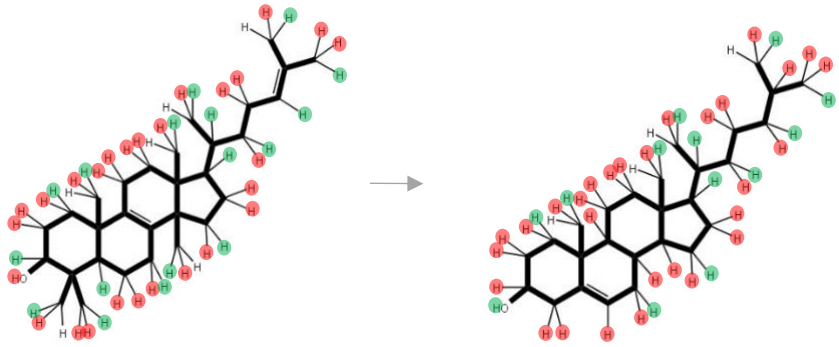

Lanosterol — 24, 25…43 → Cholesterol

SI1. Cholesterol biosynthetic pathway. Exchanged protons are given with red or green circles. The red represents deuterium, the green represents the possibility of deuterium or protium. In the synthesis from glycerol to pyruvate there are 8 enzymes involved (1-8): glycerol kinase, glycerol 3-phosphate dehydrogenase, triosephosphate isomerise, glyceraldehyde 3-phosphate dehydrogenase, phosphoglycerate kinase, phosphoglycerate mutase, enolase and pyruvate kinase. From pyruvate to Acetyl Co-enzyme A (CoA) there are three enzymes involved (9-11): pyruvate dehydrogenase, dihydrolipoyl transacetylase and dihydrolipoyl dehydrogenase which all come under the pyruvate dehydrogenase complex. For the conversion of Acetyl CoA to 3-hydroxy-3-methylglutaryl-CoA (HMG-CoA) there are two enzymatic pathways (12-13): thiolase and HMG-CoA synthase. From HMG-CoA to Melavonic acid HMG-CoA reductase is present (14). From melavonic acid to melavonate pyrophosphate there are two enzymes involved (15-16): mevalonate kinase and phosphomevalonate kinase. From melavonate pyrophosphate to isopentyl pyrophosphate (IPP) only one enzyme is used (17): mevalonate-5-pyrophosphate decarboxylase. To convert between IPP and dimethallyl pyrophosphate (DMAPP) the isopentenyl pyrophosphate isomerase enzyme is required (18). To then progress to geranyl pyrophosphate (GPP), farnesyl diphosphate synthase (FPPS) is used (19). To further progress to farnesyl pyrophosphate (FPP) the same FPPS enzyme is required (20). From FPP to squalene the enzyme farnesyl diphosphate farnesyltransferase is used (21). From squalene to lanosterol two further enzymes are required (22-23): squalene monooxygenase and oxidosqualene cyclase. There are a further 19 steps from lanosterol to cholesterol including demethylation, desaturation and reduction among others (24-43).

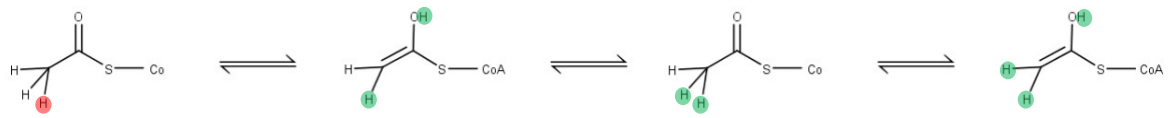

SI2. Tautomerisation of Acetyl CoA.

Table S1. All structural parameters obtained from fitting of derived model to the reflectivity curves for the DLPC + 40mol% cholesterol.

DLPC + 40% cholesterol	Thickness/Å	$\rho \times 10^{-6}$/Å^{-2}	Solvent /%	Roughness/
Si		2.07*		
SiO_2	13.3 ± 0.7**	3.47*	22 ± 3**	5.2 ± 0.5**
Solvent	6.0 ± 0.5**	0*	100*	5.1 ± 0.5**
Inner head	7.0 ± 0.3**	1.89*	26 ± 3**	5.7 ± 0.2**
Inner 1/3 core	10.1 ± 0.3**	4.6 ± 0.2**	17 ± 1**	5.7 ± 0.2**
Middle 1/3 core	10.1 ± 0.3**	2.9 ± 0.2**	17 ± 1**	5.7 ± 0.2**
Outer 1/3 core	10.1 ± 0.3**	4.8 ± 0.1**	17 ± 1**	5.7 ± 0.2**
Outer head	7.0 ± 0.3**	1.89*	26 ± 3**	5.7 ± 0.2**
Backing				5.7 ± 0.2**

* Values kept constant during the fitting process.

**The errors are given in table 3 and are calculated using a Monte-Carlo analysis as embedded in the motofit software[27].

Table S2. All structural parameters obtained from fitting of derived model to the reflectivity curves for the POPC + 40mol% cholesterol.

POPC + 40% mochol	Thickness/Å	$\rho \times 10^{-6}$/Å^{-2}	Solvent /%	Roughness/
Si		2.07*		
SiO_2	7.4 ± 0.3**	3.47*	5 ± 3**	4.3 ± 0.2**
Solvent	4.6 ± 0.3**	0*	100*	4.2 ± 0.2**
Inner head	7.2 ± 0.2**	1.89*	13 ± 3**	4.1 ± 0.1**
Inner 1/3 core	10.5 ± 0.2**	4.06 ± 0.07**	0.5 ± 0.3**	4.1 ± 0.1**
Middle 1/3 core	10.5 ± 0.2**	1.10 ± 0.08**	0.5 ± 0.3**	4.1 ± 0.1**
Outer 1/3 core	10.5 ± 0.2**	4.83 ± 0.07**	0.5 ± 0.3**	4.1 ± 0.1**
Outer head	7.2 ± 0.2**	1.89*	13 ± 3**	4.1 ± 0.1**
Backing				4.1 ± 0.1**

* Values kept constant during the fitting process.

**The errors are given in table 3 and are calculated using a Monte-Carlo analysis as embedded in the motofit software[27].

Table S3. All structural parameters obtained from fitting of derived model to the reflectivity curves for the DMPC + 40mol% cholesterol.

DMPC + 40% mochol	Thickness/Å	$\rho \times 10^{-6}$/Å^{-2}	Solvent /%	Roughness/
Si		2.07*		
SiO_2	10.4 ± 0.6**	3.47*	9 ± 3**	5.7 ± 0.3**
Solvent	5.2 ± 0.1**	0*	100*	5.8 ± 0.2**
Inner head	8.2 ± 0.6**	1.89*	8 ± 2**	5.1 ± 0.5**
Inner 1/3 core	9.9 ± 0.4**	3.2 ± 0.3**	7 ± 1**	5.1 ± 0.5**
Middle 1/3 core	9.9 ± 0.4**	1.0 ± 0.5**	7 ± 1**	5.1 ± 0.5**
Outer 1/3 core	9.9 ± 0.4**	3.9 ± 0.3**	7 ± 1**	5.1 ± 0.5**
Outer head	8.2 ± 0.6**	1.89*	8 ± 2**	5.1 ± 0.5**
Backing				5.1 ± 0.5**

* Values kept constant during the fitting process.

**The errors are given in table 3 and are calculated using a Monte-Carlo analysis as embedded in the motofit software[27].

Paper 2

LANGMUIR Article
Cite This: Langmuir 2018, 34, 472−479
pubs.acs.org/Langmuir

Localization of Cholesterol within Supported Lipid Bilayers Made of a Natural Extract of Tailor-Deuterated Phosphatidylcholine

Sarah Waldie,[†,‡,○] Tania K. Lind,[‡,○] Kathryn Browning,[§] Martine Moulin,[†] Michael Haertlein,[†] V. Trevor Forsyth,[†,∥] Alessandra Luchini,[⊥] Gernot A. Strohmeier,[#,¶] Harald Pichler,[#,∇] Selma Maric,*[,‡] and Marité Cárdenas*[,‡]

[†]Life Sciences Group, Institute Laue−Langevin, 71 Avenue des Martyrs, BP 156, 38042 Grenoble Cedex 9, France
[‡]Biofilm—Research Center for Biointerfaces and Biomedical Science Department, Faculty of Health and Society, Malmö University, Malmö 20506 Sweden
[§]Department of Pharmacy, Uppsala University, Uppsala 75237, Sweden
[∥]Life Sciences Department, Faculty of Natural Sciences, Keele University, Staffordshire ST5 5BG, U.K.
[⊥]Institute Laue−Langevin, 71 Avenue des Martyrs, BP 156, 38042 Grenoble Cedex 9, France
[#]Austrian Centre of Industrial Biotechnology, Petersgasse 14, 8010 Graz, Austria
[¶]Graz University of Technology, Institute of Organic Chemistry, NAWI Graz, Stremayrgasse 9, 8010 Graz, Austria
[∇]Graz University of Technology, Institute of Molecular Biotechnology, NAWI Graz, BioTechMed Graz, Petersgasse 14, 8010 Graz, Austria

Supporting Information

ABSTRACT: Cholesterol is an essential component of mammalian membranes and is known to induce a series of physicochemical changes in the lipid bilayer. Such changes include the formation of liquid-ordered phases with an increased thickness and a configurational order as compared to liquid-disordered phases. For saturated lipid membranes, cholesterol molecules localize close to the lipid head group−tail interface. However, the presence of polyunsaturated lipids was recently shown to promote relocation of cholesterol toward the inner interface between the two bilayer leaflets. Here, neutron reflection is used to study the location of cholesterol (both non-deuterated and per-deuterated versions are used) within supported lipid bilayers composed of a natural mixture of phosphatidylcholine (PC). The lipids were produced in a genetically modified strain of *Escherichia coli* and grown under specific deuterated conditions to give an overall neutron scattering length density (which depends on the level of deuteration) of the lipids matching that of D_2O. The combination of solvent contrast variation method with specific deuteration shows that cholesterol is located closer to the lipid head group−tail interface in this natural PC extract rather than in the center of the core of the bilayer as seen for very thin or polyunsaturated membranes.

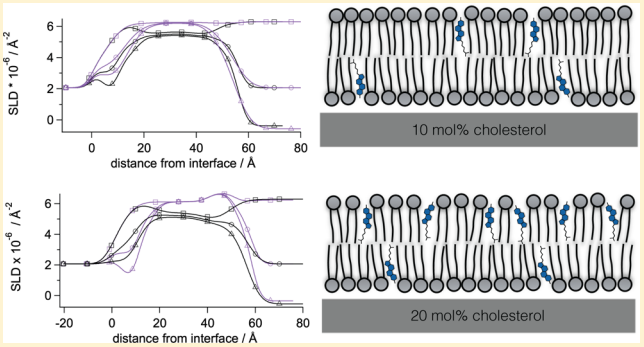

INTRODUCTION

Cholesterol is a natural component of most biological membranes.[1] Cholesterol-containing membranes have been the focus of many biophysical studies during the last 2−3 decades because of its suggested role in the formation of the so-called lipid rafts.[1] Lipid rafts are denser and thicker nano-sized domains that are believed to exist in natural membranes.[2] The role of lipid rafts has been linked to the function and regulation of transmembrane proteins and signaling processes across the cell membrane.[3] The main characteristic of cholesterol is to induce the formation of liquid-ordered phases consisting of lipid molecules that diffuse rapidly within the plane of the bilayer but retain their all-trans configuration.[4] Besides the condensation of lipid monolayers,[5] cholesterol induces changes in the thickness of both fluid and gel phase membranes[6−8] and affects the order parameter of lipid bilayers[9] and cell membranes.[10,11] These effects are explained in the "umbrella model" by the localization of cholesterol with its hydroxyl group close to the lipid head group region and its acyl tail buried in the lipid bilayer.[12] The polar head groups of phosphatidylcholine (PC) form an "umbrella" to compensate for the smaller, polar "head group" of cholesterol (the area of the hydroxyl group is only one-quarter of that occupied by the cholesterol molecule). In this way, the PC head group covers

Received: August 5, 2017
Revised: November 20, 2017
Published: December 12, 2017

DOI: 10.1021/acs.langmuir.7b02716
Langmuir 2018, 34, 472−479

the nonpolar parts of the cholesterol molecule, preventing any unfavorable contact with water. This lipid−cholesterol coupling leads to an increased order parameter of the lipid acyl chains.

Recently, it was proposed that cholesterol may localize differently in the bilayer depending on the level of saturation or thickness of the lipid tails. In particular, cholesterol was found to localize in the middle of the lipid core for bilayers containing polyunsaturated lipids[13−15] or saturated lipids with a very thin lipid core such as 1,2-dilauroylphosphatidylcholine (DLPC).[16] Relocation of cholesterol into the middle of the lipid bilayer was related to the solubility limit of cholesterol in the membrane,[17] suggesting that cholesterol has poorer solubility in polyunsaturated as compared with monounsaturated or saturated acyl chains. Moreover, small-angle neutron scattering (SANS) data suggest that cholesterol has a preference for interactions with saturated lipids, given that titration with monounsaturated or saturated lipids caused cholesterol to locate closer to the lipid head group interface [specifically, more than 50% 1-palmitoyl-2-oleoyl-*sn*-glycero-3-phosphocholine (POPC) or more than 5% 1,2-dimyristoyl-*sn*-glycero-3-phosphorylcholine (DMPC) was needed to relocate cholesterol toward the interface of the lipid head group].[15] Indeed, the presence of cholesterol was shown to create more diverse regions with distinct physical properties in natural rather than simpler model membranes.[10] It is clear that further studies of the localization of cholesterol in natural membranes are needed to fully unravel the role of unsaturated lipids in the organization of cholesterol and consequently in its effect on the lipid bilayer structure.

In this work, D_2O tailor-deuterated PC[18] and cholesterol were used as a model for natural, fluid cellular membranes. Supported lipid bilayers (SLBs) of mixed PC−cholesterol membranes were prepared by vesicle fusion, and neutron reflection (NR) used to characterize the positioning of cholesterol in the bilayers. NR is a technique that excels at determining the structure of buried interfaces with a resolution down to a few Ångstrom in the direction perpendicular to the solid−liquid interface.[19] To increase the sensitivity of the NR measurement, both nondeuterated (h-cholesterol) and perdeuterated (d-cholesterol) cholesterol were used, and all reflectivity curves were fitted using a single global model to describe the position of cholesterol in the PC membrane.

EXPERIMENTAL SECTION

Materials. D_2O was purchased from Sigma and provided by Institute Laue−Langevin, Grenoble, France. Milli-Q (MQ) water was used for all cleaning procedures and solvents. $CaCl_2$ was purchased from Sigma-Aldrich. Tris buffer was prepared by dissolving a tablet of 50 mM Tris, 150 mM NaCl, pH 7.4, in either D_2O or H_2O as specified by the producer (Sigma-Aldrich). DMPC and h-cholesterol were acquired from Avanti Polar Lipids Inc., Alabama, USA.

Production of D_2O-Matched PC. The method developed by Maric et al. (2015)[18] was used to produce a mixture of D_2O-matched PC. The *Escherichia coli* strain W3899[54] carrying the modified plasmid pAC-PCS_{lp}-Gm (P_{araB}-pcs Gm^R) was grown in minimal 100% deuterated medium[20] supplemented with deuterated glycerol ($C_3D_8O_3$) and induced with 0.2% arabinose (unlabeled; Sigma-Aldrich) in addition to 2 mM deuterated choline chloride (trimethyl-d_9, 98%; Euriso-Top), as previously described.[18,21] After incubation at 37 °C for 24 h, cells were harvested by centrifugation (10 000*g*, 20 min, 4 °C), and total lipids extracted according to a modified version of the Bligh & Dyer method.[22] Lipid extracts were separated into individual phospholipid classes according to the head group using flash chromatography on a silica-gel column using varying ratios of chloroform and methanol, as previously described.[18]

Phospholipids were further characterized by thin-layer chromatography through comparison with known standards, as previously described,[23] and the lipid amounts were estimated through the measurement of total phosphorus content according to Rouser et al.[24] Purified PC was assayed for fatty acid composition using matrix-assisted laser desorption/ionisation time-of-flight (MALDI-TOF) mass spectrometry (MS), as described previously.[25] The PC fraction was premixed in a 1:1 (v/v) ratio with 2,5-dihydroxy-benzoic acid as a matrix before deposition onto the MALDI target and was investigated by positive ion-mode MALDI-TOF MS on a Bruker Autoflex mass spectrometer (Bruker Daltonics)[26] using 30% laser power and 1000 counts on average.

Production of Perdeuterated Cholesterol. The d-cholesterol used in this study was produced by the expression from the *Pichia pastoris* strain CBS7435 Δ*his4*Δ*ku70* Δ*erg5*::p*Pp*GAP-ZeocinTM-[*DHCR7*] Δ*erg6*::pGAP-G418[*DHCR24*].[27,28] This yeast strain was adapted to growth in a deuterated minimal medium and scaled up in a high cell-density culture.[29] d-cholesterol was purified and characterized by MS and gas chromatography.

Methods. *SLB Formation.* Lipid films were made by taking the appropriate volumes from chloroform stocks of D_2O-matched PC and either h- or d-cholesterol to obtain the desired vesicle composition. The mixtures were dried under nitrogen and kept in vacuum for at least 1 h. All films were kept at −20 °C until use. Small unilamellar vesicles (SUVs) were formed by resuspending the lipid films in water or 150 mM NaCl solution to a concentration of 0.2 mg/mL. The suspension was bath-sonicated at room temperature for 1 h and then subsequently tip-sonicated for 5 min or until an optically clear solution was obtained. For optimal vesicle fusion conditions, a 0.1 mg/mL vesicle solution in 2 mM $CaCl_2$ was produced by mixing equal volumes of the freshly tip-sonicated vesicle suspension prepared in water and a 4 mM $CaCl_2$ solution. This solution was immediately introduced into the QCM-D or NR flow cell (preequilibrated to 37 °C) by pump or syringe injection, respectively, and left to incubate for 20 min at 37 °C. The cell was rinsed with water and then by a Tris buffer (50 mM Tris-HCl, 150 mM NaCl).

Quartz Crystal Microbalance with Dissipation, QCM-D. Measurements were performed using a Q-SENSE E4 system (Q-Sense, Sweden) connected to a peristaltic pump (Ismatec IPC, Switzerland). Silicon oxide sensor crystals (50 nm, Q-Sense, Sweden) were used. Cleaning protocols were used as specified by Q-Sense. Prior to experiments, the fundamental frequency (5 MHz) and five overtones (3rd, 5th, 7th, 9th, and 11th) were found and recorded in MQ water. The flow rate was set to 100 μL/min, and the temperature was kept at 37 °C throughout all experiments. A baseline was obtained in MQ water prior to injection of the vesicle solution. A constant flow of vesicles was maintained until stable signals were obtained before rinsing with excess MQ water. Experiments were repeated three times, and reproducible results were obtained.

Neutron Reflection. Specular NR was used to analyze the structure of the SLB at the solid/liquid interface. NR yields structural information perpendicular to the surface in a nondestructive manner. FIGARO,[30] a time of flight (TOF) reflectometer at the Institute Laue−Langevin (Grenoble, France) was used in this study. An incident neutron beam, with a chosen wavelength (λ), is directed on the solid/water interface and is partially reflected and refracted depending on the incident angle (θ) and the wavelength (λ). The ratio between incident and reflected beam (R) is then measured as a function of the wave vector, which is defined as $Q = 4/\lambda \sin \theta$. To obtain detailed structural information, the isotopic contrast between the molecules in the sample is important. The scattering length density (SLD) determines the isotopic contrast by highlighting different components in the sample. The SLD profile is given by the sum of the coherent scattering lengths *bj* multiplied by the number of nuclei in a given volume *nj* (SLD = $\sum j \times nj \times bj$). By exchanging hydrogen with deuterium, the SLD of a molecule increases, and the isotropic contrast can be manipulated to partially highlight specific parts of a molecule. In this study, the isotopic contrast was achieved

DOI: 10.1021/acs.langmuir.7b02716
Langmuir 2018, 34, 472−479

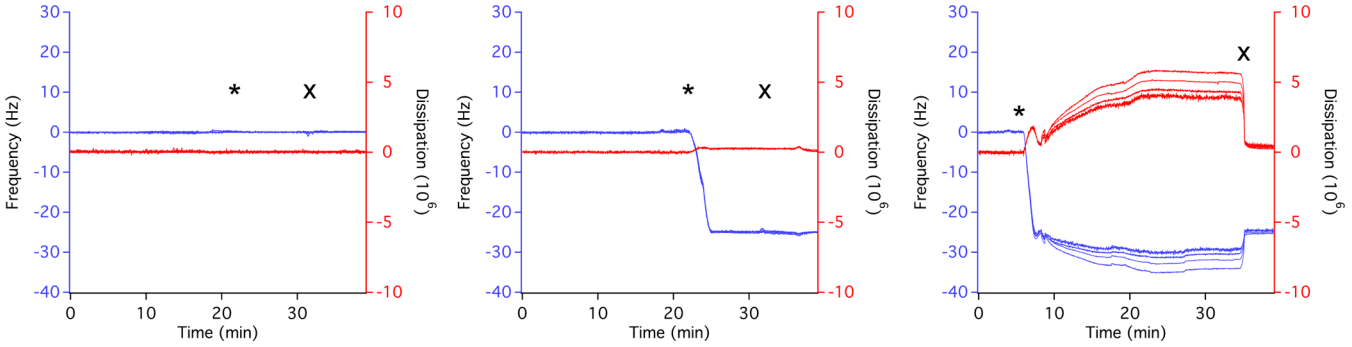

Figure 1. Fusion of DMPC vesicles containing 20 mol% cholesterol on SiO_2 as monitored by QCM-D. Deposition was performed at 37 °C in MQ water (left), 2 mM $CaCl_2$ (middle), and 150 mM NaCl (right). The star marks the point at which 0.1 mg/mL vesicles were introduced in the fluid cell at 0.1 mL/min, whereas the cross shows the point at which rinsing with MQ water was performed. Overtones 5−11th are shown.

by using both h- and d-cholesterol as well as by exchanging the bulk solvent with Tris buffers made from D_2O, H_2O, or a mixture contrast-matched to silicon (cmSi). The resolution was set to $\Delta\lambda/\lambda = 7\%$ using two incident angles of 0.8° and 3.2°. The experiments were carried out at 37 °C using homemade solid−liquid flow cells. The area exposed to the neutron beam was 3.5 × 6.5 cm^2. All cell parts made of polyether ether ketone (PEEK) were cleaned by bath sonication in 2% Hellmanex and MQ water. Silicon (111) surfaces were cooked in dilute piranha solution ($H_2O/H_2SO_4/H_2O_2$ 5:4:1) at 80 °C for 15 min followed by extensive rinsing in MQ water, drying in nitrogen, and 10 min UV−ozone cleaning (Bioforce Nanosciences Inc.). The data were analyzed using the Motofit software,[31] which uses the Abeles optical matrix method for fitting reflectometry data of thin layers. The genetic Monte Carlo minimization algorithm embedded within this software was used, allowing for error estimation of the fit parameters. The Supporting Information gives the free parameters as well as the range over which they were allowed to vary.

RESULTS AND DISCUSSION

SLBs were produced via the vesicle fusion method,[19,32] and successful SLB formation was assessed using quartz crystal microbalance with dissipation (QCM-D). For PC, successful vesicle fusion typically takes place in pure water or in buffered solvents with high ionic strength.[32] However, deposition of SLBs from vesicles of more complex composition can be challenging, and other solvents were required for deposition.[33−36] The deposition of cholesterol containing PC was optimized using QCM-D, and representative traces are presented in Figure 1. The collectively accepted QCM-D signals for successful vesicle fusion[32,37−39] are such that the QCM-D frequency (Δf) decreases because of the mass increase of the water-filled vesicles as vesicles adsorb to the surface. Simultaneously, the QCM-D energy dissipation (Δd) increases as a result of the softness and compliance of the vesicles. The collapse of the vesicles and the SLB formation lead to an increase in Δf which is consistent with loss of mass due to the release of water, and a simultaneous decrease in Δd occurs because of the formation of a thin, homogeneous membrane, which is more rigid and well-coupled to the sensor surface as compared to the adsorbed vesicle layer. This characteristic signal has led to the hypothesis that SLBs can only be formed once a critical density of vesicles have attached to the surface, which makes the adsorbed vesicles unstable and leads to their fusion and consequent formation of a continuous supported bilayer.[40] However, it has been shown that small vesicles tend to break directly upon adsorption when added in pure water or in water with low salt content.[19,41]

Figure 1 shows that no vesicle adsorption or SLB formation occurred in pure water, whereas SLBs were successfully formed using either 2 mM $CaCl_2$ or 150 mM NaCl. However, the QCM-D traces were significantly different for the two latter cases. No overshooting of Δf and Δd was observed in $CaCl_2$, whereas the characteristic overshooting of the QCM-D signals in NaCl was followed by further increase in Δd and decrease in Δf and spreading of the overtones over time. This suggests two different types of mechanisms for vesicle fusion depending on the solvent quality. For $CaCl_2$, vesicles break directly upon adsorption to the surface with no critical vesicle concentration needed for the formation of an SLB. For NaCl, on the other hand, the initial QCM-D responses correspond to the common signals related to a critical vesicle surface concentration, with further vesicle attachment taking place once the SLB was formed. However, the excess vesicles could be successfully removed upon rinsing. In previous work, fusion of cholesterol-containing vesicles was achieved by using high-salt-containing buffers.[33,42] However, high ionic strength typically increases the time required to produce small enough vesicles via tip sonication, a requirement to form SLBs of high quality (e.g., see discussions in ref 19). Extensive tip sonication could potentially lead to overheating of the sample, which should be avoided. SLBs were therefore formed using 2 mM $CaCl_2$. As control, this approach was used even for dPC SLBs in the absence of cholesterol.

Figure 2 gives neutron reflectivity profiles for an SLB formed from pure D_2O-matched d-PC vesicles. Initially, the data were fitted to a single layer model to represent the lipid bilayer (see the Supporting Information Figure S1). The resulting SLB was of high quality in terms of surface coverage (95% coverage). The layer was 41 Å thick with low roughness (4.2 Å). The SLD of this layer was determined to be 6.10 (±0.01) × 10^{-6} $Å^{-2}$, which is close to the value for D_2O (6.3 × 10^{-6} $Å^{-2}$). A three-layer (3L) model, for which the heads and tails were distinguished by the content of water, was applied to the data, and the best fit is given as solid lines in Figure 2. The inset gives the SLD profiles for the best fits found for a 3L model using the parameters given in Table 1. To decrease the number of free parameters, the coverage was fixed to 95%, and this gave a total thickness = 43.3 Å and a mean molecular area (MMA) = 61 $Å^2$, which is consistent with previous results for fluid lipids such as POPC.[41] The main lipids present in the PC extract were PC 16:0/17:0cyc, PC 16:0/15:0cyc, and PC 16:0/18:1 (POPC), as identified by MALDI-TOF MS (Supporting Information Figure S2), and thus, this result is not surprising. The compositional results are in agreement with

DOI: 10.1021/acs.langmuir.7b02716
Langmuir 2018, 34, 472−479

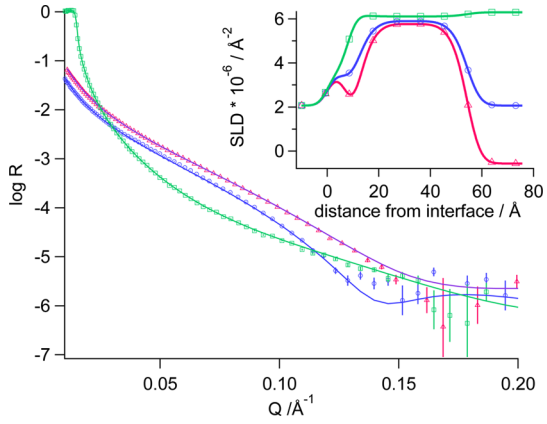

Figure 2. Neutron reflectivity profiles and best fits (solid lines) for an SLB made of D_2O-matched PC extract (upper graph). The bulk solvent contrasts were D_2O (green squares), H_2O (pink triangles), and cmSi (blue circles). The inset shows the corresponding SLD profile for the best fit.

Table 1. Parameters Used in the Best Fit to a 3L Model for Pure dPC Given in Figure 2[a]

	SLD × 10^{-6}/Å^{-2}	thickness/Å	coverage/%	MMA/Å^2
inner head	6.1 ± 0.01	6.9 ± 0.7	75 ± 2	62 ± 7
tail	6.1 ± 0.01	29.5 ± 1.2	95	65 ± 2
outer head	6.1 ± 0.01	6.9 ± 0.7	75 ± 2	62 ± 7
		43.3 ± 1.4		63 ± 9

[a]Values for molecular volumes and SLDs for other compounds are given in the Supporting Information, Table S1

a previous characterization of dPC lipids produced in a similar manner.[18] The exact composition cannot be obtained with MALDI-TOF MS because phospholipids with lower molecular weight are more sensitively detected than those with higher molecular weight.[43] However the MS data show that more than 2/3 of the dPC mixture is composed of 16:0/17:0cyc, whereas the rest contains roughly equal amounts of 16:0/15:0cyc and POPC.

D_2O-matched PC extracts containing either h- or d-cholesterol were formed using the vesicle fusion method in $CaCl_2$, Figure 1 and characterized structurally. NR data for SLBs formed by vesicles with a nominal composition of 10 and 20 mol % cholesterol are given in Figure 3A,B, respectively. The difference between the SLD for D_2O-matched PC and d-cholesterol is low (1.04×10^{-6} Å^{-2}) as compared to D_2O-matched PC and h-cholesterol (6.94×10^{-6} Å^{-2}). Three different models were used to find the best fit to the data. First, a fully symmetric 3L model (head−tails−head) was applied. Then, leaflet asymmetry was modeled using two different approaches: (1) a four-layer (4L) model for which the inner and outer leaflet tail region were clearly separated from each other and (2) a five-layer (5L) model for which the tail region was separated into three regions, and that enabled the localization of cholesterol in the middle of the SLB. In the latter model, the three tail region subsections were constrained to have equal thickness, roughness, and coverage, but each having distinctive SLD values. This choice was made to reduce the number of free parameters of the fits, and variations between them did not vary the quality of the fit significantly. For 10 mol % cholesterol, the data could be fitted using a symmetric 3L model. For 20 mol % cholesterol, on the other hand, the data could be best fitted using a 5L model. Figure S3 in the Supporting Information shows the best fits for the symmetric 3L model and the asymmetric 4L model used for the 20 mol % cholesterol NR data and gives the difference in chi2 between the different fits. For consistency, the 5L model was then applied to SLBs containing both 10 and 20 mol % cholesterol. The parameters used for the best fits to the 5L model are given in Table 2.

For 10 mol % cholesterol, SLBs of high surface coverage (>96%) were obtained. The SLD profile for the best fit shows a slight increase in the cholesterol distribution toward the outer head group region for h-cholesterol with some depletion at the center of the membrane (Figure 3A). However, the difference in SLD between these three layers is not significant when considering the fit error, and an equal distribution could thus be assumed in this case. Compared to the d-PC SLB, the total thickness of the membrane increased by 1−2 Å. Thickening of the d-PC membrane was found to be similar for h- and d-cholesterol. Moreover, the fit results show that the membranes contain 9 and 14 mol % cholesterol for the hydrogenated and deuterated version, respectively (average of the composition given in Table 2). Considering the error from the fits and the experimental conditions,[41] this is quite close to the expected values based on the nominal composition of the vesicles used to form the SLBs.

As already mentioned, the 5L model was needed to obtain a good fit for the 20 mol % cholesterol. The average composition of the SLB was also similar to the nominal composition of the vesicles from which they were made (15% and 21% for non-deuterated and deuterated cholesterol-containing SLBs, respectively). The asymmetric distribution of cholesterol within the lipid core, on the other hand, was significant (Figure 3B): cholesterol preferentially localized near the outer lipid head group for both the hydrogenated and the per-deuterated molecules with the outer and inner leaflet containing up to 55 and 2 mol % cholesterol, respectively. The data show further thickening of the membrane by 4−5 Å regardless of the level of deuteration.

The SLBs were formed at 37 °C, the temperature at which both (i) the *E. coli* cells were grown and (ii) hydrogenated POPC−hydrogenated cholesterol mixtures were reported to exist in the liquid disordered phase regardless of composition.[44] Moreover, the cyclic species in our dPC extract are known to have a main melting transition well below 0 °C.[45] For d-PC containing 20 mol % cholesterol, the SLB thickened by as much as 4 Å. Such an effect can be explained by the ability of cholesterol to reduce trans−gauche isomerization of the saturated acyl chains in their fluid state[4] and to increase the order parameter within the bilayer.[33] These results are consistent with previous findings in literature: for example, it was found that 30 mol % cholesterol induces 3−4 Å thickening of DMPC bilayers regardless of the temperature.[6] For mixed SLBs composed of POPC and cholesterol, a total bilayer thickness of 44 and 45 Å was found for 0 and 20 mol % cholesterol.[33] The presence of cholesterol in the D_2O-matched d-PC extract leads to 2 Å thicker SLBs as compared to cholesterol mixtures with POPC.[33] This can be attributed to the more complex composition of the d-PC extracts [the main species are POPC, and two cyclopropane containing PCs] (Supporting Information Figure S2). Recently, Marquardt et al.[16] reported that the localization of cholesterol in the center of lipid bilayers does not necessarily depend on the level of polyunsaturation but rather on the thickness of the lipid bilayer. In particular, the authors found that cholesterol

DOI: 10.1021/acs.langmuir.7b02716
Langmuir 2018, 34, 472−479

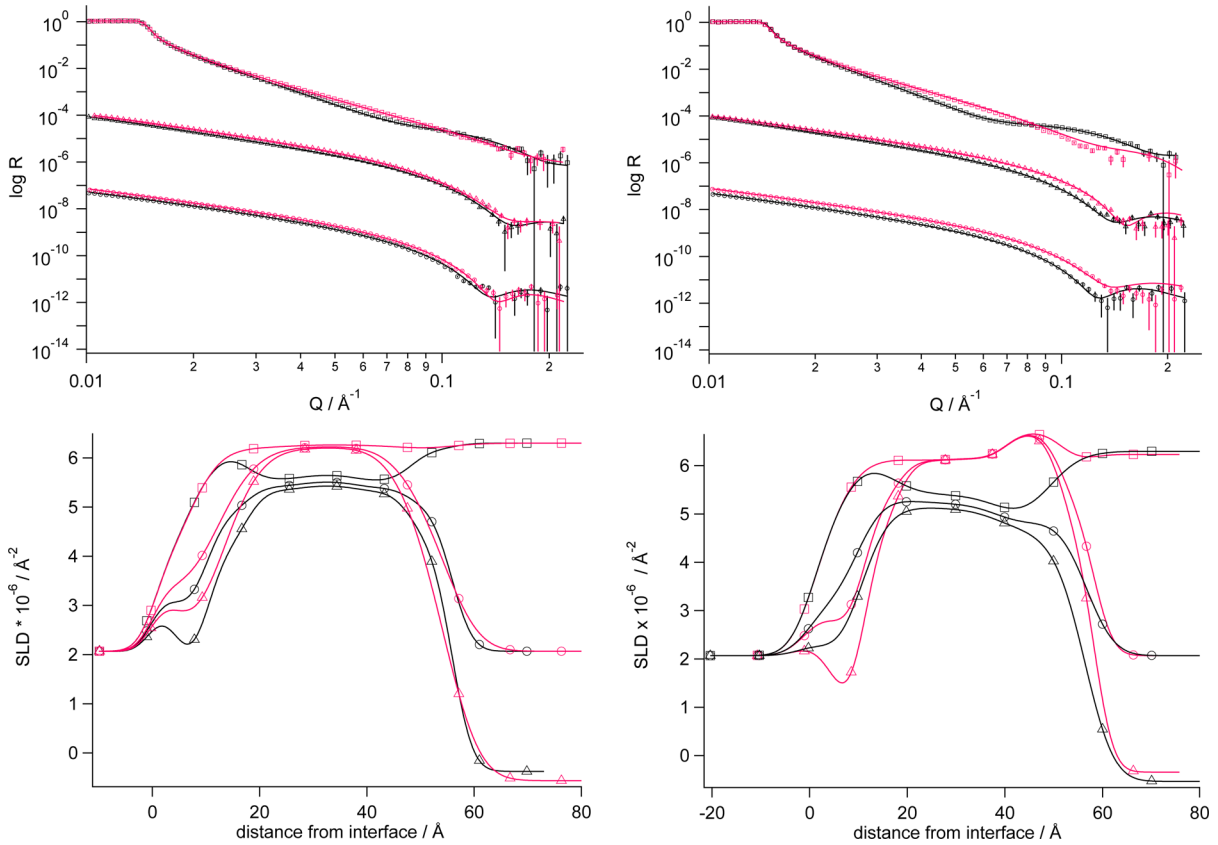

Figure 3. Neutron reflectivity profiles (upper graph), best fits (solid lines), and SLD profiles (lower graph) for SLBs made of the d-PC extract and h- or d-cholesterol (black and pink, respectively) using vesicles with 10 mol % cholesterol content or 20 mol % cholesterol content. The bulk contrasts used were D_2O, H_2O, and cmSi [squares (top), triangles (middle), and circles (bottom), respectively]. The contrasts have been offset on the *y*-scale for clarity.

Table 2. Parameters for the Best Fits Shown in Figure 3

	SLD × 10^{-6}/Å^{-2}	% lipid	thickness/Å	coverage/%	MMA/Å^2
		10 mol % h-cholesterol			
inner head	6.1		7.5 ± 0.5	67 ± 4	64 ± 6
tail	5.6/5.5/5.5(±0.1)	90/92/90(±3)	30.9 ± 0.5	97 ± 2	59 ± 2
outer head	6.1		7.7 ± 0.4	72 ± 6	58 ± 5
		average = 91	46.1 ± 0.9		60 ± 8
		10 mol % d-cholesterol			
inner head	6.1		7.2 ± 0.5	81 ± 2	55 ± 4
tail	6.22/6.32/6.23(±0.07)	89/84/86(±2)	30.8 ± 0.4	99 ± 5	57 ± 3
outer head	6.1		7.5 ± 0.5	72 ± 5	60 ± 6
		average = 87	45.5 ± 0.9		57 ± 7
		20 mol % h-cholesterol			
inner head	6.1		7.3 ± 0.5	84 ± 2	53 ± 4
tail	5.4/5.3/4.9(±0.2)	88/87/80(±3)	32.8 ± 0.6	96 ± 3	55 ± 2
outer head	6.1		7.6 ± 0.5	70 ± 5	60 ± 6
		average = 85	**47.5 ± 0.9**		56 ± 7
		20 mol % d-cholesterol			
inner head	6.1		7.0 ± 0.4	77 ± 4	60 ± 5
tail	6.12/6.15/6.70(±0.06)	98/95/45(±2)	33.5 ± 0.7	99 ± 5	51 ± 3
outer head	6.1		7.0 ± 0.5	76 ± 5	61 ± 6
		average = 80	**47.5 ± 0.9**		57 ± 8

occupied this unexpected position not only in polyunsaturated lipid membranes but also in DLPC. The common structural feature of these two bilayers was the thickness of the cholesterol containing bilayer core (28 Å). For DMPC bilayers, on the other hand, this parameter was 34 Å with the cholesterol positioned close to the head groups in an uptilt position. Here, the core of the pure dPC bilayers was 29.5 Å (Table 1), while it increased to ∼31 and ∼33 Å for 10 and 20 mol % cholesterol (Table 2), respectively. As these values are

DOI: 10.1021/acs.langmuir.7b02716
Langmuir 2018, 34, 472−479

similar to what was found for DMPC, a similar cholesterol orientation is also expected.

The asymmetry reported for SLBs made with vesicles containing 20 mol % cholesterol could be a consequence of an asymmetric distribution of cholesterol in the vesicle population prior to fusion. It is thus expected that earlier studies on cholesterol containing SLBs using vesicle fusion also presented such asymmetry, although the lack of contrast available in these studies did not allow this effect to be discriminated previously.[33] An increasing number of reports describe a tendency to form asymmetric membranes,[41,46−48] especially for two-component PC systems close to the phase separation boundary.[41] In such cases, POPC and the more rigid 1,2-dipalmitoyl-*sn*-glycero-3-phosphorylcholine (DPPC) lipids were used to form SUVs with diameters around 50 nm. In these SUVs, DPPC is expected to be preferentially localized in the outer leaflet, and thus, upon fusion, it should be preferentially located in the inner leaflet of the resulting SLB. For cholesterol containing liposomes, asymmetry in the vesicle composition was observed by SANS,[49] although in this study, the authors did not report the degree of compositional asymmetry of the vesicles. Moreover, molecular dynamics simulations of lipid vesicles composed of DMPC and cholesterol (70:30 mol %) predicted an increased density of cholesterol in the inner leaflet of vesicles with diameters smaller than 50 nm,[50] as the ones typically produced by tip sonication using protocols similar to the ones in this work.[41] The small hydroxyl group of cholesterol gives it an inverted conical shape, and thus, it is expected that cholesterol preferentially localizes in the leaflet closer to the vesicle's lumen, enriching the outer leaflet of a mixed phospholipid−cholesterol SLB after vesicle fusion. It could also be argued that the order parameter of the inner leaflet increases because of the presence of the supporting substrate, and that such asymmetric ordering across the inner and outer leaflets could lead to asymmetry in the cholesterol distribution. However, this does not seem to be the case as cholesterol prefers to localize within regions of high order, and therefore, the expected asymmetry would be opposite to that experimentally found. Interestingly, the SLB formed with vesicles containing 10 mol % cholesterol is fully symmetric. In this case, the SLB is expected to be in the fluid disordered phase and thus present high flip-flop rates for cholesterol.[51] The high flip-flop rate will, within seconds after vesicle fusion, even out the distribution of cholesterol across the SLB. For the SLB made with vesicles containing 20 mol % cholesterol, on the other hand, the actual content of cholesterol in the outer leaflet reaches up to 50 mol %. Therefore, in this case, liquid-ordered phases are expected with significantly slower flip-flop rates[52] which would favor the retention of the asymmetric structure. Indeed, recent near atomic molecular dynamics simulations on complex lipid membranes containing up to 60 lipid species suggest that the cholesterol asymmetry across the leaflet occurs when leaflet concentrations reach those expected for the formation of a liquid-ordered phase.[53]

Finally, and following the same reasoning as described for the asymmetric distribution of lipid mixtures in SUVs, it could be argued that the three main PC species are distributed differently within the two leaflets of the vesicles and thus in the resulting SLB. An asymmetric distribution of the PC species within the leaflets of the vesicles could lead to cholesterol adopting different configurations within the leaflets. If cholesterol presents preferential interactions with saturated PC species, as has been suggested previously,[15] it could be speculated that any saturated species and cholesterol preferentially enrich the inner leaflet of the vesicles and thus the outer leaflet of the SLB. This would give a strong asymmetric distribution of cholesterol in SLBs made by vesicle fusion. However, our dPC mixture does not contain saturated species, and this does not seem like a plausible explanation for the asymmetry measured for 20 mol % cholesterol. To address the effect of the specific lipid species present in our mixture (cyclic vs unsaturated acyl tails), we are currently developing preparative chromatographic protocols in our lab to separate the cyclic and the unsaturated species from our mixtures. Figure 4 presents a schematic diagram for the localization of cholesterol in SLBs on the basis of the results described here.

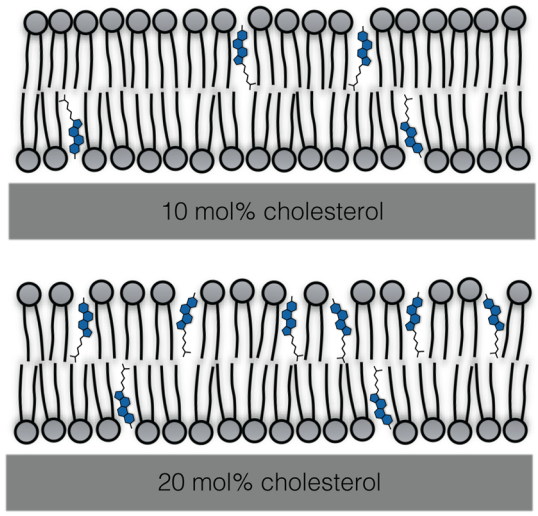

Figure 4. Schematics of cholesterol distribution in d-PC containing 10 or 20 mol % cholesterol. The thickness of the SLB increases from ∼43 to ∼46 and ∼48 Å in the absence and presence of 10 and 20 mol %, respectively.

CONCLUSIONS

In a natural lipid extract, cholesterol is embedded in the lipid bilayer in close proximity to the lipid head groups. This is in accordance with the localization of cholesterol reported for lipid bilayers of a similar core size and differs from the findings obtained from polyunsaturated or for very thin lipid bilayers. Moreover, a strong asymmetric distribution of cholesterol in SLBs is expected as the cholesterol content is raised to at least 20 mol % in PC mixtures. The data described here can be used to improve the modeling of cholesterol containing bilayers and of other biomolecular interactions involving cellular membranes. Methods to separate and purify individual PC species in the natural lipid mixture are currently being developed to further address any potential interactions with specific lipids.

ASSOCIATED CONTENT

Supporting Information

The Supporting Information is available free of charge on the ACS Publications website at DOI: 10.1021/acs.langmuir.7b02716.

NR data fitting, NR fitting for dPC using a single layer, positive ion mode MALDI-TOF for the lipid extract used in this work, and a comparison between the

DOI: 10.1021/acs.langmuir.7b02716
Langmuir 2018, 34, 472−479

different models used to fit the 20 mol % cholesterol data (PDF)

AUTHOR INFORMATION

Corresponding Authors

*E-mail: selma.maric@mah.se (S.M.).
*E-mail: marite.cardenas@mah.se (M.C.).

ORCID

Tania K. Lind: 0000-0003-0800-5650
Kathryn Browning: 0000-0002-0296-0369
Marité Cárdenas: 0000-0003-0392-3540

Author Contributions

○S.W. and T.K.L. have contributed equally.

Notes

The authors declare no competing financial interest.

ACKNOWLEDGMENTS

We thank the Institute Laue−Langevin for the time allocated at the Deuteration lab (DL-03-181 and DL-03-182) within the Life Sciences Group and at Figaro (9-13-681). Moreover, we would like to thank Anaïs Croguennec for collecting the QCM-D data used in this work. Also, thanks to Lise-Britt Wahlberg for initial tests using ellipsometry. The authors thank Professor William Dowhan and his group at the University of Texas, USA, for their kind contribution in providing the original AL95 *E. coli* strain which was further mutated for production of deuterated PC in Grenoble. M.C., T.K.L., K.B., and S.M. thank the Swedish Research Council, Nordforsk and Interreg: ESS and MaxIV Cross Border Science for funding this research. G.A.S. acknowledges the support of this work by the Federal Ministry of Science, Research and Economy (BMWFW), the Federal Ministry of Traffic, Innovation and Technology (bmvit), the Styrian Business Promotion Agency SFG, the Standortagentur Tirol, the Government of Lower Austria, and Business Agency Vienna through the COMET-Funding Program managed by the Austrian Research Promotion Agency FFG. V.T.F., M.H., and M.M. acknowledge the UK Engineering and Physical Sciences Research Council (EPSRC) for grants EP/C015452/1 and GR/R99393/01 (to Keele University) which funded the creation of the Deuteration Laboratory in ILL's Life Sciences Group.

REFERENCES

(1) Simons, K.; Ikonen, E. Functional rafts in cell membranes. *Nature* **1997**, *387*, 569−572.
(2) Armstrong, C. L.; Barrett, M. A.; Hiess, A.; Salditt, T.; Katsaras, J.; Shi, A.-C.; Rheinstädter, M. C. Effect of cholesterol on the lateral nanoscale dynamics of fluid membranes. *Eur. Biophys. J.* **2012**, *41*, 901−913.
(3) de Almeida, R. F. M.; Joly, E. Crystallization around solid-like nanosized docks can explain the specificity, diversity, and stability of membrane microdomains. *Front. Recent Dev. Plant Sci.* **2014**, *5*, 72.
(4) Vist, M. R.; Davis, J. H. Phase equilibria of cholesterol/dipalmitoylphosphatidylcholine mixtures: deuterium nuclear magnetic resonance and differential scanning calorimetry. *Biochemistry* **1990**, *29*, 451−464.
(5) Smaby, J. M.; Momsen, M.; Kulkarni, V. S.; Brown, R. E. Cholesterol-Induced Interfacial Area Condensations of Galactosylceramides and Sphingomyelins with Identical Acyl Chains. *Biochemistry* **1996**, *35*, 5696−5704.
(6) Léonard, A.; Escrive, C.; Laguerre, M.; Pebay-Peyroula, E.; Néri, W.; Pott, T.; Katsaras, J.; Dufourc, E. J. Location of Cholesterol in DMPC Membranes. A Comparative Study by Neutron Diffraction and Molecular Mechanics Simulation. *Langmuir* **2001**, *17*, 2019−2030.
(7) Karmakar, S.; Raghunathan, V. A. Structure of phospholipid-cholesterol membranes: An x-ray diffraction study. *Phys. Rev. E: Stat., Nonlinear, Soft Matter Phys.* **2005**, *71*, 061924.
(8) Gallová, J.; Uhríková, D.; Kučerka, N.; Doktorovová, S.; Funari, S. S.; Teixeira, J.; Balgavý, P. The effects of cholesterol and β-sitosterol on the structure of saturated diacylphosphatidylcholine bilayers. *Eur. Biophys. J.* **2011**, *40*, 153−163.
(9) Van Blitterswijk, W. J.; Van der Meer, B. W.; Hilkmann, H. Quantitative contributions of cholesterol and the individual classes of phospholipids and their degree of fatty acyl (un)saturation to membrane fluidity measured by fluorescence polarization. *Biochemistry* **1987**, *26*, 1746−1756.
(10) Stott, B. M.; Vu, M. P.; McLemore, C. O.; Lund, M. S.; Gibbons, E.; Brueseke, T. J.; Wilson-Ashworth, H. A.; Bell, J. D. Use of fluorescence to determine the effects of cholesterol on lipid behavior in sphingomyelin liposomes and erythrocyte membranes. *J. Lipid Res.* **2008**, *49*, 1202−1215.
(11) Golfetto, O.; Hinde, E.; Gratton, E. Laurdan Fluorescence Lifetime Discriminates Cholesterol Content from Changes in Fluidity in Living Cell Membranes. *Biophys. J.* **2013**, *104*, 1238−1247.
(12) Huang, J.; Feigenson, G. W. A Microscopic Interaction Model of Maximum Solubility of Cholesterol in Lipid Bilayers. *Biophys. J.* **1999**, *76*, 2142−2157.
(13) Harroun, T. A.; Katsaras, J.; Wassall, S. R. Cholesterol Hydroxyl Group Is Found To Reside in the Center of a Polyunsaturated Lipid Membrane. *Biochemistry* **2006**, *45*, 1227−1233.
(14) Marrink, S. J.; de Vries, A. H.; Harroun, T. A.; Katsaras, J.; Wassall, S. R. Cholesterol Shows Preference for the Interior of Polyunsaturated Lipid Membranes. *J. Am. Chem. Soc.* **2008**, *130*, 10−11.
(15) Kučerka, N.; Marquardt, D.; Harroun, T. A.; Nieh, M.-P.; Wassall, S. R.; de Jong, D. H.; Schäfer, L. V.; Marrink, S. J.; Katsaras, J. Cholesterol in Bilayers with PUFA Chains: Doping with DMPC or POPC Results in Sterol Reorientation and Membrane-Domain Formation. *Biochemistry* **2010**, *49*, 7485−7493.
(16) Marquardt, D.; Heberle, F. A.; Greathouse, D. V.; Koeppe, R. E.; Standaert, R. F.; Van Oosten, B. J.; Harroun, T. A.; Kinnun, J. J.; Williams, J. A.; Wassall, S. R.; Katsaras, J. Lipid bilayer thickness determines cholesterol's location in model membranes. *Soft Matter* **2016**, *12*, 9417−9428.
(17) Garg, S.; Castro-Roman, F.; Porcar, L.; Butler, P.; Bautista, P. J.; Krzyzanowski, N.; Perez-Salas, U. Cholesterol solubility limit in lipid membranes probed by small angle neutron scattering and MD simulations. *Soft Matter* **2014**, *10*, 9313−9317.
(18) Maric, S.; Thygesen, M. B.; Schiller, J.; Marek, M.; Moulin, M.; Haertlein, M.; Forsyth, V. T.; Bogdanov, M.; Dowhan, W.; Arleth, L.; Pomorski, T. G. Biosynthetic preparation of selectively deuterated phosphatidylcholine in genetically modified Escherichia coli. *Appl. Microbiol. Biotechnol.* **2015**, *99*, 241−254.
(19) Lind, T. K.; Cárdenas, M. Understanding the formation of supported lipid bilayers via vesicle fusion—A case that exemplifies the need for the complementary method approach (Review). *Biointerphases* **2016**, *11*, 020801.
(20) Artero, J. B.; Hartlein, M.; McSweeney, S.; Timmins, P. A comparison of refined X-ray structures of hydrogenated and perdeuterated rat γE-crystallin in H2O and D2O. *Acta Crystallogr., Sect. D: Biol. Crystallogr.* **2005**, *61*, 1541−1549.
(21) Bogdanov, M.; Heacock, P.; Guan, Z.; Dowhan, W. Plasticity of lipid-protein interactions in the function and topogenesis of the membrane protein lactose permease from Escherichia coli. *Proc. Natl. Acad. Sci. U.S.A.* **2010**, *107*, 15057−15062.
(22) Bligh, E. G.; Dyer, W. J. A rapid method of total lipid extraction and purification. *Can. J. Biochem. Physiol.* **1959**, *37*, 911−917.
(23) Maric, S.; Skar-Gislinge, N.; Midtgaard, S.; Thygesen, M. B.; Schiller, J.; Frielinghaus, H.; Moulin, M.; Haertlein, M.; Forsyth, V. T.; Pomorski, T. G.; Arleth, L. Stealth carriers for low-resolution

DOI: 10.1021/acs.langmuir.7b02716
Langmuir 2018, 34, 472−479

structure determination of membrane proteins in solution. *Acta Crystallogr., Sect. D: Biol. Crystallogr.* **2014**, *70*, 317−328.
(24) Rouser, G.; Siakotos, A. N.; Fleischer, S. Quantitative analysis of phospholipids by thin-layer chromatography and phosphorus analysis of spots. *Lipids* **1966**, *1*, 85−86.
(25) Schiller, J.; Süss, R.; Arnhold, J.; Fuchs, B.; Lessig, J.; Müller, M.; Petković, M.; Spalteholz, H.; Zschörnig, O.; Arnold, K. Matrix-assisted laser desorption and ionization time-of-flight (MALDI-TOF) mass spectrometry in lipid and phospholipid research. *Prog. Lipid Res.* **2004**, *43*, 449−488.
(26) Petkovic, M.; Schiller, J.; Müller, M.; Benard, S.; Reichl, S.; Arnold, K.; Arnhold, J. Detection of individual phospholipids in lipid mixtures by matrix-assisted laser desorption/ionization time-of-flight mass spec-trometry: phosphatidylcholine prevents the detection of further species. *Anal. Biochem.* **2001**, *289*, 202−216.
(27) Hirz, M.; Richter, G.; Leitner, E.; Wriessnegger, T.; Pichler, H. A novel cholesterol-producing Pichia pastoris strain is an ideal host for functional expression of human Na,K-ATPase $\alpha 3\beta 1$ isoform. *Appl. Microbiol. Biotechnol.* **2013**, *97*, 9465−9478.
(28) Moulin, M.; Strohmeier, G.; Hirz, M.; Thompson, K. C.; Rennie, A. R.; Campbell, R. A.; Pichler, H.; Maric, S.; Forsyth, V. T.; Haertlein, M. Perdeuteration of cholesterol for neutron scattering applicatioins using recombinant Pichia Pastoris. *Chem. Phys. Lipids* **2018** (in press).
(29) Haertlein, M.; Moulin, M.; Devos, J. M.; Laux, V.; Dunne, O.; Forsyth, V. T. Biomolecular Deuteration for Neutron Structural Biology and Dynamics. *Methods Enzymol.* **2016**, *566*, 113−157.
(30) Campbell, R. A.; Wacklin, H. P.; Sutton, I.; Cubitt, R.; Fragneto, G. FIGARO: The new horizontal neutron reflectometer at the ILL. *Eur. Phys. J. Plus* **2011**, *126*, 107.
(31) Nelson, A. Co-refinement of multiple-contrast neutron/X-ray reflectivity data using MOTOFIT. *J. Appl. Crystallogr.* **2006**, *39*, 273−276.
(32) Cho, N.-J.; Frank, C. W.; Kasemo, B.; Höök, F. Quartz crystal microbalance with dissipation monitoring of supported lipid bilayers on various substrates. *Nat. Protoc.* **2010**, *5*, 1096−1106.
(33) Vitiello, G.; Fragneto, G.; Petruk, A. A.; Falanga, A.; Galdiero, S.; D'Ursi, A. M.; Merlino, A.; D'Errico, G. Cholesterol modulates the fusogenic activity of a membranotropic domain of the FIV glycoprotein gp36. *Soft Matter* **2013**, *9*, 6442−6456.
(34) Lind, T. K.; Wacklin, H.; Schiller, J.; Moulin, M.; Haertlein, M.; Pomorski, T. G.; Cárdenas, M. Formation and characterization of supported lipid bilayers composed of hydrogenated and deuterated Escherichia coli lipids. *PLoS One* **2015**, *10*, No. e0144671.
(35) de Ghellinck, A.; Fragneto, G.; Laux, V.; Haertlein, M.; Jouhet, J.; Sferrazza, M.; Wacklin, H. Lipid polyunsaturation determines the extent of membrane structural changes induced by Amphotericin B in Pichia pastoris yeast. *Biochim. Biophys. Acta, Biomembr.* **2015**, *1848*, 2317−2325.
(36) Melby, E. S.; Mensch, A. C.; Lohse, S. E.; Hu, D.; Orr, G.; Murphy, C. J.; Hamers, R. J.; Pedersen, J. A. Formation of supported lipid bilayers containing phase-segregated domains and their interaction with gold nanoparticles. *Environ. Sci.: Nano* **2016**, *3*, 45−55.
(37) Richter, R.; Mukhopadhyay, A.; Brisson, A. Pathways of lipid vesicle deposition on solid surfaces: a combined QCM-D and AFM study. *Biophys. J.* **2003**, *85*, 3035−3047.
(38) Richter, R. P.; Brisson, A. R. Following the formation of supported lipid bilayers on mica: a study combining AFM, QCM-D, and ellipsometry. *Biophys. J.* **2005**, *88*, 3422−3433.
(39) Richter, R. P.; Bérat, R.; Brisson, A. R. Formation of solid-supported lipid bilayers: an integrated view. *Langmuir* **2006**, *22*, 3497−3505.
(40) Seantier, B.; Breffa, C.; Félix, O.; Decher, G. Dissipation-enhanced quartz crystal microbalance studies on the experimental parameters controlling the formation of supported lipid bilayers. *J. Phys. Chem. B* **2005**, *109*, 21755−21765.
(41) Åkesson, A.; Lind, T.; Ehrlich, N.; Stamou, D.; Wacklin, H.; Cárdenas, M. Composition and structure of mixed phospholipid supported bilayers formed by POPC and DPPC. *Soft Matter* **2012**, *8*, 5658−5665.
(42) Nöllmann, M.; Gilbert, R.; Mitchell, T.; Sferrazza, M.; Byron, O. The Role of Cholesterol in the Activity of Pneumolysin, a Bacterial Protein Toxin. *Biophys. J.* **2004**, *86*, 3141−3151.
(43) Schiller, J.; Süß, R.; Arnhold, J.; Fuchs, B.; Leßig, J.; Müller, M.; Petković, M.; Spalteholz, H.; Zschörnig, O.; Arnold, K. Matrix-assisted laser desorption and ionization time-of-flight (MALDI-TOF) mass spectrometry in lipid and phospholipid research. *Prog. Lipid Res.* **2004**, *43*, 449−488.
(44) Veatch, S. L.; Keller, S. L. Miscibility Phase Diagrams of Giant Vesicles Containing Sphingomyelin. *Phys. Rev. Lett.* **2005**, *94*, 148101.
(45) McGarrity, J. T.; Armstrong, J. B. Phase transition behaviour of artificial liposomes composed of phosphatidylcholines acylated with cyclopropane fatty acids. *Biochim. Biophys. Acta, Biomembr.* **1981**, *640*, 544−548.
(46) Richter, R. P.; Maury, N.; Brisson, A. R. On the effect of the solid support on the interleaflet distribution of lipids in supported lipid bilayers. *Langmuir* **2005**, *21*, 299−304.
(47) Rossetti, F. F.; Textor, M.; Reviakine, I. Asymmetric distribution of phosphatidyl serine in supported phospholipid bilayers on titanium dioxide. *Langmuir* **2006**, *22*, 3467−3473.
(48) Wacklin, H. P.; Thomas, R. K. Spontaneous formation of asymmetric lipid bilayers by adsorption of vesicles. *Langmuir* **2007**, *23*, 7644−7651.
(49) Heberle, F. A.; Petruzielo, R. S.; Pan, J.; Drazba, P.; Kučerka, N.; Standaert, R. F.; Feigenson, G. W.; Katsaras, J. Bilayer Thickness Mismatch Controls Domain Size in Model Membranes. *J. Am. Chem. Soc.* **2013**, *135*, 6853−6859.
(50) Braun, A. R.; Sachs, J. N. Determining Structural and Mechanical Properties from Molecular Dynamics Simulations of Lipid Vesicles. *J. Chem. Theory Comput.* **2014**, *10*, 4160−4168.
(51) Choubey, A.; Kalia, R. K.; Malmstadt, N.; Nakano, A.; Vashishta, P. Cholesterol Translocation in a Phospholipid Membrane. *Biophys. J.* **2013**, *104*, 2429−2436.
(52) Devaux, P.; Herrman, A. *Transmembrane Dynamics of Lipids*; John Wiley & Sons: New Jersey, 2012.
(53) Ingólfsson, H. I.; Melo, M. N.; van Eerden, F. J.; Arnarez, C.; Lopez, C. A.; Wassenaar, T. A.; Periole, X.; de Vries, A. H.; Tieleman, D. P.; Marrink, S. J. Lipid Organization of the Plasma Membrane. *J. Am. Chem. Soc.* **2014**, *136*, 14554−14559.
(54) Bogdanov, M.; Heacock, P. N.; Dowhan, W. A Polytopic Membrane Protein Displays A Reversible Topology Dependent on Membrane Lipid Composition. *EMBO J* **2002**, *21*, 2107−2116.

DOI: 10.1021/acs.langmuir.7b02716
Langmuir 2018, 34, 472−479

Supporting Information

Localization of Cholesterol within Supported Lipid Bilayers Made of a Natural Extract of Tailor-Deuterated Phosphatidylcholine

Sarah Waldie, Tania K. Lind, Kathryn Browning, Martine Moulin, Michael Haertlein, V. Trevor Forsyth, Alessandra Luchini, Gernot A. Strohmeier, Harald Pichler, Selma Maric and Marité Cárdenas.

	SLD * 10^{-6} / Å^{-2}	Volume / Å^3
Si	2.07	
SiO_2	3.47	
dPC tail	6.1	905[1]
dPC head	6.1	322[2]
h-cholesterol	0.2	622[3]
d-cholesterol	7.2	622[3]

Table S1. Theoretical SLD values and molecular volumes used.

[1] Assuming the volume of the POPC tail minus the volume of a CH_3 group, for the main 16:0/17:0 cyclo PC present in the mixture (see Figure SI1); calculated from the component volumes of CH_2, C=C, and CH_3 generated from MD simulations (Armen, Uitto et al. 1998).

[2] Calculated from component volumes of the PC headgroup generated from MD simulations (Armen, Uitto et al. 1998)

[3] Taken from (Greenwood, Tristram-Nagle et al. 2006)

The Si-SiO_2 substrate was modeled as a single layer and typical results gave a SiO_2 layer that was 6-8 Å thick, 2-3 Å rough and contained 2-10% solvent within it. A thin (3-4 Å) water layer between the silica and the lipids was required to fit all NR data. This is a common practice for fitting SLBs, see for example (Åkesson, Lind et al. 2012).

The free parameters used for each data set fit are summarised below: single, underlined values refer to fixed parameters, while a range is shown for the variable parameters. Simultaneous fitting of both h- and d- cholesterol containing dPC mixtures was performed. The roughness of the various layers of the SLB were co-fitted to the same values. The SLD values for the heads of the cholesterol containing bilayers were fixed to the value fitted for the data without cholesterol.

	SLD * 10^{-6} / $Å^{-2}$	**thickness/Å**	**coverage/%**	**roughness/Å**
Underlying substrate				
SiO_2	2.07	5-10	0-25	2-4
Solvent layer	6.35	3-7	*0*	2-4
without cholesterol				
Inner head	6-6.5	35-45	90-100	2-5
with cholesterol				
Inner head	6.1	6.0 - 8.5	18- 40	2-5
Tail	6.1-7.3 (d)/0-6.1 (h)	9-12 (*3)	90-100	
Outer head	6.1	6.0 - 8.5	18- 40	

Table S2. Parameters and range of values used to fit the NR data.

Figure S1 NR data for a dPC SLB including the best fit (solid lines) to a one-layer model. The bulk solvent contrasts were D_2O, H_2O and cmSi (green squares, purple triangles and blue circles, respectively). The graph below shows the corresponding scattering length density profiles for the best fit.

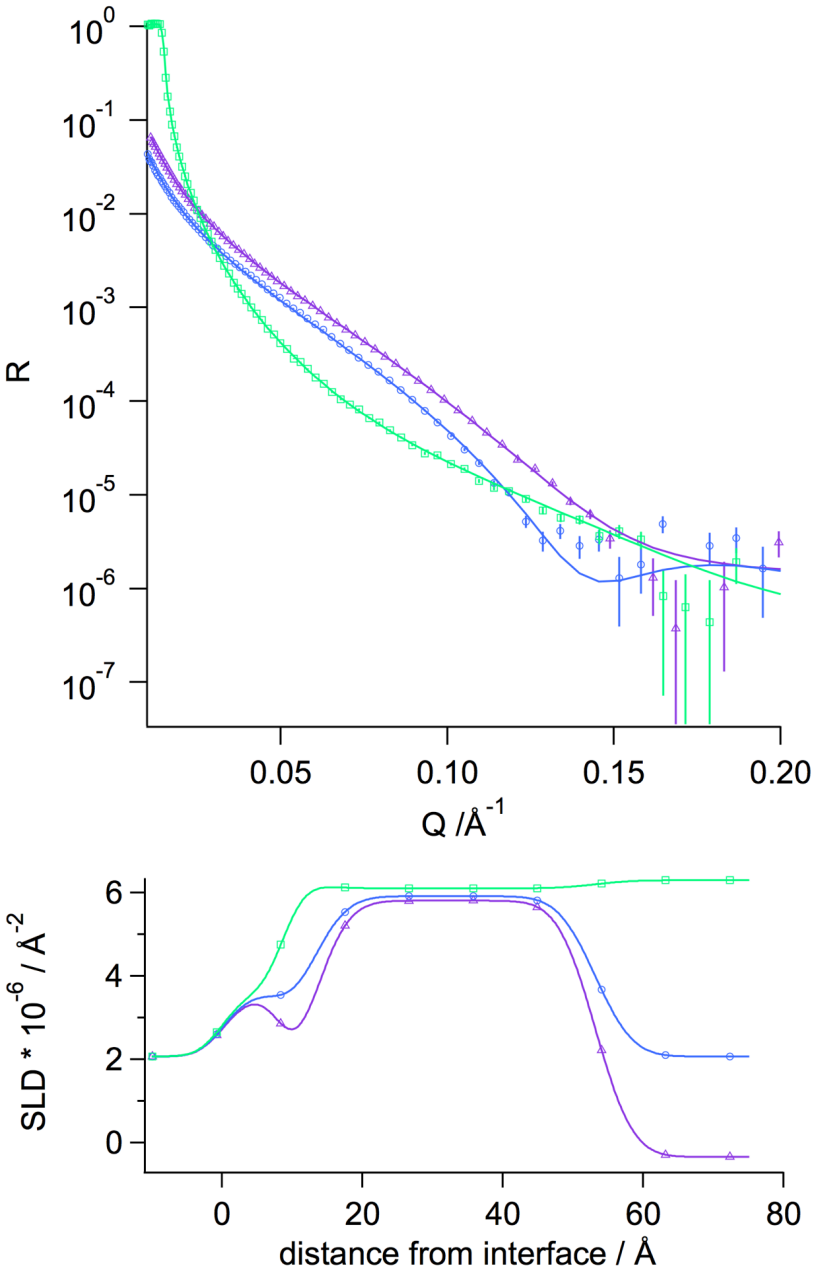

Figure S2. Positive ion mode MALDI-TOF mass spectrum of phospholipid species extracted from adapted AL95 cells grown in ~100 % D_2O supplemented with deuterated glycerol (Sigma Aldrich) and labeled choline (trimethyl- d_9, 98%; Eurisotop). Spectra were recorded in the presence of 9-aminoacridine as the matrix. Only the most abundant species (16:0/17:0 cyclo) were investigated in more detail and compositional details are given exclusively for these species.

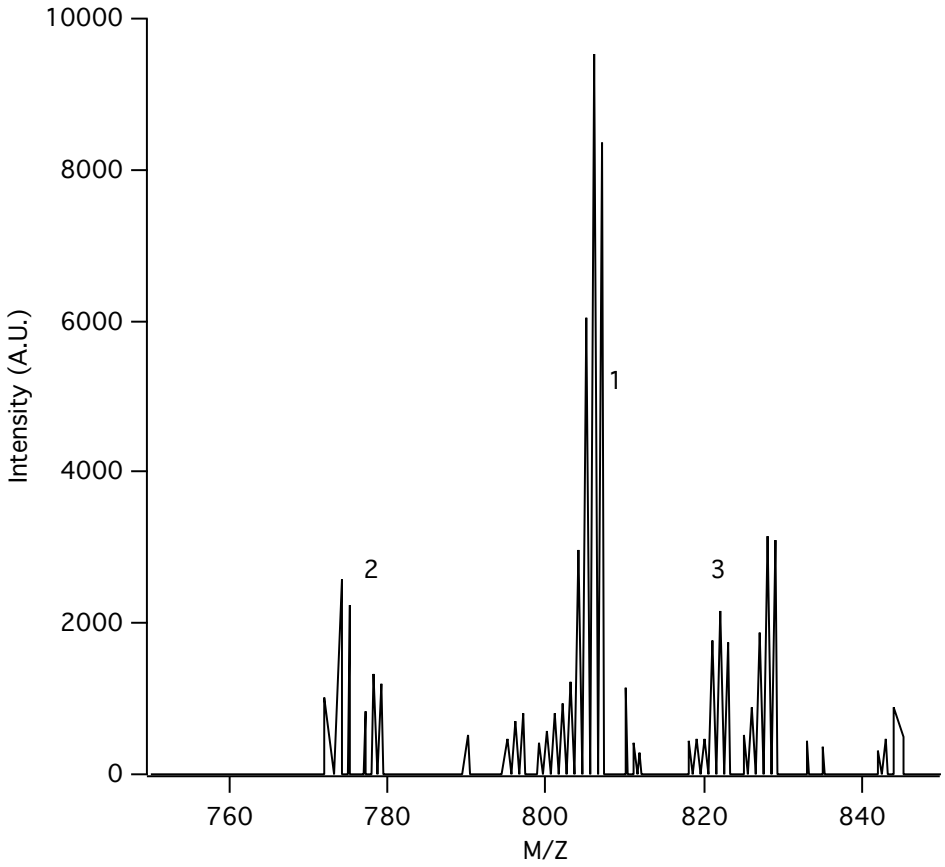

Main PC lipids found in order of abundance:

1. PC 16:0/17:0cyc + H^+,$C_{41}H_{23}D_{58}NO_8P$, theoretical mass: 806.4 Da, Na^+ adduct: 828.4 Da

2. PC 16:0/15:0cyc + H^+, $C_{39}H_{23}D_{54}NO_8P$, theoretical mass: 774.33 Da, Na^+ adduct: 796.33 Da

3. PC 16:0/18:1 + H^+, $C_{42}H_{21}D_{61}NO_8P$, theoretical mass: 822.4 Da, Na^+ adduct: 844.4 Da

Figure S3. NR data for a dPC SLB containing 20 mol% h- or d-cholesterol (black and pink, respectively), including best fit (solid lines) to an asymmetric 4L (A) or a symmetric 3L (B) model. The figure includes the corresponding SLD profiles (below) for the best fit shown in the figure above. The bulk contrasts were D_2O, H_2O and cmSi (squares (top), triangles (middle) and circles (bottom), respectively). The contrasts have been offset on the *y*-scale for clarity. The best Chi^2 fit values are 23.3, 16.2 and 9.6 for a symmetric 3L, an asymmetric 4L, and an asymmetric 5L model respectively.

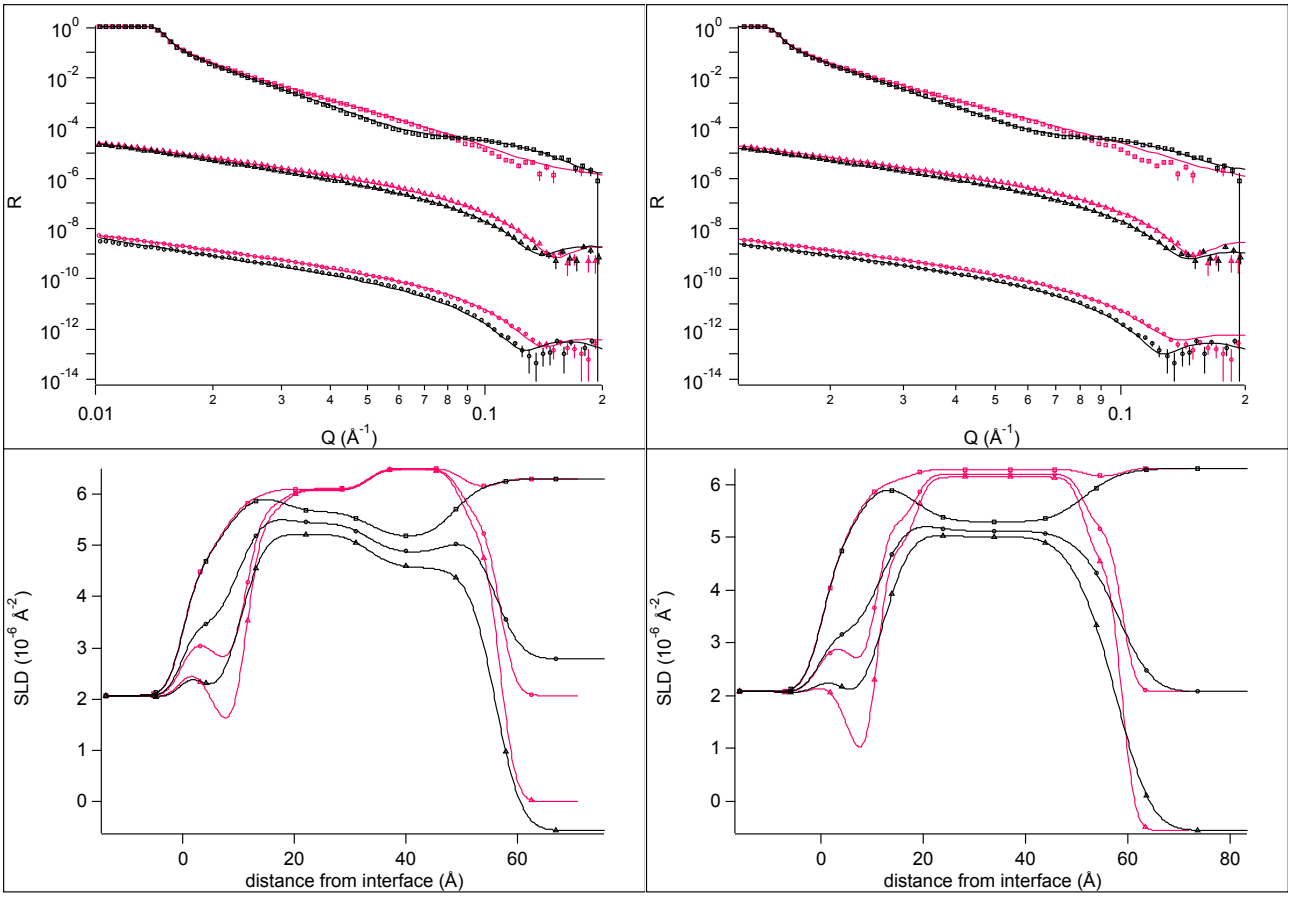

References

Åkesson, A., T. Lind, N. Ehrlich, D. Stamou, H. P. Wacklin and M. Cardenas (2012). "Composition and structure of mixed phospholipid supported bilayers formed by POPC and DPPC." Soft Matter **8**(20): 5658-5665.

Armen, R. S., O. D. Uitto and S. E. Feller (1998). "Phospholipid Component Volumes: Determination and Application to Bilayer Structure Calculations." Biophys J **75**: 734-744.

Greenwood, A. I., S. Tristram-Nagle and J. F. Nagle (2006). "Partial molecular volumes of lipids and cholesterol." Chem. Phys. Lipids **143**: 1-10.

Paper 3

BBA - Molecular and Cell Biology of Lipids 1865 (2020) 158769

Contents lists available at ScienceDirect

BBA - Molecular and Cell Biology of Lipids

journal homepage: www.elsevier.com/locate/bbalip

Lipoprotein ability to exchange and remove lipids from model membranes as a function of fatty acid saturation and presence of cholesterol

Sarah Waldie[a,b,1], Federica Sebastiani[a], Kathryn Browning[c], Selma Maric[d], Tania K. Lind[a], Nageshwar Yepuri[e], Tamim A. Darwish[e], Martine Moulin[b,1], Gernot Strohmeier[f,g], Harald Pichler[f,h], Maximilian W.A. Skoda[i], Armando Maestro[b], Michael Haertlein[b,1], V. Trevor Forsyth[b,j,1], Eva Bengtsson[k], Martin Malmsten[c,l], Marité Cárdenas[a,*]

[a] Department of Biomedical Science and Biofilms – Research Center for Biointerfaces, Malmö University, 20506 Malmö, Sweden
[b] Institut Laue-Langevin, 71 Avenue des Martyrs, 38042 Grenoble, Cedex 9, France
[c] Department of Pharmacy, Copenhagen University, Universitetsparken 2, 2100 Copenhagen, Denmark
[d] MAX IV Laboratory, Fotongatan 2, 225 92 Lund, Sweden
[e] National Deuteration Facility, Australian Nuclear Science and Technology Organisation, New Illawarra Road, Lucas Heights, NSW 2234, Australia
[f] Austrian Centre of Industrial Biotechnology, Petersgasse 14, 8010 Graz, Austria
[g] Graz University of Technology, Institute of Organic Chemistry, NAWI Graz, Stremayrgasse 9, 8010 Graz, Austria
[h] Graz University of Technology, Institute of Molecular Biotechnology, NAWI Graz, BioTechMed Graz, Petersgasse 14, 8010 Graz, Austria
[i] STFC, Rutherford Appleton Laboratory, ISIS, Harwell, Didcot OX11 0QX, UK
[j] Faculty of Natural Sciences, Keele University, Staffordshire ST5 5BG, UK
[k] Department of Clinical Sciences, Malmö, University of Lund, Clinical Research Center, Jan Waldenströms gata 35, 214 28 Malmö, Sweden
[l] Department of Physical Chemistry 1, University of Lund, SE-22100 Lund, Sweden

ARTICLE INFO

Keywords:
Lipoproteins
Cholesterol
Neutron reflection
Lipid removal
Saturated fats

ABSTRACT

Lipoproteins play a central role in the development of atherosclerosis. High and low-density lipoproteins (HDL and LDL), known as 'good' and 'bad' cholesterol, respectively, remove and/or deposit lipids into the artery wall. Hence, insight into lipid exchange processes between lipoproteins and cell membranes is of particular importance in understanding the onset and development of cardiovascular disease. In order to elucidate the impact of phospholipid tail saturation and the presence of cholesterol in cell membranes on these processes, neutron reflection was employed in the present investigation to follow lipid exchange with both HDL and LDL against model membranes. Mirroring clinical risk factors for the development of atherosclerosis, lower exchange was observed in the presence of cholesterol, as well as for an unsaturated phospholipid, compared to faster exchange when using a fully saturated phospholipid. These results highlight the importance of membrane composition on the interaction with lipoproteins, chiefly the saturation level of the lipids and presence of cholesterol, and provide novel insight into factors of importance for build-up and reversibility of atherosclerotic plaque. In addition, the correlation between the results and well-established clinical risk factors suggests that the approach taken can be employed also for understanding a broader set of risk factors including, e.g., effects of triglycerides and oxidative stress, as well as local effects of drugs on atherosclerotic plaque formation.

1. Introduction

Atherosclerosis is the largest killer in the west and accounted for an estimated 17.9 million deaths in 2016 [1]. It is a leading cause of cardiovascular disease (CVD), which in turn originates from the build-up of plaque on artery walls. This plaque build-up arises from the deposition of lipoproteins, which are subsequently oxidised, in turn initiating an active inflammatory process and taken up by macrophages. The macrophages develop into foam cells filled with lipids and cholesterol, over time forming a hard plaque. If this plaque ruptures, blood will be exposed to thrombogenic material, which can result in a heart attack or stroke [2]. Although plaque formation is a complex process, involving not only endothelial cells but also connective tissue, as well as calcification and onset of oxidative and other processes [3,4],

* Corresponding author.
E-mail address: marite.cardenas@mau.se (M. Cárdenas).
[1] Partnership for Structural Biology (PSB), 71 Avenue des Martyrs, 38042 Grenoble, Cedex 9, France.

https://doi.org/10.1016/j.bbalip.2020.158769
Received 23 March 2020; Received in revised form 11 May 2020; Accepted 19 July 2020
Available online 23 July 2020

lipoprotein deposition nevertheless constitutes a key initial step. Despite this, the initial interaction of lipoprotein particles with the membrane wall remains poorly understood, notably in relation to lipid exchange from lipoprotein to the cell membrane and vice versa.

Lipoproteins are particle-like aggregates which consist of a core of cholesterol esters and triglycerides, encased by a monolayer of lipids and apolipoproteins [5]. Among the diverse family of lipoproteins [5], high- and low-density lipoproteins (HDL and LDL) are particularly important in atherosclerosis. HDL and LDL differ in structure, composition and their role in atherogenic processes [6]. It has been shown clinically that LDL deposits into artery walls, aiding the development of atherosclerosis, whilst HDL plays a preventive role by removing cholesterol from the lipid-filled foam cells in a process known as reverse cholesterol transport (RCT) [7,8]. For these reasons, HDL and LDL are frequently referred to as 'good' and 'bad' cholesterol, respectively.

In RCT, HDL removes free cholesterol from blood vessel walls via various pathways [9,10] and eventually transports it to the liver where it is removed from the body. An inverse relationship has been demonstrated between RCT efficiency and the risk of CVD [10], illustrating the importance of this step and the role of HDL in the prevention of atherosclerosis. However, the situation is complex as the quantity of HDL alone does not determine suppression of the risk of CVD, and increased levels of HDL have also been found to result in no effect [11] or even in an increased risk for CVD [12]. Having said that, the ratio of HDL to LDL is of importance [13]. This suggests that there is a delicate equilibrium in the transport of cholesterol and other fats in both directions between the lipoproteins and the endothelial membranes, which determines the onset of atherosclerosis. There are also several other fat components important in the development of atherosclerosis, also transported by lipoproteins. These include triglycerides and lipids with either saturated or unsaturated fatty acid tails.

Whilst the dietary guidelines for the prevention of CVD include the reduction of saturated fats with preference for unsaturated fats, there are further layers of complexity in the types of fats present in foods and their origin in the diet. Reflecting this, there is a striking lack of consensus of whether or not dietary saturated fats can be directly correlated to the development of various lipoprotein types and in turn CVD [14]. There is also little evidence that the presence of cholesterol in the diet impacts the risk of CVD [15].

In our previous work, we developed methodologies to quantify lipid exchange from model cell membranes by lipoproteins (Fig. 1) using both neutron reflection [16] and small angle neutron scattering [17]. Such methodologies allow mechanistic studies of the impact of membrane composition on the capacity of lipoproteins to exchange and remove lipids. For example, neutron reflection results have demonstrated that increasing the content of negatively charged lipids in the membrane (as in cancerous cells [18]) resulted in an increased removal of lipids from the cell membrane bilayer in both HDL and LDL systems [19]. This mirrors the strong interaction of LDL with negatively charged surfaces, mediated by electrostatic interactions with the positive residues in the ApoB protein in LDL [20], and has clinical implications related to calcium signalling in atherosclerotic development [21]. While thus showing promise as a tool for mechanistic studies of lipoprotein-membrane exchange, these previous investigations did not address effects of cholesterol and lipid saturation, widely important for atherosclerotic plaque formation, but with poorly understood underlying mechanisms. Considering this, we hereby employ neutron reflection to distinguish the effects of acyl chain saturation and the presence of cholesterol on the ability of lipoproteins to exchange lipids to/from model membranes.

2. Materials and methods

D_2O (99.9% deuterated, Sigma-Aldrich) was provided by the Institut Laue-Langevin, Grenoble, France and by the ISIS Neutron Source, Didcot, UK. MilliQ water (18.2 Ω cm^{-1}) was used for all cleaning procedures and solvent preparations. Calcium chloride ($CaCl_2$) and Tris buffer saline tablets were from Sigma-Aldrich. Tris buffer (50 mM Tris, 150 mM NaCl, pH 7.4) was prepared by dissolving a tablet in H_2O or D_2O as specified by the producer. 1,2-Dimyristoyl-d54-sn-glycero-3-phosphocholine (dDMPC; > 99%) was from Avanti Polar Lipids (Alabaster, AL). 1-palmitoyl, 2-oleoyl-sn-glycero-3-phosphocholine (POPC) in perdeuterated form (dPOdPC, d77; overall purity 95%) and tail-deuterated form (dPOhPC, d67; overall purity 95%) were both provided by the deuteration facility at ANSTO, produced and purified as previously described [22]. Bradford was from Sigma while *infinite* triglyceride and cholesterol enzymatic assays were from ThermoFisher.

2.1. D_2O-matched PC production

Selectively deuterated phosphatidylcholine (dPC) was produced as reported previously [23]. The *Escherichia coli* strain AL95 (pssA::kan^R lacY::Tn9 cam^R), containing the plasmid pAC-PCS_{lp}-Sp-Gm (P_{araB}-pcs Sp^R Gm^R), was grown in 100% deuterated minimal medium [24] with the incorporation of deuterated d8-glycerol, 0.2% arabinose (unlabelled; Sigma-Aldrich) and 2 mM deuterated choline chloride (trimethyl-d9, 98%; Eurisotop) [23]. After incubation at 37 °C for 24 h, cells were harvested by centrifugation (10,000*g*, 20 min, 4 °C). Total lipids were extracted by the Bligh and Dyer method [25] and separated according to phospholipid head group via chromatography on a silica-gel column using varying ratios of chloroform and methanol [23].

Thin-layer chromatography was used to further characterise the phospholipids by comparison to known standards [26] and quantitatively assessed through phosphate analysis [27]. The fatty acid composition of the purified dPC was determined previously to be PC 16:0/17:0cyc (where 'cyc' refers to the cyclic unsaturation, also known as propyl unsaturation), PC 16:0/15:0cyc and PC 16:0/18:1 in order of abundance [28].

2.2. Deuterated cholesterol production

Perdeuterated cholesterol was produced and purified as reported previously [29]. The Pichia pastoris strain CBS7435 Δhis4Δku70 Δerg5::pPpGAP-ZeocinTM-[DHCR7] Δerg6::pGAP-G418[DHCR24] was grown in 100% deuterated basal salts medium in the presence of d8-glycerol (Eurisotop). After 7 days in a fermenter at 28 °C, the batch phase was complete and the fed-batch phase was initiated by constant feeding of d8-glycerol for a further 12 days. The cells were harvested and then isolated using an organic solvent extraction method followed by HPLC to obtain pure cholesterol, verified by GCMS.

The production of dPC and deuterated cholesterol made full use of the Deuteration Laboratory (D-lab) within ILL's Life Sciences Group [30]; this facility is widely used for in vitro production of biomolecules in the interests of biological neutron scattering [31–37].

2.3. Model membrane preparation

Lipid films were prepared from chloroform stocks of the different PC lipids and cholesterol to obtain the desired compositions. Chloroform was evaporated under a stream of nitrogen and the resulting films placed under vacuum overnight.

Prior to use, the lipid films were hydrated to a concentration of 0.2 mg mL^{-1} in MilliQ water and bath sonicated for 1 h. The lipids were then tip sonicated for 5 min (20% power, 5 s on, 5 s off) immediately before use. To optimise vesicle fusion, lipids were deposited at a concentration of 0.1 mg mL^{-1} in the presence of 2 mM $CaCl_2$ [38,39]; freshly tip-sonicated lipids were mixed with an equal volume of 4 mM $CaCl_2$ solution [16,28], and immediately introduced into the solid-liquid flow cell (pre-equilibrated at 37 °C) by syringe injection. The lipids were incubated for 20 min before rinsing with water, followed by 50 mM Tris saline buffer, pH 7.4. This process leads to a supported lipid bilayer or *'model membrane'*.

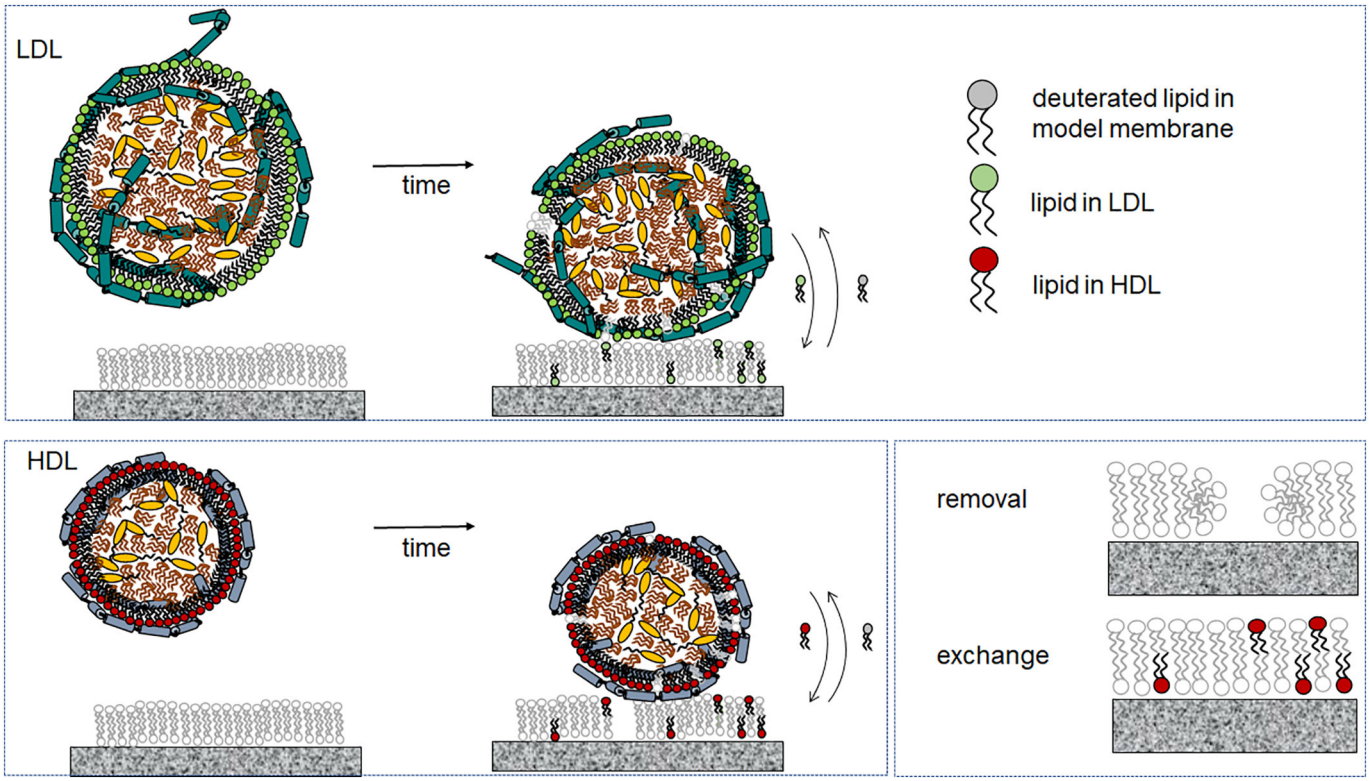

Fig. 1. Schematic illustration of the incubation of lipoprotein particles with the model membranes (not-to-scale: LDL is two to three times larger in diameter than HDL). Deuterated lipids in the model membrane can be exchanged by hydrogenated lipids from the lipoproteins and also removed via uptake by lipoproteins. Neutron reflection can distinguish between deuterated and hydrogenated lipids in the bilayer, and allows quantification of these processes (Cholesterol has not been included in the schematic illustration for clarity, since some systems contain cholesterol and others do not).

2.4. Lipoprotein preparation

Lipoprotein particle preparation was carried out as described before [40]. Human plasma from three healthy males was purified by sequential ultracentrifugation resulting in isolated LDL and HDL at densities of 1.019 and 1.065 g mL^{-1}, respectively. These purified samples were then pooled and stored in 50% sucrose, 150 mM NaCl, 24 mM EDTA, pH 7.4 at −80 °C, and further fractionated via size exclusion chromatography at 25 °C (Superose 6 Increase 10/300 GL column, GE Healthcare) before use in 25 mM Tris, 150 mM NaCl at pH 7.4. Samples were stored at 4 °C, in an inert atmosphere away from light, ready to be used within one week. The Bradford assay was used to determine protein concentration, which in turn was used to calculate lipoprotein concentration. Triglyceride and total cholesterol assays were used as described by the manufacturer. Three different pooled preparations were used for various neutron experiments and the protein, triglyceride, and cholesterol concentrations were used to calculate the total composition in mass ratio (Supporting Information, Table S1). Prior to injection, the lipoprotein solution was diluted to a protein concentration of 0.1 mg mL^{-1} for LDL and 0.132 mg mL^{-1} for HDL in 50 mM Tris saline buffer, pH 7.4. These values were chosen to ensure constant lipoprotein particle concentration giving the same number of HDL and LDL particles incubating with each bilayer. The same values were also used in previous studies, enabling direct comparison [16,19]. Samples were injected into the solid liquid flow cells at 1 mL min^{-1} by a syringe pump via an injection port. The experiments were carried out at 37 °C to resemble the physiological environment and to ensure the fluidity of lipids in the model biomembrane as well as in the core in low density lipoprotein, the latter being solid below 20 °C [40].

2.5. Neutron reflectometry

Neutron reflection data were collected on FIGARO [41,42], a time-of-flight reflectometer, at the Institut Laue-Langevin (Grenoble, France), and at INTER [43] and OFFSPEC [44], both at the ISIS Neutron Facility (Didcot, UK). In specular conditions, an incident neutron beam with wavelength, λ, is directed towards the solid/liquid interface at an incident angle, θ. The reflectivity as a function of the momentum transfer, $q = 4\pi sin(\Theta)/\lambda$, is measured and corresponds to the ratio of incident and reflected intensities. The resulting $R(q)$ profile is linked to a plane-averaged scattering length density (SLD) profile perpendicular to the surface. SLD profiles describe the structure and composition in the direction perpendicular to the surface plane and can be modelled by a series of layers normal to the substrate characterised by a thickness, roughness and SLD.

Momentum transfer ranges of $0.01 > q > 0.3$ $Å^{-1}$ were measured using wavelengths $2 < \lambda < 20$ Å and two incident angles, 0.8° and 2.3° on FIGARO, $1.5 < \lambda < 16$ Å and 0.7° and 2.3° on INTER, and $1.0 < \lambda < 14$ Å and 0.55° and 1.8° on OFFSPEC, with a spatial resolution ($\Delta q/q$) of 7% at the ILL and 3% at ISIS. The area exposed to the neutron beam was 30 × 60 mm^2. The experiments were carried out in reflection-up mode to ensure that any aggregated particles settled at the bottom of the cell, away from the surface being measured.

The experiments were carried out using bespoke solid-liquid flow cells at 37 °C. The alternative experimental design of performing the experiments at a fixed temperature difference above the melting transition (e.g., T_m + 10 °C) of the respective lipid system was not deemed suitable for the present investigation due to the vastly different transition temperatures in the systems investigated. Thus, DMPC has T_m = 24 °C and hence the experimental temperature used here is not too far off T_m + 10 °C. However, T_m = −2 °C for POPC and thus T_m + 10 °C = 8 °C. At 8 °C, lipoproteins would behave entirely

differently with, for example, the fluidity of the LDL core depending on temperature which for healthy individuals has a $T_m \approx 30$ °C [40]. Thus, at 8 °C the core in LDL is effectively a gel, dramatically skewing exchange kinetics.

The silicon (111) blocks were cleaned in Piranha solution (H_2SO_4/H_2O_2, 7:3 in volume) for 10 min at 80 °C before being thoroughly rinsed with MilliQ water. The polyether ether ketone (PEEK) and O-ring components of the cells were intensively cleaned in 2% (v/v) Hellmanex solution twice and MilliQ water via bath sonication, with MilliQ rinsing between each sonication. Buffer contrasts were changed via HPLC pump. Contrasts used were 50 mM Tris saline buffers prepared in D_2O, H_2O, and a mixture of 38:62 D_2O:H_2O in volume to contrast match the SLD of the silicon block (cmSi). The use of the deuterium isotope increases the SLD of components and can be used to highlight specific parts of the molecule, while the buffer contrasts allow differences to be seen.

Experimental data for the bilayers in the three isotropic contrasts were fitted simultaneously using the MOTOFIT software [45], while the genetic Monte Carlo minimisation algorithm within the software was used to determine error estimation of the fits. Error bars are calculated from the error of the fit and correspond to a single measurement. Initially the silicon surfaces were characterised to ensure they were clean and to determine the thickness and roughness of the oxide layer; these were then fixed alongside the three solvent contrasts for fitting the model membranes. This resulted in a five-layer model consisting of a silicon oxide layer in contact with the silicon block, a small solvent layer, followed by the bilayer. The bilayer itself is split into 3 layers: an inner headgroup (closest to the silicon block), a tail region, and an outer headgroup exposed to the solvent. The three contrasts were fitted simultaneously in order to constrain the fit. The bilayer was fitted to be symmetrical, i.e., the thickness, SLD, and coverage of the inner and outer headgroups were constrained to be equal to each other during the fitting process, whilst the roughness was constrained to be the same across the whole bilayer. These initial parameters were then used as the starting point to fit the characterisations of the membranes after the incubation with the lipoprotein particles. Upon lipoprotein interaction, the silicon oxide layer was kept constant, while the parameters of the other layers were allowed to vary to accommodate the changes (details in Supporting Information; Tables S3 and S4). In order to obtain an acceptable fit and in agreement with our previous work [16], membranes incubated with HDL required one extra layer while the membranes incubated with LDL required two extra layers, likely due to the larger size of LDL over HDL. The size of the extra HDL layer and the first LDL layer were found to be similar (ca. 60 Å), however, the second layer required for the LDL fit was slightly thicker (ca. 120 Å). All neutron reflectivity results summarized in the figures in the main manuscript are also given in Supporting Information Tables S3 and S4 to enable the reader to enjoy the specific details so that own calculations can be made. All figures on neutron reflectometry results in the paper are based on the data in these tables.

3. Results

In this work, neutron reflection was used to monitor HDL and LDL lipid exchange with model membranes consisting of either saturated or unsaturated phospholipids, both in the absence and presence of cholesterol. Neutron reflection can differentiate between deuterium-labelled and hydrogen-rich lipids as shown schematically in Fig. 1, allowing quantification of both lipid exchange and lipid removal from the model membranes by lipoproteins. Neutrons can thus differentiate between lipid exchanged by another lipid, and lipid replaced by solvent, by following the SLD change and the solvent content of the lipid tail region, respectively. The use of tail-deuterated lipids in a non-deuterated solvent (i.e., H_2O buffer) provides the best contrast to follow these phenomena by neutron reflection. The neutron reflection profiles were analysed via a layer model as described in the Materials and methods section. During the fitting process, the model was constrained to describe the three isotropic contrasts measured simultaneously (the bulk solution was exchanged from H_2O buffer, to a mixture of H_2O and D_2O buffer (38% D_2O), to pure D_2O buffer). This increases sensitivity of the method and allows decoupling of lipids exchanged (deuterated membrane lipids being replaced by hydrogenated lipoprotein lipids) from those removed (deuterated lipids removed and replaced by solvent). All pristine bilayers prior to incubation were found to have a surface coverage of 95% or more. Any minor defects below this were found not to influence resulting trends in lipoprotein interactions. The neutron reflection data, best fits, and layer models used to analyse the model membrane neutron reflectometry profiles can be found as Supporting Information (Tables S3 and S4, Figs. S1 and S2).

3.1. Effect of phospholipid unsaturation

Using the approach and model described above, saturated and unsaturated model membranes were found to behave very differently in terms of lipid exchange. First, we compared the interaction of HDL with saturated and unsaturated phospholipid model membranes. The results show a vast difference in the relative quantity of lipids exchanged and removed depending on phospholipid fatty acid saturation (Fig. 2). As different pooled lipoprotein samples varied slightly in composition (Supporting Information Fig. S1), Fig. 2 shows data for each model membrane relative to the incubation with the dDMPC membrane for the same lipoprotein sample. Corresponding absolute values are found in Supporting Information Table S4.

Overall, the quantities of lipids exchanged and removed were lower for the unsaturated phospholipids compared to the saturated phospholipids, regardless of lipoprotein type. For HDL, the amount of lipids exchanged with the unsaturated dPC membrane was ca. 80% lower than for saturated dDMPC. Analogously, the quantity of lipids removed (and replaced by solvent), for the unsaturated dPC membrane was significantly reduced compared to dDMPC (ca. 90%). For LDL, incubation with unsaturated dPC membranes led to a similar reduction in lipids exchanged as for HDL (ca. 80%). However, a smaller difference (ca. 60%) was observed between the saturated and unsaturated phospholipids removed. The absolute quantities of lipids exchanged and removed for dDMPC were also lower for LDL than for HDL (Supporting Information, Table S4). Both types of lipoproteins display preferential uptake of saturated lipids as compared to unsaturated ones, although HDL has a greater affinity for these than LDL. This is in agreement with previous results, showing HDL to have a higher affinity than LDL for exchanging and removing saturated lipids [16].

3.2. Effect of cholesterol in model membranes

Endothelial cellular membranes contain between 10 and 20 mol% of cholesterol [46]. Consequently, we investigated the effect of 10 or 20 mol% cholesterol on the capacity of lipoproteins to exchange lipids from model membranes (Fig. 2). The presence of cholesterol reduces the quantity of lipids exchanged and removed by HDL. For cholesterol-containing saturated membranes, there was an inverse relationship between the quantity of lipids exchanged and the amount of cholesterol in the model membrane. The presence of cholesterol also reduced the amount of lipids removed compared to dDMPC alone. In contrast, the presence of cholesterol in unsaturated dPC membranes did not affect the extent of lipids exchanged, while the amount removed was slightly increased.

A slightly different trend was observed in the presence of LDL. For saturated dDMPC membranes, exchange in the presence of 20 mol% cholesterol was comparable to that for dDMPC alone, while the quantity of lipids removed decreased with increased levels of cholesterol in the membranes. For unsaturated dPC containing 20 mol% cholesterol, there was little effect on the level of lipids exchanged as compared to the unsaturated dPC membrane alone. However, the amount of lipids

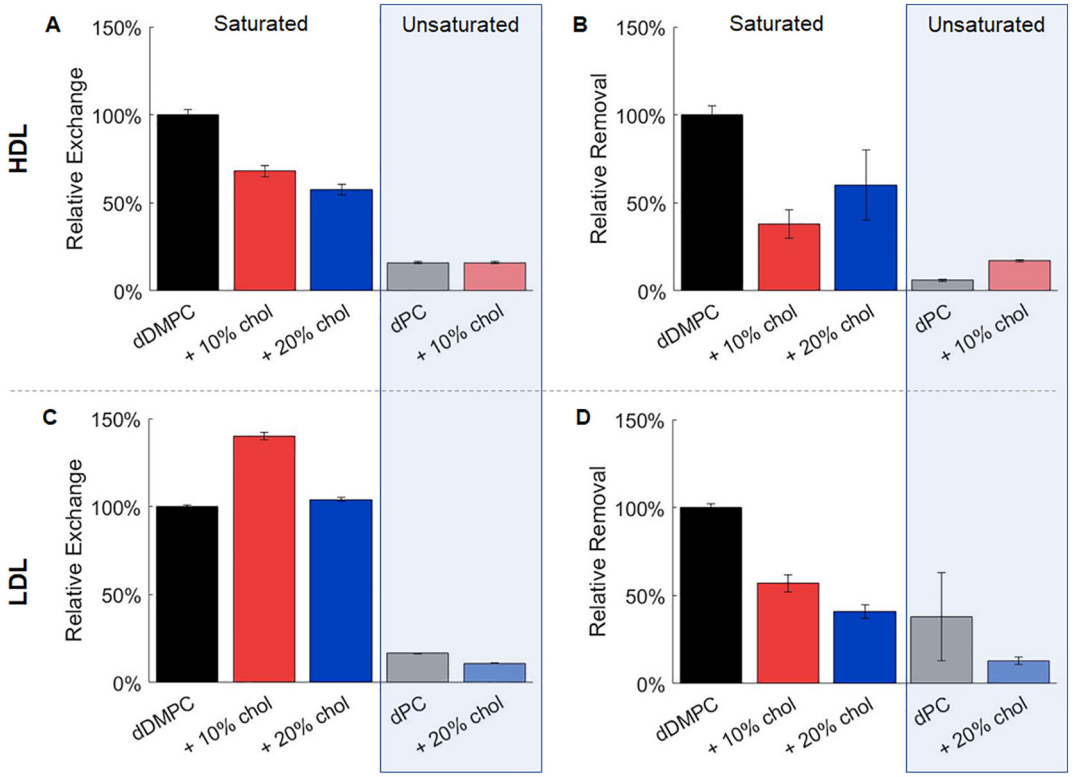

Fig. 2. Relative lipid exchange and removal for HDL or LDL particles interacting with membranes formed with saturated (dDMPC) and unsaturated (dPC) phospholipids with and without cholesterol. Results are shown for HDL (A, B) and LDL (C, D) regarding exchange (A, C) and removal (B, D).

removed by LDL decreased when including 20 mol% cholesterol in unsaturated phospholipid membranes.

3.3. Effect of lipid exchange by LDL as a function of LDL composition

Fig. 3 compares absolute values of lipid exchange according to lipoprotein particle content (the fat and protein content in the HDL and LDL fractions hereby used are given in Supporting Information Table S1). As seen, an increase in lipid exchange was found with increasing protein content in LDL, paralleled by a decreasing total fat content (cholesterol and triglyceride). In contrast, no pronounced dependency on lipoprotein composition was seen for phospholipid removal from the membrane (Supporting Information Table S4). For HDL, in turn, lipoprotein composition had only minor effects on lipids both exchanged and removed (Supporting Information Table S4).

In these experiments, the protein concentration was kept constant. This implies that the increase in protein content across the particles corresponds to a decrease in particle size, assuming a constant number of proteins per particle [47]. Thus, smaller LDL particles seem to have an improved ability to exchange lipids. This is well in line with clinical observations, in which smaller sized LDL sub-fractions were reported to display higher atherosclerotic effects, which can more easily penetrate artery walls and become a source of fat and cholesterol for the development of plaque [48,49].

3.4. Effect of headgroup deuteration on lipid exchange and removal by HDL

Since deuteration is a pre-requisite for performing these studies, we investigated the effect that the degree of headgroup deuteration have on lipid exchange by HDL. Fig. 4 gives the percentage of lipids exchanged or removed by HDL in model membranes consisting of either dPC (composed of a mixture of unsaturated PC and cyclopropane-containing PC), perdeuterated POPC (dPOdPC) or tail-deuterated POPC

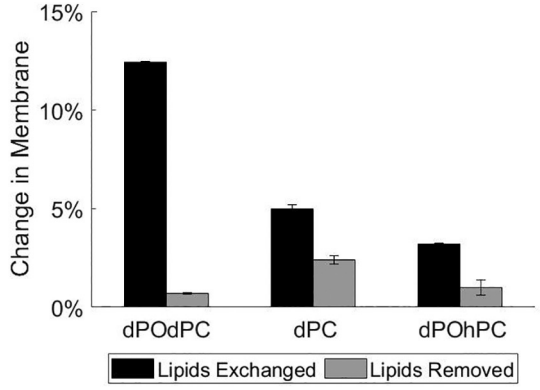

Fig. 3. Exchange of dDMPC by LDL as a function of the protein and total fat content of the latter.

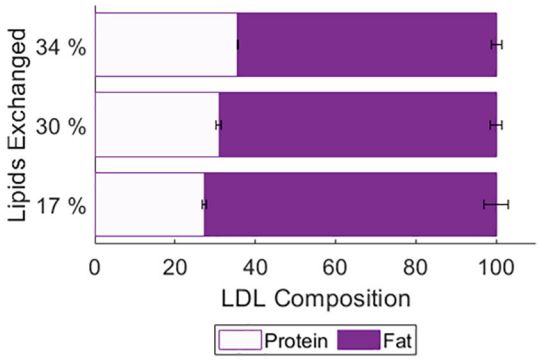

Fig. 4. HDL-induced lipid exchange and removal, for unsaturated dPOdPC, dPC and dPOhPC.

(dPOhPC). These deuterated phospholipids have different levels of deuteration in their phosphatidylcholine groups: 100%, 78%, and 0% in dPOdPC, dPC, and dPOhPC, respectively. Since the experimental temperature ensured full fluidity in all model membranes, the interaction data highlight the difference in the exchange and removal induced by deuteration of the headgroup of the model membranes. We found that the higher level of deuteration in the headgroup correlated to a stronger capacity of HDL to exchange lipids. However, phospholipid removal from the membrane (i.e., lipids being replaced by solvent) is not significantly influenced by headgroup deuteration, all samples showing 0.5–2.5% phospholipid removal from the model membranes. Hence, headgroup deuteration does have an effect on this type of exchange study in terms of absolute values of lipids exchanged. This can be explained by deuteration affecting bond vibrations, molecular motions and hydrogen bonding. Thus, we hypothesise that specific protein-lipid interactions are directly involved in the recognition of lipids within the model membrane by lipoproteins [50,51]. In particular, the minor effects observed for dPC as compared to dPOhPC could be correlated with this lipid having deuteration only on the amine methyl groups of the phosphatidylcholine headgroup [23], these amine group is not involved on hydrogen bonding. Even though deuteration in the headgroups could impact lipid-protein interactions, deuteration in the lipid tails can be used with no influence on the exchange data since these are not involved on specific interactions with apolipoproteins in LDL or HDL.

4. Discussion

Summarising the lipid exchange data for dDMPC with HDL and LDL (Table S4), and comparing these with previously reported data [19], we note that the absolute quantities are similar for most preparations and thus there is good reproducibility despite small variability in the lipoprotein composition. For HDL, the absolute quantities of lipids removed and exchanged are within error to those reported by Browning et al. [19]. For LDL, on the other hand, we observe a dependency of lipid exchange with the lipoprotein composition for denser LDL (Fig. 3). Therefore, our results suggest that lipoproteins have similar capacities to exchange and remove lipids, except for LDL with total protein content lower than 30%. This implies that the pooled LDL samples (presenting higher lipid exchange capacity) could be enriched in the more atherogenic [52], smaller and denser type of LDL, even though the individuals were considered to be healthy. Thus, our data may reflect the properties of different LDL sub-types to exchange fats [14]. This is the first time that differences in lipid exchange capacity have been reported for LDL fractions presenting distinctive compositions.

Our data clearly show that the saturation level of the phospholipids present in the bilayers strongly affects the ability of lipoproteins to exchange and further remove lipids from model membranes (Fig. 2). This is seen most prominently with HDL. The difference in the ease of lipid removal may be attributed to protein-lipid binding affinity of HDL and LDL particles with the model membranes. Indeed, the conformation of the protein present in reconstituted HDL particles greatly impacts lipoprotein binding affinity for unsaturated phospholipids [53]. The lipoprotein particle composition may impose conformational restrictions on apolipoproteins, which could translate as modified binding to lipid molecules present in the model membranes. It may also be noted here that HDL therapy, based on the re-modelling of the plaque by fat-poor HDL, results in a decrease of both saturated fats and cholesterol in atherosclerotic plaque [54,55], although studies suggest that the total amount of HDL alone does not suppress the risk for atherosclerosis [11]. This highlights the need to understand which molecular properties of HDL contribute to its lipid exchange capacity.

The different affinity for saturated and unsaturated phospholipids may be related to their different mobility. A recent inelastic neutron scattering study showed that saturated phospholipids have greater mobility both in the fluid and gel phases compared to unsaturated phospholipids [56]. Our data show that saturated lipids are more easily taken up by lipoproteins compared to unsaturated fats. Thus, lipids with greater mobility seem to be more accessible to lipoprotein binding, in turn facilitating lipid exchange. Earlier studies for lipid exchange between lipid aggregates (bicelles versus vesicles) showed that lipid exchange strongly depended on the length of the acyl chain as well as the type and size of the lipid aggregate [57]. However, these experiments were performed at 10 °C at which strong van der Waals interactions are expected. Moreover, in these experiments the molecular identity of the lipid aggregates did not change over time (bicelles exchange lipids with bicelles of the same composition or vesicles exchange lipids with vesicles of the same composition). This is clearly not the case for our experiments where lipids from the lipoproteins (presenting a very complex lipid type and acyl chain composition as measured by lipidomics [17]), replace the model membrane lipids, and vice versa. Thus, the findings from the present study on increased exchange and removal of saturated lipids add important new insight into lipid exchange between lipoprotein and lipid membranes.

The presence of cholesterol in the model membranes impacts the quantity of lipids exchanged and further removed. As with the level of saturation, this is most noticeable in the presence of HDL (Fig. 2). The normal cholesterol content in plasma membranes is 10–20 mol% [46]. Even though cholesterol is known to increase the order and hydrophobicity of membranes [46,58], differential scanning calorimetry (DSC) data of the model membranes hereby used (Supporting Information, Fig. S3) indicate that these membranes are fluid at 37 °C, in agreement with literature [59]. It is possible, however, that the cholesterol suppresses the mobility of saturated phospholipids to form liquid ordered bilayers, as previously demonstrated from in-plane diffusion studies [60]. At the same time, however, cholesterol may induce complex local ordering and other effects as well [61], which may influence lipoprotein-membrane lipid exchange. Experimentally, we did not observe any systematic trends for either lipoproteins due to cholesterol (Fig. 2), thus, it is unlikely that the effects observed are related alone to decreased mobility in the model membrane by increased cholesterol content. Furthermore, cholesterol molecules were reported to interact preferentially with saturated phospholipids [62,63]. Additionally, LDL was shown to bind preferentially to raft domains, rich in saturated fats and cholesterol [64], and to modify the cell membrane area covered by rafts [65]. Therefore, it seems likely that specific interactions between the apolipoproteins in the lipoproteins and the lipids in the model membrane determine the exchange of fats observed. We observed different lipid exchange by denser LDL (Fig. 3), suggesting that the properties of ApoB-100 (the main apolipoprotein in LDL) may be influenced by LDL density. Indeed, it was reported that small and medium-sized LDLs have altered epitopes between ApoB-100 residues 4342 and 4536, as compared with VLDLs, IDLs, and large LDL [47]. The altered expression of these epitopes in small and medium dense LDL coincides with altered accessibility of protease-sensitive sites elsewhere in the ApoB structure [66]. These findings suggest a major change in the configuration of the ApoB on the LDL surface due to increased density. Moreover, the sequence region that includes these epitopes is believed to form alpha helices which are the motives found in the exchangeable apolipoproteins (mainly A, C, E) that are known to bind lipids [67]. Indeed, we showed recently that lipoprotein binding to the model membrane is an important step for lipid exchange, since the exchange via solution or via simple collision is limited [17]. Such direct contact might favour protein-lipid interactions. However, further studies with reconstituted lipoproteins using specific apolipoproteins are needed to clarify this point.

Although debated, it has been shown that whilst dietary cholesterol intake does not in itself increase the risk of CVD [68], the intake of dietary saturated fats increases the risk of CVD [69]. Conversely, the replacement of saturated fats with mono- and polyunsaturated ones has been found to decrease the risk of CVD [70]. Such replacement has further been shown to lower total cholesterol, LDL cholesterol, and triglyceride levels in blood [70,71]: known markers for CVD risk

[49,72,73]. Furthermore, a diet with increased fat content has been shown to induce HDL production and also result in an increase in the total liver cholesterol content [74]. Mirroring this, our data show efficient lipid removal of unsaturated phospholipids also in the presence of cholesterol. Therefore, cholesterol intake together with a fatty diet based on unsaturated fats may give rise to high HDL values despite high cholesterol values in the liver. In contrast, as suggested by a pronounced effect of cholesterol content in saturated membranes in the present investigation as well as an overall large lipid exchange in the case of saturated phospholipids, a diet rich in saturated fats and cholesterol may result not only in high cholesterol values, but also affect HDL exchange in atherosclerotic plaque remodelling.

While neutron reflectivity provides novel insight on lipid exchange and removal on lipoprotein interactions with bilayers of different saturation and cholesterol content, it should be recognized that these findings have been observed for highly simplified models, which obviously do not fully represent the full biological system. For example, DMPC is present in endothelial membranes only in very small quantities, and DPPC would have represented a physiologically more relevant lipid. However, the melting temperature of the latter lipid is 41 ˚C, and DPPC is therefore not fluid at 37 ˚C. To use another temperature than 37 ˚C is unsuitable not only from a physiological relevance perspective, but also since other temperatures might induce phase transition of the core in low density lipoproteins to become gel-like [40]. Sphingomyelin, in turn, has a high melting temperature but currently we lack known biosynthetic/organic approaches for its deuterated form. The use of DPPC or ideally sphingomyelin in combination with POPC and cholesterol can give rise to “raft like” domains which are of interest to study in the future due to their biological relevance. Furthermore, deuteration in the backbone of the phosphatidylcholine headgroup has some effect on lipid exchange, which also demonstrates a limit on to how far one should draw the comparison with the full biological system endorsing the use of mainly tail deuterated lipids instead. With such considerations in mind, however, it seems clear that the experimental approach taken captures key effects of lipid saturation and presence of cholesterol for lipoprotein-associated lipid exchange and removal, well suited for comparison with biological results of larger biological relevance, but for which mechanistic studies are precluded.

5. Conclusions

In this work, we present data of lipid exchange between pooled lipoprotein fractions extracted from human blood (of healthy donors) and model membranes composed of either saturated or unsaturated phospholipids, in the presence or absence of cholesterol. Despite the simplicity of the model system, the exchange data mirror key clinical findings since: 1) HDL was found to remove lipids to a larger extent than LDL, 2) saturated fats were cleared to a larger extent by HDL than by LDL, while the presence of cholesterol in the membrane significantly reduced the ability of lipoproteins to exchange lipids, 3) lipoproteins present low affinity for unsaturated phospholipids which explains why HDL therapy is able to re-model plaque composition, and 4) denser LDL (with higher protein content) deposit more lipids on model membranes in agreement with the atherogenic characteristics of smaller and denser LDL sub-fractions. This suggests that the approach captures key physiological aspects of atherosclerotic plaque formation, while still allowing the mechanisms of lipid exchange to be investigated in detail. As such, it can likely be applied to unravel mechanistic information and to investigate other contexts relating to atherosclerosis such as LDL fractions arising from patients with a defined clinical condition such as high cholesterol, high triglyceride, or presence of lipoprotein(A); and to determine the capacity of these fractions to deposit and remove fats, as well as systematic studies with reconstituted HDL fractions of known composition both in terms of lipids and apolipoproteins.

CRediT authorship contribution statement

Sarah Waldie: Investigation, Project administration, Formal analysis, Writing - original draft. **Federica Sebastiani**: Formal analysis, Writing - original draft. **Kathryn Browning**: Investigation, Writing - original draft. **Selma Maric**: Investigation, Writing - original draft. **Tania K. Lind**: Investigation, Writing - original draft. **Nageshwar Yepuri**: Investigation, Writing - original draft. **Tamim A. Darwish**: Investigation, Writing - original draft. **Martine Moulin**: Investigation, Project administration, Supervision, Formal analysis, Writing - original draft. **Gernot Strohmeier**: Investigation, Writing - original draft. **Harald Pichler**: Writing - original draft. **Maximilian W.A. Skoda**: Investigation, Writing - original draft. **Armando Maestro**: Investigation, Writing - original draft. **Michael Haertlein**: Supervision, Writing - original draft. **V. Trevor Forsyth**: Supervision, Writing - original draft. **Eva Bengtsson**: Writing - original draft. **Martin Malmsten**: Writing - original draft. **Marité Cárdenas**: Project administration, Investigation, Formal analysis, Writing - original draft, Funding acquisition, Supervision.

Declaration of competing interest

The authors declare that they have no known competing financial interests or personal relationships that could have appeared to influence the work reported in this paper.

Acknowledgements

The authors thank Irena Ljungcrantz for LDL purification and biochemical analysis, and Anne-Mette Bjerg Pedersen who produced the dPC used in the first experiment. We thank Professor Karin Schillén for access to the DSC instrument. We thank the neutron facilities ILL and ISIS for granted beamtime with DOIs: https://doi.org/10.5291/ILL.DATA.9-13-681 and https://doi.org/10.5286/ISIS.E.RB1810104. The National Deuteration Facility in Australia is partly funded by The National Collaborative Research Infrastructure Strategy (NCRIS) an Australian Government initiative. This work was partially funded by the Swedish Research Council (M.C. project 2014-3981 and M.Ma. project 2016-05157) and a PhD studentship by the ILL. VTF thanks the EPSRC for grants GR/R99393/01 and EP/C015452/1 which funded the creation of the Deuteration Laboratory in ILL's Life Science Group. This work benefitted from the platforms of the Grenoble Instruct centre (ISBG; UMS 3518 CNRS-CEA-UGA-EMBL) with support from FRISBI (ANR-10-INBS-05-02) and GRAL (ANR-10-LABX-49-01) within the Grenoble Partnership for Structural Biology (PSB).

Appendix A. Supplementary data

Supplementary data to this article can be found online at https://doi.org/10.1016/j.bbalip.2020.158769.

References

[1] WorldHealthOrganization, Cardiovascular Disease, https://www.who.int/news-room/fact-sheets/detail/cardiovascular-diseases-(cvds), (2017).
[2] D.J. Rader, A. Daugherty, Translating molecular discoveries into new therapies for atherosclerosis, Nature 451 (2008) 904–913.
[3] J.F. Bentzon, F. Otsuka, R. Virmani, E. Falk, Mechanisms of plaque formation and rupture, Circ. Res. 114 (2014) 1852–1866.
[4] P. Libby, P.M. Ridker, G.K. Hansson, Progress and challenges in translating the biology of atherosclerosis, Nature 473 (2011) 317–325.
[5] A. Jonas, Lipoprotein structure, Biochem. Lipids Lipoproteins Membr. (2002), https://doi.org/10.1042/bst0100143a.
[6] L. Badimon, G. Vilahur, LDL-cholesterol versus HDL-cholesterol in the atherosclerotic plaque: inflammatory resolution versus thrombotic chaos, Ann. N. Y. Acad. Sci. 1254 (2012) 18–32.
[7] B.A. Ference, et al., Low-density lipoproteins cause atherosclerotic cardiovascular disease. 1. Evidence from genetic, epidemiologic, and clinical studies. A consensus statement fromthe European Atherosclerosis Society Consensus Panel, Eur. Heart J.

38 (2017) 2459–2472.
[8] J.E. Feig, B. Hewing, J.D. Smith, S.L. Hazen, E.A. Fisher, HDL and atherosclerosis regression: evidence from pre-clinical and clinical studies, Circ. Res. 114 (2014) 205–213.
[9] L.R. Marques, et al., Reverse cholesterol transport: molecular mechanisms and the non-medical approach to enhance HDL cholesterol, Front. Physiol. 9 (2018) 1–11.
[10] R.S. Rosenson, et al., Cholesterol efflux and atheroprotection: advancing the concept of reverse cholesterol transport, Circulation 125 (2012) 1905–1919.
[11] B.F. Voight, et al., Plasma HDL cholesterol and risk of myocardial infarction: a mendelian randomisation study, Lancet 380 (2012) 572–580.
[12] C.M. Madsen, A. Varbo, B.G. Nordestgaard, Extreme high high-density lipoprotein cholesterol is paradoxically associated with high mortality in men and women: two prospective cohort studies, Eur. Heart J. 38 (2017) 2478–2486.
[13] M.L. Fernandez, D. Webb, The LDL to HDL cholesterol ratio as a valuable tool to evaluate coronary heart disease risk, J. Am. Coll. Nutr. 27 (2008) 1–5.
[14] N.G. Forouhi, R.M. Krauss, G. Taubes, W. Willett, Dietary fat and cardiometabolic health: evidence, controversies, and consensus for guidance, BMJ 361 (2018) 1–15.
[15] G.A. Soliman, Dietary cholesterol and the lack of evidence in cardiovascular disease, Nutrients 10 (2018) E780.
[16] K.L. Browning, et al., Human lipoproteins at model cell membranes: effect of lipoprotein class on lipid exchange, Sci. Rep. 7 (2017).
[17] S. Maric, et al., Time-resolved small-angle neutron scattering as a probe for the dynamics of lipid exchange between human lipoproteins and naturally derived membranes, Sci. Rep. 9 (2019) 7591.
[18] B. Chen, et al., Targeting negative surface charges of cancer cells by multifunctional nanoprobes, Theranostics 6 (2016) 1887–1898.
[19] K.L. Browning, et al., Effect of bilayer charge on lipoprotein lipid exchange, Colloids Surf. B: Biointerfaces 168 (2018) 117–125.
[20] G. Camejo, S.O. Olofsson, F. Lopez, P. Carlsson, G. Bondjers, Identification of Apo B-100 segments mediating the interaction of low density lipoproteins with arterial proteoglycans, Arteriosclerosis 8 (1988) 368–377.
[21] S.P. Allen, S. Khan, P. Batten, M. Yacoub, Native low density lipoprotein-induced calcium transients trigger VCAM-1 and E-selectin expression in human endothelial cells, FASEB J. 11 (1997).
[22] N.R. Yepuri, et al., Synthesis of Perdeuterated 1-Palmitoyl-2-oleoyl-sn-glycero-3-phosphocholine ([D 82]POPC) and characterisation of its lipid bilayer membrane structure by neutron reflectometry, Chempluschem 81 (2016) 315–321.
[23] S. Maric, et al., Biosynthetic preparation of selectively deuterated phosphatidylcholine in genetically modified Escherichia coli, Appl. Microbiol. Biotechnol. 99 (2015) 241–254.
[24] J.B. Artero, M. Härtlein, S. McSweeney, P. Timmins, A comparison of refined X-ray structures of hydrogenated and perdeuterated rat γE-crystallin in H2O and D2O, Acta Crystallogr. Sect. D Biol. Crystallogr. 61 (2005) 1541–1549.
[25] E. Bligh, W. Dyer, A rapid method of total lipid extraction and purification, Can. J. Biochem. Physiol. 37 (1959) 911–917.
[26] S. Maric, et al., Stealth carriers for low-resolution structure determination of membrane proteins in solution, Acta Crystallogr. Sect. D Biol. Crystallogr. 70 (2014) 317–328.
[27] G. Rouser, A. Siakotos, S. Fleischer, Quantitative analysis of phospholipids by thin-layer chromatography and phosphorus analysis of spots, Lipids 1 (1996) 85–86.
[28] S. Waldie, et al., Localization of cholesterol within supported lipid bilayers made of a natural extract of tailor-deuterated phosphatidylcholine, Langmuir 34 (2018) 472–479.
[29] M. Moulin, et al., Perdeuteration of cholesterol for neutron scattering applications using recombinant Pichia pastoris, Chem. Phys. Lipids 212 (2018) 80–87.
[30] M. Haertlein, et al., Biomolecular deuteration for neutron structural biology and dynamics, Methods in Enzymology 566 (2016).
[31] O. Dunne, et al., Matchout deuterium labelling of proteins for small-angle neutron scattering studies using prokaryotic and eukaryotic expression systems and high cell-density cultures, Eur. Biophys. J. 46 (2017) 425–432.
[32] I. Josts, et al., Conformational states of ABC transporter MsbA in a lipid environment investigated by small-angle scattering using stealth carrier nanodiscs, Structure 26 (2018) 1072–1079.
[33] J. Nitsche, et al., Structural basis for activation of plasma-membrane Ca2+-ATPase by calmodulin, Commun. Biol. 1 (2018) 1–10.
[34] A.W. Yee, et al., A molecular mechanism for transthyretin amyloidogenesis, Nat. Commun. 10 (2019) 1–10.
[35] M.G. Cuypers, et al., Macromolecular structure phasing by neutron anomalous diffraction, Sci. Rep. 6 (2016) 31487.
[36] M. Grimaldo, et al., Protein short-time diffusion in a naturally crowded environment, J. Phys. Chem. Lett. 10 (2019) 1709–1715.
[37] A.W. Yee, et al., Impact of deuteration on the assembly kinetics of Transthyretin monitored by native mass spectrometry and implications for amyloidoses, Angew. Chem. Int. Ed. 55 (2016) 9292–9296.
[38] A. Åkesson, et al., Composition and structure of mixed phospholipid supported bilayers formed by POPC and DPPC, Soft Matter 8 (2012) 5658–5665.
[39] S. Waldie, et al., The Production of Matchout- Deuterated Cholesterol and the Study of Bilayer-Cholesterol Interactions, 9 (2019), p. 5118.
[40] S. Maric, T.K. Lind, J. Lyngsø, M. Cárdenas, J.S. Pedersen, Modeling small-angle X-ray scattering data for low-density lipoproteins: insights into the fatty core packing and phase transition, ACS Nano 11 (2017) 1080–1090.
[41] R.A. Campbell, H.P. Wacklin, I. Sutton, R. Cubitt, G. Fragneto, FIGARO: the new horizontal neutron reflectometer at the ILL, Eur. Phys. J. Plus 126 (2011) 1–22.
[42] R.A. Campbell, H.P. Wacklin, I. Sutton, R. Cubitt, G. Fragneto, Erratum to: FIGARO: the new horizontal neutron reflectometer at the ILL, Eur. Phys. J. Plus 126 (107) (2011), https://doi.org/10.1140/epjp/i2011-11107-8 (Eur. Phys. J. Plus 130, 1 (2015)).
[43] J. Webster, S. Holt, R. Dalgliesh, INTER the chemical interfaces reflectometer on target station 2 at ISIS, Phys. B Phys. Condens. Matter 385–386 (2006) 1164–1166.
[44] R.M. Dalgliesh, S. Langridge, J. Plomp, V.O. De Haan, A.A. Van Well, Offspec, the ISIS spin-echo reflectometer, Phys. B Condens. Matter 406 (2011) 2346–2349.
[45] A. Nelson, Co-refinement of multiple-contrast neutron/X-ray reflectivity data using MOTOFIT, J. Appl. Crystallogr. 39 (2006) 273–276.
[46] W.K. Subczynski, M. Pasenkiewicz-Gierula, J. Widomska, L. Mainali, M. Raguz, High cholesterol/low cholesterol: effects in biological membranes: a review, Cell Biochem. Biophys. 75 (2017) 369–385.
[47] X. Wang, R. Pease, J. Bertinato, R.W. Milne, Well-defined regions of apolipoprotein B-100 undergo conformational change during its intravascular metabolism, Arterioscler. Thromb. Vasc. Biol. 20 (2000) 1301–1308.
[48] M. Austin, et al., Low-density lipoprotein subclass patterns and risk of myocardial infarction, JAMA 260 (1988) 1917–1921.
[49] E.A. Ivanova, V.A. Myasoedova, A.A. Melnichenko, A.V. Grechko, A.N. Orekhov, Small dense low-density lipoprotein as biomarker for atherosclerotic diseases, Oxidative Med. Cell. Longev. 2017 (1273042) (2017).
[50] S. Scheiner, C. Martin, Relative stability of hydrogen and deuterium bonds, J. Am. Chem. Soc. (1996) 1511–1521, https://doi.org/10.1021/ja9530376.
[51] F.P. Guengerich, Kinetic deuterium isotope effects in cytochrome P450 reactions, Methods Enzymol. (2017) 217–238, https://doi.org/10.1016/bs.mie.2017.06.036. Kinetic.
[52] R.M. Krauss, P.J. Blanche, R.S. Rawlings, H.S. Fernstrom, P.T. Williams, Separate effects of reduced carbohydrate intake and weight loss on atherogenic dyslipidemia, Am. J. Clin. Nutr. 83 (2006) 1025–1031.
[53] M.A. Tricerri, et al., Interaction of apolipoprotein A-I in three different conformations with palmitoyl oleoyl phosphatidylcholine vesicles, J. Lipid Res. 43 (2002) 187–197.
[54] M.R. Ward, G. Pasterkamp, A.C. Yeung, C. Borst, Mechanisms and Clinical Implications, 27 (2011), pp. 1186–1191.
[55] B.G. Brown, X.Q. Zhao, D.E. Sacco, J.J. Albers, Lipid lowering and plaque regression: new insights into prevention of plaque disruption and clinical events in coronary disease, Circulation 87 (1993) 1781–1791.
[56] H. Nanda, et al., Relaxation dynamics of saturated and unsaturated oriented lipid bilayers, Soft Matter 14 (2018) 6119–6127.
[57] Y. Xia, et al., Effects of nanoparticle morphology and acyl chain length on spontaneous lipid transfer rates, Langmuir 31 (2015) 12920–12928.
[58] M.B. Sankaram, T.E. Thompson, Cholesterol-induced fluid-phase immiscibility in membranes, Proc. Natl. Acad. Sci. U. S. A. 88 (1991) 8686–8690.
[59] P.F.F. Almeida, W.L.C. Vaz, T.E. Thompson, Lateral diffusion in the liquid phases of dimyristoylphosphatidylcholine/cholesterol lipid bilayers: a free volume analysis, Biochemistry 31 (1992) 6739–6747.
[60] G. Orädd, G. Lindblom, P.W. Westerman, Lateral diffusion of cholesterol and dimyristoylphosphatidylcholine in a lipid bilayer measured by pulsed field gradient NMR spectroscopy, Biophys. J. 83 (2002) 2702–2704.
[61] H. Martinez-Seara, T. Róg, M. Karttunen, I. Vattulainen, R. Reigada, Cholesterol induces specific spatial and orientational order in cholesterol/phospholipid membranes, PLoS One 5 (2010) e11162.
[62] J. Yang, J. Martí, C. Calero, Pair interactions among ternary DPPC/POPC/cholesterol mixtures in liquid-ordered and liquid-disordered phases, Soft Matter 12 (2016) 4557–4561.
[63] M. Pitman, F. Suits, A. MacKerell, S. Feller, Molecular-level organization of saturated and polyunsaturated fatty acids in a phosphatidylcholine bilayer containing cholesterol, Biochemistry 43 (2004) 15318–15328.
[64] L.J. Pike, Rafts defined: a report on the keystone symposium on lipid rafts and cell function, J. Lipid Res. 47 (2006) 1597–1598.
[65] A.J. Guarino, S.P. Lee, S.P. Wrenn, Interactions between sphingomyelin and cholesterol in low density lipoproteins and model membranes, J. Colloid Interface Sci. 293 (2006) 203–212.
[66] G.C. Chen, et al., Conformational differences in human apolipoprotein B-100 among subspecies of low density lipoproteins (LDL). Association of altered proteolytic accessibility with decreased receptor binding of LDL subspecies from hypertriglyceridemic subjects, J. Biol. Chem 269 (1994) 29121–29128.
[67] J.P. Segrest, M.K. Jones, H. De Loof, N. Dashti, Structure of apolipoprotein B-100 in low density lipoproteins, J. Lipid Res. 42 (2001) 1346–1367.
[68] T. Dawber, R. Nickerson, F. Brand, J. Pool, Eggs, serum cholesterol, and coronary heart disease, Am. J. Clin. Nutr. 36 (1982) 617–625.
[69] E. Yu, F.B. Hu, Dairy products, dairy fatty acids, and the prevention of cardiometabolic disease: a review of recent evidence, Curr. Atheroscler. Rep. 20 (2018) 24.
[70] F.M. Sacks, et al., Dietary fats and cardiovascular disease: a presidential advisory from the American Heart Association, Circulation 136 (2017) e1–e23.
[71] R.P. Mensink, Effects of saturated fatty acids on serum lipids and lipoproteins: a systematic review and regression analysis, World Heal. Organ. (2016) 1–63.
[72] Z. Chen, et al., Cholesterol in human atherosclerotic plaque is a marker for underlying disease state and plaque vulnerability, Lipids Health Dis. 9 (2010) 61.
[73] B.G. Talayero, F.M. Sacks, The role of triglycerides in atherosclerosis, Curr. Cardiol. Rep. 13 (2011) 544–552.
[74] T. Hayek, et al., Dietary fat increases high density lipoprotein (HDL) levels both by increasing the transport rates and decreasing the fractional catabolic rates of HDL cholesterol ester and apolipoprotein (Apo) A-I, J. Clin. Invest. 91 (1993) 1665–1671.

Supporting Information

Lipoprotein ability to exchange and remove lipids from model membranes as a function of fatty acid saturation and presence of cholesterol

Sarah Waldie[1,2,2b], Federica Sebastiani[1], Kathryn Browning[3], Selma Maric[4], Tania K. Lind[1], Nageshwar Yepuri[5], Tamim A. Darwish[5], Martine Moulin[2], Gernot Strohmeier[6,7], Harald Pichler[6,8], Maximilian W. A. Skoda[9], Armando Maestro[2], Michael Haertlein[2], V. Trevor Forsyth[2,2b,10], Eva Bengtsson[11], Martin Malmsten[3,12] and Marité Cárdenas[1]*

* corresponding author marite.cardenas@mau.se

[1] Department of Biomedical Science and Biofilms – Research Center for Biointerfaces, Malmö University, 20506 Malmö, Sweden.

[2] Institut Laue-Langevin, 71 Avenue des Martyrs, 38042 Grenoble, Cedex 9, France

[2b] Partnership for Structural Biology (PSB), 71 Avenue des Martyrs, 38042 Grenoble, Cedex 9, France

[3] Department of Pharmacy, Copenhagen University, Universitetsparken 2, 2100 Copenhagen, Denmark

[4] MAX IV Laboratory, Fotongatan 2, 225 92 Lund, Sweden

[5] National Deuteration Facility, Australian Nuclear Science and Technology Organisation, New Illwarra Road, Lucas Heights NSW 2234, Australia

[6] Austrian Centre of Industrial Biotechnology, Petersgasse 14, 8010 Graz, Austria

[7] Graz University of Technology, Institute of Organic Chemistry, NAWI Graz, Stremayrgasse 9, 8010 Graz, Austria

[8] Graz University of Technology, Institute of Molecular Biotechnology, NAWI Graz, BioTechMed Graz, Petersgasse 14, 8010 Graz, Austria

[9] STFC, Rutherford Appleton Laboratory, ISIS, Harwell, Didcot OX11 0QX, UK

[10] Faculty of Natural Sciences, Keele University, Staffordshire ST5 5BG, UK

[11] Department of Clinical Sciences, Malmö, Clinical Research Center, Jan Waldenströms gata 35, 214 28, Malmö, Sweden

[12] Department of Physical Chemistry 1, University of Lund, SE-22100, Lund, Sweden

Table S1. HDL and LDL composition in % mass.

	HDL			LDL		
	Prep. 1	**Prep. 2**	**Prep. 3**	**Prep. 1**	**Prep. 2**	**Prep. 3**
Protein	77.7 ± 0.6	54.8 ± 0.3	65.8 ± 0.4	30.9 ± 0.6	27.3 ± 0.6	35.6 ± 0.2
Cholesterol	19.0 ± 0.8	42.3 ± 0.5	27.7 ± 0.7	61.8 ± 1.3	61.1 ± 0.9	54.9 ± 0.4
Triglyceride	3.3 ± 2.8	2.9 ± 1.5	6.5 ± 2.2	7.3 ± 0.5	11.6 ± 3	9.6 ± 1.2

Table S2. Lipid composition for each model membrane exposed to either HDL or LDL. A letter (superscript) identifies the lipid composition of the model membrane and the lipoprotein used for the neutron reflection data (Figure S1) and parameters (Table S3 and Table S4) for best fits.

HDL			LDL		
Prep. 1	**Prep. 2**	**Prep. 3**	**Prep. 1**	**Prep. 2**	**Prep. 3**
FIGARO	**OFFSPEC**	**INTER**	**INTER**	**FIGARO**	**INTER**
dDMPC[1.A] (INTER)	dDMPC[E]	dPOdPC[G]	dDMPC[1.I]	dDMPC[J]	dDMPC[M]
dDMPC 10%dchol[B]	dDMPC 20%chol[F]	dPOhPC[H]		dDMPC 10%dchol[K]	dPC[N]
dPC[C]				dDMPC 20%dchol[L]	dPC 20%chol[O]
dPC 10%dchol[D]					

1. Browning KL, Lind TK, Maric S, Barker RD, Cárdenas M, Malmsten M. Effect of bilayer charge on lipoprotein lipid exchange. *Colloids Surfaces B Biointerfaces*. 2018;168:117-125. doi:10.1016/j.colsurfb.2018.01.043

All NR data, best fits and SLD profiles are given below for each substrate before and after exposure to lipoproteins following the nomenclature in Table S2. The parameters used for the best fits are given in Table S3 and S4 prior and after 8H of lipoprotein incubation, respectively. The range of errors for the values is given at the top unless otherwise stated. The roughness across all the bilayers were between 4-6 Å. Values were allowed to vary unless otherwise stated.

Table S3. Parameters for pristine SLBs.

Bilayer	Layer	Thickness (Å) E± 0.1-1	SLD (*10^{-6} Å^{-2}) E± 0.01-0.3	Solvent (%) E± 0.5-5
A[1]	Inner Head	9.3*	1.89*	42*
	Tail	26.4*	6.58*	0*
	Outer Head	9.3*	1.89*	42*
B	Inner Head	9	1.89*	49
	Tail	30	6.75	8
	Outer Head	9	1.89*	49
C**	Bilayer	43.5	6.1	7.2
D**	Bilayer	43.8	6.18	4.9
E	Inner Head	8	1.89*	23.4
	Tail	26	6.7	2
	Outer Head	8	1.89*	23.4
F	Inner Head	10	1.89*	37
	Tail	29.4	6.78	1.3
	Outer Head	10	1.89*	24
G	Inner Head	8.2	6.1*	17.4
	Tail	24.5	6.29	4.8
	Outer Head	8.2	6.1*	17.4
H	Inner Head	6.7	1.89*	25.8
	Tail	29.2	6.3	0.8
	Outer Head	6.7	1.89*	25.8
I[1]	Inner Head	9.1*	1.84*	42*
	Tail	27.5*	6.58*	0*
	Outer Head	9.1*	1.84*	42*
J	Inner Head	6.9	1.89*	20.1
	Tail	26.6	6.7	1.3
	Outer Head	6.9	1.89*	20.1
K	Inner Head	7.1	1.89*	7.7
	Tail	28	6.8	1.8
	Outer Head	7.1	1.89*	7.7
L	Inner Head	6.9	1.89*	19
	Tail	32.7	7	2.9
	Outer Head	6.9	1.89*	19

M	Inner Head	7.1	1.89*	8
	Tail	24.4	6.7	0.8
	Outer Head	7.1	1.89*	8
N	Inner Head	7.2	6.1*	14
	Tail	27.3	6.1*	3.2
	Outer Head	7.2	6.1*	14
O	Inner Head	8.2	6.2*	20.6
	Tail	30.8	6.2*	4.5
	Outer Head	8.2	6.2*	20.6

*Values fixed during fitting process (or previously reported – Bilayers A and I, ref 1)

** For dPC and dPC with 10 mol% cholesterol, the SLD is constant for heads and tails and equally good fits are obtained for a three layer or a one layer model.

Table S4. Parameters for SLBs after 8H incubation with lipoproteins and absolute exchange and removal values. SLBs were exposed to HDL/LDL preparations as given in Table S2. Note that total deuterated lipid removal is the sum of both the exchanged and the further removal (*i.e.,* replaced with solvent) while the deposited hydrogenated lipids equals the exchanged.

Bilayer	**Layer**	**Thickness (Å)** E± 0.1-1	**SLD (*10^{-6} Å^{-2})** E± 0.1-0.3	**Solvent (%)** E± 0.5-6	**% Lipids Exchanged**	**% Lipids Removed**
A[1]	Inner Head	8.8*	1.84*	62*		
	Tail	28.6*	4.47*	9*	31 ± 1	8 ± 2
	Outer Head	17.3*	1.84*	63*		
	HDL	87.5*	2.02*	97*		
B	Inner Head	10	1.89*	50		
	Tail	28	5.3	23	21 ± 1	15 ± 3
	Outer Head	12	1.89*	39 ± 8		
	HDL	52 ± 2	2.02*	94		
C**	Bilayer	43.3	5.76	9.6	5 ± 0.2	2.4 ± 0.2
D**	Bilayer	43.6	5.85	11.7	5 ± 0.2	6.8 ± 0.2
E	Inner Head	8	1.89*	38		
	Tail	31	4.43	44	33 ± 1	42 ± 8
	Outer Head	8	1.89*	38		
	HDL	60 ± 8	2.02*	97		
F	Inner Head	9.1	1.89*	60		
	Tail	31.3	5.4	26	19 ± 1	25 ± 8
	Outer Head	8.7	1.89*	40		
	HDL	50 ± 5	2.02*	98		

G	Inner Head	6.8	6.1*	8	12.55 ± 0.07	3 ± 1
	Tail	26.8	5.5	4.8		
	Outer Head	6.8	6.1*	8		
	HDL	155 ± 5	2*	97		
H	Inner Head	6.6	1.89*	23	3.2 ± 0.01	1 ± 0.7
	Tail	28.6	6.1	1.6		
	Outer Head	6.6	1.89*	23		
	HDL	146 ± 8	2*	98.9		
I[1]	Inner Head	9.1*	1.84*	64*	30 ± 1*	0 ± 2*
	Tail	27.5*	4.51*	0*		
	Outer Head	17.3*	1.84*	65*		
	LDL	75*	2.12*	96*		
	LDL	80*	2.12*	98*		
J	Inner Head	9	1.89*	19	16.29 ± 0.06	18.5 ± 0.3
	Tail	29.8	5.6	19.7		
	Outer Head	9.2	1.89*	21 ± 14		
	LDL	73 ± 4	2*	93		
	LDL	117 ± 4	2*	95.2		
K	Inner Head	7.4	1.89*	27	22.7 ± 0.3	11 ± 1
	Tail	31.4	5.2	12		
	Outer Head	11.2	1.89*	37		
	LDL	73 ± 4	2*	89.2		
	LDL	131 ± 6	2*	95.3		
L	Inner Head	12.1	1.89*	25	16.9 ± 0.2	7.5 ± 0.7
	Tail	35.1	5.8	10.3		
	Outer Head	9.2	1.89*	32 ± 7		
	LDL	71 ± 3	2*	94		
	LDL	106 ± 5	2*	95.3		
M	Inner Head	7.3	1.89*	25.1	33.7 ± 0.4	8 ± 2
	Tail	28.8	4.3	9.1		
	Outer Head	9.6	1.89*	24 ± 9		
	LDL	69 ± 5	2*	94		
	LDL	141 ± 7	2*	97.4		
N	Inner Head	7.7	5.5	12	5.6 ± 0.1	3 ± 2
	Tail	26.8	5.7	7		
	Outer Head	7.7	5.9	15		
	LDL	75 ± 4	2*	94.7		
	LDL	155 ± 5	2*	96.5		
O	Inner Head	5.5	6.0	5	4.8 ± 0.1	0.6 ± 0.2
	Tail	28.2	5.9	5.1		
	Outer Head	5.5	6.0	5		

	LDL	66 ± 4	2*	98.9
	LDL	107 ± 7	2*	98.7

*Values fixed during fitting process (or previously reported – Bilayers A and I, ref 1)

** For dPC and dPC with 10 mol% cholesterol, the SLD is constant for heads and tails and equally good fits are obtained for a three layer or a one layer model.

Example of the quality of fitted data for one bilayer (M), before and after incubation with lipoprotein with SLD insets, figures S1 and S2 respectively.

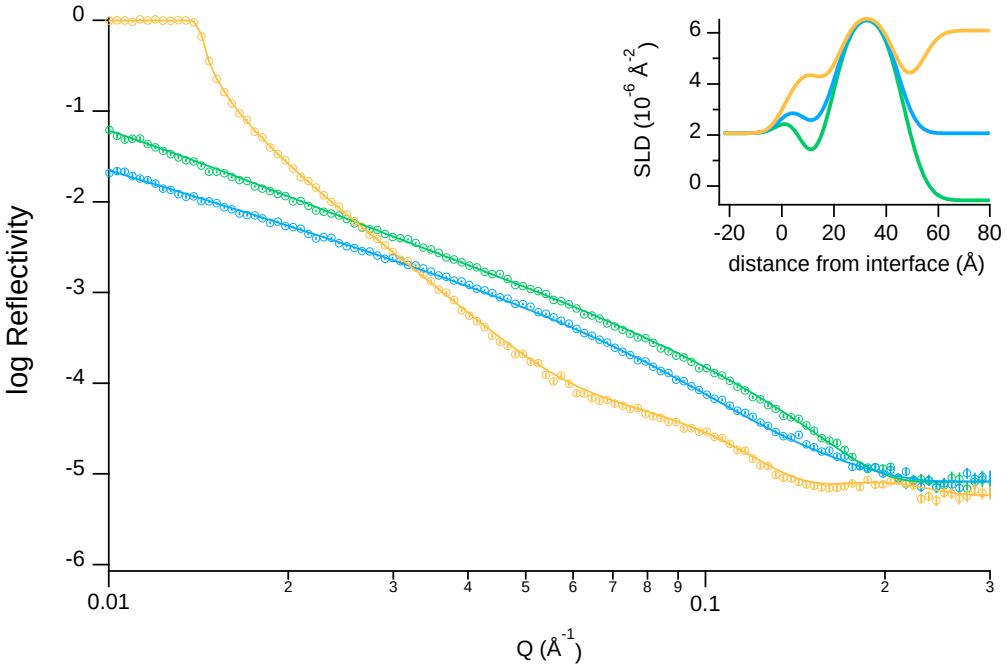

Figure S1. Pristine bilayer M pre-incubation with LDL. Data points, best fits and SLD curves for contrasts D_2O, H_2O and cmSi shown in yellow, green and blue respectively.

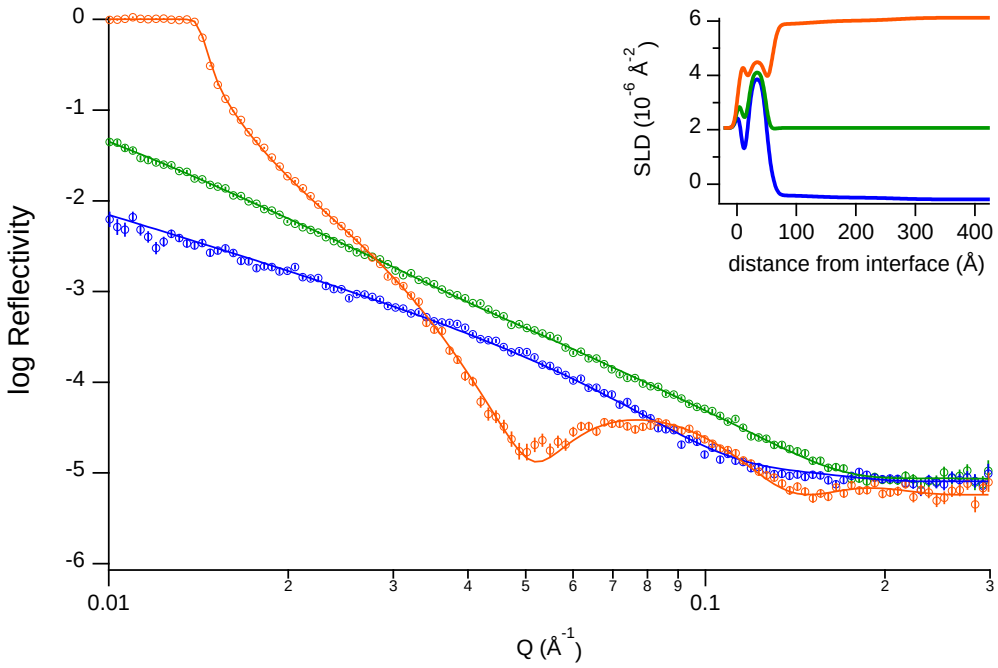

Figure S2. Bilayer M post incubation with LDL. Data points, best fits and SLD curves for contrasts D_2O, H_2O and cmSi shown in orange, green and blue respectively.

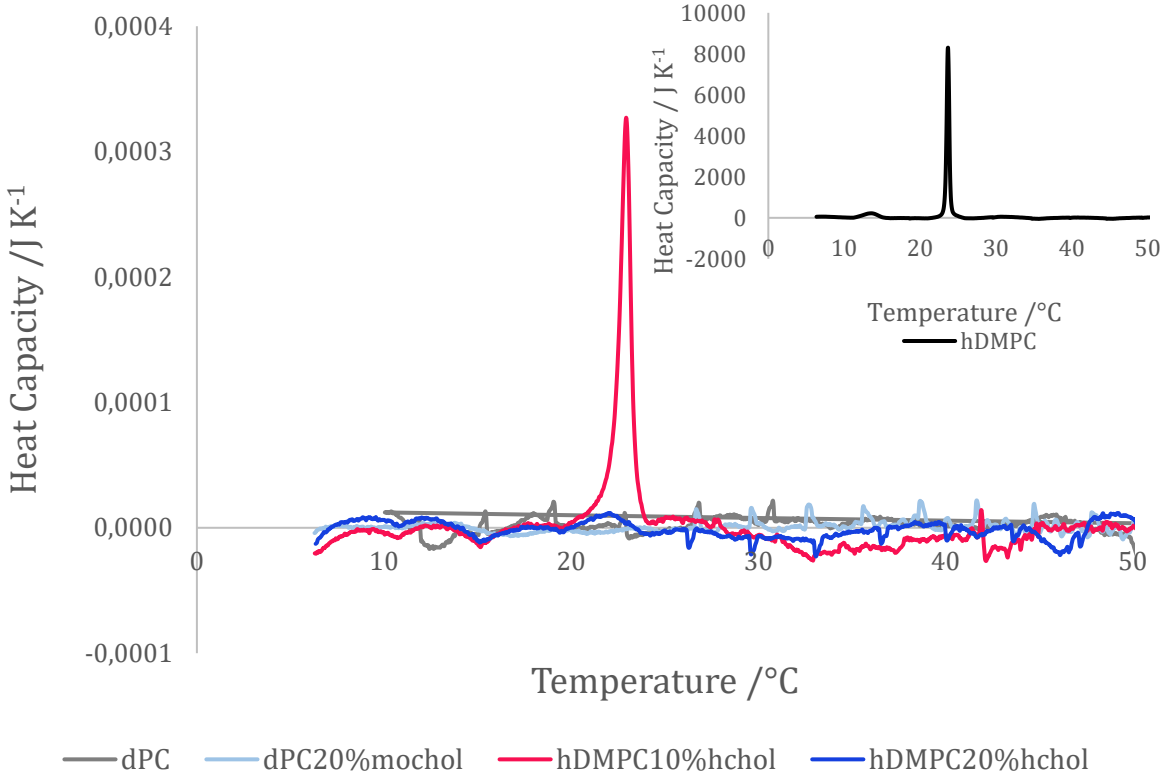

Figure S3. Differential scanning calorimetry data for the lipids used showing at 37 °C all lipids are in the fluid phase.

Paper 4

The interaction of ApoE and ApoE nascent-like HDL particles with model cellular membranes: Effect of protein allele and membrane composition

Sarah Waldie[1,2,2b], Federica Sebastiani[1], Martine Moulin[2,2b], Yuri Gerelli[2], Sylvain Prevost[2], Felix Roosen-Runge[1], John C. Voss[3], Tamim A. Darwish[4] Nageshwar Yepuri[4], Rita Del Giudice[1], Gernot Strohmeier[5,6], Harald Pichler[5,7], Selma Maric[8], V. Trevor Forsyth[2,2b,9], Michael Haertlein[2,2b] and Marité Cárdenas[1]*

* corresponding author marite.cardenas@mau.se

[1] Department of Biomedical Science and Biofilms – Research Center for Biointerfaces, Malmö University, 20506 Malmö, Sweden.

[2] Institut Laue-Langevin, 71 Avenue des Martyrs, 38042 Grenoble, Cedex 9, France

[2b] Partnership for Structural Biology (PSB), 71 Avenue des Martyrs, 38042 Grenoble, Cedex 9, France

[3] Department of Biochemistry and Molecular Medicine, University of California, Davis, CA 95616, USA

[4] National Deuteration Facility, Australian Nuclear Science and Technology Organisation, New Illwarra Road, Lucas Heights NSW 2234, Australia

[5] Austrian Centre of Industrial Biotechnology, Petersgasse 14, 8010 Graz, Austria

[6] Graz University of Technology, Institute of Organic Chemistry, NAWI Graz, Stremayrgasse 9, 8010 Graz, Austria

[7] Graz University of Technology, Institute of Molecular Biotechnology, NAWI Graz, BioTechMed Graz, Petersgasse 14, 8010 Graz, Austria

[8] MAX IV Laboratory, Fotongatan 2, 225 92 Lund, Sweden

[9] Faculty of Natural Sciences, Keele University, Staffordshire ST5 5BG, UK

Abstract

Apolipoprotein E (ApoE) plays a large role in diseases such as atherosclerosis and Alzheimer's. The allele variants (ApoE3 and ApoE4), differ only slightly in composition, varying in only one amino acid. However, this difference has drastic consequences in the roles they play in physiological processes. In this paper, the interaction of lipid-free ApoE variants with model membranes is studied as a function of saturation in the bilayer; the structural characterisation of reconstituted HDL-like particles is also reported; along with the interaction of said particles with model membranes in the presence and absence of cholesterol. The protein alleles interact differently with the model membranes, adopting different protein conformations, with ApoE3 varying depending on saturation of the bilayer also. The ApoE based lipid particles form elliptical disc like structures, similar to nascent or discoidal HDL. The ApoE based particles when interacting with model membranes do not remove cholesterol but rather exchange saturated lipids, as seen in the brain, whereas ApoA1 based particles remove and exchange lipids to a greater extent as seen elsewhere in the body.

1. Introduction

Disorders in lipid metabolism are related to a range of diseases, among them atherosclerosis and Alzheimer's disease (AD). In atherosclerosis, the leading cause of death in western society, high levels of high density lipoproteins (HDL) are thought to have counter-atherosclerotic properties[1]. However, the presence of HDL has more recently been shown to play a neutral[2] or even negative[3] role in aiding the prevention of this disease. While HDL has been used to help combat the onset of atherosclerosis (via HDL therapy or plaque remodelling therapy)[4,5], some recent medical trials have proved to be disappointing due to lack of effectiveness against atherosclerosis[6,7].

In general, HDL consist of a core of triglycerides and cholesterol esters, encased in a monolayer of lipids and cholesterol surrounded by protein. There are many different subclasses of HDL each with slightly varying size and composition[8]: in particular, the lipid poor, nascent HDL (also known as Pre-HDL) is thought to be discoidal in shape and it transforms into a spherical, mature HDL particle upon esterification of cholesterol and transfer, into its lipid core. While ApolipoproteinA1 (ApoA1) constitutes around 70% of total protein content in human serum, there are various other proteins which are also key to the structure and function of HDL particles[8]. One of these is ApolipoproteinE (ApoE)[9] which is found on most HDL particles but mainly on the largest, most buoyant mature particles (HDL2) that contain triglycerides and are lipid rich[10]. ApoE is also the most commonly found apolipoprotein in cerebrospinal fluid[11]. It plays a large role in cholesterol transport while maintaining a local homeostasis of cholesterol within the brain[12].

ApoE has three alleles: E2, E3 and E4 varying at only two amino acid residues, 112 and 158 (E2: 112Cys, 158 Cys; E3: 112Cys, 158Arg; E4: 112Arg, 158Arg)[13]. These differences largely contribute the proteins' structure and function and therefore can determine specific contributions to their behaviour in the body[14,15]. These differences are most notably apparent in the roles they play in certain diseases such as atherosclerosis and AD. The presence of ApoE2 is associated with very low risk of AD[16,17] and generally thought to be protective against atherosclerosis, however is also linked to type III hyperlipoproteinemia and in such cases leads to reduced binding to the LDL receptor in turn impairing the ability to clear triglyceride rich VLDL remnants from plasma and giving rise to increased atherosclerotic risk. On the other hand, ApoE3 is neutral and ApoE4 is indicative of both atherosclerotic advancement and the onset of AD[15]. Understanding their differences in interaction with membranes is key to understanding the specific roles they play in these developments.

The roles of lipoproteins in the development of atherosclerosis and (most likely) in AD, heavily involves lipid exchange. Indeed, cholesterol and other lipids were found to coexist in amyloid plaques in the brain[18]. The type of lipid exchange occurring – namely deposition or removal – highly depends on the lipoprotein type present[19]. Previously HDL was shown to remove lipids from the cell membrane which gave rise to the idea behind HDL therapy. Reconstituted HDL, comparable to discoidal pre-HDL, exhibits similar lipid transfer properties to that of mature HDL[20]. To mimic this, discoidal nanoparticles of

phospholipids solubilised by encircling ApoA1 are used as artificial HDL, also known as reconstituted HDL (rHDL), and are used as one of the strategies in HDL therapy[4,5]. Another approach is the use of ApoA1-like peptides to replicate the function of the rHDL[21,22]. While less is known about the lipid exchange properties of ApoE, some promising results have shown ApoE-based rHDL to be a potential route to explore for athereosclerosis treatment upon further testing[23].

In this paper, the interaction of ApoE3 and ApoE4 with saturated or unsaturated supported lipid bilayers (SLBs) is first explored using neutron reflectometry (NR). ApoE shares a similar structure to ApoA1 but is larger (34 kDa compared to 28 kDa)[24]. ApoE is able to solubilise lipids in a similar way but the rHDL structure is less characterised in the literature as for ApoA1. Here, the formation and structural characterisation of ApoE based rHDL is followed with small angle neutron scattering (SANS), and their subsequent interaction with SLBs is explored by NR. As ApoE is the main apolipoprotein in the brain and there is a local homeostasis of cholesterol, the bilayers in question are in the absence and presence of cholesterol to determine the potential differences between these interactions. Comparisons are done to ApoA1 based rHDL and mature HDL pooled from three healthy male volunteers[25].

2. Materials and Methods

Materials

MilliQ water (18.2 Ω cm^{-1}) was used for all experiments, solvent preparations and cleaning procedures. D_2O (99.9% deuterated, Sigma-Aldrich) was provided by the Institut Laue-Langevin (ILL), Grenoble, France. Bradford, calcium chloride ($CaCl_2$) and Tris buffer saline tablets were from Sigma-Aldrich. Tris buffer (50 mM Tris, 150 mM NaCl, pH 7.4) was prepared by dissolving a tablet in H_2O or D_2O as specified by the producer. 1,2-dimyristoyl-sn-glycero-3-phosphocholine (hDMPC; >99%), 1,2-dimyristoyl-d54-sn-glycero-3-phosphocholine (dDMPC; >99%) and cholesterol (h-cholesterol; >98%) were from Avanti Polar Lipids (Alabaster, AL). 1-palmitoyl, 2-oleoyl-sn-glycero-3-phosphocholine (POPC) in tail-deuterated form (dPOhPC, d67; overall tail deuteration 95%) were provided by the deuteration facility at ANSTO, produced and purified as previously described[26].

Protein Expression and Purification

Plasmids containing ApoE3 and ApoE4 were transferred into BL21DE3 *Escherichia coli* cells with ampicillin resistance. Cells were cultivated in Terrific Broth (TB) medium (12 g L^{-1} tryptone, 24 g L^{-1} yeast extract, 4 mL L^{-1} glycerol, dipotassium phosphate 9.4 g L^{-1} and potassium dihydrogen phosphate 2.2 g L^{-1}) at 37 °C. When cultures reached an OD_{600} nm of 0.6-0.8, protein expression was induced with 1mM isopropyl-beta-thiogalactopyranoside (IPTG) and incubated for a further 90 min. The cells were then harvested by centrifugation (19000 rpm, JLA 9.1000 rotor 20 min, 4 °C) after which the cell pellets were resuspended in TBS buffer and sonicated on ice for 10 min (50% power,

30 sec on, 30 sec off). DMPC suspended in water was added to the protein at a concentration of 100 mg per 1 L culture and dialysed against TBS at room temperature overnight. The DMPC is added to protect the hinge region of ApoE when cleaving with thrombin. After dialysis, thrombin was added in excess for 6 h at 24 °C. The sample was verified by SDS-PAGE to ensure all fusion protein had been cleaved. Potassium bromide was added to the ApoE-DMPC mixture to a density of ~1.21 g mL^{-1}. Ultra-clear tubes (Beckman) are filled two-thirds with a ~1.12 g mL^{-1} density solution (16% w/v potassium bromide solution dissolved in 20 mM Tris pH 7.4 and 0.05% w/v sodium azide) and underlayed with the lysate solution. Samples were spun for 16 hours at 38000 rpm in a SW41 rotor (Beckman) at 15 °C with the break off to preserve the gradient. The resulting 'floating pellet' was recovered and dialysed against TBS to remove the potassium bromide salts. The ApoE-DMPC complexes were lyophilised and can be frozen at this point. When fresh protein is required the pellets are delipidated against methanol and resuspended in 6 M Guanadine Hydrochloride (GuHCl) 50 mM Tris pH 8 and 0.5% beta-mercaptoethanol (BME), dialysed against 4 M GuHCl, 10 mM Tris pH 7.5, 1 mM EDTA and 0.1% BME; further against 0.1 M ammonium bicarbonate; and finally into TBS. The protein is then purified via gel-permeation column chromatography on 2 S200 columns in series and ready to use.

Protein-Lipid Particle Production and Purification

To form the ApoE-DMPC particles equal volumes of fresh protein are mixed with freshly extruded hDMPC vesicles at a final molar ratio of 1:100 ApoE:DMPC. The hDMPC vesicles were extruded 41 times using an Avanti extruder and a filter of 100 nm pore size (Millipore). The solution is left at 24 °C for 12 hours or overnight. Verification of the particle formation is carried out via dynamic light scattering (DLS) due to a slight reduction in the peak intensity for the 100 nm vesicles and the presence of a small peak at roughly 10-15 nm. The rHDL particles are purified via gel-permeation column chromatography using a Superose 6 10/300 column.

Deuterated Cholesterol Production

The production of tailor deuterated cholesterol made use of the Deuteration Laboratory within the Life Sciences Group[27] at the ILL. Matchout-deuterated cholesterol (mo-cholesterol) was produced and purified as reported previously[28]. The *Pichia pastoris* strain CBS7435 Δhis4Δku70 Δerg5::pPpGAP-ZeocinTM-[DHCR7] Δerg6::pGAP-G418[DHCR24] was grown in 100% deuterated basal salts medium in the presence of non-deuterated glycerol as the sole carbon source. The batch phase was complete after 7 days in a fermenter at 28 °C; the fed-batch phase was initiated by constant feeding of glycerol for a further 12 days. The cells were harvested and then isolated using an organic solvent extraction method followed by HPLC to obtain pure cholesterol, verified by GCMS.

Model Membrane Preparation

Lipid films were prepared from chloroform stocks of DMPC, POPC, h- and mo-cholesterol. The films were dried under a stream of nitrogen and placed under vacuum overnight. Before use, the lipid films were hydrated in MilliQ water and bath sonicated for 1 h. Immediately prior to injection the lipids were tip sonicated for 5 min (20% power, 5 sec on, 5 sec off), mixed with an equal volume of 4 mM $CaCl_2$ and injected into the pre-equilibrated NR solid-liquid flow cells by syringe port[19,28]. The presence of 2 mM $CaCl_2$ and concentration of 0.1 mg mL^{-1} of lipids were used to optimise vesicle fusion[29,30]. The lipids were incubated for 20 min before rinsing with water, followed by 50 mM Tris saline buffer, pH 7.4. This process leads to a supported lipid bilayer or *'model membrane'*.

Scattering

SANS and NR data were collected, where scattered intensity and reflectivity, respectively, as a function of momentum transfer, $q=4\pi sin(\theta)/\lambda$, were measured, where θ and λ are the incidence angle and neutron radiation wavelength respectively.

Neutron Reflectometry

Neutron reflectometry data were collected on FIGARO[31,32], a time-of-flight reflectometer, at the ILL (Grenoble, France). Momentum transfer ranges of $0.01 > q > 0.3$ $Å^{-1}$ were measured using wavelengths $2 < \lambda < 20$ Å and two incident angles, 0.8° and 2.3°, with a spatial resolution ($\Delta q/q$) of 7%. The area exposed to the neutron beam was 30 x 60 mm^2. Specular reflection was used to obtain a scattering length density (SLD) profile perpendicular to the surface. The experiments were carried out in reflection-up mode to ensure no aggregated particles could settle on the surface being measured.

The silicon (111) blocks were treated with Piranha solution (H_2SO_4:H_2O_2, 7:3) for 10 min at 80 °C before extensive rinsing with MilliQ water. The polyether ether ketone (PEEK) and O-ring components of the cells were thoroughly cleaned in Hellmanex 2% (v/v) solution and MilliQ water twice via bath sonication, with rinsing of MilliQ water between each sonication. Solvent contrasts were changed *in situ* via HPLC pump. Three contrasts were used: 100% h-Tris (Tris made using H_2O), 100% d-Tris (Tris made using D_2O) and 38% d-Tris or cmSi (Tris made using 38% D_2O) to contrast-match the silicon block.

The MOTOFIT programme[33] was used to fit the experimental data and the Monte Carlo minimisation algorithm within the software was used to determine the error of the fits. The three contrasts were fitted simultaneously to constrain the fit. The clean silicon surfaces were characterised initially to determine the thickness and roughness of the oxide layer and were then used alongside the three buffer contrasts to fit the model membranes. This resulted in either a four- or five-layer model for the membranes, where some samples required an extra solvent layer between the silicon oxide and the bilayer. The bilayer itself was fitted to be symmetrical and was split into three layers: an inner headgroup (closest to the silicon surface), a tail region and an outer headgroup (exposed to the buffer contrast). The symmetry of the bilayer allowed the thickness, coverage and

SLD of the headgroups to be the same for both, and the roughness was constrained across all regions of the bilayer.

After the bilayers were characterised, the ApoE protein or protein-lipid particles were introduced into the solid-liquid flow cells via syringe pump at a rate of 1 mL min^{-1}. The concentrations of the protein and protein-lipid particles were 0.075 mg mL^{-1} and 0.132 mg mL^{-1} respectively. After either 6 or 8 h of incubation, the bilayers were rinsed with buffer and re-characterised in all buffer contrasts.

When fitting the bilayers post-interaction, the initial parameters were used as a starting point and the silicon oxide layer was kept constant. For some bilayers, the thickness of the head and tail regions also remained constant allowing only the solvent and SLD values to vary. However, this approach gave no suitable fits for some other bilayers forcing the use of the thickness of these regions as an additional fitting parameter. An extra layer on top of the bilayer was necessary in all cases corresponding to either the protein or rHDL particles still attached to the bilayer.

Small Angle Neutron Scattering

Small angle neutron scattering data were collected on the D11 instrument at the ILL. The experiments were carried out at 25 °C with a momentum transfer range of $0.002 < q < 0.3$ $Å^{-1}$ by using detector distances of 1.5, 8 and 39 m.

The protein-lipid particles were measured in three contrasts: 100% h-Tris, 100% d-Tris and 42% d-Tris to contrast-match the protein. The data were corrected for the empty cell, background and used in absolute scale compared to the direct beam measurement. The cells were 1 mm thick quart glass Helma SANS cuvettes and the data reduction was carried out using BerSANS. The SasView programme was used to fit the experimental data. The three contrasts were fitted simultaneously to constrain the fit.

3. Results

This work follows three main parts: the use of NR to study the interaction of apolipoproteins with model membranes; the use of SANS to study the structure of protein-lipid complexes; and the use of NR to study the interaction of said complexes with model membranes.

NR and SANS are techniques that can distinguish between deuterated and non-deuterated components. Therefore, the use of deuteration in samples allows highlighting of certain components and the buffer contrasts enable differences to be seen. In both interaction NR studies, the model membranes are made up of tail-deuterated lipids and, in some membranes, the presence of non-deuterated or matchout-deuterated cholesterol. The injected protein or protein-lipid particles are fully non-deuterated. The differences between the components allows the level of interaction to be determined. The change in the SLD of the tail region gives information on the level of protein incorporation or lipid exchange, while the change in the solvent quantity in the tail region gives information on

the amount of lipids that were removed and replaced by protein or solvent. During the interaction process, the samples were measured in non-deuterated buffer as this gives the best contrast against the deuterated membrane layer, while full characterisations of the bilayers before and after interactions were measured in three contrasts (100% h-Tris, 100% d-Tris and 38% d-Tris) to increase the sensitivity of the information obtained. The layer models describing the model membranes are determined from simultaneous fitting of the isotropic contrasts and allow for the analysis of the membrane composition and the decoupling of the information regarding protein incorporation/lipid exchange and lipid removal as described in the methods section. Figure 1 gives pictorial representations of the protein and nanodisc interactions with the bilayers. Representative structural parameters for the pristine SLBs are summarised in Table 1 and are in agreement with the literature[19].

The samples measured by SANS were non-deuterated and were measured in three contrasts: 100% h-Tris, 100% d-Tris and 42% d-Tris. The different buffers used give varying levels of contrast for example the 42% d-Tris and 100% h-Tris highlights the lipids and the proteins respectively, whereas the 100% d-Tris buffer gives the largest contrast against the sample. Using all three contrasts simultaneously allows for higher sensitivity in the model determination.

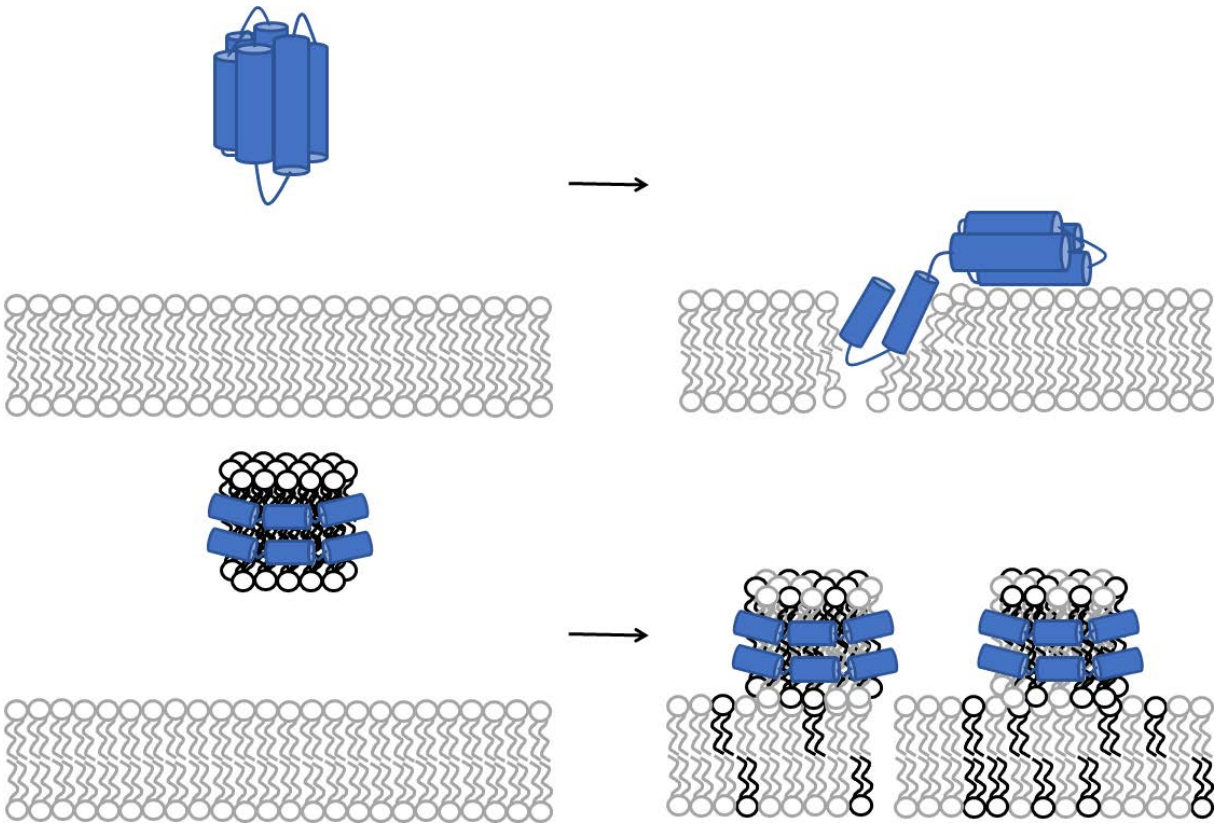

Figure 1. Pictorial representation of the protein incorporation into the phospholipid bilayer (above) and the lipid exchange between the rHDL and the phospholipid bilayer (below). The light grey colour represents deuterated lipids while the black colours represent non-deuterated lipids.

Table 1. Representative structural parameters for the SLB used. Corresponding NR profiles and best fits are given in the SI.

	Head group thickness /Å	Tail thickness /Å	Headgroup coverage /%	Tail coverage /%	Mean molecular area/Å^2
dDMPC	8.98 ± 0.02	27.2 ± 0.2	62 ± 1	96 ± 1	59 ± 2
dPOPC	8.8 ± 0.2	28.6 ± 0.4	54 ± 2	86 ± 1	73 ± 3
dDMPC-mo cholesterol	8.5 ± 0.2	32.1 ± 0.2	71 ± 1	98 ± 1	52 ± 4
dDMPC-h cholesterol	7.7 ± 0.4	30.7 ± 0.5	85 ± 5	94 ± 1	51 ± 4

3.1 Protein interaction with model membranes

The binding of ApoE3 or ApoE4 to SLBs made of saturated or unsaturated phospholipids was followed by NR to determine if the mode or rate of interaction differed between the protein alleles or was affected by the saturation level in the bilayer. In general, ApoE4 has a slightly stronger interaction in terms of lipid removal and exchange by protein adsorption (reflected by the SLD change in the SLB core) than ApoE3 for saturated lipids but the opposite seems to be true for unsaturated lipids (Figure 2A,B). With unsaturated lipids, for both ApoE alleles most of the interaction happens mainly within the first three hours of incubation after which steady-state is reached. For saturated lipids, a slightly different behaviour is observed among the ApoE alleles: on one hand, ApoE3 shows a similar initial pattern to that of unsaturated lipids but this is followed by a slower increase change, possibly suggesting a gradual and slower removal of saturated lipids over longer time periods. On the other hand, ApoE4 follows a more linear increase with time, with only a slight slowing down towards the end of the incubation time (6 hours). This implies a difference in the mode of interaction of the proteins when interacting with saturated bilayers as compared to unsaturated ones, which is allele dependant.

After the incubation period was over, NR data was collected on three isotropic contrasts to enable quantifying the extent of lipid removal (calculated from change in solvent penetration) and protein adsorption both in the SLB core and as an additional layer on top. This additional 28 Å layer represents most of the compact protein in a lipid-free state, allowing for some part to rearrange and integrate itself into the bilayer[34]. The main lipid-binding region is the C-terminal[35] so it is possible the protein would rearrange itself to allow maximum binding of lipids to this area. For membranes incubated with ApoE3, few changes were required from the pristine bilayer structure: the lipid head and tail thicknesses remained constant, while there were some changes in the lipid tail SLD and both head and tail solvation. On the other hand, interaction with ApoE4 also required changes in the head and tail thicknesses to obtain better fits to the NR data. The increased

modifications to the bilayers for the ApoE4 than ApoE3 follow the trend seen in the increased levels of embedded protein. When looking at the net lipid removal (or increase in solvation) and protein adsorption (due to changes in SLD of the SLB core) upon incubation with ApoE, both alleles remove more saturated than unsaturated lipids (Figure 2C). Lipids are removed and replaced by protein adsorption in the bilayer core (Figure 2D) with more protein adsorbing to unsaturated than saturated membranes. The latter in turn indicates that the protein is more prone to remain bound to the unsaturated membrane without actually removing lipids. Additionally, a further protein layer is formed on top of the SLB (Figure 2E). This layer has a greater coverage for ApoE3 than for ApoE4 regardless of membrane type. This indicates that ApoE3 preferentially interacts with the lipid headgroups compared to ApoE4. Interestingly, and regardless of membrane type, the protein fraction that binds to the lipid core is larger for ApoE4 than ApoE3: 70 and 76% of the ApoE4 protein is colocalised within the core for saturated vs. unsaturated SLBs, while these fractions decrease to 54 and 62% when ApoE3 is used instead respectively. The NR data highlight a difference between the proteins that while interaction is preferred with the unsaturated bilayers by both ApoE alleles, the ApoE4 isoform binds to a larger extent to the lipid core than the ApoE3 isoform and the conformation it takes (the fraction colocalised within the lipid core) is less sensitive to the type of lipid in the SLB.

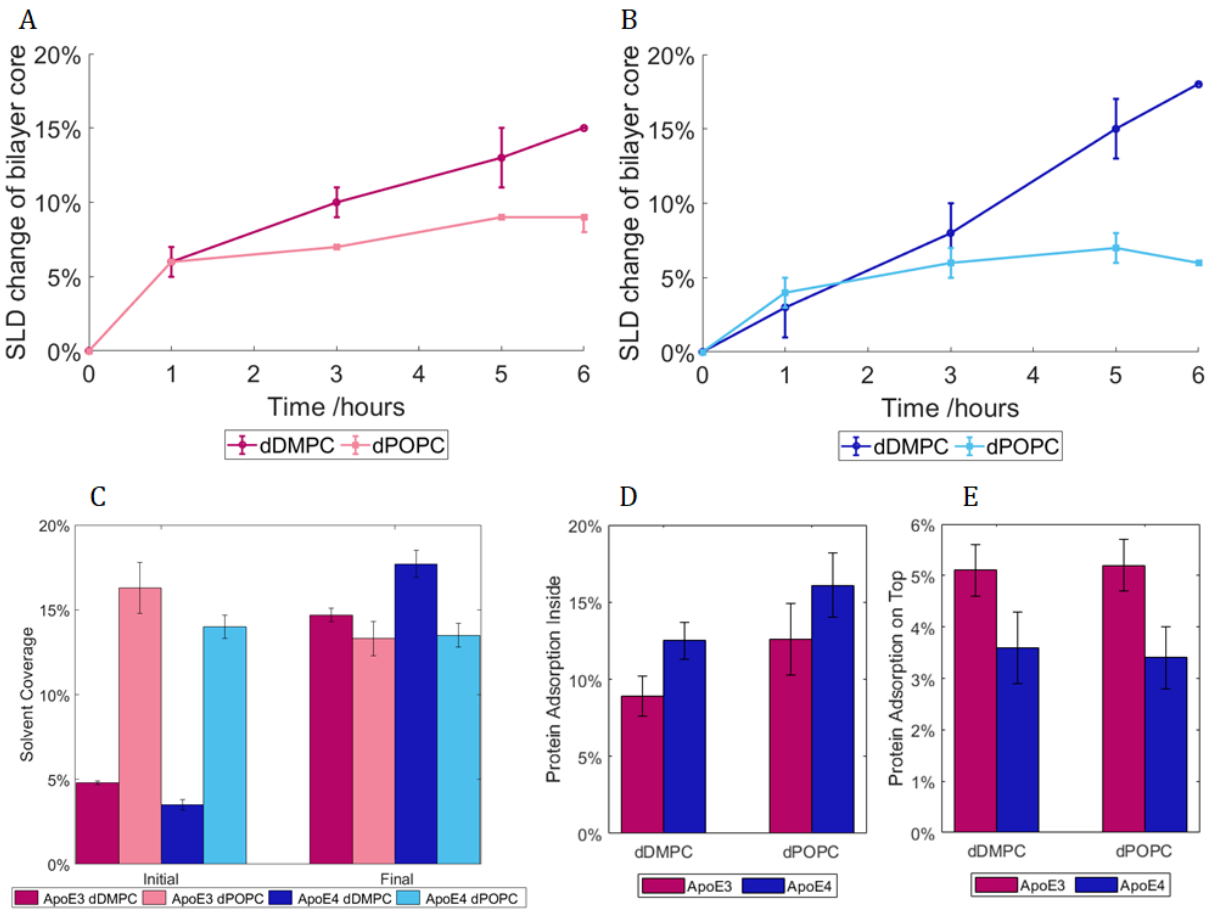

Figure 2. ApoE interaction with saturated (DMPC) or unsaturated (POPC) SLBs: kinetics of lipid replacement in terms of the relevant change in SLD of the lipid core, taking into account solvent change also, are given for ApoE3 (A) and ApoE4 (B). Relative solvent changes within the bilayers (C) and protein adsorption within (D) or on top of (E) the SLBs upon 6 hours of incubation and rinsing with Tris buffer. The NR profiles and best fits are shown in the SI.

3.2 ApoE-based nascent-like HDL particle structure

rHDL made of ApoE and DMPC were prepared using the vesicle solubilisation approach and purified by size exclusion chromatography (Fig. 3A). The discs were structurally characterised by SAXS and SANS in three isotropic contrasts to highlight different parts of the "discs" and increase the accuracy of the fit as already mentioned (Fig 3B).

The model adopted was that of a 'nanodisc' like structure consisting of an elliptical bilayer encased by protein and is depicted in the inset of Figure 3A, with values both fitted and calculated found in Table 2. These discs aim to model nascent HDL, mainly present in cerebrospinal fluids but also important as ApoE containing lipoproteins are responsible for the clearance of lipids in the liver via binding to ApoE receptors[36].

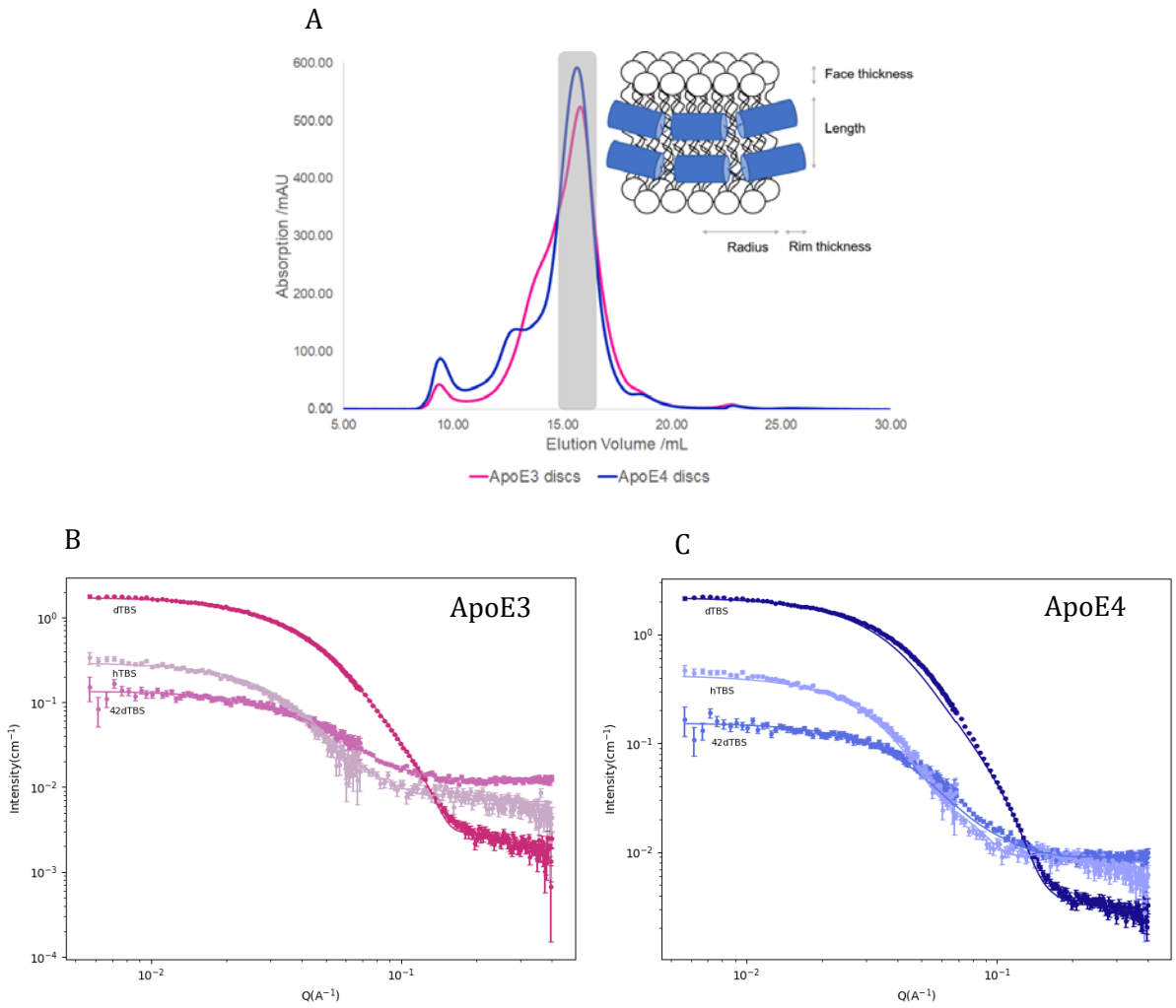

Figure 3A. Size exclusion chromatograms for ApoE3 and ApoE4 rHDL with inset of model used for fitting and B. SANS data in 3 contrasts for the ApoE3 and C. ApoE4 rHDL.

Table 2. Fitted and calculated parameters for the protein-DMPC particles. *Fitted values. ** Calculated values. * Fixed value.**

Parameters	ApoE3	ApoE4
Radius* Å	39.6	43.3
Ellipticity ratio*	1.8	1.5
Protein rim thickness* Å	9	9.8
Lipid headgroup thickness* Å	7.9	7.6
Lipid core thickness*** Å	28	28
Short-long axis disc diameter** Å	97.2-160.6	106.2-149.5
Disc circumference** Å	417	407
No. amino acids**	278	272
Area per Lipid** Å^2	55.9	55.9
No. Lipids per leaflet**	159	158
No. Proteins per disc**	2	2

The calculated values from Table 1 are determined as follows. The equation used for circumference determination takes into account the ellipticity of the particles as used previously[37]:

$$\text{Circumference} = 2\pi\sqrt{([(\text{rminor} + \text{dbelt})^2 + (\text{rmajor} + \text{dbelt})^2]/2)}$$

From this the number of amino acids in contact with the bilayer can be determined. This was done by using an average length per amino acid of 1.5 Å. With 299 residues per protein this gives a maximum circumference of ~ 448 Å which is slightly larger than what was calculated here, however leaves room for flexibility in the protein and possible expansion. Previously reported data on related particles prepared with similar proteins have also allowed for some residues to not be in contact with the bilayer: roughly 20 amino acids per protein were estimated not to be in direct contact with the lipid core[37,38], in agreement with our results. The resulting area of the bilayer region gives 159 or 158 lipids (for ApoE3 and ApoE4 respectively) per leaflet and each disc contains 2 proteins (one per leaflet). This number of lipids per leaflet agrees with data provided for similar length apolipoprotein-like proteins[39]. The disc diameter is larger compared to ApoA1 discs prepared in a similar manner[40], however ApoE is substantially longer than ApoA1 resulting in larger discs. The diameter of the particles in is agreement with DLS data measured for both ApoE3 and ApoE4 based discs which gave values between 10 – 15 nm prior to SANS measurements (results not shown). Both ApoE3 and ApoE4 gave similar structured discs with the same number of lipids per leaflet and number of proteins as each other. This is not surprising due to the same protein length and very similar sequence, only differing in one amino acid. The main structural difference in the discs found between the alleles was the ellipticity, with ApoE3-rHDL being more elliptical than ApoE4-rHDL. Finally, allowing the lipid core thickness to vary did not significantly improve the fit quality.

3.3 ApoE-based nascent-like HDL particle interactions with model membranes

As ApoE alleles play different roles in the onset and development of atherosclerosis and AD, it is important to look at their specific influence on the exchange or removal of lipids when in the form of rHDL or nascent-like HDL. To this end ApoE-based rHDL particles were incubated with model membranes to follow their interaction by NR. dDMPC bilayers both in the absence and presence of cholesterol were used. Both non-deuterated and deuterated cholesterol was used to determine whether the ApoE particles specifically targeted the cholesterol molecules.

There was little change in the surface coverage of the bilayer upon interaction with ApoE based r-HDL: all bilayers started with at least 95% coverage and finished with no less than 90% coverage. Such small capacity for lipid removal cannot be compared to mature HDL (purified from 3 male, healthy adult donors[25]) at similar protein concentration, which can remove roughly 40% of the bilayer[25]. This shows that while some excess lipids were removed in certain cases, lipid removal is not the main role of the ApoE based nascent like HDL particles. Since HDL contains a large number of apolipoproteins associated to it[41], we

also present data for ApoA1 based rHDL against a cholesterol containing saturated membrane (these discs were also prepared by the vesicle solubilisation method[42,43]). For ApoA1 based rHDL, significant lipid removal occurred though to a lesser extent than mature HDL. Although both the HDL and ApoA1-rHDL samples were incubated for 8 hours (as noted by the asterisk in Fig. 4A) rather than 6 hours for ApoE-rHDL against cholesterol containing membranes, the quantity is significantly greater for these samples indicating more than just the increased incubation time is at play. Indeed, kinetics of lipid exchange show that equilibrium was reached after 6 hours for ApoE3-rHDL (Fig 4C) and ApoA1 (SI figure SI 1) while continuous increase was observed for ApoE4-rHDL (Fig. 4D) regardless of membrane composition.

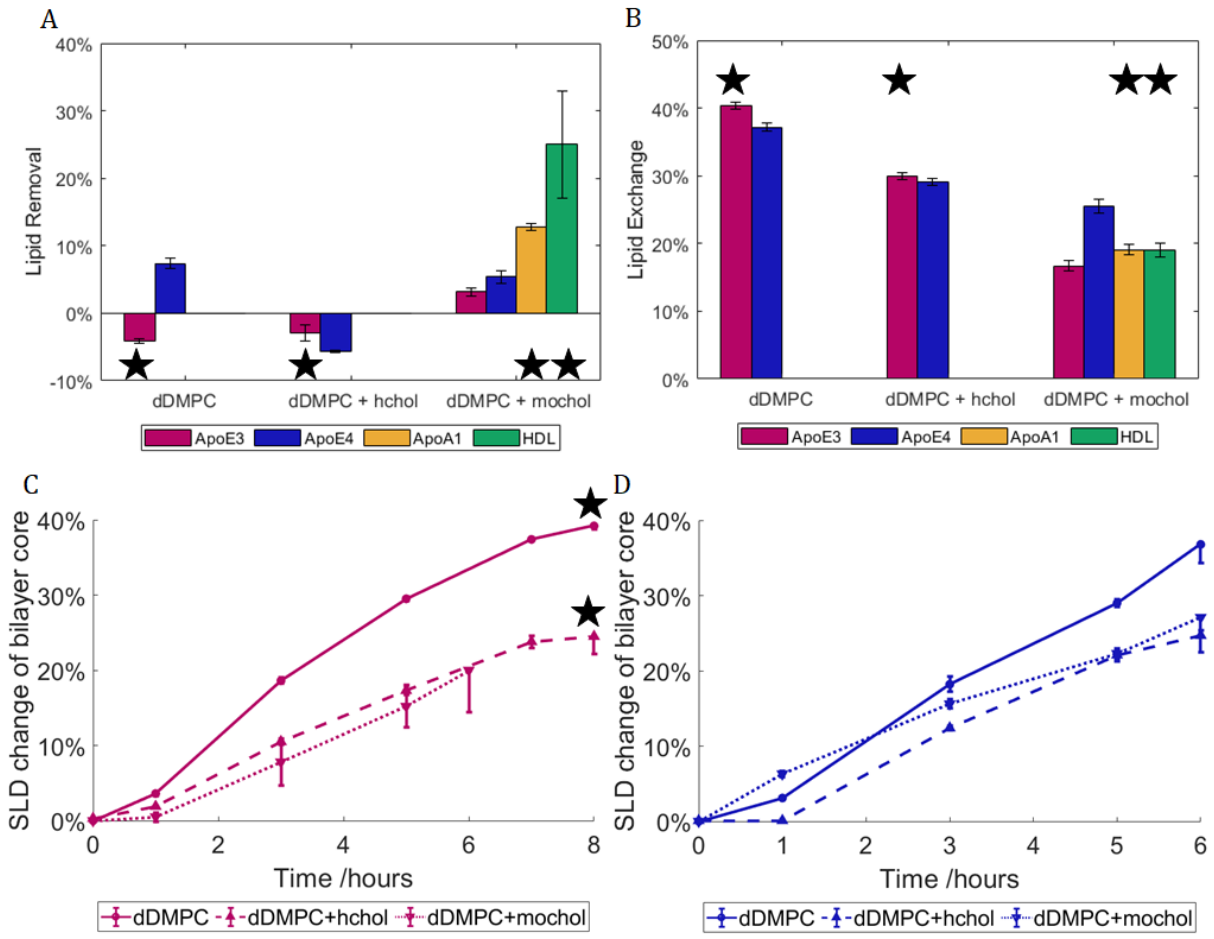

Figure 4. Lipid removal (A) and lipid exchange (B) across model membranes for ApoE3 and ApoE4 based particles. Included data for mature HDL and ApoA1-rHDL against the cholesterol containing bilayers[25]. The asterisk indicates an incubation time of 8 h compared to 6 h for those without. Kinetics of lipid exchange for rHDL containing ApoE3 (C) and ApoE4 (D) in terms of the relative change in SLD of the solvated lipid core over time. HDL data is replotted from Ref 25. The NR profiles and best fits are given in the SI.

Lipid exchange (Fig. 4B) is hereby defined as lipids removed from the bilayer and replaced with lipids from the rHDL particles and is calculated from the SLD change within the tail

region. In this case, a significant proportion of the lipids were exchanged by ApoE-rHDL. For the saturated bilayers both with and without h-cholesterol, the extent of lipid exchange was similar regardless of the ApoE allele present. For the DMPC bilayers, 40.4% ± 0.5% and 37.2% ± 0.6% lipid exchange occurred for ApoE3 and ApoE4-rHDL respectively, while 30.0% ± 0.5% (ApoE3) and 29.1% ± 0.5% (ApoE4) lipid exchange took place in DMPC + h-cholesterol. Bearing in mind the difference in incubation time (ApoE3-rHDL were incubated 2 hours longer than ApoE4-rHDL, see Figure 4C-D), this strongly indicates that ApoE4-rHDL has the ability to exchange more lipids than ApoE3-rHDL. This is indeed confirmed when observing the quantities of lipids exchanged in the DMPC + mo-cholesterol bilayers where the samples were incubated for the same time period (6 hours) and the values differ more drastically: 16.7% ± 0.8% and 25% ± 1% for ApoE3 and ApoE4. The trend is clear that ApoE4-rHDL exchanged more lipids than the ApoE3-rHDL regardless of membrane composition. In Figure 4B the extent of lipid exchange for both ApoA1-rHDL and mature HDL upon 8 hour incubation has similar lipid exchange capacity to ApoE3-rHDL, while ApoE4-rHDL has much greater affinity for lipid exchange than any of the other samples tested.

To be able to determine if cholesterol was being preferentially exchanged by either ApoE allele, both deuterated and non-deuterated cholesterol were used. If cholesterol was exchanged preferentially over the phospholipids, a net difference would be seen in the final quantity of lipids exchanged across these two membranes due to lack of contrast between h-cholesterol and the h-DMPC lipids in the rHDL or mature HDL samples. This is not the case as shown in Figure 4B, which suggests that the phospholipid molecules were primarily exchanged rather than the cholesterol molecules.

Mirroring the NR data for protein incubation alone on SLBs, the bilayers exposed to ApoE4-rHDL required greater changes to obtain a satisfactory fit to the experimental data. ApoE3-rHDL incubated with saturated bilayers with and without h-cholesterol were fitted with head and tail region thicknesses kept constant, whereas the remaining bilayers including ApoE3-rHDL with DMPC + mochol and all of the bilayers incubated with ApoE4-rHDL required changes to the head and tail thicknesses to find suitable fits. All variations were tested: from keeping them all the same; to only altering the head thickness; to varying all regions. It was found that better fits were possible when allowing greater variation when incubated with ApoE4-rHDL, again indicating greater level of interaction occurred in the presence of ApoE4 compared to ApoE3. This could in part be due to slight embedding of ApoE4 into the core of the SLB, although the resulting membranes were found to maintain, within error, a constant area per molecule within tails and head suggesting that the bilayer structure is retained in all cases.

4. Discussion

While the variance in the ApoE alleles' structure is subtle[14], clear differences can be seen in their resulting behaviour upon interaction with bilayers: in particular, ApoE4 binds to

a larger extent to the lipid bilayer core than ApoE3 (Fig 2D) although roughly the same amount of protein sits on top of the bilayer regardless of allele (Fig. 2E). These changes impact the ability of ApoE to bind lipids. In particular, ApoE4 has a greater ability to bind lipids due to structural differences in the helical segments of the C-terminal (CT) leading to a reduced ability of the protein to form tetramers, in turn giving a higher proportion of monomers and therefore increasing lipid binding ability, as tetramers are less capable of binding lipids[44,45]. AopoE4's increased affinity for lipid binding is also seen where ApoE4 preferentially binds to very low-density lipoproteins (VLDL, for which its surface is roughly 60% lipids) rather than HDL compared to ApoE3 which binds preferentially to HDL (for which its surface is roughly 80% protein). Futhermore, ApoE4 lacks flexibility in its CT domain leading to a preference for the lower curvature of the VLDL particles[46]. The increased affinity for VLDL leads to an increased clearance of VLDL from plasma via ApoE receptors in the liver. However, this in turn leads to LDL receptors being downregulated raising overall levels of plasma LDL and giving an increased risk for atherosclerosis[47,48].

The rate of lipid binding was explored by vesicle solubilisation showing a biexponential decay when solubilising DMPC vesicles at their melting temperature of 24 °C[49]; with ApoE4 having a higher rate constant than ApoE3. A two-rate kinetic process can also be seen here with the protein incorporation into bilayers (Fig. 2A-B) where an initial increase occurs rapidly followed by a slowing down of the interaction process. Another study showed the increased ability of ApoE4 to disrupt DMPC vesicles compared to ApoE3 by measuring the release of fluorescent dye within[50].

Recently, our group showed that native HDL, through its apolipoproteins, present a lower ability to exchange and replace unsaturated lipids as compared to saturated ones[25]. Both ApoE alleles mirror this trend and remove more saturated than unsaturated lipids. Atherogenic and amyloid plaques are rich in saturated lipids and cholesterol[18,51]. In a recent study, a link between AD and the disruption of the metabolism of unsaturated fats such as omega 3 was found, which could provide an explanation for ApoE4's affinity for the unsaturated membrane[52]. Indeed, previous reports states that supplementing mono- and poly-unsaturated fats in the diet reduce the risk to AD, whereas saturated fats increase this risk[53].

The fact that a larger fractions of ApoE4 binds the lipid core than ApooE3 and that it has less sensitivity to the lipid type in the membrane (Fig. 2D, E) could be linked to a decreased flexibility in the ApoE4 molecule: its greater rigidity forces it to maintain a more compact conformation around the lipid core which in turn could render it less able to bind to HDL. Earlier, ApoE4 was shown to disrupt the lipid membrane to a larger extent than ApoE3[15], in agreement with our results that show larger ApoE4 incorporation into the bilayers and greater structural changes in the SLBs required to fit the NR data after protein incubation. Indeed, ApoE4 could retain a more compact structure folded back on itself due to the Arg-61:Glu-255 salt bridge that could restrain the protein structurally even when associated with lipids[54,55].

Regarding the nascent HDL structure, there are some reports on the structural determination of ApoE-based particles mainly by electron microscopy[56] and also

regarding size determination by SDS-PAGE[55,57]. These reports are in agreement with the size of particles reported here: 10-15 nm in diameter (Figure 3 and Table 2). Contrary to ApoE based rHDL, ApoA1- or membrane scaffold protein (MSP)-based nanodiscs form particles that are about 8-12 nm in diameter[37–39,43]. A variation of models have been presented when describing protein-lipid particles from the picket-fence model[58], to the double superhelix[59] or double belt-like structure[40,60], though some of these have faced opposition within the nanodisc community[61,62]. The main structural difference in the nanodiscs formed by the two alleles studied is the ellipticity, with ApoE4 forming less elongated discs. Our data agrees well with the double belt structure since the data suggest that there are 2 proteins present per nanodisc, well in agreement with ApoA1-based nanodiscs. Previously reported data on ApoE-based nanodiscs show the presence of 2 or more proteins per disc[55,57,63]. There has been some debate as to whether ApoE3 and ApoE4 form nanodiscs in a different manner giving structural differences to the protein conformation[64] and in turn their lipid exchange ability. Hypotheses suggested include ApoE3 forming more of an extended belt conformation around the whole perimeter of the disc due to increased flexibility[57]. The more compact structure of ApoE4 could lead to potentially more ApoE4 proteins per nanodisc compared to ApoE3[65]. However, the same number of proteins was found to be present in both of the nanodisc variants presented here. The NR lipid exchange data (Fig. 4) though suggest that the proteins adapt slightly different conformations giving rise to their differing exchange capabilities.

Where some reports have shown incremental size increase of nanodiscs with increasing protein length[38,66], it is of no surprise that the ApoE-based rHDL particles reported here are of a slightly larger size than previously reported for ApoA1-based ones as the ApoE protein length is longer still. In turn, the number of lipids per nanodisc is also higher for ApoE than ApoA1-based nanodiscs which does not seem to have an effect on the ability of these nanodiscs to exchange lipids: when comparing ApoE3 and ApoE4 based rHDL of similar size, their functional capabilities are different depending on the ApoE allele present since clear differences were observed in their lipid exchange and removal affinity (Fig. 4 A, B).

Moreover, the lipid exchange (Fig. 4B) was similar between ApoE3 and ApoA1-based nanodiscs while it was different between ApoE alleles, despite them being of similar size but larger than ApoA1 (sine the nanodisc concentration was constant across samples, smaller discs imply lower lipid concentration in the case of ApoA1). Therefore, it is clear that the rHDL size (area of the lipid nanodisc) does not determine the extent of lipid exchange; rather, specific apolipoprotein – lipid interactions must be behind the observed phenomena.

ApoA1 and ApoE have similar structures comprising of amphipathic alpha-helices that enable them to form nascent HDL like structures by solubilising phospholipids[24]. However, neither ApoE3 nor ApoE4 remove many excess lipids from the membrane but ApoA1-rHDL does although to a lesser extent than mature HDL (Fig. 4A). ApoA1 is the main protein in the human serum and its function is to clear lipids so the results here suggest that indeed it removes more lipids than it exchanges. Our results suggest that the

function of ApoE cannot be related to mainly the lipid exchange, but rather to binding ApoE-receptors in the liver. In turn, the fact that ApoE4 conformation is more compact might affect how it binds to ApoE and other LDL receptors in the liver[67]. However, ApoE based HDL are the main lipoproteins found in the brain, being produced there and lacking the ability to cross the blood brain barrier[36]. The ApoE in the brain is the second most abundant place for ApoE production in the body after the liver[48]. ApoE plays an important role in maintaining the homeostasis of cholesterol concentration in the brain which homes the highest quantity of cholesterol in the body (roughly 20-25% of the body's total cholesterol)[68]. Where HDL in the rest of the body undergoes cholesterol efflux thereby removing cholesterol from artery walls, ApoE-based HDL in the brain maintains constant cholesterol levels[12]. Indeed, the hereby reported data clearly show that lipid exchange was not affected by the level of deuteration in cholesterol (Fig. 4) suggesting that ApoE does not interact with cholesterol significantly. These results suggest that ApoE enriched HDL rather removes saturated lipids than cholesterol or unsaturated lipids. By regulating the ratio of saturated lipids in cellular membranes. ApoE-based HDL could probably maintain membrane elasticity, which is key for the healthy function of the cell. Interestingly, cholesterol crystal nucleation starts sooner in unsaturated than saturated containing model bile salts[69], which suggests a higher saturation concentration prior to forming crystals in saturated than unsaturated membranes. Thus, ApoE4 can potentially favour an increase in membrane saturation with cholesterol by exchanging and removing more saturated fats than ApoE3, which could potentially lead to cholesterol crystallisation in the brain.

Even though ApoE4 has a higher affinity to bind lipids than ApoE3 as demonstrated here and elsewhere[70], the ability of ApoE alleles to efflux cholesterol has been disputed: some studies suggest it is not ApoE allele dependant[71] while others have found that ApoE4 has a lesser ability to perform cholesterol efflux compared to ApoE3 especially in relation to neurons in the brain[65,72,73]. This lack of ability of ApoE4 to remove and deposit cholesterol in the brain efficiently has been proposed to be one of the main reasons for the onset of AD[64,65]. Our simplified model that enables controlled experimental conditions show that neither ApoE allele has a special affinity for taking up cholesterol and we could hypothesise that there is no significant difference in their capacity to efflux cholesterol.

Conclusions

Neutron reflection has been used to show that ApoE4 adopts a different conformation to ApoE3 at model membranes, and that this conformation differs between saturated and unsaturated membranes for ApoE3 only. Moreover, neither ApoE allele removes a significant amount of unsaturated lipids but can remove saturated lipids to similar extents. Small angle neutron scattering was used to demonstrate that the structure of nascent like HDL particles made with DMPC and either ApoE3 or ApoE4 is quite similar, forming elliptical disc like structures. Neutron reflection is then used to quantify the extent of lipid exchange and lipid removal by nacent-like rHDL particles and model membranes. The data show that rHDL particles made with both ApoE alleles have a low

ability to remove saturated lipids as compared to ApoA1-based rHDL particles or mature HDL. The extent of lipid exchange, on the other hand is similar between the alleles and is impaired by the presence of cholesterol. Finally, ApoE does not exchange or remove cholesterol molecules but rather saturated lipids. The results here mirror the physiological roles of ApoE-based HDL and ApoA1-based HDL particles in the brain and in serum respectively. This demonstrates that our models are suitable to study the function of these particles as a function of a range of experimental conditions.

Acknowledgements

We thank the ILL neutron facility for granted beamtimes with DOIs: The National Deuteration Facility in Australia is partly funded by The National Collaborative Research Infrastructure Strategy (NCRIS) an Australian Government initiative. MC thanks the Swedish Research Council for financial support. This work was also partly funded by a PhD studentship at the ILL. VTF thanks the EPSRC for grants GR/R99393/01 and EP/C015452/1 which funded the creation of the Deuteration Laboratory in ILL's Life Science Group. This work benefited from the use of the SasView application, originally developed under NSF award DMR-0520547.

Competing interests

Authors declare no competing interests.

Corresponding Authors

Marité Cárdenas

References

1. Gordon, D. J. *et al.* High-Density Lipoprotein Cholesterol and Cardiovascular Disease Four Prospective American Studies. 8–15 (1988).
2. Voight, B. F. *et al.* Plasma HDL cholesterol and risk of myocardial infarction: A mendelian randomisation study. *Lancet* **380**, 572–580 (2012).
3. Madsen, C. M., Varbo, A. & Nordestgaard, B. G. Extreme high high-density lipoprotein cholesterol is paradoxically associated with high mortality inmen and women: Two prospective cohort studies. *Eur. Heart J.* **38**, 2478–2486 (2017).
4. Gille, A., Easton, R., D'Andrea, D., Wright, S. D. & Shear, C. L. CSL112 enhances biomarkers of reverse cholesterol transport after single and multiple infusions in healthy subjects. *Arterioscler. Thromb. Vasc. Biol.* **34**, 2106–2114 (2014).
5. Van Capelleveen, J. C., Brewer, H. B., Kastelein, J. J. P. & Hovingh, G. K. Novel therapies focused on the high-density lipoprotein particle. *Circ. Res.* **114**, 193–204 (2014).
6. Toth, P. P. *et al.* High-density lipoproteins : A consensus statement from the National Lipid Association. *J. Clin. Lipidol.* **7**, 484–525 (2013).
7. Angeloni, E. *et al.* Lack of protective role of HDL-C in patients with coronary artery disease undergoing elective coronary artery bypass grafting. 3557–3562 (2013) doi:10.1093/eurheartj/eht163.
8. Jonas, A. *Lipoprotein structure*. *Biochemistry of Lipids, Lipoproteins and Membranes* (2002). doi:10.1042/bst0100143a.
9. Utermann, G. Isolation and Partial Characterization of an Arginine-Rich Apolipoprotein From Human Plasma Very-Low-Density Lipoproteins: Apolipoprotein E. *Hoppe Seylers Z Physiol Chem* **356**, 1113–21 (1975).
10. Davidson, W. S. *et al.* Proteomic analysis of defined HDL subpopulations reveals particle-specific protein clusters: Relevance to antioxidative function. *Arterioscler. Thromb. Vasc. Biol.* **29**, 870–876 (2009).
11. Ladu, M. J. O., Reardon, C., Eldik, L. V. A. N. & Getz, G. S. Lipoproteins in the Central Nervous System. 167–175 (1801).
12. Mahley, R. W. Central Nervous System Lipoproteins: ApoE and Regulation of Cholesterol Metabolism. *Arterioscler. Thromb. Vasc. Biol.* **36**, 1305–1315 (2016).
13. Weisgraber, K. H., Rall, S. C. & Mahley, R. W. Human E Apoprotein Heterogeneity. (1981).
14. Chou, C. Y. *et al.* Structural variation in human apolipoprotein E3 and E4: Secondary structure, tertiary structure, and size distribution. *Biophys. J.* **88**, 455–466 (2005).
15. Mahley, R. W., Weisgraber, K. H. & Huang, Y. Apolipoprotein E : structure determines function , from atherosclerosis to Alzheimer ' s disease to AIDS. 183–188 (2009) doi:10.1194/jlr.R800069-JLR200.
16. Reiman, E. M. Exceptionally low likelihood of Alzheimer ' s dementia in APOE2 homozygotes from a 5,000-person neuropathological study. doi:10.1038/s41467-019-14279-8.
17. Wu, L., Zhao, L. & Ph, D. ApoE2 and Alzheimer ' s disease : time to take a closer look. **11**, 412–413 (2020).

18. Kiskis, J. *et al.* Plaque-associated lipids in Alzheimer ' s diseased brain tissue visualized by nonlinear microscopy. *Nat. Publ. Gr.* 1–9 (2015) doi:10.1038/srep13489.
19. Browning, K. L. *et al.* Human lipoproteins at model cell membranes: effect of lipoprotein class on lipid exchange. *Sci. Rep.* **7**, (2017).
20. Davidson, W. S. *et al.* Effects of Acceptor Particle Size on the Efflux of Cellular Free Cholesterol. vol. 270 17106–17113 (1995).
21. Garber, D. W. *et al.* A new synthetic class A amphipathic peptide analogue protects mice from diet-induced atherosclerosis. *J. Lipid Res.* **42**, 545–552 (2001).
22. White, C. R., Garber, D. W. & Anantharamaiah, G. M. Anti-inflammatory and cholesterol-reducing properties of apolipoprotein mimetics: A review. *J. Lipid Res.* **55**, 2007–2021 (2014).
23. Valanti, E. K., Dalakoura-Karagkouni, K. & Sanoudou, D. Current and emerging reconstituted hdl-apoa-i and hdl-apoe approaches to treat atherosclerosis. *J. Pers. Med.* **8**, 1–12 (2018).
24. Lund-Katz, S. & Phillips, M. C. High Density Lipoprotein Structure-Function and Role in Reverse Cholesterol Transport. *Subcell Biochem.* **51**, 183–227 (2010).
25. Waldie, S. *et al.* Lipoprotein ability to exchange and remove lipids from model membranes as a function of fatty acid saturation and presence of cholesterol. *Biochim. Biophys. Acta - Mol. Cell Biol. Lipids* 2020 (2020).
26. Yepuri, N. R. *et al.* Synthesis of Perdeuterated 1-Palmitoyl-2-oleoyl-sn-glycero-3-phosphocholine ([D 82]POPC) and Characterisation of Its Lipid Bilayer Membrane Structure by Neutron Reflectometry. *Chempluschem* **81**, 315–321 (2016).
27. Haertlein, M. *et al. Biomolecular Deuteration for Neutron Structural Biology and Dynamics*. *Methods in Enzymology* vol. 566 (2016).
28. Waldie, S. *et al.* The Production of Matchout- Deuterated Cholesterol and the Study of Bilayer-Cholesterol Interactions. **9**, 5118 (2019).
29. Åkesson, A. *et al.* Composition and structure of mixed phospholipid supported bilayers formed by POPC and DPPC. *Soft Matter* **8**, 5658–5665 (2012).
30. Waldie, S. *et al.* Localization of cholesterol within supported lipid bilayers made of a natural extract of tailor-deuterated phosphatidylcholine. *Langmuir* **34**, 472–479 (2018).
31. Campbell, R. A., Wacklin, H. P., Sutton, I., Cubitt, R. & Fragneto, G. FIGARO: The new horizontal neutron reflectometer at the ILL. *Eur. Phys. J. Plus* **126**, 1–22 (2011).
32. Campbell, R. A., Wacklin, H. P., Sutton, I., Cubitt, R. & Fragneto, G. Erratum to: FIGARO: The new horizontal neutron reflectometer at the ILL (Eur. Phys. J. Plus (2011), 126, (107), 10.1140/epjp/i2011-11107-8). *Eur. Phys. J. Plus* **130**, 1 (2015).
33. Nelson, A. Co-refinement of multiple-contrast neutron/X-ray reflectivity data using MOTOFIT. *J. Appl. Crystallogr.* **39**, 273–276 (2006).
34. Chen, J., Li, Q. & Wang, J. Topology of human apolipoprotein E3 uniquely regulates its diverse biological functions. **108**, 2–7 (2011).
35. Li, X., Kypreos, K., Zanni, E. E. & Zannis, V. Domains of apoE Required for Binding To apoE Receptor 2 and To Phospholipids : Implications For The Functions Of apoE in the Brain †. **1**, 10406–10417 (2003).

36. Pitas, R. E., Boyles, J. K., Lee, S. H., Hui, D. & Weisgraber, K. H. Lipoproteins and their receptors in the central nervous system. *J. Biol. Chem.* **262**, 14352–14360 (1987).
37. Skar-Gislinge, N. *et al.* Elliptical structure of phospholipid bilayer nanodiscs encapsulated by scaffold proteins: Casting the roles of the lipids and the protein. *J. Am. Chem. Soc.* **132**, 13713–13722 (2010).
38. Denisov, I. G., Grinkova, Y. V., Lazarides, A. A. & Sligar, S. G. Directed Self-Assembly of Monodisperse Phospholipid Bilayer Nanodiscs with Controlled Size. *J. Am. Chem. Soc.* **126**, 3477–3487 (2004).
39. Bayburt, T. H. & Sligar, S. G. Membrane protein assembly into Nanodiscs. *FEBS Lett.* **584**, 1721–1727 (2010).
40. Midtgaard, S. R., Pedersen, M. C. & Arleth, L. Small-Angle X-Ray Scattering of the Cholesterol Incorporation into Human ApoA1-POPC Discoidal Particles. *Biophys. J.* **109**, 308–318 (2015).
41. Maric, S. *et al.* Time-resolved small-angle neutron scattering as a probe for the dynamics of lipid exchange between human lipoproteins and naturally derived membranes. *Sci. Rep.* **9**, 7591 (2019).
42. Giudice, R. Del, Nilsson, O., Domingo-espín, J. & Lagerstedt, J. O. Synchrotron radiation circular dichroism spectroscopy reveals structural divergences in HDL-bound apoA-I variants. 1–9 (2017) doi:10.1038/s41598-017-13878-z.
43. Del, R. *et al.* Structural determinants in ApoA-I amyloidogenic variants explain improved cholesterol metabolism despite low HDL levels. *BBA - Mol. Basis Dis.* **1863**, 3038–3048 (2017).
44. Chetty, P. S., Mayne, L., Lund-katz, S., Englander, S. W. & Phillips, M. C. Helical structure, stability, and dynamics in human apolipoprotein E3 and E4 by hydrogen exchange and mass spectrometry. *PNAS* **114**, (2017).
45. Garai, K., Baban, B. & Frieden, C. Dissociation of apoE oligomers to monomers is required for high affinity binding to phospholipid vesicles. **50**, 2550–2558 (2011).
46. Nguyen, D. *et al.* Molecular Basis for the Differences in Lipid and Lipoprotein Binding Properties of Human Apolipoproteins E3 and E4. **49**, 10881–10889 (2010).
47. Dong, L. & Weisgraber, K. H. Human Apolipoprotein E4 Domain Interaction. **271**, 19053–19057 (1996).
48. Mahley, R. W. Apolipoprotein E : from cardiovascular disease to neurodegenerative disorders. *J. Mol. Med.* 739–746 (2016) doi:10.1007/s00109-016-1427-y.
49. Segall, M. L. *et al.* Influence of apoE domain structure and polymorphism on the kinetics of phospholipid vesicle solubilization. **43**, (2002).
50. Ji, Z. S. *et al.* Apolipoprotein E4 potentiates amyloid β peptide-induced lysosomal leakage and apoptosis in neuronal cells. *J. Biol. Chem.* **277**, 21821–21828 (2002).
51. Touboul, D. & Gaudin, M. Lipidomics of Alzheimer's disease. *Bioanalysis* **6**, (2014).
52. Snowden, S. G. *et al.* Association between fatty acid metabolism in the brain and Alzheimer disease neuro- pathology and cognitive performance : A nontargeted metabolomic study. 1–19 (2017) doi:10.1371/journal.pmed.1002266.

53. Morris, M. C. Diet and Alzheimer ' s Disease : What the Evidence Shows. **6**, 1–6 (2020).
54. Drury, J. & Narayanaswami, V. Examination of lipid-bound conformation of apolipoprotein E4 by pyrene excimer fluorescence. *J. Biol. Chem.* **280**, 14605–14610 (2005).
55. Raussens, V. *et al.* The Low Density Lipoprotein Receptor Active Conformation of Apolipoprotein E. **273**, 25825–25830 (1998).
56. Newhouse, Y., Peters-Libeu, C. & Weisgraber, K. H. Crystallization and preliminary X-ray diffraction analysis of apolipoprotein E-containing lipoprotein particles. *Acta Crystallogr. Sect. F Struct. Biol. Cryst. Commun.* **61**, 981–984 (2005).
57. Narayanaswami, V. *et al.* Helix Orientation of the Functional Domains in Apolipoprotein E in Discoidal High Density Lipoprotein Particles *. **279**, 14273–14279 (2004).
58. Jonas, A. & Wald, J. H. Defined Apolipoprotein A-I Conformations in Reconstituted High Density Lipoprotein Discs *. 4818–4824 (1989).
59. Wu, Z. *et al.* Double superhelix model of high density lipoprotein. *J. Biol. Chem.* **284**, 36605–36619 (2009).
60. Segrest, J. P. *et al.* A Detailed Molecular Belt Model for Apolipoprotein A-I in Discoidal High Density Lipoprotein *. **6**, 31755–31759 (1999).
61. Approach, A. C. C. Assessment of the Validity of the Double Superhelix Model for Reconstituted High Density Lipoproteins. **285**, 41161–41171 (2010).
62. Gogonea, V. & Miller, N. E. Structural Insights into High Density Lipoprotein : Old Models and New Facts. **6**, (2016).
63. Yamamoto, T., Choi, H. W. & Ryan, R. O. Apolipoprotein E isoform-specific binding to the low-density lipoprotein receptor. *Anal. Biochem.* **372**, 222–226 (2008).
64. de Chaves, E. P. & Narayanaswami, V. Apolipoprotein E and cholesterol in aging and disease in the brain. *Futur. Lipidol.* **3**, 505–530 (2008).
65. Gong, J. *et al.* Apolipoprotein E (ApoE) Isoform-dependent Lipid Release from Astrocytes Prepared from Human ApoE3 and ApoE4 Knock-in Mice *. **277**, 29919–29926 (2002).
66. Denisov, I. G., McLean, M. A., Shaw, A. W., Grinkova, Y. V. & Sligar, S. G. Thermotropic phase transition in soluble nanoscale lipid bilayers. *J. Phys. Chem. B* **109**, 15580–15588 (2005).
67. Ruiz, J. *et al.* The apoE isoform binding properties of the VLDL receptor reveal marked differences from LRP and the LDL receptor. *J. Lipid Res.* **46**, 1721–1731 (2005).
68. Michikawa, M. Role of cholesterol in amyloid cascade : cholesterol-dependent modulation of tau phosphorylation and mitochondrial function. **114**, 21–26 (2006).
69. Halpern, Z., Moshkowitz, M., Laufer, H., Peled, Y. & Gilat, T. Effect of phospholipids and their molecular species on cholesterol solubility and nucleation in human and model biles. 110–115.
70. Saito, H. *et al.* Effects of Polymorphism on the Lipid Interaction of Human Apolipoprotein E. *J. Biol. Chem.* **278**, 40723–40729 (2003).

71. Krimbou, L. *et al.* Molecular interactions between apoE and ABCA1 : impact on apoE lipidation. **45**, (2004).
72. Huang, Y., Eckardstein, A. Von, Wu, S. & Assmann, G. Effects of the Apolipoprotein E Polymorphism Cell-derived Cholesterol in Plasma. **96**, 2693–2701 (1995).
73. Michikawa, M., Fan, Q., Isobe, I. & Yanagisawa, K. Apolipoprotein E Exhibits Isoform-Specific Promotion of Lipid Efflux from Astrocytes and Neurons in Culture. (2000).

Supporting Information

The interaction of ApoE and ApoE nascent-like HDL particles with model cellular membranes: Effect of protein allele and membrane composition

Sarah Waldie[1,2,2b], Federica Sebastiani[1], Martine Moulin[2,2b], Yuri Gerelli[2], Sylvain Prevost[2], Felix Roosen-Runge[1], John C. Voss[3], Tamim A. Darwish[4] Nageshwar Yepuri[4], Rita Del Giudice[1], Gernot Strohmeier[5,6], Harald Pichler[5,7], Selma Maric[8], V. Trevor Forsyth[2,2b,9], Michael Haertlein[2,2b] and Marité Cárdenas[1]*

* corresponding author marite.cardenas@mau.se

[1] Department of Biomedical Science and Biofilms – Research Center for Biointerfaces, Malmö University, 20506 Malmö, Sweden.

[2] Institut Laue-Langevin, 71 Avenue des Martyrs, 38042 Grenoble, Cedex 9, France

[2b] Partnership for Structural Biology (PSB), 71 Avenue des Martyrs, 38042 Grenoble, Cedex 9, France

[3] Department of Biochemistry and Molecular Medicine, University of California, Davis, CA 95616, USA

[4] National Deuteration Facility, Australian Nuclear Science and Technology Organisation, New Illwarra Road, Lucas Heights NSW 2234, Australia

[5] Austrian Centre of Industrial Biotechnology, Petersgasse 14, 8010 Graz, Austria

[6] Graz University of Technology, Institute of Organic Chemistry, NAWI Graz, Stremayrgasse 9, 8010 Graz, Austria

[7] Graz University of Technology, Institute of Molecular Biotechnology, NAWI Graz, BioTechMed Graz, Petersgasse 14, 8010 Graz, Austria

[8] MAX IV Laboratory, Fotongatan 2, 225 92 Lund, Sweden

[9] Faculty of Natural Sciences, Keele University, Staffordshire ST5 5BG, UK

Table S1. Pristine bilayers before incubation with either lipid-free protein or ApoE-based rHDL. The parentheses detail which sample was incubated on that SLB.

Bilayer	**Layer**	**Thickness (Å)** E± 0.1-1	**SLD (*10^{-6} Å^{-2})** E± 0.01-0.3	**Solvent (%)** E± 0.2-5	**MMA (Å²)** E±1-5
dDMPC (E3 prot)	Inner Head	8.98	1.89	35	56
	Tail	25.2	6.46	4.8	65
	Outer Head	8.98	1.89	35	56
dPOPC (E3 prot)	Inner Head	7.8	1.89	31	60
	Tail	28.4	6.45	16	78
	Outer Head	7.8	1.89	31	60
dDMPC (E4 prot)	Inner Head	8.98	1.89	37.7	58.2
	Tail	27.2	6.45	3.5	59.6
	Outer Head	8.98	1.89	37.7	58.2
dPOPC (E4 prot)	Inner Head	8.8	1.89	46.4	70
	Tail	28.6	6.25	14	76
	Outer Head	8.8	1.89	46.4	70
dDMPC (E3 disc)	Inner Head	9.46	1.89	38	55.6
	Tail	26.2	6.34	4.4	62.4
	Outer Head	9.46	1.89	38	55.6
dDMPChch (E3 disc)	Inner Head	7.7	1.89	15	50
	Tail	30.7	5.7	6	53
	Outer Head	7.7	1.89	15	50
dDMPCdch (E3 disc)	Inner Head	8.5	1.89	29	54
	Tail	32.1	6.58	2	48.5
	Outer Head	8.5	1.89	29	54
dDMPC (E4 disc)	Inner Head	9.4	1.89	33	52
	Tail	26	6.22	0.5	61
	Outer Head	9.4	1.89	33	52
dDMPChch (E4 disc)	Inner Head	9.45	1.89	26	46.6
	Tail	31.3	5.7	5.8	51.7
	Outer Head	9.45	1.89	26	46.6
dDMPCdch (E4 disc)	Inner Head	8.9	1.89	26	49.5
	Tail	26.3	6.43	3.2	59.9
	Outer Head	8.9	1.89	26	49.5

dDMPCdch (A1 disc)	Inner Head	6.9	1.89	19	58
	Tail	33.6	6.59	5.4	48
	Outer Head	6.9	1.89	19	58

Table S2. Parameters for bilayers after incubation with either lipid-free protein or ApoE-based rHDL.

Bilayer	**Layer**	**Thickness (Å)** E± 0.1-1	**SLD (*10^{-6} Å^{-2})** E± 0.01-0.3	**Solvent (%)** E± 0.2-5	**MMA (Å^2)** E±1-5
dDMPC E3 prot	Inner Head	8.98	1.89	49.2	71
	Tail	25.2	6.08	14.7	73
	Outer Head	8.98	1.89	44.2	65
	Protein	28	2.99	94.9	
dPOPC E3 prot	Inner Head	7.82	1.89	35	64
	Tail	28.4	5.75	13	76
	Outer Head	7.82	1.89	42	71
	Protein	28	2.99	94.8	
dDMPC E4 prot	Inner Head	8.8	1.89	42	64
	Tail	26.8	5.94	17.7	71
	Outer Head	7.1	1.89	39	75
	Protein	28	2.99	96.4	
dPOPC E4 prot	Inner Head	8.8	1.89	47.2	70
	Tail	29.4	5.78	13.5	73
	Outer Head	7.6	1.89	41	73
	Protein	28	2.99		
dDMPC E3 disc	Inner Head	9.46	1.89	40.3	57.7
	Tail	26.2	3.65	0.3	59.9
	Outer Head	9.46	1.89	43	60
	Disc	44	2.56	98.9	
dDMPChch E3 disc	Inner Head	7.7	1.89	14	49
	Tail	30.7	3.61	3.2	51
	Outer Head	7.7	1.89	18	52
	Disc	44	2.56	99	
dDMPCdch E3 disc	Inner Head	6.7	1.89	20	61
	Tail	30.9	5.26	5.2	51.2
	Outer Head	9.2	1.89	25	47
	Disc	44	2.76	98.7	

dDMPC E4 disc	Inner Head Tail Outer Head Disc	7.5 32.3 6.2 44	1.89 3.86 1.89 2.52	40 7.9 30 98.9	73 53 75
dDMPChch E4 disc	Inner Head Tail Outer Head Disc	10.9 30.9 9.3 44	1.89 3.67 1.89 2.52	36.8 0 21 98.8	47 49.3 44
dDMPCdch E4 disc	Inner Head Tail Outer Head Disc	6.6 29 8.2 44	1.89 4.67 1.89 2.52	23 8.6 38 97.2	64 56.6 64
dDMPCdch A1 disc	Inner Head Tail Outer Head Disc	6.7 34.6 9.4 44	1.89 5.12 1.89 2.5	35 18.8 31 96.8	75 54 50

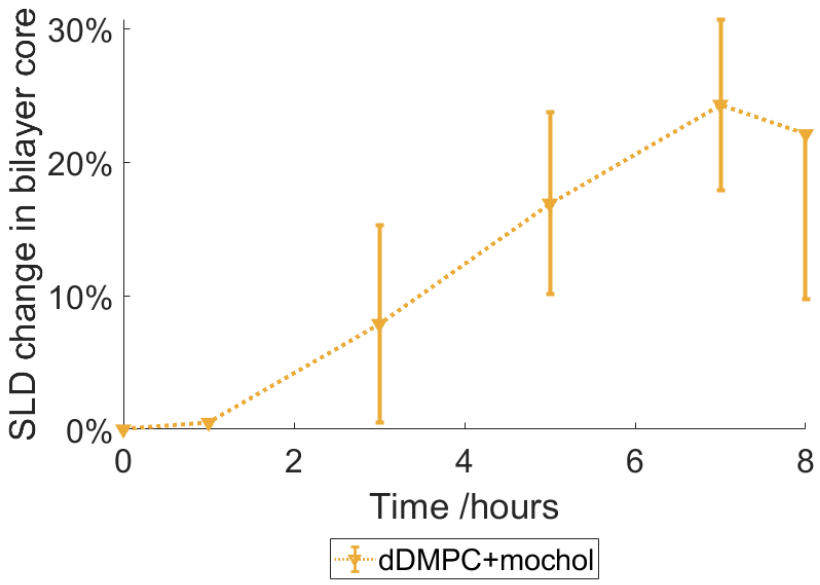

Figure S1. Kinetics of incubation of ApoA1-rHDL with dDMPC-chol SLB.

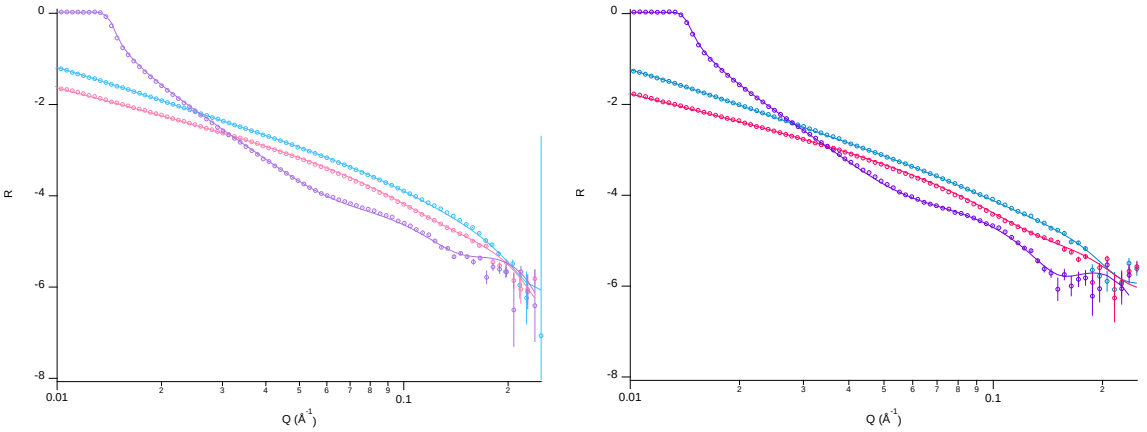

Figure S2. NR data of dDMPC SLB before incubation (left) and after incubation (right) with ApoE3 protein. dTBS, cmSi and hTBS contrasts shown in purple, pink and blue respectively.

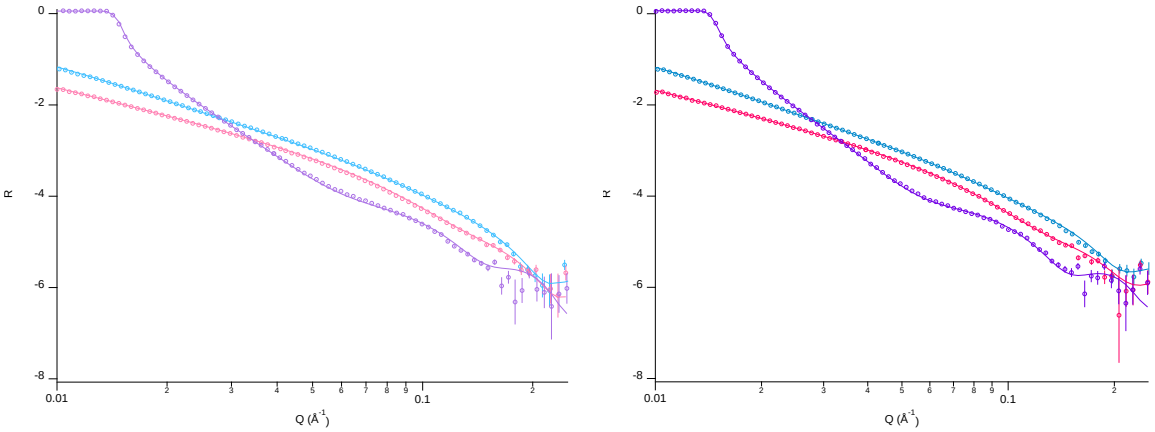

Figure S3. NR data of dPOPC SLB before incubation (left) and after incubation (right) with ApoE4 protein. dTBS, cmSi and hTBS contrasts shown in purple, pink and blue respectively.

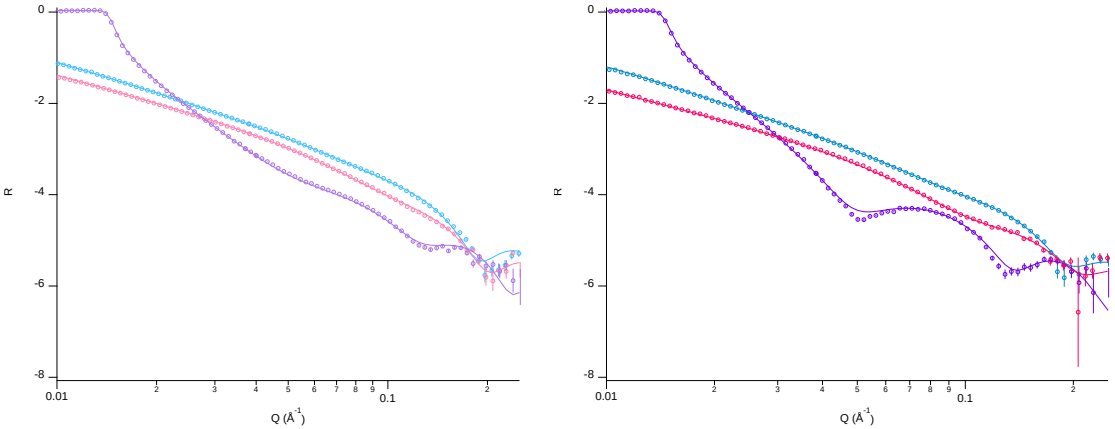

Figure S4. NR data of dDMPC+moChol SLB before incubation (left) and after incubation (right) with ApoE3 based rHDL. dTBS, cmSi and hTBS contrasts shown in purple, pink and blue respectively.

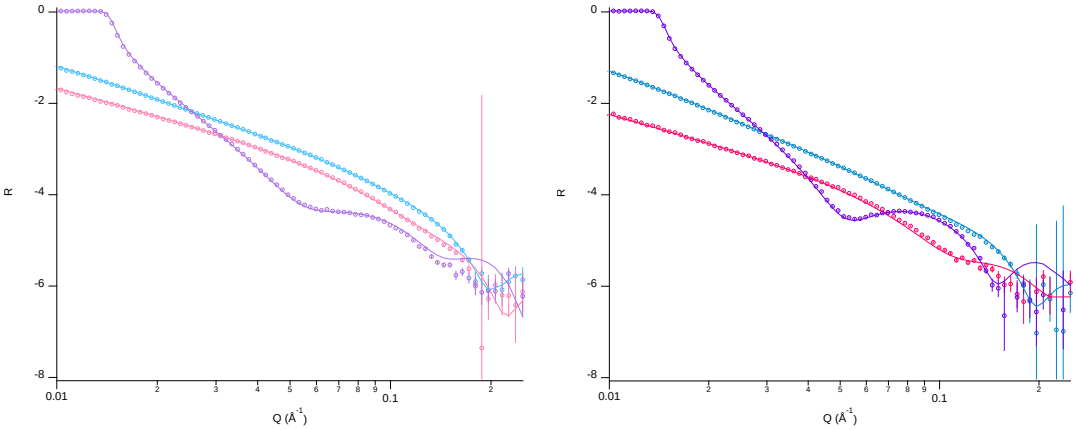

Figure S5. NR data of dDMPC+hChol SLB before incubation (left) and after incubation (right) with ApoE3 based rHDL. dTBS, cmSi and hTBS contrasts shown in purple, pink and blue respectively.

Malmö University Health and Society Doctoral Dissertations

Ross, M. W. Typing, doing and being. A study of men who have sex with men and sexuality on the Internet. 2006:1

Stoltz, P. Searching for meaning of support in nursing. A study on support in family care of frail aged persons with examples from palliative care at home. 2006:2

Gudmundsson, P. Detection of myocardial ischemia using real-time myocardial contrasts echocardiograpy. 2006:3

Holmberg, L. Communication in palliative home care, grief and bereavement. A mother's experiences. 2007:1

Ny, P. Swedish maternal health care in a multiethnic society – including the fathers. 2007:2

Schölin, T. Etnisk mångfald som organisationsidé. Chefs- och personalpraktiker i äldreomsorgen. 2008:1

Svensson, O. Interactions of mucins with biopolymers and drug delivery particles. 2008:2

Holst, M. Self-care behaviour and daily life experiences in patients with chronic heart failure. 2008:3

Bahtsevani, C. In search of evidence-based practices. Exploring factors influencing evidence based practice and implementation of clinical practice guidelines. 2008:4

Andersson, L. Endocytosis by human dendritic cells. 2009:1

Svendsen, I. E. *In vitro* and *in vivo* studies of salivary films at solid/liquid interfaces. 2009:2

Persson, K. Oral health in an outpatient psychiatric population. Oral status, life satisfaction and support. 2009:3

Hellman, P. Human dendritic cells. A study of early events during pathogen recognition and antigen endocytosis. 2009:4

Baghir-Zada, R. Illegal aliens and health (care) wants. The cases of Sweden and the Netherlands. 2009:5

Stjernswärd, S. Designing online support for families living with depression. 2009:6

Carlsson, A. Child injuries at home – prevention, precautions and intervention with focus on scalds. 2010:1

Carlson, E. Sjuksköterskan som handledare. Innehåll i och förutsättningar för sjuksköterskors handledande funktion i verksamhetsförlagd utbildning – en etnografisk studie. 2010:2

Sinkiewicz, G. Lactobacillus reuteri in health and disease. 2010:3

Tuvesson, H. Psychiatric nursing staff and the workplace. Perceptions of the ward atmosphere, psychosocial work environment, and stress. 2011:1

Ingvarsdotter, K. Mental ill health and diversity. Researching human suffering and resilience in a multicultural context. 2011:2

Hamit-Eminovski, J. Interactions of biopolymers and metal complexes at biological interfaces. 2011:3

Mellgren, C. What´s neighbourhood got to do with it? The influence of neighbourhood context on crime and reactions to crime. 2011:4

Annersten Gershater, M. Prevention of foot ulcers in patients with diabetes mellitus. Nursing in outpatient settings. 2011:5

Pooremamali P. Culture, occupation and occupational therapy in a mental care context- the challenge of meeting the needs of Middle Eastern immigrants. 2012:1

Gustafsson A. Aspects on sepsis: treatment and markers. 2012:2

Lavant, E. Multiplex HLA-DR-DQ genotyping. For genetic epidemiology and clinical risk assessment. 2012:3

Wangel, A-M. Mental ill-health in childbearing women. Markers and risk factors. 2012:4

Scaramuzzino, R. Equal opportunities? - A cross-national comparison of immigrant organisations in Sweden and Italy. 2012:5

Ivert, A-K. Adolescent mental health and utilisation of psychiatric care - The role of parental country of birth and neighbourhood of residence 2013:1

Znamenskaya, Y. Effect of hydration on thermodynamic, rheological and structural properties of mucin. 2013:2

Andersson, F. The female offender. Patterning of antisocial and criminal activity over the life-course. 2013:3

Lindroth, M. Utsatthet och sexuell hälsa – en studie om unga på statliga ungdomshem. 2013:4

Hulusjö, A. The multiplicities of prostitution experience – narratives about power and resistance. 2013:5

Falk, M. Direct electron transfer based biofuel cells. Operation in vitro and in vivo. 2014:1

Finnbogadóttir, H. Exposure to domestic violence during pregnancy. Impact on outcome, midwives' awareness, women´s experience and prevalence in the south of Sweden. 2014:2

Fagerström, A. Effects of surfactant adjuvants on barrier properties of plant leaf cuticle. 2014:3

Lamberg, P. Design and characterization of direct electron transfer based biofuel cells including tests in cell cultures. 2014:4

Richert, T. Överdoser, försörjningsstrategier och riskhantering – livsvillkor för personer som injicerar narkotika. 2014:5

Örmon, K. Experiences of abuse during the life course. - Disclosure and the care provided among women in a general psychiatric context. 2014:6

Sjöblom, I. Planerade hemförlossningar i Norden - kvinnors och barnmorskors perspektiv. 2014:7

Albèr, C. Humectants and Skin - Effects of hydration from molecule to man. 2015:1

Kisch M., A. Allogeneic stem cell transplantation. – Patients' and sibling donors' perspectives. 2015:2

Weiber, I. Children in families where the mother has an intellectual or developmental disability – incidence, support and first person perspectives. 2015:3

Schlyter, M. Myocardial infarction, Personality factors, Coping strategies, Depression and Secondary prevention 2016:1

Carlström, C. BDSM – Paradoxernas praktiker. 2016:2

El-Schich, Z. Novel imaging technology and tools for biomarker detection in cancer. 2016:3

Boonsatean, W. Living with type 2 diabetes in Thai population: Experiences and socioeconomic characteristics. 2016:4

Vejzovic, V. Going through a colonoscopy and living with inflammatory bowel disease: Children's and parents' experiences and evaluation of the bowel cleansing quality prior to colonoscopy. 2016:5

Isma, G.E. Overweight and obesity in young children: Preventive work in child health care with focus on nurses' perceptions and parental risk factors. 2016:6

Brännvall, M. Frigörelse med förhinder – Om polisanmälan när kvinnor tar sig ur mäns våld i nära relationer. 2016:7

Pankratov, D. Self-charging biosupercapacitors. 2016:8

Guidi, P. Social work assessment of families with children at risk: Similarities and differences in Italian and Swedish public social services. 2016:9

Jakobsson, J. The process of recovery after colorectal cancer surgery: Patients' experiences and factors of influence. 2017:1

Gerell, M. Neighborhoods without community. Collective efficacy and crime in Malmö, Sweden. 2017:2

Wierzbicka, C. New fractionation tools targeting elusive post-translational modifications. 2017:3

Afzelius, M. Families with parental mental illness: Supporting children in psychiatric and social services. 2017:4

Nordgren, J. Making drugs ethnic – Khat and minority drug use in Sweden. 2017:5

Nilsson, E-L. Parental socialization and adolescent offending. 2017:6

Sixtensson, J. Härifrån till framtiden. Om gränslinjer, aktörskap och motstånd i tjejers vardagsliv. 2018:1

Vasiljevic, Z. Ambulatory risk assessment and intervention in the prison services. Using Interactive Voice Response to assess and intervene on acute dynamic risk among prisoners on parole. 2018:2

González Arribas, E. Flexible and transparent biological electric power sources based on nano-structured electrodes. 2018:3

Svalin, K. Risk assessment of intimate partner violence in a police setting. Reliability and predictive accuracy. 2018:4

Andersson, M. Hate crime victimization: consequences and interpretations. 2018:5

Djampour, P. Borders crossing bodies. The stories of eight youth with experience of migrating 2018:6

Yeung, S.Y. Stimuli-responsive lipid bilayer mimics for protein, virus and cell recognition. 2018:7

Holst-Hansson, A. On a journey for survival: everyday life during radiation therapy from the perspectives of women with breast cancer and their families. 2018:8

Berlin Hallrup, L. Experiences of Everydaylife and Participation for People with Intellectual Disabilities -From four Perspectives. 2019:1

Aleksejeva, O. Blue copper proteins as bioelements for bioelectronics devices 2019:2

Wendel, L. Dokumentation, profession och hälso- och sjukvård. Rättsliga perspektiv. 2019:3

Larsson, H. Existentiell ensamhet hos sköra äldre personer: ett närståendeperspektiv. 2020:1

Sundström, M. Existentiell ensamhet hos sköra äldre personer: Vårdpersonals och volontärers erfarenheter och behov av stöd. 2020:2.

Kvist, M. Varken resurs eller problem. Om lågutbildade ungas etablerings- och försörjningsmöjligheter. 2020:3

Waldie, S. Model Membranes and Their Interactions with Native and Artificial Lipoproteins 2020:4

The publications are available on-line.
https://mau.diva-portal.org/